Universidade de Lisboa
Faculdade de Medicina
Instituto de Medicina Molecular

INTERACTIONS OF *PLASMODIUM* BLOOD AND LIVER STAGES WITHIN A SINGLE HOST

Sílvia Vilar Portugal

A dissertation for the degree of Doctor of Philosophy in Biomedical Sciences
Specialization in Biopathological Sciences

Supervised by **Maria Manuel Mota,** M.Sc, Ph.D
Principal Investigator of Unidade de Malária in Instituto de Medicina Molecular
Auxiliary Professor at Faculdade de Medicina da Universidade de Lisboa

2010

A impressão desta dissertação foi aprovada pela Comissão Coordenadora do Conselho Cientifico da Faculdade de Medicina da Universidade de Lisboa em reunião de 13 de Abril de 2010.

As opiniões expressas nesta publicação são da responsabilidade do seu autor.

The research described in this thesis was performed at the Instituto de Medicina Molecular, Lisboa, Portugal, and was financially supported by Fundação para a Ciência e Tecnologia, Portugal (SFRH/BD/31523/2006).

O trabalho de investigação descrito nesta tese foi realizado no Instituto de Medicina Molecular, Lisboa, Portugal, e foi financiado pela Fundação para a Ciência e Tecnologia, Portugal (SFRH/BD/31523/2006).

Preface

This dissertation assembles data obtained during my Ph.D research project, developed at Faculdade de Medicina da Universidade de Lisboa, Instituto de Medicina Molecular, Unidade de Malaria, under the supervision of Prof. Maria M. Mota, from October 2006 to April 2010.

This thesis is structures in 5 chapters, preceded by a summary both in Portuguese and English, outlining the aims, results and outcomes of this project.

The first chapter provides an insight on previous malaria knowledge, and the aims of this work.

The second chapter contains the description of the methods and materials employed to carry out the present work.

The third chapter contains the original data regarding this project.

Chapter four encloses an overall discussion and conclusions of the studies performed, together with a section where future perspectives of the work developed are described.

In the Appendix is included a table with the information obtained with a microarray analysis performed during the course of this work.

The data described in this dissertation is the result of my own work. This work has never been previously submitted for any degree at this or any other university

Acknowledgements

The ones who got to know me during my time in Lisbon, know that I like a lot to work, always as much as I can, and have it done as soon as possible. But most of the times, in order to be able to do almost as much as what I planned for, I counted with many important people without whom it would have been impossible to achieve all this.

Thank you Jeremie for the photo.

À Maria, por achar que valia a pena ter-me no laboratório desde o dia em que me propus vir. Pela responsabilidade que me foi gradualmente atribuindo e que me permitiu crescer no laboratório até hoje. E pela pressão boa, que sempre me fez sentir, para estar à altura do que precisava o trabalho.

Obrigada pelo projecto que deu origem a esta tese, e obrigada por tantas vezes teres acreditado que a solução estava já ali na próxima experiência, e obrigada ainda por muitas e muitas vezes teres minimizado o facto de que não tínhamos encontrado solução nenhuma...

À Mar, porque me ensinou a mexer na bancada, me deixou participar activamente no seu trabalho, e no final me delegou responsabilidades efectivas na finalização de projectos seus. E por ter feito isto tudo com um carinho sempre presente e sempre muito visível.

À AnaGomes, à Mosq e ao Johny, por tantas vezes serem correio de caixas com gelo seco e amostras, ou por me levarem e trazerem ao lab às hora que tenho que lá estar, por aceitarem os meus horários e ainda me ouvirem falar das experiências durante o jantar sempre atrasado. E a AnaGomes fez isto vezes sem conta!!

Sem vocês seria efectivamente muito mais difícil ou incrivelmente mais aborrecido.

To Unidade de Malária, to everyone i met in the *several* UMAs I crossed since the summer of 2005. All of you, I'm sure, at a certain moment contributed to the work presented here, and to the fun I had producing it.

In particular I thank Céline for the contribution with the analysis of the microarray results and for helping me interpret them with so much patience.

Depois em particular quero dizer muito obrigada à Vanessa pelo trabalho que deram as minhas amostras em Munique e pela imensa disponibilidade para discutir trabalho ou ajudar com um casaco de Elton John ou um gorro de Nikita; à Carina pelas discussões científicas ou as conversas da vida quando ficámos a trabalhar até às mil; ao Miguel pelas críticas eficientes e por exemplo, por atravessar meia cidade comigo de mota, para repor antes das 10h o tremos que parti da UBD; à Sá, à Pamplona e à Margarida Vigário por ajudarem nas minhas dúvidas de imunologia; à Sá por me ensinar a esplectomizar ratinhos, à Fernanda por me permitir pedidos de mosquitos fora de tempo e por encurtar as minhas ausências da casa dos animais com uma injecção aqui ou ali enquanto viajo; e à Eliana pela prontidão com que me aceitou na sua casa que me permitiu experiências relâmpago em Paris.

To Mario Recker for the great help in producing the model that allowed fitting the results produced in the lab during this thesis, with field observation in malaria endemic settings.

To Chris Newbold, Hal Drakesmith and Andy Armitage for the input on the hepcidin experiments, and for the help preparing the final article.

À Lígia pela contribuição com os hepatócitos primários, e por tornar agradáveis dias a produzir muito menos células do que as que gostaríamos.

Ao Cláudio Marinho por gostar de falar comigo sobre o projecto que levou a esta tese, e pelas tantas perguntas que fez sempre.

Ao João Ferreira e ao Bruno Silva Santos que enquanto Comité desta tese me questionaram e me incentivaram a perseguir os objectivos. E por perguntarem sempre *como é que está?!* o mistério.

A todo o staff das casas dos animais do IMM e do IGC, e à Alina, à Dolores e ao Manel em particular por me deixarem abusar, atender os pedidos de ratinhos em cima da hora, usar a câmara de fluxo sem marcação, por acreditarem que era importante eu poder trabalhar tudo o que quisesse.

À Rosa Maria pela prontidão com que produziu os vários anticorpos que usei ao longo deste trabalho.

To all of you that read parts of this thesis_ Miguel, Pat, Teresa, Bruno, Margarida, Vanessa, Pamplona, and Andy

Thank you for your time, your comments, corrections, and suggestions. I hope I did it right!

Ao Ruben, ao Daniel e ao Pedro obrigada por tratarem do meu computador.

À Cati e ao seu amigo Manel que me ajudaram a identificar o nome do que escolhi para a capa desta tese. E ao César que aceitou imprimir.

À prima Paula que no início me deu a sua casa por mais de um ano.

Depois à Ana por não se importar de partilhar casa com uma quase sempre ausente, por se preocupar que durma, que coma, que descanse.

Aos meus pais por participarem activamente agora como antes, desde o tempo em que o meu pai vendia os calendários dos escuteiros que deveria vender eu, até a tempos mais recentes em que a minha mãe forra as gaiolas dos mosquitos com rede e nastro que nos servem a todos no lab. E à Quel que tantas segundas-feira me levou ao comboio a horas indecentes para que pudesse começar a trabalhar a horas decentes. E à Di por me perdoar os tantos ratinhos sacrificados.

Obrigada por me deixarem continuar a ser cuidada por vocês.

E ao Ricardo pelo ímpeto que me dá o seu amor, em tudo e mais no trabalho.

Obrigada por me ouvires já demasiado tarde e ainda sobre trabalho, por vires comigo ao lab em noites ou madrugadas em que devíamos só namorar, por leres as coisas que escrevo ainda que tarde, e por perguntares e se fosse assim...? por ajudares no nome da tese e por arranjares os artigos acabados de sair do prelo ou da "arca da velha", aos quais não tenho acesso.

Resumo

A infecção pelo agente causador da malária, o parasita *Plasmodium*, encontra-se ainda hoje disseminada pelas populações de 108 países no mundo. A malária produz sintomas que variam entre febres ligeiras até ao coma, anemia severa, síndrome respiratória aguda ou malária cerebral. Só em 2008 esta infecção foi responsável por mais de 800000 mortes, das quais a maioria se ficou a dever ao parasita *Plasmodium falciparum*. Adicionalmente a malária é ainda responsável por uma redução de 1.3% no crescimento económico dos países de maior endemicidade.

O parasita *Plasmodium*, pertence ao filo Apicomplexa e partilha com o Homem a presença na Terra desde o próprio aparecimento da espécie humana, tendo a adaptação parasita-hospedeiro vindo a evoluir ao longo do tempo, procurando um balanço entre a transmissão do parasita e a sobrevivência do hospedeiro.

É com a picada de uma fêmea de mosquito *Anopheles* que o parasita chega ao hospedeiro mamífero. Depois de uma passagem pela pele, os esporozoítos migram via corrente sanguínea até ao fígado onde depois de atravessar vários hepatócitos, invadem um último com a formação de um vacúolo parasitário. No hepatócito dá-se um processo de crescimento e replicação que no homem demora vários dias até à formação de vários milhares de merozoítos que serão libertados de novo na corrente sanguínea. Uma vez no sangue os merozoítos entram numa nova fase de reprodução assexuada, com sucessivos ciclos de invasão de eritrócitos, replicação e libertação para a corrente sanguínea e nova invasão de eritrócitos. É nesta fase da infecção que todos os sintomas associados à malária surgem.

Ocasionalmente, o ciclo de reprodução assexuada dentro dos eritrócitos para formação de novos merozoítos é substituído pela formação de gametócitos femininos ou masculinos que poderão ser aspirados durante uma nova picada de mosquito. É no hemocélio deste vector que se dá a fase sexual do parasita da malária com a formação de um zigoto e subsequente oocineto que migra para a lâmina basal onde se transforma num oocisto. A partir da esquizogonia dos oocistos surgem novos esporozoítos que uma vez chegados às glândulas salivares do mosquitos estão prontos para que se inicie uma nova infecção.

Em zonas de alta transmissão de *Plasmodium* é provável a ocorrência de sobreposição das fases hepática e sanguínea num só hospedeiro, bastando para isso que uma picada infecciosa ocorra num indivíduo que alberga já uma infecção circulante proveniente de uma picada anterior. Apesar de potencialmente importantes, as possíveis interacções entre as diferentes fases de desenvolvimento do parasita e o hospedeiro que os acolhe nunca foram objecto de estudo.

O objectivo desta tese prende-se precisamente com o estudo das interacções que surgirão desta situação a que damos o nome de re-infecção. Quão efectivos serão os esporozoítos na infecção do fígado de indivíduos com *Plasmodium* no sangue, quando comparados com a infecção do fígado de indivíduos sem qualquer parasita de malária presente?

Fazendo uso de modelos animais previamente estabelecidos e diferentes clones de parasitas, que nos permitiram distinguir as infecções hepática e sanguínea nos animais re-infectados, verificámos uma redução fortíssima na infecção no fígado de animais re-infectados. A capacidade dos esporozoítos para infectar hepatócitos de ratinhos com infecção sanguínea a decorrer apareceu altamente limitada quando comparada com a mesma capacidade para infectar hepatócitos de ratinhos naive.

O estudo detalhado deste fenómeno permitiu-nos relacionar a redução da infecção hepática com a diminuição tanto do número como do desenvolvimento das formas exo-eritrocíticas (EEF no original) no fígado. Esta redução verificou-se independente do nível da parasitémia da infecção primária, desde que esta se encontrasse acima de um valor que se mostrou ser baixo e rapidamente atingido. Mais ainda, verificou-se que a administração de um tratamento anti-malárico aos ratinhos infectados com *Plasmodium* no sangue antes da re-infecção, resulta na perda deste efeito protector.

Várias hipóteses, baseadas em trabalhos anteriores a este e num estudo de expressão genética que realizámos para melhor compreender as alterações hepáticas em resposta à presença de *Plasmodium* no sangue, foram colocadas na tentativa de entender o mecanismo pelo qual se observa tamanha redução na infecção de fígado de ratinhos re-infectados. Diversas moléculas associadas ao sistema imunitário, à inflamação e à apoptose no fígado foram testadas por meio de ratinhos transgénicos, ou pelo uso de anticorpos depletantes ou drogas bloqueantes sem que nenhum dos factores testados indicasse ser relevante.

A infecção de hepatócitos co-cultivados com eritrócitos infectados com *Plasmodium*, não mostrou ser eficiente em produzir o mesmo tipo de redução, afastando a hipótese de um factor solúvel libertado pelo eritrócito infectado.

Ao avaliar alterações no fígado relacionas com a disponibilidade de nutrientes verificámos que o gene codificante da hormona reguladora do ferro, hepcidina se encontrava sobre-expresso no fígado de animais com parasitas no sangue. Sabendo que a disponibilidade de ferro pode limitar o crescimento de vários patogénios incluindo o *Plasmodium*, perguntámo-nos se seria esse o cerne da redução na infecção verificada.

A expressão do gene codificante da hepcidina provou estar intimamente ligada à presença de eritrócitos infectados no sangue de ratinhos, subindo rapidamente com poucos ciclos replicativos de *Plasmodium* no sangue, e voltando rapidamente a valores basais com o tratamento anti-malárico, o que rapidamente reduz a parasitemia para zero permitindo então que a infecção hepática se processe como em ratinhos naive. Além disso, pôde verificar-se uma redistribuição de ferro no fígado, perdendo-se parte do conteúdo nos hepatócitos para incrementar o conteúdo em macrófagos residentes e infiltrados no fígado.

Adicionalmente, mostrou-se que a hepcidina *per se* pode reduzir a infecção hepática. A administração a ratinhos de um adenovírus expressando o gene codificante desta hormona reguladora de ferro confirmou que este componente promovido pelo parasita no sangue, mesmo na sua ausência, pode actuar limitando a infecção por esporozoítos.

Ao tentar perceber a implicação destes resultados na malária humana, deparámo-nos com dados epidemiológicos há muito conhecidos mas parcamente explicados. Em áreas altamente endémicas é conhecido consistentemente que a incidência da infecção aumenta inicialmente com a idade das crianças para depois decrescer, possivelmente pela acção da imunidade adquirida. Ao mesmo tempo, a complexidade da infecção, em número de clones de parasitas diferentes no sangue de indivíduos, aumenta à medida que as crianças crescem em idade.

Divisando um modelo baseado unicamente na existência de um valor mínimo de parasitémia que inibisse o estabelecimento da infecção hepática, tal como foi observado no decurso desta tese, e assumindo o há muito estabelecido, que a densidade de parasitas no sangue decresce com a idade dos indivíduos. Institui-se então que a probabilidade de um picada infecciosa produzir infecção depende do nível de parasitémia no momento

da infecção e da história clínica do hospedeiro no que concerne a episódios prévios. Sob estas assumpções mínimas o modelo criado prevê correctamente um aumento inicial de infecções nas crianças seguindo-se um declínio à medida que os indivíduos adquirem imunidade devido a repetidas infecções. Quer isto dizer que uma densidade mínima de parasitas no sangue, da qual dependa a inibição de novas infecções de *Plasmodium* no fígado, pode por si justificar o aumento do risco de infecção e crescente complexidade das mesmas em crianças novas.

A aplicação do modelo com os resultados esperados é mais proeminentemente observada quando testado segundo áreas com taxas de transmissão moderadas ou elevadas, e permite explicar ainda algumas diferenças de incidência da doença ao longo da idade das crianças em áreas com diferentes taxas de transmissão.

O ciclo de vida do *Plasmodium* tem vindo a desenvolver-se ao longo de milhões de anos de co-evolução das interacções hospedeiro-parasita, com implicações importantes para a saúde humana. A infecção de eritrócitos acima de uma densidade mínima eleva a produção da hormona reguladora do ferro, hepcidina, que redistribuindo o ferro protege o nicho do parasita existente, inibindo o estabelecimento de uma infecção secundária, prevenindo assim a superinfecção. Este fenómeno actua independentemente e de forma complementar à imunidade adquirida e vem aclarar observações epidemiológicas prévias, podendo ainda ter implicações em futuras intervenções na luta contra a malária.

Palavras-chave: malária, re-infecção, superinfecção, hepcidina, ferro

Summary

In regions of high malaria transmission, infected individuals are constantly exposed to potential re-infection. Mosquito bites transmit liver-tropic sporozoites into subjects who already have blood-stage parasitaemia. How these two stages of the *Plasmodium* life cycle interact within their host is unknown. Here, using a rodent model, we show ongoing blood stage infections impair the growth of subsequently inoculated sporozoites. Secondary infections are arrested in liver hepatocytes and fail to compete for colonization of red blood cells. This protection of the erythrocyte niche only occurs beyond a certain threshold of blood parasite density, and so is phenotypically akin to quorum sensing. We eliminate *Plasmodium*-secreted factors, host cell survival and innate or adaptive immunity as explanations for this observation. Instead, we find parasitized erythrocytes induce expression of the host iron regulatory hormone hepcidin, which by diverting iron from hepatocytes to macrophages, limits *Plasmodium* growth in the liver. Presuming a similar interaction between malaria and the human host we demonstrate how parasite threshold-density dependent growth inhibition alone can explain the epidemiological patterns of age-related risk and complexity of infections in young children. Our findings thus have broad implications for malaria and have general relevance for understanding host-pathogen interactions.

CQ	Chloroquine
EEF	Exo-Erythocytic Forms
EIR	Entomological Inoculation Rate
gfp	Green Fluorescent Protein
hamp	Hepcidin
hprt	Hypoxanthine Guanine Phosphoribosyltransferase
iRBC	Infected Red Blood Cell
PbA	*P. berghei* ANKA
PbNK	*P. berghei* NK65 iRBCs
RBC	Red Blood Cell

Introduction

From the beginning…

Malaria

Descriptions of malaria appear in history prior to its name in several ancestral civilizations. Ancient Chinese manuscripts dating as early as 2700 BC have descriptions of patients with fever accompanied by enlarged spleen (reviewed in [1]). Later, Indian and Egyptian manuscripts also recorded indications of malaria infection. Furthermore, DNA of one of the species causing malaria, *Plasmodium falciparum* was recently isolated from an approximately 4000 year old Egyptian mummy [2] and *Plasmodium falciparum* DNA was also found in the mummy of Egyptian King Tutankhamun and three members of his family [3]. Reports by Hippocrates in 400 BC described for the first time the various periodic malaria fevers. In the *Corpus Hippocraticum*, he distinguished the intermittent malarial fever from the continuous fever of other infectious diseases, and also noted the daily, every-other-day, and every-third-day increase in body temperature (reviewed in [4]).

Fig. I1. **La Mal'aria** (1850-1851), oil over canvas by the French artist Antoine Auguste Ernest Hébert (1817-1908). Reproduction rights requested to Museé d'Orsay and Museé Hébert.

The name Malaria appears later from the Italian *mal'aria*, translating into *bad air*, as in Rome, where the disease raged for centuries, it was commonly believed until the 20th century that swamp and marshes produced the illness (reviewed in [5]).

In world history, the disentanglement of the Greek Empire is attributed to malaria and the disease is also believed to have stopped armies of European and Asian empires on different occasions [1]. Now as then, malaria still limits civilizations. Indeed, in the second half of the 20th century, countries with intensive malaria showed an average increase of gross domestic product (GDP) 5 times lower than that observed for non-malarial countries [6].

The clinical features of malaria infection, which made it so recognisable throughout centuries, occur only during the asexual cycles of *Plasmodium* parasite inside red blood cells (RBCs). In humans, symptoms range from mild fever to coma, severe anaemia, respiratory distress or cerebral malaria [7]. The 2009 World Malaria Report of the World Health Organization (WHO) states that 108 countries were endemic for malaria in 2009, and that 863000 deaths were attributable to malaria in 2008, the majority of which were African children under 5 years of age [8]. Moreover, the disease is estimated to be responsible for an annual average reduction of 1.3% in the economic growth for those countries with the highest burden [9].

From the very beginning…

Plasmodium phylogeny and its co-evolution with man

Plasmodium is the causative agent of malaria and belongs to the Apicomplexa phylum. Apicomplexans have probably been present on earth since the earliest animals appeared and modern *Plasmodium* species descend from apicomplexans that interacted and adapted to increasingly sophisticated hosts over hundreds of millions of years [10]. Species of the genus *Plasmodium* have co-existed with humankind throughout its

evolution. *P. falciparum, P. vivax, P. ovale* and *P. malariae* are the species that systematically infect humans. In addition, a fifth one, *P. knowlesi*, a natural parasite of macaque monkeys in southeast Asia, was recently reported to infect considerable numbers of humans [11], besides several reports on isolated cases in several Asian regions [12,13]. Likewise, recent work reports that *P. falciparum* infections are not rare in gorillas [14]. These species represent only a glimpse of the systematic and ecological diversity of *Plasmodium* and related genera of Apicomplexa parasites. Several hundreds of malaria parasite species use squamat reptiles, birds, and mammals as vertebrate hosts along with many genera of dipteran vectors [15], but the evolutionary and ecological events that led to this diversification and success remain poorly resolved. Recent genetic data challenged the classical systematic classification of malaria parasites, both within the *Plasmodium* genus, and in its relations among the currently recognized genera of the order Haemosporidiae of Apicomplexa parasites. A study recovering multi-gene phylogeny of malaria parasites, including the analysis of sequencing data from 4 genes, indicated that parasites identified as *Plasmodium* species fall in two major clades, each clade being associated with a unique vector family, one clade containing parasites of mammals, and other of lizards and birds. Within the mammalian parasite clade, there are 4 monophyletic lineages: the human parasite, *P. falciparum*, a ‘‘primate” lineage that contains *P. vivax* and *P. knowlesi*, a lineage of parasites that infect African rodents, and the three samples of *Hepatocystis* isolated from bats [16].

Evolutionarily, *Plasmodium* emergence was accompanied by a major change in parasite’s life cycle that differed from other genera. In addition to an initial round of asexual replication in fixed tissues that was general for all parasites, the *Plasmodium* life cycle includes additional rounds of asexual reproduction in blood cells, revealing increasing complexity when compared to ancestral parasites. There was also a shift to the use of

mosquito vectors, which seems to have made the exploitation of a greater variety of vertebrate taxa as hosts possible [16].

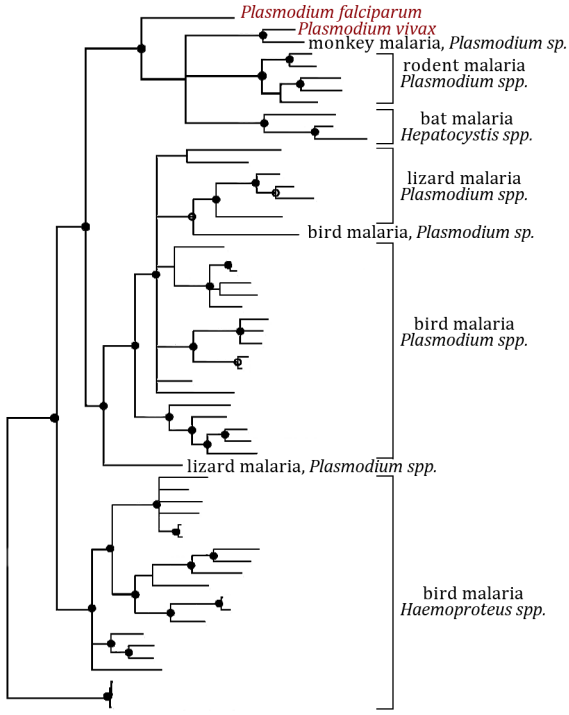

Fig. I2. **Phylogenetic tree of malaria causing parasites** Adapted from a multy-gene analysis study performed by Ellen S. Martinsen and collaborators, using 11 mammalian parasite species, 7 species that infect lizards, and 39 lineages from avian hosts.

It has been established that *Plasmodium* entered mammals only once, coincident with a switch from Culicine to Anopheline mosquitoes [17]. All known vectors of mammalian-infecting *Plasmodia* belong to the *Anopheles* genus [18], indicating that the shift of *Plasmodium* into mammals was associated with specialization to anopheline vectors. It is well accepted that the closest identified sister taxon of *P. falciparum* is *P. reichenowi* whose host is the chimpanzee [19]. It was recently proposed that extant *P. falciparum* populations originated from *P. reichenowi* as late as 1.5 million years ago,

likely by a single host transfer [20], an event that appears to have happened frequently between primates, including humans [19]. Others believe that the appearance of *P. falciparum* occurred even later during the initiation of agriculture, ten thousand years ago [21]. Still, there is some controversy around these proposals and the relationship between *P. falciparum* and *P. reichenowi* is not yet completely clear.

Nevertheless, it is clear that *Plasmodium* (or its ancestors) and their hosts had millions of years to co-evolve and co-adapt, leading to a balance between parasite replication and host survival enabling transmission to other hosts. A possible explanation for *P. falciparum* being the most virulent species infecting humans is the fact that, being much more recent than other *Plasmodium* species, it has not yet had the necessary time to fine-tune its effects on the host population.

Despite the significant burden of malaria-related mortality only a small proportion of infections lead to severe disease or death. *Plasmodium* infections in malaria endemic regions most often go unnoticed even in children, who are the most affected sector of the population. In children, around half of all infectious bites produce no infection, about a quarter leads to asymptomatic infections, roughly the other quarter gives rise to uncomplicated malaria with mild symptoms, and only a very small proportion of the infective bites will induce severe malaria with manifestations such as coma, cerebral malaria, respiratory distress, or severe anaemia [22] that can ultimately lead to death. Still, the prevalence of *P. falciparum* is high enough to kill more than half a million children every year in sub-Saharan-Africa.

Evidence for the adaptation of *Plasmodium* to man, and man's strategies to circumvent malaria infection can be seen in how the infection has modulated certain human genes in affected populations, selecting for resistance. As Haldane hypothesised and Allison demonstrated [23], malaria is

known to be a strong evolutionary force of selection in the recent history of the human genome. Sickle-sell disease, thalassemia, and glucose-6-phosphatase deficiency, among other erythrocyte defects that together comprise the most common Mendelian human diseases, are under *Plasmodium* infection selection force, and can aid understanding the genetic basis of resistance shown by some exposed populations. Indeed, different resistant alleles have been identified for sickle cell trait in different areas and at different times, suggesting convergent evolution (reviewed in [24]).

Plasmodium *modus operandi…*

The *Plasmodium* life cycle in mammals

Alfonse Laveran identified the exflagelating malaria parasite in human blood in 1880 [25]. Eight years later, using an avian model, Ronald Ross attributed the transmission of malaria disease to the anopheline mosquito [26]. The first observation of the pre-erythrocytic stage parasite was described later in 1948 by H. E. Short and P. C. Garnham in the liver of a simian model [27]. The three stages of malaria infection were then described, and from there on research tries to fill in the gaps, and understand the exact details of the entire life cycle, what the parasite's needs are, and how host and vector molecules contribute to or fight infection.

During its life cycle the malaria parasite takes many forms, shifting between invasive and replicative stages both in the vertebrate host and in the anopheline vector.

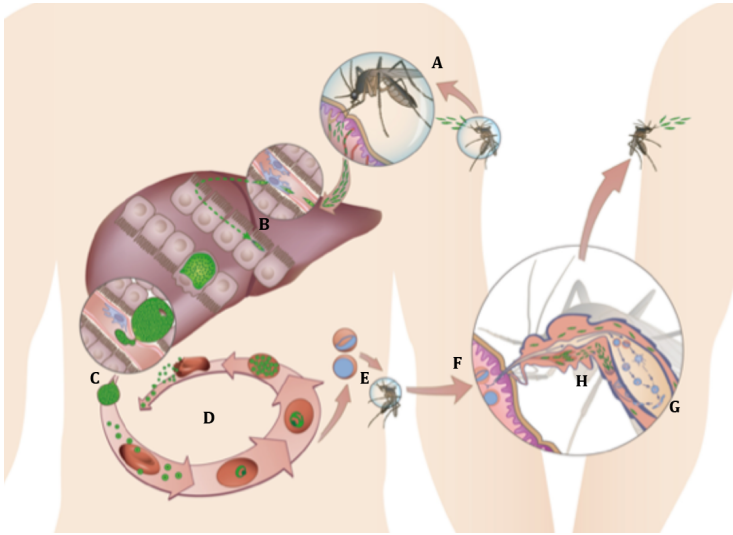

Fig. I3. ***Plasmodium* life cycle** (**A**) During a blood meal an anopheline mosquito injects *Plasmodium* sporozoites into the host dermis. (**B**) After reaching a blood vessel, sporozoites will travel to the liver where after traversing several hepatocytes, sporozoites invade a final one. (**C**) After asexual replication and development inside a hepatocyte, merozoites are released into the blood stream. (**D**) Merozoites infect red blood cells during cycles of asexual replication. (**E**) Occasionally replication cycles will originate female and male gametocytes. (**F**) Through another blood meal, a mosquito ingests gametocytes into its midgut. (**G**) Fertilization of gametes occurs in the mosquito midgut with the formation of ookinetes and later the oocysts. (**H**) Sporozoites released from the oocyst migrate to the salivary gland of the mosquito awaiting the next blood meal.

Deposition in the skin. All natural human malaria infections start with the deposition of *Plasmodium* sporozoites by a female anopheline mosquito in the host's dermis, during a blood meal. Each sporozoite is approximately 10 μm long and 1 μm wide, and once in the dermis, one of four possible fates will determine its future: (i) it can invade a blood vessel and reach the liver [27], (ii) it can invade a lymphatic vessel and accumulate in the draining lymph node [28], (iii) it can remain in the dermis [29], or (iv) it can be re-ingested into the mosquito gut during the blood meal [30]. Only the first of these fates allows infection to proceed.

In the avascular tissues of the dermis, sporozoites actively glide forward in random directions. This movement however, seems to be specific to its substrate, as it differs from the one observed in salivary gland ducts and from that exhibited *in vitro* [28]. Like other apicomplexan parasites, *Plasmodium* sporozoites display a unique kind of locomotion, known as gliding motility, defined by the lack of obvious modification in the moving cell shape, and the need for a supporting substrate [31]. The parasite glides both to achieve motility and to invade cells, and the two mechanisms are made possible by the same acto-myosin motor located in the cortical space in between the plasma membrane and the inner membrane complex (IMC), a continuous layer of flattened vesicles underneath the plasma membrane [31-34]. In this space, trans-membrane proteins displaying adhesive extracellular domains and anchored to the motor trigger either forward locomotion or penetration into the host cells [31,35,36]. One such molecule of particular importance is the thrombospondin-related anonymous protein (TRAP), whose expression is restricted to *Plasmodium* sporozoites [37,38].

Most sporozoites remain in the dermis for at least 5 minutes, as the removal of the biting site 5 minutes after the bite greatly reduces the number of infections in mice. However, a similar removal 15 minutes after the mosquito bite does not cause any significant alteration in the outcome of liver infection [39], showing that during this timeframe following inoculation a significant and sufficient proportion of the sporozoites leave the biting site to find a blood vessel, which will later lead to infection of hepatocytes. Nevertheless, it takes one hour for half of the inoculated sporozoites to leave the dermis, either into blood or lymphatic vessels, and sporozoites have been found in the dermis up to 7 hours after injection [40]. During this period in the skin, sporozoites might trigger the first line of immune response.

To leave the dermis sporozoites may make use of their ability to traverse cells [41], disrupting membranes of endothelial cells and penetrating vessels. Several proteins have been identified as essential for cell traversal, such as the sporozoite microneme protein essential for cell traversal (SPECT) [42], SPECT2 [43], cell traversal protein for ookinetes and sporozoites (CelTOS) [44] or phospholipase (PL) [45]. Indeed, sporozoites lacking SPECT are unable to reach blood vessels [41].

Close to one third of sporozoites inoculated into mice through mosquito bite are later found in lymphatic vessels [28]. From there, only a few sporozoites can be rescued back to blood circulation, while the rest are drained to the closest lymph node. Once there, some sporozoites have been observed to develop into young and small Exo-Erythocytic Forms (EEFs) during the first hours. This initial development is not continued and, instead, these small EEFs are then cleared, which seems to contribute to the initiation of an immune response [46].

The mechanism of invasion of the blood vessels is still not fully understood. It has been described that gliding speed is decreased when sporozoites are in contact with the vessels and it is known that the entry process lasts less than a minute [47].

The liver stage. Once inside the vessel, sporozoites are carried in the blood flow at the same speed as erythrocytes [40], and will later be arrested in the liver by not completely understood mechanisms. Circumsporozoite protein (CSP), a protein encoded by a single copy gene, and the major coat protein of *Plasmodium* sporozoites [48], has been shown to be involved in this process. Indeed recombinant CSP binds specifically to sulfated glycoconjugates [49]. It has been proposed that heparan sulfate proteoglycans (HSPGs) of stellate cells extending through endothelial fenestrations to the sinusoidal lumen, can attract and arrest sporozoites. These cells synthesize proteoglycans that are eight times more sulphated than those of hepatocytes and incorporate

twice the amount sulphate into heparan sulphate, known to be preferentially attractive to sporozoites [50]. Being unable to pass through fenestrations of the liver sinusoid, sporozoites must migrate through cells, mostly Kupffer cells, using their capacity to traverse barriers and finally access the liver parenchyma [51]. Still, this is a matter of controversy and some authors have proposed that the passage through Kupffer cells occurs by a mechanism akin to phagocytosis [52]. Once having gaining free access to the liver parenchyma, sporozoites traverse several hepatocytes, disrupting their plasma membranes to get in and out of cells [53], until they ultimately invade a final hepatocyte with formation of a parasitophorous vacuole (PV). Different studies have shown hepatocyte traversal makes sporozoites prone for final hepatocyte infection, either by activating sporozoites to form a PV [54,55] or by leading to the release of hepatocyte growth factor, which sustains host cell viability [56]. Importantly, although demonstrated to be beneficial for infection, traversal ability of *Plasmodium* sporozoites has been shown not to be essential for hepatocyte invasion *in vitro*, since parasites lacking essential proteins for cell migration as SPECT, CelTOS or PL still invade hepatocytes and complete liver stage development similarly to wild type parasites [42-44]. Not much is known about the signal to stop migration and invade, but mouse studies indicate that sporozoites are activated to initiate the invasion process in the presence of cells expressing high levels of sulfated HSPGs [50,54].

To invade hepatocytes, *Plasmodium* sporozoites, like other apicomplexan parasites, release proteins from apical organelles termed rhoptries, micronemes and dense granules, and attach to host cells using cell-adhesive domains of some of these proteins. TRAP seems to be essential to this process [57]. Although adhesion to the host cell is initially reversible, it later becomes irreversible, forming tight junctions that will allow the parasite to move forward propelled by its acto-myosin motor, allowing it to enter the

cell. With the completion of the tight junctions, the sporozoite is included inside the host cell surrounded by the PV membrane [58].

Inside hepatocytes, sporozoites develop and replicate originating thousands of merozoites that ultimately will proceed to blood infection. The astonishing replication rate observed most certainly implies strong cellular and molecular host-parasite interactions. Although little is known about the intra-hepatic development of *Plasmodium* parasites, recent studies have provided a new and more comprehensive insight into gene expression and protein abundance profiles of *Plasmodium* liver stage [59]. *Plasmodium* sporozoite and liver stage asparagine-rich protein (SLARP) has been observed to be essential for initiation of EEF development, as parasites mutant for this protein are arrested in very early development [60]. Other parasite proteins have been shown to be essential for development inside hepatocytes. Parasites deficient for the microneme protein P36p present reduced invasion and impaired development [61], and up-regulated in infective sporozoites genes 3 an 4 (UIS3)- or (UIS4)-deficient parasites present impaired development [62]. *Plasmodium* Fatty Acid Synthesis II pathway enzymes were found to be modulated during infection, and later functional studies revealed that type 2 fatty acid synthesis is important for liver stage development [63] and, more specifically, essential for the late steps of liver stage development [64]. Another recent study showed that cGMP dependent protein kinase (PbPKG) disruption in sporozoites leads to an arrest of liver stages [65].

Host molecules have also proven to be important for complete development of the *Plasmodium* parasite inside hepatocytes. The expression of several host genes is modulated during liver infection, as shown recently in a microarray study comparing infected and non-infected cells patterns of gene expression over the time course of infection [66]. In functional studies, tetraspanin CD81 [67] and scavanger receptor B1 [68] have been shown to be

important for liver stage development. Their absence reduces liver infection to very low levels in rodent models. Yet another functional screen, aimed at the host kinome, has linked an efficient parasite infection with several human kinases [69].

During the liver stage, as will later be shown for the blood stage, *Plasmodium* parasites seem to export proteins beyond the PV to the cytosol of the hepatocyte or even to the hepatocyte nucleus. Up to now this has been shown for CSP, and mutant parasites incapable of this export movement show impaired development [70].

By the end of exoerythrocytic stage, merozoites are released in the blood-stream within large vesicles known as merosomes [71]. These budding structures full of merozoites squeeze through endothelial cells, and are initially hidden from the host's innate immune system by being covered with a hepatocyte-derived membrane.

The blood stage. After reaching circulation, merosomes release the merozoites into the blood-stream. This seems to occur only when merosomes reach the lung microvasculature. Although the reason behind is not known, it has been speculated that low macrophage density and reduced blood velocity with reduced shear forces within the lung microvasculature enhances the ability of merozoites to invade erythrocytes, since once merozoites are free in circulation they quickly have to find a red blood cell to infect. [72].

Merozoites invade RBCs, highly differentiated cells, whose main purpose is oxygen distribution throughout the body. However, RBCs lack several cellular functions as they are anucleated, transcriptionally and translationally inactive, lack any secretory apparatus, have only a limited repertoire of solute and iron transporters, and are readily removed from circulation when damaged (reviewed in [73]).

Invasion of RBCs follows sequential steps: cell recognition, merozoite binding, reorientation and deformation of the RBC, junction formation and parasite entry. In in *P. falciparum* alone, more than 50 surface and secreted proteins have been identified as playing a role in these events [74]. Initial host-parasite contact is believed to be random but, once it has happened, merozoite surface proteins (MSP) immediately mediate adhesion to the host cell [75]. The merozoite's surface is covered in glycosylphosphatidylinositol (GPI)-anchored proteins and their partners [76]. Many of these proteins seem to act as ligands for RBCs. Besides sharing GPI-anchors, surface proteins of the merozoite also share with sporozoites and gametes the cysteine-rich domains that have been shown to potentiate adherence [77] of *Plasmodium* species. As such, it is believed they play similar roles in the cytoadherance during the blood stage of infection. In order to invade RBCs, merozoites make use of complex mechanisms, evidencing great adaptation to their host. Some parasite strains that depend on sialic-acid receptors, for example, can even shift their invasion pathway to a sialic-acid independent entry process [78].

After this initial binding, there is a reorientation of the merozoite in order to position its apical and secretory ornanelles (rhoptries, micronemes and dense granules) in contact with the RBC membrane. An indentation is then formed in the contact zone. A number of proteins of the apical organelles bind to specific erythrocyte receptors. Apical membrane antigen 1 (AMA-1) is known to establish the apical interaction through parasite adhesins initially located at the neck of the rhoptries and in the micronemes [79]. Recently, parasites with green fluorescent protein (GFP)-tagged AMA-1 were used in live imaging studies that revealed this protein's crucial function [80].

The actual invasion process involves two major protein families, the Duffy binding-like (DBL) protein family [81], and the *P. falciparum* reticulocyte

binding protein homolog (PfRh) family [82]. DBL and PfRh proteins are important for merozoite invasion of RBCs, but are not considered essential, as gene disruption for each of them in different *P. falciparum* lines still show normal blood-stage growth rates [83-87]. This might be due to complementation between different family members or to a great level of adaptation of *Plasmodium* to its host cell. When the apical interaction is formed, the merozoite establishes a tight junction, which is accompanied by the release of more proteins from the microneme and rhoptry organelles. When attachment is finally achieved, the merozoite is hypothesised to discharge mediators into the RBC, and although these have not yet been identified, visualization of merozoite invasion by electron migrographs suggests material transfer [88]. Entry is then mediated by activation of the acto-myosin motor in the pellicle of the invading merozoite [89]. At the end of the invasion process, the RBC bilayer envelops the invading merozoite in a new vacuole [90], which lacks normal proteins of the RBC membrane. Proteins like Band 3 are cleaved by proteolytic enzymes secreted by the parasite [91] and are replaced by recruitment of detergent-resistant membrane (DRM) raft proteins, making the PV richer in lipid rafts and its proteins [90].

Inside the normally quiescent environment of a RBC, the merozoite undergoes some rounds of nuclear division, transforming sequentially in ring, trophozoite and schizont stages. It eventually egresses and releases 16 to 32 new merozoites that will follow the same sequence of events. In *P. falciparum*, the ring stage lasts approximately 24h, accounting for half of the entire erythrocytic cycle [92].

Following entry, and throughout all the developmental and replication processes, the parasite modifies the permeability and adhesive properties of its host cell, possibly to promote its own survival.

The ring stage is followed by the trophozoite stage, during which most of the cytoplasm of the RBC is consumed, a process that leads to the

degradation of 60 to 80% of the haemoglobin present in the RBC [93]. This is followed by the schizont stage, during which 4 to 5 rounds of binary replication take place, originating merozoites that will later invade other RBCs. The most common and concentrated molecule inside RBCs is haemoglobin that is degraded by *Plasmodium*. Haemoglobin proteolysis yields haem besides amino acids as end products. Haeme is not metabolized or recycled by the parasite. Instead, it is stored as hemozoin, a polymer that confers the characteristic pigmentation to the organs of infected individuals [94,95]. The amino acids of the haemoglobin polypeptide chain are used in the synthesis of parasite's proteins [96] and appear to be used as an energy source [95]. The recovery of the amino acids is essential for the parasite as it has limited capacity of *de novo* synthesis [94]. However, the recycling of amino acids originating from haemoglobin degradation is not sufficient for parasite maintenance as haeomglobin lacks some essential amino acids, which the parasite is able to withdraw from the host plasma [97]. The feeding of the parasite in the RBC occurs through a cytostome, an invagination of the PV membrane and the parasite plasma membrane, which ingests small packets of haemoglobin from the host cytosol. Budding vesicles full of haemoglobin are transported and fused to an acidic digestive vacuole (DV) where haemoglobin is degraded and haeme is detoxified by the action of several proteases [98] acting like haemoglobinases. Data suggest that this degradation process is ordered and requires, among other reactions, an initial aspartic protease-mediated cleavage, followed by secondary aspartic protease and cysteine protease cleavages. The aspartic proteases have been shown to be Plasmepsin I and II and the cysteine protease has been identified has Falcipain [99,100]. Different patterns of gene expression are observed during the erythrocytic cycle, suggesting that their functions are not exactly the same. Several other Plasmepsin proteins were later identified both inside and outside the DV. Their functional redundancy was

shown when independent disruption of Plasmepsin I, II, IV or histidine aspartic protease (HAP) was obtained and very little effect on the parasite growth was observed [101,102].

Plasmodium has the ability to export hundreds of its own proteins beyond its plasma membrane and the PV to the cytosol of the erythrocyte [103]. This represents 5% of its whole genome. Although the function of many of these proteins remains unknown, some of them have been associated with virulence, promoting cell adhesion and/or rigidity of the erythrocyte [104,105]. To be exported, proteins must first enter the secretory pathway [106] showing a recessed amino-terminal hydrophobic endoplasmatic reticulum (ER) signal sequence that allows transport across the plasma membrane of the parasite but not the PV membrane. Most proteins exported across the PV membrane require an additional sequence element known as *Plasmodium* export element (PEXEL), or a vacuolar transport sign (VTS) that is found downstream of the ER signal sequence [107]. This export movement has recently been proposed to be performed by a proteinaceous translocon within the PV membrane, an ATP-powered complex containing heat shock protein 101, a novel protein PTEX150 and a known parasite protein identified as exported protein 2 (EXP2) that potentially works as the common portal through which most or all exported proteins must pass [108]. Moreover Plasmepsin V was recently shown to be the protease responsible for cleavage of the PEXEL motif of proteins to be exported, thereby allowing their traversal of the PV and trafficking to the RBC surface [109,110]. Following this export via this translocon at the PV membrane, exported proteins have to reach different destinations in the host RBC, such as the cytoplasm or the plasma membrane. Because RBCs have no secretory system, the parasite builds its own to allow its proteins to reach the host cell plasma membrane. Maurer's cleft is a central structural component of this “extracellular” protein export system [111]. These stacks of flattened lamellae of long slender

membranes with a translucent lumen were identified more than a century ago and are located below the erythrocyte plasma membrane [112,113]. Several parasite proteins are synthesized in the parasite's ER and then transferred to the cleft [114,115]. It is still not completely clear whether the Maurer's cleft is part of a continuous network that connects the PV to the erythrocyte cell surface like some imaging reconstructions of thin sections seem to suggest [116], or if the cleft is a well-defined structure continuously supplied with vesicles budding from the membrane lining the PV. Subsequently, vesicles bud out from the cleft and migrate towards the erythrocyte cell surface, with secretion of their contents into the medium and incorporation of some proteins in the erythrocyte plasma membrane [74].

The very strong remodelling of the host RBC eventually leads to its distortion, with positively charged knobby protrusions. Using atomic force microscopy, the knob was shown to consist of two subunits that might be central to the phenomenon of cyto-adherence in *P. falciparum* malaria [117]. Indeed, in *P. falciparum* infections, schizonts are known to barely circulate [118]. Instead, they are sequestered in different organs by adhering to the endothelial cells of the vessels. Knobs are created by the deposition of parasite proteins, such as knob-associated histidine-rich protein (KAHRP) and the adhesion protein *P. falciparum* erythrocyte membrane 1 (PfEMP1), which are inserted in the RBC membrane.

PfEMP1 is restricted to *P. falciparum*, and undergoes clonal antigenic variation switching, changing its antigen type at high frequencies during intra-erythrocytic cycles [119,120]. PfEMP1 belongs to a large polymorphic gene family called *var*, in which each individual gene encodes a different form of the protein, and only one is expressed at a time through a mutually exclusive mechanism. It comprises three regions: the cytoplasmatic or acidic terminal segment (ATS) that is anchored to the knobs; the transmembrane regions that are inside the RBC membrane; and the

ectodomain or N-terminal segment followed by the DBL domains and the Cys-rich interdomain regions (CIDR) (reviewed in [74]) that interact with endothelial cell receptors, leading to sequestration and thus preventing destruction of infected RBC (iRBC) in the spleen [121]. PfEMP1 is highly related to virulence as it is believed that the adherence it promotes triggers much of the associated pathology, including cerebral malaria end preganancy-associated malaria (reviewed in [122]).

Following this period (whose length varies between different *Plasmodium* species) where *Plasmodium* replicates with the consumption of the RBC cytoplasm, parasites leave the RBC by a process called egress that happens very fast and must be tightly regulated. Several hypothetical models explain egress. Although these vary by disagreeing on whether the PV membrane or the RBC membrane disintegrates first, all the models accept that proteases play a critical role. Protease inhibitors have been shown to prevent *P. falciparum* iRBC rupture, and to promote accumulation of mature schizonts *in vitro* due to egress blocking [123], which was later attributed to prevention of the proteolytic effect of serine repeat antigen (SERA)-5 [124]. Further studies showed that different protease inhibitors have different effects on egress [125]. Still, the mechanism by which egress is regulated is only beginning to be understood. It has been recently reported that just prior to egress essential serine protease PfSUB1 is discharged from *Plasmodium* organelles called exonemes, from the merozoite into the PV [126], where it mediates the proteolytic maturation of members of SERA family that have been previously implicated in egress [127]. Furthermore PfSUB1 has been shown to directly mediate primary proteolytic processing of MSP1, MSP6 and MSP7. PfSUB1 seems to prepare not only the merozoite for release from the erythrocyte but also to ensure that, once in circulation, merozoites get inside a new cell without delay [128], avoiding exposure to the host response.

Shifting to sexual stages. Differentiation and sexual commitment happen prior to schizogeny during asexual replication cycles inside RBCs. All siblings of a schizont are either asexual, female gametocytes or male gametocytes [129], but the mechanism that determines which of these possibilities occurs remains unknown. Translational repression and mRNA turnover have been shown to be key players in determining stage-specific gene expression in *Plasmodium*. More specifically, development of zygote inhibited RNA helicase (DOZI) was identified in the female gametocyte and shown to have a central role in the silencing and maintenance of steady-state levels of a population of gametocyte-specific transcripts, allowing the coordinated production of essential proteins for the further development and establishment of infection inside the mosquito [130].

Inside the mosquito. Mature gametocytes in the blood can later be engorged during a mosquito blood meal. The abrupt environmental change inside the mosquito triggers gametocytes to round up and emerge from the RBC within minutes [131]. The presence of xanthurenic acid allows the male gametocyte to transform into eight motile microgametes after three rounds of exceedingly fast genome replication followed by nuclear division and axoneme assembly, and the female emerges from the erythrocyte as a roundshaped non-motile gamete [132]. Exflagelation of the male gametocyte and the vibratory movements in waves of its microgametes allow it to penetrate into the female gamete, and fertilization to occur [133]. The resulting zygote will be the only parasite survivor in the aggressive environment of the mosquito gut, and further develops into a tetraploid [134] motile ookinete that is the only invasive form of the whole cycle that is not originated by replication. There is a great loss of ookinetes during traversal of the midgut epithelial cells to reach the basal lamina, due to host protective mechanisms [135]. Once in the basal lamina, ookinetes become sessile and, after meiosis [136], transform into oocysts that are the only extracellular developmental stage

of the whole cycle. Oocysts make use of their capsule to recruit nutrients from the hemolymph [137] to grow, 50 to 60 μm in diameter, and originate sporozoites. CSP, the protein that will cover all of sporozoites, starts to be expressed and accumulate in the oocyst plasma membrane even prior to sporozoite formation [138]. With the retraction on the oocyst plasma membrane, several lobes called sporoblasts appear in this form [139]. CSP is essential for this formation [140], and also seems to be essential for the organization of the microtubule organizing centres (MTOCs) [138] that will later lead to the formation of the apical complex and nuclei positioning in the daughter sporozoites.

Sporozoite release into the hemolymph occurs asynchronously [141] and was shown to be dependent on proteinase activity, including that of egress cysteine protease 1 (ECP1) [142]. Once released in the hemocoel, sporozoites can be spread in the whole mosquito body but only recognize specific host receptors in the basal lamina of the salivary glands [139]. Invasion occurs only in this organ and several parasite ligands, like CSP [143], TRAP [144] or MAEBL [145], have been identified as being important for recognition and invasion. After attaching, sporozoites breach the basal lamina and invade through the basal membrane of salivary secretory acinar cells with the brief formation of a vacuole that will allow them to emerge from the apical side of these same cells into the salivary gland duct [146].

Sporozoites are now ready to infect a new mammalian host when the infected mosquito takes another blood meal.

Malaria outcome…

Malaria transmission and naturally acquired immunity

Measuring malaria endemicity or *Plasmodium* prevalence in a geographical area has been the subject of an active debate for decades. Surveys of

splenomegaly across a population [147], examination of peripheral blood for asexual malaria parasites [148], stability/instability of transmission, entomological inoculation rates (EIR) [149] or haemoglobin measurements [150] were, and are, some of the metrics to establish classes of endemicity in which a given population should fall. Considering Africa alone, the existing endemic populations show rates of transmission that can differ in intensity by 100-fold.

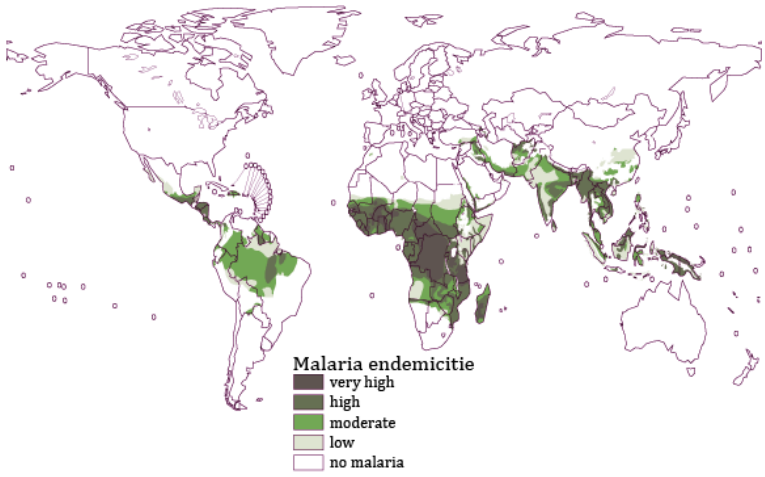

Fig.I4. **Global distribution of malaria transmission risk.** Adapdted from WHO World Malaria Report 2005.

Clinical presentations of *P. falciparum* malaria vary according to different transmission intensities, but the biological interactions promoting these different outcomes are not easily understood. Studies across fifty years of field research in areas with different rates of transmission, in several communities with different access to health systems or treatment, and with variations in the prevalence of infection occurring from year to year in a given place, allow all sorts of interpretations concerning how mortality and morbidity vary with transmissions rates. There is, however, a consensus in

accepting that the mean age of severe malaria disease decreases as *P. falciparum* transmission increases. The frequency of cerebral malaria declines with increasing transmission rates while anaemia takes over the clinical burden (reviewed in [151]). It is generally accepted that in low to moderate transmission settings, the incidence of severe disease grows after the first year of age, while in high transmission areas the peak in severe disease happens between the fifth and the seventh month of age, after which it declines significantly before the first birthday (reviewed [152]). Common to all settings is the fact that for the first 3 months of age the incidence of severe disease is very low, most likely due to the presence of maternal antibodies [153]. In addition, the much lower risk of severe disease after 5 years of age indicates that some degree of immunity is acquired early in life. However, under very low transmission regions the risk of clinical malaria is extended until adulthood [154].

An extensive study in an area with decreasing parasite prevalence over 16 years showed that although transmissions decreased significantly in the first ten years, there were no major alterations in clinical cases reported. Only later, when parasite prevalence fell below a certain threshold, could a drop in hospital admissions be observed. At the same time, as parasite prevalence dropped, the mean age of slide-positive children increased [155]. Moreover in cross-sectional studies with increasing malaria transmission, there is an initial increase in the rate of hospital admissions with malaria, but thereafter, the risk of hospitalization rises either more slowly or plateaus at intermediate ranges of transmission intensity and may decrease slightly in areas of very high transmission [156].

Very strong evidence that protection against malaria increases with age more than with any other factors comes from a study performed in Mali where it was observed that older children treated with chloroquine were better able to clear chloroquine-resistant *P. falciparum* parasites than

younger children treated in a similar way [157], again pointing towards an effective acquired immune response.

However, although in endemic settings older children and adults are resistant to severe morbidity and death, they are still susceptible to infection [158], showing that only a certain level of immunity can be developed against malaria. This natural immunity is acquired at the cost of very high early mortality and is still defective, as multiple infections are required before clinical protection is achieved, and persistent infection is typical. Indeed, back in 1900, Robert Koch compared areas of different endemicities and deduced that there was the need for heavy and continued exposure to the parasite in order to acquire protection against malaria. Later, in 1920, the essential features of naturally acquired immunity against *Plasmodium* were described: it was accepted that natural immunity was (i) effective in adults after uninterrupted lifelong heavy exposure, (ii) lost upon cessation of exposure, (iii) species specific, (iv) somewhat stage specific, and (v) acquired at a rate which was dependent upon the degree of exposure (reviewed in [159]).

In spite of these premises, very little is known about the mechanisms through which immunity against malaria is acquired. Early studies with humans, showed that antibodies can protect against malaria infection [160], and several antigens have later been shown to be associated with malaria protection. Antibodies against MSP1 [161], MSP2 [162] or MSP3 [163] were found significantly elevated in the sera of protected individuals in different endemic areas and are thought to correlate with protection. These associations vary between studies, and antigens encountered until now show considerable polymorphisms through the existence of alternative allelic forms [164] and through antigenic variation [165], limiting their use as possible targets for vaccination and treatment. Also, the antibody response to the most common merozoite antigens is believed to be short-lived [166],

peaking one week after the malaria episode and rapidly decaying to very low levels within 6 to 8 weeks. The reason for such a short half-life is still not understood. It might be that the catabolic half-life of these antibodies is just shorter, but other hypothesis have been raised such as the predilection towards IgG3 which is known to be short lived [167], or the poor development of memory or long-lived plasma cells [168]. Independent of the mechanism behind it, this short half-life of anti-malaria antibodies continues to create problems when planning an intervention strategy toward an effective vaccine against malaria.

Liver stage naturally acquired immunity is not believed to be strong enough or acquired fast enough to provide any kind of protection in endemic populations. Still, it cannot be said that natural immunity against *Plasmodium* pre-erythrocytic stage is not involved in the final outcome observed. Indeed, infection of both humans and mice with *Plasmodium* sporozoites followed by chloroquine treatment that abrogates the establishment of blood stages protects individuals from subsequent infections [169,170]. It is true, however, that early studies performed in humans, bypassing the hepatic phase of the infection through direct blood stage infection, showed that immunity could be maintained (reviewed in [162]). However, vaccine development efforts have invested a significant effort in pre-erythrocytic immunization and proven efficient in rendering protection for variable periods of time, probably because of the very high numbers of attenuated sporozoites used [171], which are very different from the very low numbers of sporozoites that mosquitoes inject during a blood meal [172]. Both attenuated forms of the parasite [173] and live sporozoites [170] can completely protect humans, making them resistant to infection. However, so far the most advanced vaccine candidate against *Plasmodium falciparum* is RTS,S. It is a recombinant, yeast-expressed subunit vaccine using hepatitis B virus

surface antigens carrying epitopes from *P. falciparum* CSP [174] the major coat protein of sporozoites.

In areas with very high EIRs, as children get older malaria attacks become less frequent after an initial peak at young age, and parasite levels between manifestations steadily decrease. Although the child seems to be acquiring immunity, they remain parasitized, often with higher parasitaemias than other children at greater risk of clinical disease from areas with lower EIRs [175]. This protection against clinical disease is the product of acquired immunity that is able to control parasitaemia but does not fully abrogate infection, producing only non-sterilizing immunity [176]. Several reports of *Plasmodium* superinfection describe single individuals hosting more than one *Plasmodium* species, or different genotypes of the same *Plasmodium* species infecting RBCs [177-179]. However, these observations have been much more frequent among asymptomatic carriers than in clinical cases [180], and have been shown to depend on the age of individuals in a population [175,181-183].

Premunition or concomitant immunity is the protection against infections and clinical disease that associates with persistence of multiple infections, providing protection against new infections by maintaining a low-grade and generally asymptomatic parasitaemia and high levels of antibodies (reviewed in [159,184]). A better understanding of mechanisms behind premunition is clearly central to the comprehension of naturally acquired immunity to malaria. Periodic blood-stage infection presumably serves to boost a pre-existing immune response and maintain high frequencies of effector cells in areas of high transmission. Exposure to a greater variety or antigens of families with associated variance increases the repertoire that each individual recognises [185].

Antigenic variation creates distinct waves of parasitemia that must be chased by different antibody responses, on the one hand promoting long

infections that might endanger the host, while on the other hand allowing eventual acquisition of disease-controlling immunity. Effective antiparasitic immunity is, if ever, achieved only after very many and frequent infections [149,186].

So, the doubt remains, whether reducing the risk of *Plasmodium* infection will always lead to a decrease in the threat of severe malaria throughout life. This is a concern that was raised 50 years ago, when wondering if altering the natural risk of exposure to parasite, by reducing vector or transmission itself, would change the epidemiology of severe disease [187]. Knowing that increasing exposure to *Plasmodium* parasites is reflected in increasingly rapid acquisition of immune responses that limits life-threatening effects of malaria, the full understanding of the transmission/immunity associations is of major importance in defining malaria control interventions.

Aims

Plasmodium passage through the skin followed by infection of liver hepatocytes and, later, of blood erythrocytes, are natural and sequential steps of *Plasmodium* life cycle in the mammalian host and should not be seen as independent entities. The sophistication and complexity of *Plasmodium* life cycle are evidence for co-evolution with man, and are reflected in the complicated nature of relationships between transmission rates, immunity and disease severity in endemic areas. Importantly, liver and blood stages of *Plasmodium* infection may frequently occur simultaneously in the same individual where transmissions rates allow it.

Indeed, after infecting the hepatocyte for approximately a week, *P. falciparum* can infect RBCs for weeks or even months after that [188]. Thus, a new infection initiated by a mosquito bite may occur while the parasites from a previous one are still replicating inside erythrocytes. Very little is known about the interactions between the two different stages of a malaria

infection. So far it has been shown that malaria blood-stage can be immunosuppressive [189], but it is clear that very close interactions are established between parasite and host throughout the parasite's life cycle.

The objective of the work presented here arises from intending to clarify effects of one stage on another in individuals dually infected with blood and posterior liver stage malaria, and try to understand how re-infection fits what is known so far regarding different patterns of infection in different EIR settings.

To access *Plasmodium* blood stage/liver stage interactions new tools were used to outwit past limitations, we have made use of wild-type *Plasmodium* parasites to start blood stage infections and of *gfp*-expressing or luciferase-expressing *Plasmodium* parasites to initiate liver stage infections. Using transgenic parasites we were able to distinguish the two infections circumventing the lack of specific liver stage markers. Because the GFP or luciferase genes are under the control of a *Plasmodium* housekeeping gene promoter, their expression correlates with *Plasmodium* liver load.

The study of the temporal coincidence of *Plasmodium* blood and liver stages in a single host at a given time was mostly performed in rodent models of infection to answer 4 major questions:

What would be the impact of an ongoing blood stage infection on the establishment of a secondary sporozoite infection in the liver?

By what molecular mechanisms do any interactive effects between blood and liver stages occur?

What, if any are the consequences of such interaction for the re-infected individual?

How such interactions adjust to established relations between patterns of infection and transmission rates in different endemic settings?

Materials and Methods

Mice. C57BL/6, BALB/c, Balb-SCID as well as mice deficient in RagII, IL-10, caspase 3, MyD88 or Kit W-sh/W-sh deficient were bred in the specific pathogen-free facilities of the Instituto de Gulbenkian de Ciência (Oeiras, Portugal). RAGII/γ_c deficient mice were kindly provided by James Di Santo (Cytokines and Lymphoid Development unit, Institut Pasteur, Paris, France). NOS2- (B6.129P2-Nos2tm1Lau/J), TCRdelta- (B6.129P2-Tcrdtm1Mom/J), and C5a- (B10.D2-Hc0.H2d.H2-T18c/oSnJ) deficient mice were purchased at The Jackson Laboratory along with their respective wild type littermates. All mice were housed in the Instituto de Medicina Molecular (IMM) facilities and the IMM Animal Care Committee approved all protocols. IFN-γ deficient mice were kindly provided by Rui Appelberg (Microbiology and Immunology of Infection laboratory, Instituto de Biologia Molecular e Celular-IBMC, Porto, Portugal). Experiments with IFN-γ deficient mice were performed at IBMC, and IBMC Animal Care Committee approved all protocols. All transgenic mice were genotyped by tail genomic DNA PCR to confirm their respective mutations.

***Plasmodium* blood infection.** Primary blood stage infection of mice was achieved by 30 minutes exposure of mice to 15 *Anopheles* mosquitoes infected with *P. berghei* ANKA (parasite line GFPcon259cl2), or by intra-peritoneal inoculation of the designated quantity of red blood cells infected with *P. berghei* ANKA (1.49L), *P. berghei* NK65, *P. yoelii* 17X NL or *P. chabaudi chabaudi* AS. Peripheral blood parasitaemia was determined by Giemsa staining followed by microscopic counting of iRBCs and results are expressed as percentage of RBCs. On Fig. 1 C parasitemia was verified by real time *in vivo* imaging using the *in vivo* IVIS® Lumina Imaging System [190] as described bellow. And on Fig. 1 E parasitemia was determined by flow cytometry, measuring red blood cells infected with *gfp*-expressing *P. berghei* ANKA. The results are expressed as percentage of infected red blood cells, as previously described [191].

***Plasmodium* liver infection.** Green fluorescent protein (*gfp*)-expressing *P. berghei* ANKA (parasite line GFPcon259cl2) or *gfp*-expressing *P. yoelii* sporozoites [191,192] were obtained by dissection of *Anopheles stephensi* infected mosquitoes bred in the insectarium of IMM. Mice were infected by intra-venous inoculation of the designated quantity of GFP sporozoites, or by 30 minutes exposure of mice to 15 *Anopheles* mosquitoes infected with *P. berghei* ANKA. Parasite liver load was quantified 40, 48 or 72h post-infection.

Real time *in vivo* imaging luminescent *Plasmodium*. Naïve mice (control) and blood stage infected (PbA in Fig. 1A and PbNK in Fig. 1B and Fig. 1C), were intra-peritoneally injected with 200µl of anaesthesia mixture (80 mg/kg Ketamine and 10 mg/kg Xylazine) diluted in PBS in order to allow each mouse exposure to 15 *Anopheles* mosquitoes infected with luciferase expressing *P. berghei* (parasite line 354cl4). After 30 minutes of mosquito bites, mice were shaved in the abdomen. Forty h post-infection for Fig. 1A and 1B and 6 days post-infection for Fig. 1C, D-luciferin dissolved in PBS (150 mg/kg; Caliper Life Sciences, USA) was injected subcutaneously in the neck. Animals were anesthetized again as described above for the whole duration of measurements (performed within 5 to 10 minutes after the injection of D-luciferin). Bioluminescence imaging was acquired with a 12.5 cm field of view (FOV), medium binning factor and an exposure time of 180 seconds. Luciferase activity in animals was visualized through imaging of whole bodies using the i*n vivo* IVIS® Lumina Imaging System [190].

qReal-Time PCR quantification of liver infection. Livers were collected and homogenized in denaturing solution (4 M guanidine thiocyanate; 25mM sodium citrate pH 7, 0.5% N-Lauroylsarcosineand, 0.7% β-Mercaptoethanol in DEPC-treated water). Total RNA was extracted using RNeasy Mini kit (Qiagen), and then reverse transcribed into cDNA using Transcriptor First

Strand cDNA Synthesis kit (Roche), according to the manufacturers' protocols. Infection load in the liver was determined as previously described by qRT-PCR using classic PbA 18S *rRNA* [193] specific primers or *gfp* specific primers (*gfp* expression correlates with PbA 18S *rRNA*, fig. S1). qRT-PCR reactions used Power SYBR Green PCR Master Mix (Applied Biosystems) and were performed according to the manufacturer's instructions on an ABI Prism 7000 system (Applied Biosystems). Relative amounts of PbA 18S *rRNA* and *gfp* mRNA were calculated against the Hypoxanthine Guanine Phosphoribosyltransferase (*hprt*) housekeeping gene, following a prime denaturation of 10 minutes at 95°C, then 50 cycles of 95°C for 15 seconds and 60°C for 1 minute. PbA 18S *rRNA*, *gfp* and *hprt* specific primer sequences were: 5'-CGG CTT AAT TTG ACT CAA CAC G-3' and 5'-TTA GCA TGC CAG AGT CTC GTT C-3' for PbA 18S *rRNA*, 5'- GTC AGT GGA GAG GGT GAA GG– 3' and 5' – ACT TCA GCA CGT GTC TTG TAG TTC – 3' for *gfp* and 5' – TGC TCGAGA TGT GAT GAA GG – 3´ and 5' – TCC CCT GTT GAC TGG TCA TT – 3' for mouse *hprt*. External standardization was performed using plasmids encoding the full-length genes cDNA cloned in TOPO TA (Invitrogen).

Chloroquine treatment. Mice infected 4 days previously with *P. berghei* NK65 and control mice received 0.8 mg of chloroquine (CQ) by intra-peritoneal injection for 1 or 2 days before re-infection, a protocol leading to decrease in peripheral blood parasitaemia until zero by day 2 of treatment.

Liver slice histopathology, morphometric analysis and immunofluorescence. Liver tissues were harvested from control or re-infected mice 40 h after sporozoite infection. Tissues were fixed in 4% paraformaldehyde for 15 minutes, washed three times in PBS and then sliced into 50 μm sections using a vibratome (VT1000S, Leica). Sections were later permeabilized and blocked overnight in 0.3% Triton X-100

(Calbiochem) and 1% Bovine Serum Albumin (Sigma) to avoid non-specific reactivity. Sections were then incubated overnight at 4°C in the same solution containing anti-GFP IgG Alexa flour 488 congugate antibody (Invitrogen), Alexa 594 phaloidin (Invitrogen) and 4',6-diamidino-2-phenylindole (DAPI, Sigma). After mounting 15 to 20 sections on slides, the areas of the sections were measured using a scope, the EEFs were counted using the Leica DM5000B Widefield Fluorescence Microscope, and the sizes of 20 randomly chosen EEFs of each mouse were measured using a Zeiss LSM 510 META Point Scanning Confocal Microscope. All images of immunofluorescence-stained sections were analysed using the ImageJ 1.42b software. Areas and numbers of EEF were normalized to the total area observed.

Cells. Huh7 cells, a human hepatoma cell line, were cultured in RPMI (Gibco/Invitrogen) medium supplemented with 10% fetal calf serum (FCS, Gibco/Invitrogen), 1% penicillin/streptomycin (pen/strep, Gibco/Invitrogen), 1% glutamine (Gibco/Invitrogen) at pH 7 and maintained at 37°C with 5% CO_2.

Isolation of murine primary hepatocytes. Mouse primary hepatocytes were isolated as previously described [194]. Briefly, cells were initially obtained by perfusion of mouse liver lobules with liver perfusion medium and liver digest medium (Gibco/Invitrogen) at 37°C using a peristaltic pump. Hepatocytes were then purified using a 1.12 g/ml, 1.08 g/ml and 1.06g/ml Percoll gradient. Cells were cultured in William´s E medium containing 4% FCS, 1% pen/strep in 24-well plates coated with 0.2% Gelatine in PBS. Cells were maintained in culture at 37°C and 5% CO_2.

Sporozoite infection and development in contact with infected blood. Mouse primary hepatocytes and Huh7 cells, a human hepatoma cell line, were cultured as described above in complete William's E or RPMI

(Gibco/Invitrogen) in transwell system plates (COSTAR/Corning). In the lower chamber, liver-derived cells were infected with 20,000 *P. berghei* ANKA sporozoites, and allowed to share medium with upper chambers containing serum (CTRL), non-infected blood (NI) or blood containing 6 x 10^5 *P. berghei* NK65 iRBCs (PbNK). After 36h of co-culture, hepatoma cells were collected and treated for FACS analysis and primary hepatocytes were fixed in 4% paraformaldehyde for 10 minutes, washed three times in PBS, and later permeabilized and blocked 1h in 0.3% Triton X-100 (Calbiochem) and 1% Bovine Serum Albumin (Sigma) to avoid non-specific reactivity. Coverslips were then incubated 1h at 4°C in the same solution containing anti-GFP IgG Alexa flour 488 congugate antibody (Invitrogen), Alexa 594 phaloidin (Invitrogen) and DAPI (Sigma). After mounting coverslips on slides, EEFs were counted using the Leica DM5000B Widefield Fluorescence Microscope, and the sizes of 20 randomly chosen EEFs of each coverslip were measured using a Zeiss LSM 510 META Point Scanning Confocal Microscope. All immunofluorescence-stained images were analysed using the ImageJ 1.42b software.

Fluorescence activated cell sorting (FACS) analysis of sporozoite infection. FACS analysis of sporozoite-infected Huh7 hepatoma cell cultures at 36h post-sporozoite addition was performed to determine the percentage of parasite-containing cells and parasite-GFP intensity within infected cells. Cell samples for FACS analysis were processed as previously described [195].

Transcription profiling. Total RNA from livers of naïve mice (control group), mice infected with 10^6 *P. berghei* NK65 iRBCs for 7 days (Blood stage group, BS), mice infected with $5x10^4$ *P. berghei* ANKA-GFP sporozoites for 40h (Liver stage group, LS), and mice infected with 10^6 *P. berghei* NK65 iRBCs for 7 days then re-infected with $5x10^4$ *P. berghei* ANKA-GFP sporozoites for 40h (Reinfection group, Reinf) was extracted using RNeasy

Mini kit (Qiagen), following the manufacturer's instructions. Three biological replicates were analysed for each group. RNA quality and quantity was assessed on a Bioanalyser nanochip (Agilent). Total RNA was reverse transcribed and end-labelled as cRNA using the GeneChip WT Amplified Double-Stranded cDNA Synthesis Kit and the GeneChip WT Terminal Labeling Kit as recommended by Affymetrix. Hybridisation to an Affymetrix Mouse Gene 1.0 ST Array was carried out at 45°C for 16h under rotation (60 rpm). Arrays were washed on an Affymetrix FS450 and scanned using an Affymetrix Genechip Scanner 3000 7G. Fluorescence intensities were background adjusted, quantile normalised and median polished into expression values using the robust multi-array averaging program RMA [196] in R/Bioconductor suite [197] (software package: affy [198]) To assess significance and differential expression (DE), each infected group was compared to the non-infected group, and out of 28815 main probesets represented on the array, 6273 transcript clusters were classified as significant (F-test, $p<0.05$) with 1704 being DE at a fold change of 2 (software packages: limma [199] and gplots). Each cluster separated from the non-hierarchical clustering was subjected to a Gene Ontology Biological Process enrichment analysis using a hypergeometric test (software package: GOstats [200]. Original data was submitted to Array Express and is accessible in the reviewer's user account: Username: Reviewer_E-TABM-839, and Password: 1257429875724.

Depletions using monoclonal antibodies. (**i**) IL-6. Mice infected with *P. berghei* NK65 and control mice received 1 mg of IL-6 specific monoclonal antibody (clone MP520F3, Rat IgG1) 3h, 3 days, and 5 days after inoculation with infected blood, a protocol leading to IL-6 depletion at the time of sporozoite infection, 7 days post- *P. berghei* NK65 infection.

(**ii**) IFNγ. Mice infected with *P. berghei* NK65 and control mice received 0.4 mg of IFNγ specific monoclonal antibody (clone R46A2, Rat IgG1) 1, 2 and 3 days, after inoculation with infected blood, a protocol leading IFNγ depletion at the time of sporozoite infection, 5 days post-*P. berghei* NK65 infection.

(**iii**) TNFα. Mice infected with *P. berghei* NK65 and control mice received 0.4 mg of TNF specific monoclonal antibody (clone XT3.11, Rat IgG1) 4 and 6 days after inoculation of infected blood, a protocol leading to TNFα depletion at the time of sporozoite infection, 5 days post-*P. berghei* NK65 infection.

Nω-Nitro-L-arginine methyl ester hydrochloride treatment. Mice infected with *P. berghei* NK65 and control mice received 50mg/kg of Nω-Nitro-L-arginine methyl ester hydrochloride (L-NAME, Sigma) 3, 4, 5 and 6 days after inoculation of infected blood, a protocol leading to NOS inhibition at the time of sporozoite infection, 7 days post- *P. berghei* NK65 infection.

S-methyl-isothiourea treatment. Mice infected with *P. berghei* NK65 and control mice received 100 μg of S-methyl-isothiourea (SMT, Sigma) 3, 4, 5 and 6 days after inoculation of infected blood, a protocol leading to iNOS inhibition at the time of sporozoite infection, 7 days post- *P. berghei* NK65 infection.

C3a receptor antagonist treatment. C5a deficient (B10.D2-Hc0.H2d.H2-T18c/oSnJ) naïve or *P. berghei* NK65 infected mice received 0.5 mg of C3a receptor antagonist (SB290157, Calbiochem) 4h before sporozoite re-infection, 5 days post-*P. berghei* NK65 infection.

Kupffer cell depletion using clodronate liposomes [201,202]**.** Kupffer cells were eliminated from naïve and *P. berghei* NK65 infected mice by injection of 200 μl clodronate liposomes (liposome-encapsulated dichloromethylene

diphos-phonate; clodLip) daily, from day one after *P. berghei* NK65 infection until the day of sporozoite infection (4 days post-blood stage infection). As controls, the same volume of PBS containing liposomes was injected into naïve or *P. berghei* NK65 infected mice. Clodronate was a gift from Roche Diagnostics GmbH (Mannheim, Germany). It was encapsulated into liposomes, as previously described [203]. Kupffer cell depletion was verified by immunofluorescence microscopy. Livers were collected and 50 μm sections obtained and fixed, as described above. Sections were then incubated overnight at 4°C in a solution containing rat anti-mouse pan tissue fixed macrophages antibody (Fitzgerald) and Alexa 660 phaloidin (Invitrogen). After washing twice with PBS, sections were incubated for 6h with secondary Alexa fluor 595 donkey anti-rat IgG (Invitrogen) and DAPI (Sigma). After mounting sections on slides, sections were imaged on a Zeiss LSM 510 META Point Scanning Confocal Microscope. Images of immunofluorescence-stained sections were analysed using the ImageJ 1.42b software.

Splenectomy. Intra-peritoneal injection of 250 μl of anaesthesia mixture (80 mg/kg Ketamine and 10 mg/kg Xylazine) was administered to mice 10 to 15 min before surgery. After observing the animals for response to anaesthesia, the animals were laid on their right side; and the fur removed with a razor. A 1.5 to 2 cm long skin incision was made in the left hypochondrium, the connective tissue under the skin was loosened and another incision in the peritoneal wall was made. Gently the spleen was pulled onto the exterior surface of the peritoneum. The artery, attached to the hilum of the spleen, close to the stomach was tied off with a single knot using 3-0 plain CATGUT suture. The efferent venule attached at the other end of the spleen was tied off similarly by a single knot using 3-0 plain CATGUT. Cutting away the mesentery and connective tissue, the spleen was removed. Peritoneal wall and underlying muscles were closed with plain

CATGUT (3-0) and the skin incisions closed with wound clips. Mice with accessorial spleen were excluded from the study. The control group underwent a sham surgery and they were maintained in the same conditions.

Liver hepcidin (*hamp1*) quantification. After RNA extraction and cDNA conversion as described above, hepcidin (*hamp1*) mRNA expression in the liver was determined by TaqMan qRT-PCR using TaqMan Gene Expression Master Mix (Applied Biosystems) and Applied Biosystems inventoried gene expression assays for *hamp1* (ABI TaqMan Gene Expression Assay probe/primer set Mm00519025_m1) and *gapdh* (Glyceraldehyde-3-phosphate dehydrogenase) (ABI TaqMan Gene Expression Assay probe/primer set Mm99999915_g1), according to the manufacturer's instructions. qRT-PCR was carried out using an ABI Prism 7500 FAST system (Applied Biosystems). Changes in *hepcidin* mRNA expression between control and re-infected mouse livers were calculated using the 2^{-DDCt} method with *gapdh* as the endogenous control gene.

Ferritin staining. Livers were collected and 50 μm sections were obtained and fixed as described above. Sections were then incubated overnight at 4°C in a solution containing rabbit anti-mouse heavy and light ferritin chain antibody (a kind gift by Paolo Arosio, Faculty of Medicine, Brescia, Italy) and Alexa 660 phaloidin (Invitrogen). After washing twice with PBS, sections were incubated for 6h with secondary Alexa fluor 595 donkey anti-rat IgG (Invitrogen) and DAPI (Sigma). Sections were imaged on a Zeiss LSM 510 META Point Scanning Confocal Microscope. Images of immunofluorescence-stained sections were analysed using the ImageJ 1.42b software.

Total non-heme iron quantification. Total non-heme iron was measured as described previously [204], in brief after drying samples (spleens and primary hepatocytes) for 48h at 45°C, tissues were weighed, and digested

for 48h in 10% trichloroacetic acid/10% HCl at 65°C. Two hundred microliters of the extract were then added to 1 ml of chromogen solution (0.01% bathophenanthroline-disulfonic acid, 0.1% thioglycolic acid, 2.5 M sodium acetate) and after 15 minutes of incubation, absorbance was measured at 535 nm. A standard curve performed for known iron concentrations between 10 and 500 μg/ml revealed a linearity of response with a slope of ~1. Samples were diluted appropriately to fall within the linear range. Values were expressed as % of control, in micrograms of iron per gram of dry weight.

HAMP adenovirus *in vivo* infection. Mice were infected with adenoviral $5x10^{11}$ pu of pAd.CMV.GFP (control) or pAd.CMV.Hamp.ires.GFP.Wpre (HAMP.adV) kindly provided by Stefano Rivella for (Weill Cornell Medical College, USA) 48h prior to sporozoite infection, hepcidin expression was 2 fold upregulated by the Hamp.adv compared to uninfected and GFP.adv control groups. All mice were then infected with $2x10^4$ *P. berghei* ANKA (1.49L) sporozoites, and 40h later livers were collected and liver infection was determined by expression of PbA 18S *rRNA*.

Iron treatments. (**i**) *In vitro:* Ferric Ammonium Citrate (FAC, Sigma) bathophenanthrolinedisulfonate (BPS, Acros) and Desferrioxamine (DFO, Sigma) solutions were prepared in at the designated concentrations. Huh7 cells were incubated with different concentrations of FAC, BPS or DFO, using water as control for FAC and PBS as control for BPS and DFO respectively, 24h prior to sporozoite infection and for 36h post-infection, after which cells were collected for FACS analysis.

(**ii**) *In vivo:* DFO (Sigma) solution was prepared in PBS at the designated concentration. Mice were inoculated intra-peritonealy with 250 mg/Kg of DFO using PBS as control 24h prior to sporozoite infection.

Tunel detection of apoptosis. Liver tissues were harvested from wild type and caspase 3-deficient mice infected with *P. berghei* NK65 for 8 days along with non-infected wild type mice. Tissues were frozen in OCT freezing medium and then sliced into 16 μm sections using a cryostat. Analysis of DNA fragmentation by transferase-mediated dUTP nick-end labelling (TUNEL) was performed using the In Situ Cell Death Detection kit, POD and DAB Substrate kits (Roche, USA) following the manufacturer's instructions, and later stained with DAPI (Sigma) for general nuclei count. Sections were imaged on a Zeiss LSM 510 META Point Scanning Confocal Microscope. Quantification of positive cells was determined counting a total of 1000 cells/section and calculating the proportion of stained nuclei. Images of immunofluorescence-stained sections were analysed using the ImageJ 1.42b software.

Cardiac puncture, blood collection and serum production. Mice were maintained under general inhalant anesthesia, a needle was inserted through intact skin and between ribs and up to 1ml of blood was quickly withdrawn from heart using a 1ml plastic syringe with 25ga. needle. Mice were euthanized by cervical dislocation. The blood was allowed to cloth for a while, after what the cloth is removed and the remaining liquid centrifuged for 20min, 3000rpms. Supernatant was collected and injected to mice intra-venously.

Cholesterol measurements. (**i**) Serum. Total cholesterol, HDL- and LDL-cholesterol in the serum were biochemically determined by DNAtech (INETI, Portugal).

(**ii**) Liver. The amounts of cholesterol in a sample of liver collected after perfusion with PBS were measured using the Amplex Red cholesterol assay kit (Invitrogen), according to the manufacturer's instructions. Briefly, cholesterol is oxidised by cholesterol oxidase to yield hydrogen peroxide

and ketones. The hydrogen peroxide reacts with 10-acetyl-3, 7-dihydroxyphenoxazine (Amplex Red reagent) to produce highly fluorescent resorufin, which is measured by excitation at 550 nm and emission detection at 590 nm. A standard curve was performed with serial dilutions with a linearity of response with a slope of ~1. Samples were diluted appropriately to fall within the linear range. Values were expressed as % of control.

***Toxoplasma* infection.** *Toxoplasma gondii* tachyzoites (Toxo-GFP/LacZ kindly provided by Markus Meissner, Departament of Parasitology, University Hospital Heidelberg, Germany) were grown in VERO cells and maintained in Dulbecco's modified Eagle's medium (DMEM) supplemented with 10% fetal calf serum, 1% glutamine and 20 µg/ml gentamicin. 10^4 freshly released tachizoites were intra-peritonealy injected into mice 4 days prior to *Plasmodium* sporozoite challenge.

Model description. A stochastic, individual-based model was used to follow a cohort of *N* individuals for up to 20 years in a low, medium and high transmission setting (with according annual EIR of 2, 20 and 200, respectively). At each time point t_i the probability of an individual becoming infected, *P*, is given as the product of the probability of being bitten by an infected mosquito, p_{bite} (=1-1/EIR), times the probability of this bite leading to successful blood stage infection which itself is dependent on the immune history of the host, p_{imm}, and the parasite density of a possible ongoing infection, p_{dens}. That is, $P(\text{infection}) = P(p_{bite} \cap p_{imm} \cap p_{dens})$. We assumed that the average parasite density per infection decreases with age [175,181,205] given as $\pi_{age} = \pi_{\max}\left(1 + k\exp(-age)\right)$, and that mean parasitaemia level also decreases over the course of infection [206]; for simplicity we assumed this to be linear although the actual functional form does not change the results presented here. We further assumed that there exists a threshold parasite

density, p_{crit}, above which the host is mostly protected from super-infections. This threshold density then defines the probability of a successful inoculation as a function of infection length and is given as $p_{dens} = \prod_i \left(1 + \exp(\tau_i - \Delta t_i)^{\beta}\right)^{-1}$, where i is the number of concurrent infections, Δt_i is the time since infection i, and $\tau_i = T_i\left(1 - \pi_{crit}/\pi_{\max}\right)$ is the time when the probability of a new blood stage infection is approximately half; $1/T_i$ is the clearance rate of infection i. For reasons of simplicity and because we are here more concerned with the inhibitory effect on new liver-stage infections, we do not take into account the full complexity of super-infections (see e.g. [178]) and assume infections and their respective clearance rates to be independent. A graphical representation of the relationship between parasitaemia and probability of infection is given in Supplementary Information. Finally we assumed acquired immunity to be driven by exposure, or rather the number of life-time blood stage infections. We chose this to be non-linear to take into account antigenic diversity of and immunity against the various life-stages of the parasite; again, the exact functional form does not have a significant effect on the results presented. The probability of an infection not being blocked by immunity is then given as $p_{imm} = \prod_{i=1..n} \sqrt{\frac{D-i}{D}}$, where n is the life-time number of blood stage infections and D can be understood as a measure of antigenic diversity and which defines the rate of acquired protection with infection history (see SI). The parameter values used for the simulations are as follows: N=500, p_0=5000, k=2, b=2, p_{crit}=3000, T~normal(100) and D=500. Note, our results are robust to a wide range of parameter values; however, we do not attempt to fit the outcome to actual epidemiological data but here are more concerned with the qualitative behaviour of the model.

Statistical analysis. All experiments were performed with a minimum number of 5 mice per group, and all shown results are one representative of at least three independent experiments, or the cumulative result of at least three independent experiments. In all bar graphs, bars represent average and error bars represent standard deviation. Significance is indicated by * and its value is identified in every graph legend. For samples in which $n > 5$, statistical analysis was performed using unpaired Student t or variance (ANOVA) parametric tests. Normal distributions were confirmed using the Kolmogorov-Smirnov test.

Results

Blood stage *Plasmodium* parasites suppress co-infection in the liver

Silvia Portugal[1,4], Céline Carret[1], Mario Recker[2], Andrew E. Armitage[3], Lígia A. Gonçalves[4], Sabrina Epiphanio[1§], Chris I. Newbold[3], Hal Drakesmith[3] and Maria M. Mota[1,4]

[1]Instituto de Medicina Molecular, Faculdade de Medicina da Universidade de Lisboa, 1649-028 Lisboa, Portugal

[2]Department of Zoology, University of Oxford, Oxford OX1 3PS, UK

[3]Weatherall Institute of Molecular Medicine, John Radcliffe Hospital, University of Oxford, Oxford OX3 9DS, UK

[4]Instituto Gulbenkian de Ciência, 2780-156 Oeiras, Portugal

§ current address: Departamento de Ciências Biológicas, Universidade Federal de São Paulo, Diadema, Brasil.

Correspondence to M.M.M. (mmota@fm.ul.pt)

In regions of high malaria transmission, infected individuals are constantly exposed to potential re-infection. Mosquito bites transmit liver-tropic sporozoites into subjects who already have blood-stage parasitaemia. How these two stages of the *Plasmodium* life-cycle interact within their host is unknown. Here, we show that ongoing blood stage infections in a rodent model impair the growth of subsequently inoculated sporozoites. Secondary infections are arrested in liver hepatocytes and fail to compete for colonization of red blood cells. This protection of the erythrocyte niche only occurs beyond a certain threshold of blood parasite density. Parasitized erythrocytes induce expression of the host iron regulatory hormone hepcidin, which, by diverting iron away from hepatocytes, limits *Plasmodium* growth in the liver. We show that this effect of parasite threshold-density dependent growth inhibition could explain the epidemiological patterns of age-related risk and complexity of infections in young children.

Plasmodium sporozoites, initially deposited in the skin by *Anopheles* female mosquitoes, subsequently travel to the liver where they infect hepatocytes. Once there, each sporozoite replicates into thousands of merozoites, which then infect red blood cells (RBCs) and cause malaria associated pathology [58,207]. In human malaria, apart from hypnozoites, hepatocytes remain infected for one to two weeks [58], whereas infection of RBCs continues for months [188]. We asked what the impact would be of an ongoing blood stage infection on a subsequent *Plasmodium* sporozoite liver infection. We infected mice via mosquito bite with a wild-type *P. berghei* parasite and as soon as parasites appeared in the bloodstream (peripheral blood parasitemia 0.99±0.03%), we challenged the mice by mosquito bite of a luciferase-expressing *P. berghei.* Liver stage development was monitored relative to controls by light emission from the liver 40h later and found to be dramatically inhibited (Fig. 1A). Identical results were obtained if mice were first infected with blood stage parasites and later challenged via mosquito bite with luciferase expressing *P. berghei* (Fig. 1B) and most strikingly, luciferase-labelled parasites never reached detectable levels in the blood (Fig. 1C). To quantify this effect we challenged infected mice with sporozoites constitutively expressing *gfp* and used qRT-PCR of *gfp* mRNA as readout (fig. S1). A potent and significant reduction in *P. berghei* liver load was confirmed in mice with an ongoing blood stage infection, when compared to naïve controls (Fig. 1D). Once again, no *gfp*-expressing parasites were ever found in blood (Fig. 1E). Mice carrying blood stage infections with *P. berghei* NK65, *P. berghei* ANKA, *P. chabaudi chabaudi* AS or *P. yoelii* 17X parasites and later challenged with *gfp*-expressing *P. berghei* ANKA sporozoites, all showed a very strong reduction in *Plasmodium* liver infection when compared with control mice ($P<0.01$; Fig. 1D). Likewise, *P. berghei* NK65 blood stage infection caused a strong reduction in liver

infection by *gfp*-expressing *P. yoelii* 17X sporozoites ($P<0.05$; Fig. 1F). This effect was thus neither species- nor strain-specific.

Besides, this decrease in liver parasite load was consistently observed from day 3 to day 15, regardless of differences in peripheral blood parasitaemia (1.24±0.24 – 15.53±3.80%; $P<0.05$; Fig. 1G). However, if an ongoing blood stage infection was treated with the antimalarial drug chloroquine then inhibition of liver stage development was abrogated (Fig. 1H).

To investigate in more detail the nature of the inhibition we examined thick liver sections from control and re-infected mice and observed that both the number and size of exoerythrocytic forms (EEFs) were decreased in the presence of blood stage parasites. (Fig. 2A-D). No EEFs were present 72hr after sporozoite infection in mice with a blood stage infection (fig. S2).

We thus conclude from these data that the inhibition of EEF development is independent of species, transient and results in very small EEFs that disappear and never give rise to blood stage infection. The data are consistent with a critical density of blood stage parasites inhibiting the development of the liver stage, resembling a quorum sensing mechanism described for bacteria [208], by which the blood stage is able to protect its niche from the threat of superinfection. What then is the mechanism by which this occurs?

We ruled out the involvement of a soluble factor secreted in the blood stage, since infection of both mouse primary hepatocytes and hepatoma cells by *P. berghei* sporozoites is not affected when co-cultured with iRBCs (fig. S3). In addition and contrary to a previous report [209], we found that sporozoite infection was similar in primary hepatocytes isolated either from blood-infected or naïve mice (fig. S3). We next examined the differences in liver stage transcription between naïve mice (NI), sporozoite infected mice (LS),

mice carrying a blood stage infection alone (BS) or after secondary sporozoite infection (Reinf) by genome wide microarray analysis. Analysis of these data showed first that immune-related genes were upregulated in BS or Reinf mice, and that genes associated with a defense response were upregulated in the latter (fig. S4 and table S1). We therefore hypothesized that impaired liver stage development could be caused by a blood stage initiated immune response. However, using either splenectomised mice, genetically deficient mice or depletion methods, we showed that the impairment of *Plasmodium* liver infection is independent of T or B cells; liver macrophages, NK or γδ T cells; IFN-γ, TNF-α, NOS, IL-10, IL-6, TLR/MyD88 signalling; the complement system or mastocytes (Fig. 3A and fig. S5). This set of experiments provided no support for a role of adaptive immunity or aspects of innate immunity in the phenotype observed.

Plasmodium blood stages increase apoptosis in hepatocytes [210] and our microarray data showed a robust pro-apoptotic stimulus in the livers of mice with an ongoing blood stage infection (highlighted in table S1). However, although a significantly reduced level of apoptosis was observed in *P. berghei* NK65 blood stage infected caspase-3 deficient mice (fig. S6), blood stage infection in these mice still impairs a secondary *P. berghei* ANKA liver infection ($P<0.05$; Fig. 3B). Thus, hepatocyte apoptosis does not explain the observed protection.

The fact that both the number and size of EEF are reduced in the presence of a blood infection (Fig. 2) suggested that some nutrient or growth factor might be limiting liver stage development. Our microarray data showed that *hamp*, the gene encoding the iron regulatory hormone hepcidin, is significantly overexpressed in mouse livers with ongoing blood stage infection (2.7-fold increase in Reinf, $P<0.05$, highlighted in table S1). To confirm this, we compared *hamp* expression levels in mice infected with

Plasmodium sporozoites and in re-infected mice. Mice with an ongoing blood stage infection show a 7-fold increase in *hamp* expression levels, when compared to controls ($P<0.05$; Fig. 3C), consistent with previous findings of increased hepcidin in human blood stage infection [211,212]. Hepcidin regulates iron homeostasis by triggering the degradation of the iron exporter protein ferroportin, which is strongly expressed by enterocytes and macrophages [213,214]. We found that increased *hamp* expression during blood stage infection re-distributes iron, promoting its sequestration inside macrophages in the liver (Fig. 3E) and in the spleen (Fig. 3F) and that should happen in enterocytes as well. In addition, the level of iron in hepatocytes is reduced (Fig. 3G). The increase in hepcidin is immediately reversed to normal levels after treatment of infected mice with chloroquine ($P<0.05$; Fig. 3D), which also allows the liver stage infection to grow (Fig. 1F).

Previous reports make a connection between iron availability and *Plasmodium* infection of both red blood cells [215] and hepatocytes.[216-218] In addition, a recently performed microarray analysis shows that, in *Plasmodium*-infected hepatoma cells, while the expression of the iron exporter protein ferroportin is significantly reduced (47.0±0.2% reduction, $P<0.0001$), that of divalent metal transporter 1 (DMT1) is significantly increased (2.0±0.2 fold increase, $P<0.0001$) [66]. This suggests that iron acquisition and retention might be essential for complete *Plasmodium* development inside its host cells. Reducing iron availability (using iron chelators bathophenanthrolinedisulfonate (BPS) and desferrioxamine (DFO)) in host cells led to a significant and dose-dependent reduction of *Plasmodium* EEF development (Fig. 3G, H and fig. S7) whereas iron supplementation (using Ferric Ammonium Citrate (FAC)) increased development (Fig. 3H and I and fig. S7). These effects can be reproduced in mice infected with *P. berghei* sporozoites (Fig. 3J). Most importantly,

hepcidin *per se* (introduced by the administration of *hamp*-expressing adenovirus to mice), prior to sporozoite infection, can on its own reduce significantly liver stage infection (Fig. 3K).

Altogether, our data shows that an ongoing blood stage infection leads to a rapid increase in liver hepcidin levels, which results in a redistribution of iron in infected mice. This limits iron availability necessary for *Plasmodium* EEF development/replication inside hepatocytes.

What are the possible implications of our findings for human malaria? Epidemiological studies from highly endemic areas consistently show that the incidence of infection first increases with age in young children before it declines presumably as a result of acquired immunity (e.g. [175,183]). At the same time, the complexity of infection, i.e. the average number of clones per infection, also increases as hosts get older [175,181-183]. A previous attempt to explain these observations relied on the biting preference of mosquitoes towards older individuals [219]. Here we propose an alternative solution depending only on a threshold-density dependent inhibitory effect reported in this work. We devised a simple agent-based model to simulate infection histories in a number of individuals which we followed over time whilst recording the average annual infection rates as well as the number of co-infecting clones (see Materials and Methods). According to epidemiological observations the model assumes that the average parasite density per infection decreases with age [175, 181, 205]. The probability of an infectious bite leading to a new infection then depends on the level of a current blood-stage infection as well as the host's infection history. Under these minimal assumptions the model correctly predicts an initial increase in infection rates, which subsequently declines as individuals acquire immune protection through repeated exposure (Fig. 4A and C). As a result of a higher risk of infection and reduced inhibitory effect in older individuals we also

observe an increase in the multiplicity of infection (Fig. 4B and D). We tested the model under various assumptions regarding the relationship between an ongoing blood-stage infection and the probability of superinfection and find that no other inhibitory effect (including acquired immunity) can explain the observed data (Fig. 4A and B). This means that threshold-density dependent inhibition of new liver-stage infections alone can account for the increase in infection risk and complexity of infections in young individuals. Crucially, however, our results show that this effect is strongly dependent on the transmission intensity and most prominently observed under moderate to high transmission settings (Fig. 4C and D). Our findings therefore provide an explanation for some of the differences in age-dependent risk of infection within the endemicity spectrum. A recent clinical trial of iron supplements to children under five years of age showed a statistically significant increase in the number of malaria infections in those receiving iron [220]. It may be that altered iron availability due to dietary factors could also modify the threshold-density dependent inhibitory effect modelled in Fig. 4.

The sophisticated lifecycle of *Plasmodium* has resulted from millions of years of parasite/host co-evolution and communication, having broad implications for evolution and human health. *Plasmodium* infection of RBCs, above a critical threshold, leads to an increase in the level of the host hormone hepcidin that, by re-distributing iron, protects the parasite niche (and thus the host) from the risk of superinfection. This phenomenon, which acts independently of and in addition to acquired immunity, explains many previous epidemiological observations and has important implications for future anti-malarial interventions.

Acknowledgments

We would like to thank Laurent Renia (Agency for Science, Technology and Research, Singapore) for helpful comments and reagents, as well as Rui Appelberg (Instituto de Biologia Molecular e Celular, Porto, Portugal), James Di Santo (Institut Pasteur, Paris, France) and Juan Rivera (National Institutes of Arthritis and Musculoskeletal and Skin Diseases, Bethesda, USA) for IFN-γ, RAG2/γ_c and Kit W-sh transgenic mice, Stefano Rivella (Weill Cornell Medical College, New York, USA) for *gfp* and *hamp.gfp*-expressing adenovirus, and Paolo Arosio, (Faculty of Medicine University of Brescia, Italy) for anti-mouse heavy and light ferritin chain antibody.

This work was supported by Fundação para a Ciência e Tecnologia (FCT, Portugal), European Science Foundation (EURYI to MMM), Howard Hughes Medical Institute and the Medical Research Council UK. H.D. is a Beit Memorial Fellow for Medical Research and an MRC New Investigator. S.P. and C.C. were supported by FCT fellowships (SFRH/BD/31523/2006 and SFRH/BPD/40965/2007 respectively). M.R. is supported by a Royal Society University Research Fellowship.

Fig. 1. Malaria blood-stage infection confers protection against a secondary *Plasmodium* liver infection. (**A**) *Plasmodium* liver load measured by radiance signal 40h post-infection by mosquito bite of 15 *Anopheles* mosquitoes infected with luciferase-expressing *P. berghei* sporozoites in the livers of naïve mice (control) and mice that had been infected 6 days previously by mosquito bite of 15 *Anopheles* mosquitoes infected with *P. berghei* ANKA (PbA), imaged in the IVIS® Lumina Imaging System, 5-10 minutes after injecting luciferin into mice. (**B**) *Plasmodium* liver load measured by radiance signal 40h post-infection by mosquito bite of 15 *Anopheles* mosquitoes infected with luciferase-expressing *P. berghei* sporozoites in the livers of naïve mice (control) and mice infected 5 days previously with 10^6 *P. berghei* NK65 iRBCs (PbNK), imaged in the IVIS® Lumina Imaging System, 5-10 minutes after injecting luciferin into mice. (**C**) *Plasmodium* load measured by radiance signal in the whole body of naïve mice (control) and mice infected 5 days previously with 10^6 *P. berghei* NK65 iRBCs (PbNK), 5 days post infection by mosquito bite of 15 *Anopheles* mosquitoes infected with luciferase-expressing *P. berghei* sporozoites, imaged in the IVIS® Lumina Imaging System, 5-10 minutes after injecting luciferin into mice. (**D**) *Plasmodium* liver load 40h post 5 x 10^4 *P. berghei* ANKA-GFP sporozoite injection into naïve mice (control), mice transfused 5 days previously with non-infected blood (NI) or mice infected 5 days previously with 10^6 *P. berghei* ANKA (PbA), *P. berghei* NK65 (PbNK), *P. chabaudi* AS (Pcc) or *P. yoelii* 17X (Py) iRBCs respectively. (**E**) Peripheral blood parasitaemia after injection of 5 x 10^4 *P. berghei* ANKA-GFP sporozoite into naïve mice (control) and mice infected 5 days previously with 10^6 *P. berghei* NK65 (PbNK), measured by FACS, counting only GFP positive RBCs. (**F**) *Plasmodium* liver load 40h post 5 x 10^4 *gfp*-expressing *P. yoelii* 17X sporozoite injection into naïve mice (control) or mice infected 5 days previously with 10^6 *P. berghei* NK65 (PbNK) iRBCs. (**G**) *Plasmodium* liver load (bars) 40h post 5 x 10^4 *P. berghei* ANKA-GFP sporozoite injection into naïve mice (control), and mice infected 2-14 days previously with 10^6 *P. berghei* NK65 iRBCs; gray line represents the peripheral blood parasitaemia at the time of re-infection by *Plasmodium* sporozoites. (**H**) *Plasmodium* liver load 40h post 5 x 10^4 *P. berghei* ANKA-GFP sporozoite injection into naïve mice (control), mice treated with chloroquine for 2 days before sporozoite injection (CQ control), mice infected 5 days previously with 10^6 *P. berghei* NK65 iRBCs (∅CQ PbNK), or mice infected 5 days previously with 10^6 *P. berghei* NK65 iRBCs and treated with chloroquine for 1 or 2 days before *Plasmodium* sporozoite injection (d1CQ or d2CQ respectively); gray line represents the peripheral blood parasitaemia at the time of re-infection by *Plasmodium* sporozoites. (**P* <0.05; ***P* <0.01, Ttest). Results are expressed as the mean ± s.d. of 3 independent infections each counting with a minimum of 5 mice per group.

Fig. 1

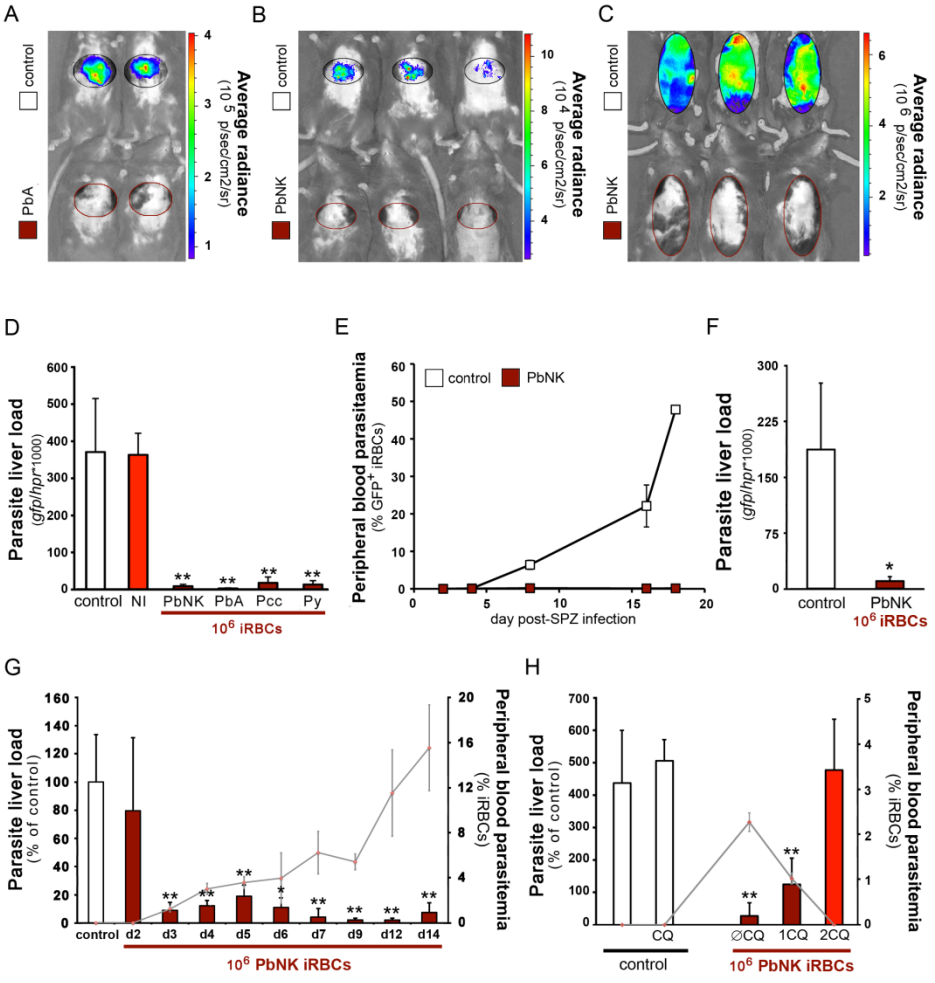
A
control
PbA
Average radiance
(10 5 p/sec/cm2/sr)
B
control
PbNK
Average radiance
(10 4 p/sec/cm2/sr)
C
control
PbNK
Average radiance
(10 6 p/sec/cm2/sr)
D
Parasite liver load
(gfp/hpr*1000)
control NI PbNK PbA Pcc Py
10^6 iRBCs
E
Peripheral blood parasitaemia
(% GFP+ iRBCs)
control PbNK
day post-SPZ infection
F
Parasite liver load
(gfp/hpr*1000)
control PbNK
10^6 iRBCs
G
Parasite liver load
(% of control)
Peripheral blood parasitemia
(% iRBCs)
control d2 d3 d4 d5 d6 d7 d9 d12 d14
10^6 PbNK iRBCs
H
Parasite liver load
(% of control)
Peripheral blood parasitemia
(% iRBCs)
CQ ∅CQ 1CQ 2CQ
control
10^6 PbNK iRBCs

Fig. 2. Ongoing malaria-blood stage infection causes reduction in the number and development of *Plasmodium* EEFs in hepatocytes. (**A**) Fifty μm liver sections, 40h after *P. berghei* ANKA-GFP infection of naïve mice (control) and mice infected 5 days previously with 10^6 *P. berghei* NK65 iRBCs (PbNK); EEFs shown as white spots exemplified by arrows. Bar = 100μm. (**B**) Representative EEF in liver sections of naïve mice (control) or mice infected 5 days previously with 10^6 *P. berghei* NK65 iRBCs (PbNK), 40h post 5 x 10^4 *P. berghei* ANKA- *gfp*-expressing sporozoite infection. (Blue = DNA, red = polymerized actin, and green = GFP (EEF); Bar = 10μm.). (**C**) *P. berghei* ANKA-GFP size (area) and density (number) in liver sections of naïve mice (control) or mice infected 5 days previously with 10^6 *P. berghei* NK65 iRBCs (PbNK), 40h post 5 x 10^4 *P. berghei* ANKA-GFP sporozoite infection, in three independent experiments. (**D**) Comparison of microscopy and qRT-PCR quantification of infection in the liver 40h post 5 x 10^4 *P. berghei* ANKA-*gfp*-expressing sporozoite injection in naïve mice (control) or mice infected 5 days previously with 10^6 *P. berghei* NK65 iRBCs (PbNK), in three independent experiments. (**P* <0.05; ***P* <0.01, Ttest). Results are expressed as the mean ± s.d. of 3 independent infections each counting with a minimum of 5 mice per group.

Fig. 2

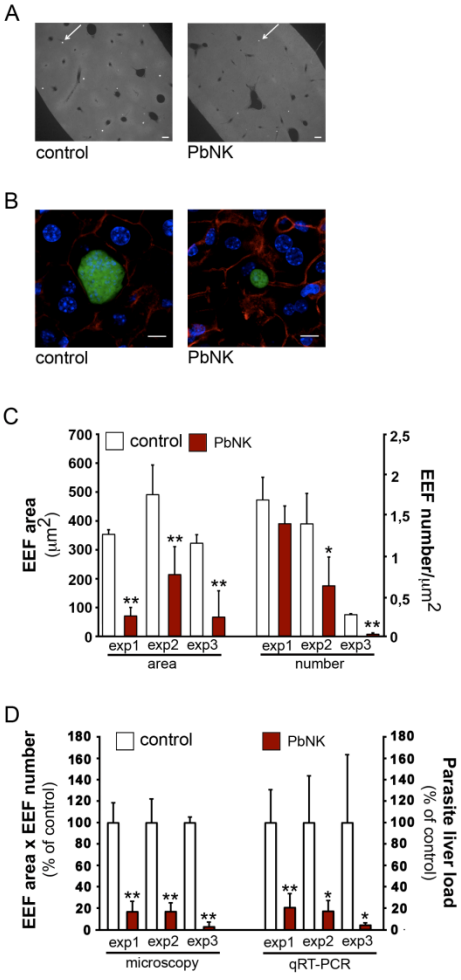
A
control
PbNK
B
control
PbNK
C
control
PbNK
EEF area (µm2)
EEF number/µm2
exp1 exp2 exp3
area
exp1 exp2 exp3
number
D
control
PbNK
EEF area x EEF number (% of control)
Parasite liver load (% of control)
exp1 exp2 exp3
microscopy
exp1 exp2 exp3
qRT-PCR

Fig. 3. An increase in *hepcidin* levels during blood stage infection leads to a redistribution of iron in infected mice, which restricts *Plasmodium* sporozoite development/replication. (**A**) *Plasmodium* liver load 40h post 5 x 10^4 *P. berghei* ANKA-GFP sporozoite injection into naïve mice (control), and mice infected 5 days previously with 10^6 *P. berghei* NK65 iRBCs (PbNK), using mice with different genotypes (RAGII-/-), (MyD88-/-) and (IFNγ-/-), after monoclonal antibody treatment (anti-IL-6), or after Nω-Nitro-L-arginine methyl ester hydrochloride (L-NAME) and clodronate liposome treatment (clodLip), all compared to wild-type C57BL/6 mice. (**B**) *Plasmodium* liver load 40h post 5 x 10^4 *P. berghei* ANKA-GFP sporozoite injection into naïve mice (control), and mice infected 5 days previously with 10^6 *P. berghei* NK65 iRBCs (PbNK), using wild-type (C57BL/6) and caspase3 deficient (caspase3-/-) mice. (**C**) *Plasmodium* liver load (left axis), and relative hepcidin expression levels (right axis), 40h post 5 x 10^4 *P. berghei* ANKA-GFP sporozoite injection into naïve mice (control) or mice infected 5 days previously with 10^6 *P. berghei* NK65 iRBCs (PbNK), measured by qRT-PCR. (**D**) *Plasmodium* liver load (left axis), and relative hepcidin expression levels (right axis), 40h post 5 x 10^4 *P. berghei* ANKA-GFP sporozoite injection into naïve mice (control), mice infected 5 days previously with 10^6 *P. berghei* NK65 iRBCs (PbNK) and mice infected 5 days previously with 10^6 *P. berghei* NK65 iRBCs and treated with chloroquine for 2 days before *Plasmodium* sporozoite injection (CQ PbNK), measured by qRT-PCR. (**E**) EEF and ferritin distribution in liver sections of naïve mice (control) or mice infected 5 days previously with 10^6 *P. berghei* NK65 iRBCs (PbNK), 40h post 5 x 10^4 *P. berghei* ANKA- *gfp*-expressing sporozoite infection. (Blue = DNA, green = GFP (EEF), red = ferritin, white = polymerized actin; bar = 10μm.). (**F**) Spleen total non-heme iron quantification 40h post 5 x 10^4 *P. berghei* ANKA-GFP sporozoite injection into naïve mice (control) or mice previously infected 5 days previously with 10^6 *P. berghei* NK65 iRBCs (PbNK). (**G**) Primary hepatocyte total non-heme iron quantification of primary hepatocytes isolated from naïve mice (control) and mice infected 5 days previously with 10^6 *P. berghei* NK65 iRBCs (PbNK). (**H**) Effect of iron chelator bathophenanthrolinedisulfonate (BPS) titration on *P. berghei* ANKA-GFP EEF development inside Huh7 hepatoma cells, measured by flow cytometry 36h after sporozoite addition. (**I**) Representative EEFs in Huh7 hepatoma cells 36h post-2 x 10^4 *P. berghei* ANKA- *gfp*-expressing sporozoite infection of untreated cells (control), cells treated 24h before infection with iron chelator Desferrioxamine (DFO) and cells treated 24h before infection with Ferric Ammonium Citrate (FAC). (Blue = DNA, and green = GFP (EEF); bar = 10μm.). (**J**) *Plasmodium* liver load 40h post 5 x 10^4 *P. berghei* ANKA-GFP sporozoite injection into naïve mice (control) or mice treated 24h previously with 250 mg/kg of iron chelator Desferrioxamine (DFO). (**K**) *Plasmodium* liver load 40h post 5 x 10^4 *P. berghei* ANKA sporozoite injection into mice infected 48h previously with 5 x 10^{11} units of *gfp* adenovirus (GFP.adV) or 5 x 10^{11} units of *hamp* expressing adenovirus (HAMP.adV) compared with non previously infected mice (control). (**P* <0.05; ***P* <0.01, Ttest). Results are expressed as the mean ± s.d. of 3 independent infections each counting with a minimum of 5 mice per group.

Fig. 3

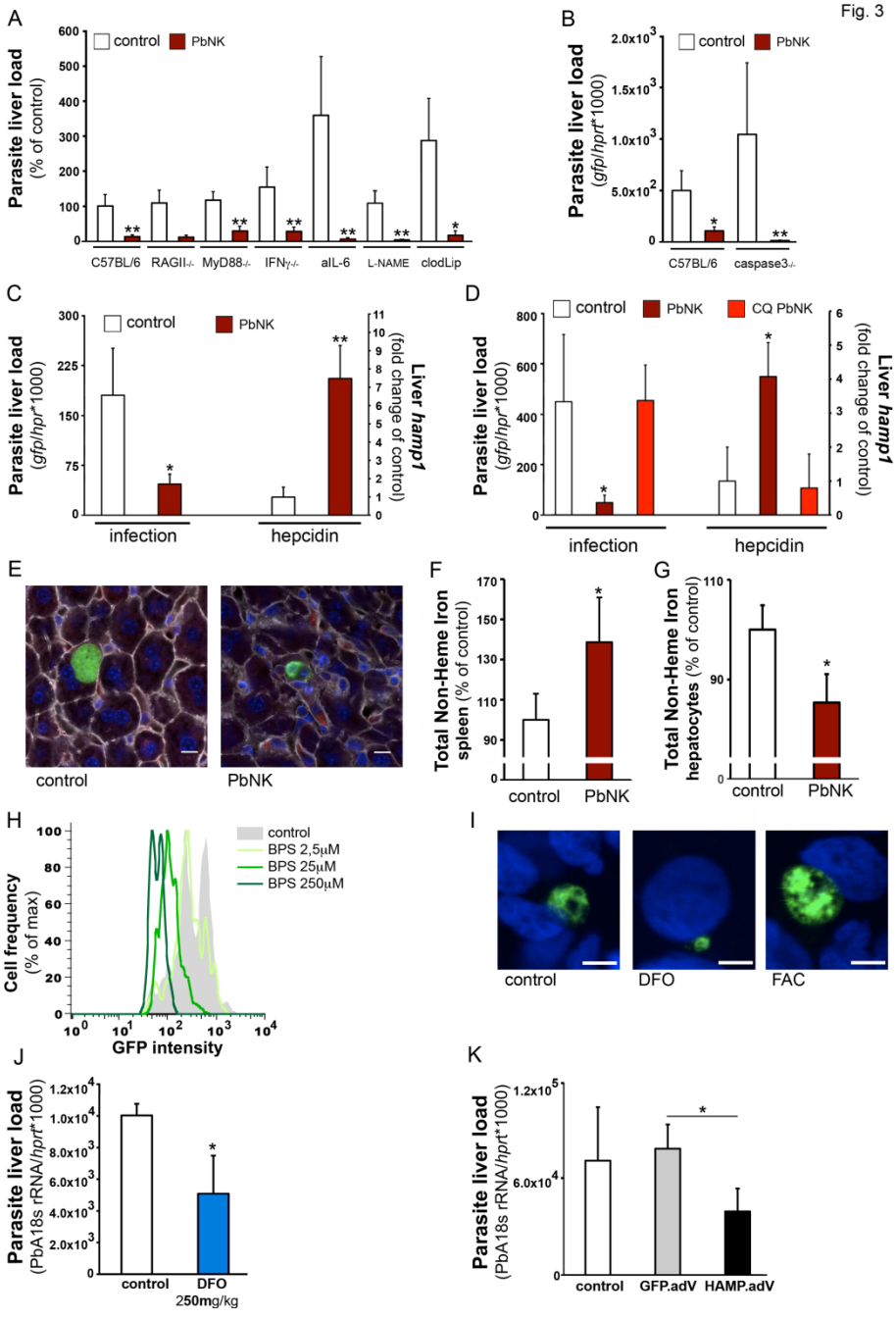
A
Parasite liver load (% of control)
control
PbNK
C57BL/6
RAGII-/-
MyD88-/-
IFNγ-/-
aIL-6
L-NAME
clodLip
B
Parasite liver load (gfp/hprt*1000)
C57BL/6
caspase3-/-
C
Parasite liver load (gfp/hprt*1000)
Liver hamp1 (fold change of control)
infection
hepcidin
D
CQ PbNK
E
control
PbNK
F
Total Non-Heme Iron spleen (% of control)
G
Total Non-Heme Iron hepatocytes (% of control)
H
BPS 2,5μM
BPS 25μM
BPS 250μM
Cell frequency (% of max)
GFP intensity
I
DFO
FAC
J
Parasite liver load (PbA18s rRNA/hprt*1000)
DFO 250mg/kg
K
GFP.adV
HAMP.adV

Figure 4. Model predictions for age-related incidence and multiplicity of infections. (**A** and **B**) We tested four different assumptions regarding a possible inhibitory effect of a blood-stage infection: (i) density-dependent, where the probability of infection directly correlates with parasite density; (ii) classical premunition, where a new infection can only be established after an ongoing infection is essentially cleared; (iii) no protection, where the probability of infection is independent of an ongoing infection; and (iv) critical threshold dependent, where a new infection can only be established once the blood-stage parasite density falls below a certain level. Only the presence of a critical threshold density results in an initial increase in both infection rate and multiplicity of infection, which then decline due to acquired immunity. (**C** and **D**) The results reveal a strong dependency on transmission intensities and predict that the observed age-dependency in the rates of infection and multiplicity will be lost under low levels of transmission.

Fig. 4

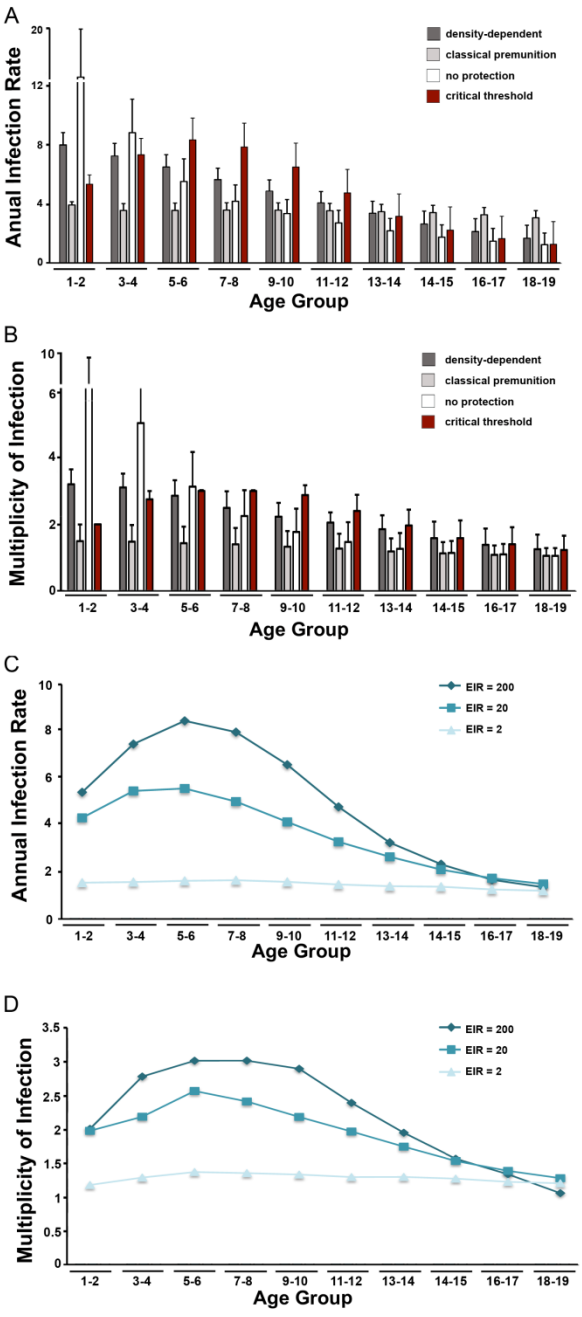
A
Anual Infection Rate
density-dependent
classical premunition
no protection
critical threshold
1-2
3-4
5-6
7-8
9-10
11-12
13-14
14-15
16-17
18-19
Age Group
B
Multiplicity of Infection
density-dependent
classical premunition
no protection
critical threshold
Age Group
C
Annual Infection Rate
EIR = 200
EIR = 20
EIR = 2
Age Group
D
Multiplicity of Infection
EIR = 200
EIR = 20
EIR = 2
Age Group

fig. S1. Correlation between expression levels of 18S *rRNA* and *gfp* cDNA in mouse livers, 40h post 5 x 10^3, 2 x 10^4, 5 x 10^4 and 1.5 x 10^5 *P. berghei* ANKA-GFP sporozoite injection. Dots show the average expression of 4 mice and the black line represents the positive correlation between the two parameters measured.

fig. S1

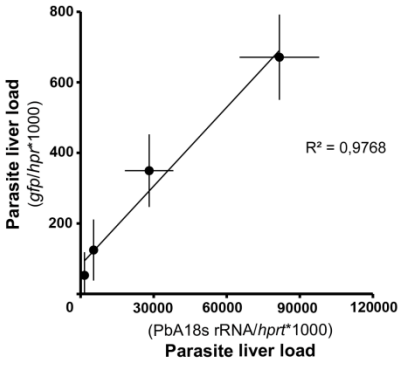
800
600
400
200
0
30000
60000
90000
120000
R² = 0,9768
Parasite liver load
(gfp/hprt*1000)
(PbA18s rRNA/hprt*1000)
Parasite liver load

fig. S2. (**A**) *Plasmodium* liver load 40 and 48h post 5 x 10^4 *P. berghei* ANKA-GFP sporozoite injection into naïve mice (control) and mice infected 5 days previously with 10^6 *P. berghei* NK65 (PbNK). (**B**) Representative EEF in liver sections of naïve mice (control) or mice infected 5 days previously with 10^6 *P. berghei* NK65 iRBCs (PbNK), 40 and 48h post 5 x 10^4 *P. berghei* ANKA *gfp*-expressing sporozoite infection. (Blue = DNA, red = polymerized actin, and green = GFP (EEF); Bar = 10µm.). (**C**) *Plasmodium* liver load 40 and 72h post 5 x 10^4 *P. berghei* ANKA-GFP sporozoite injection into naïve mice (control) and mice infected 5 days previously with 10^6 *P. berghei* NK65 (PbNK), compared to a non-infected group (NI). (**D**) Magnification of 72h post infection of 5 x 10^4 *P. berghei* ANKA-GFP sporozoite injection into naïve mice (control) and mice infected 5 days previously with 10^6 *P. berghei* NK65 (PbNK), and non infected control group shown in (**C**). (**P* <0.05; ***P* <0.01, Ttest). Results are expressed as mean ± s.d. of 3 independent infections each counting with a minimum of 5 mice per group.

fig. S2

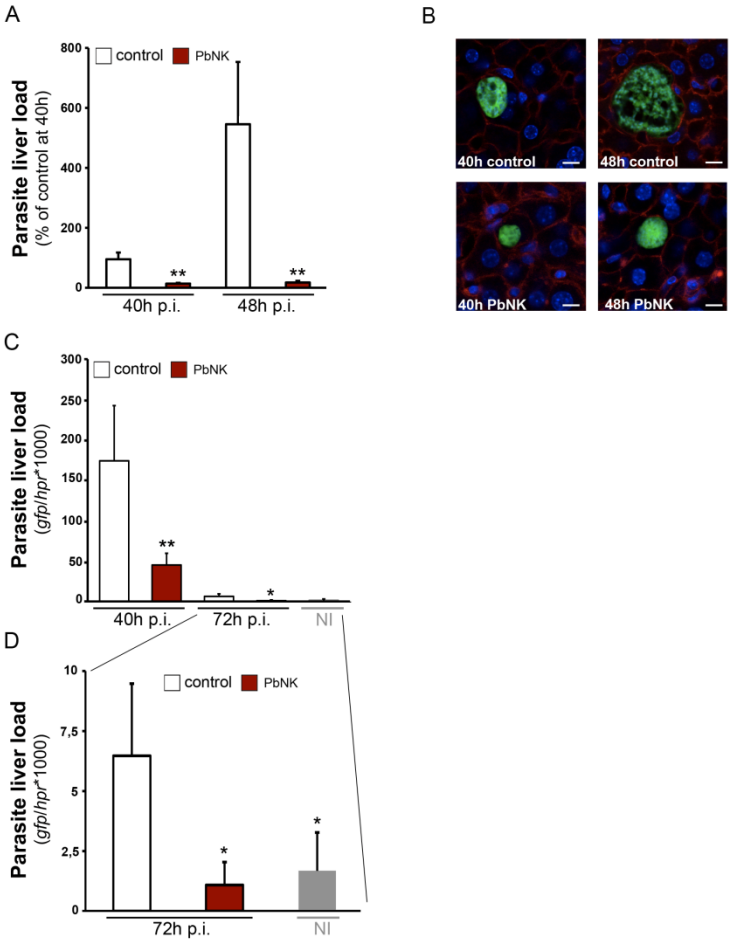
A
control
PbNK
Parasite liver load
(% of control at 40h)
800
600
400
200
0
**
**
40h p.i.
48h p.i.
B
40h control
48h control
40h PbNK
48h PbNK
C
control
PbNK
Parasite liver load
(gfp/hpr*1000)
300
250
200
150
100
50
0
**
*
40h p.i.
72h p.i.
NI
D
control
PbNK
Parasite liver load
(gfp/hpr*1000)
10
7,5
5
2,5
0
*
*
72h p.i.
NI

fig. S3. (**A**) Effect of *Plasmodium* iRBC supernatants on sporozoite hepatocyte infection. Hepatocytes grown in the lower chamber of a transwell system where infection by sporozoites (green crescents) takes place, contacting with mouse serum (control), non-infected blood (NI) or blood containing 6 x 10^5 *P. berghei* NK65 iRBCs (PbNK) within the upper chamber. (**B**) Sporozoite infection (% infected cells) of mouse primary hepatocytes in the three conditions described above 40h post-2 x 10^4 *P. berghei* ANKA *gfp*-expressing sporozoite addition, analysed by wide field microscopy. (**C**) EEF development (EEF area) in mouse primary hepatocytes in the three conditions described above 40h post-2 x 10^4 *P. berghei* ANKA *gfp*-expressing sporozoite addition, analysed by confocal microscopy. (**D**) Sporozoite infection (% infected cells) of Huh7 cells, in the three conditions described above 36h post-2 x 10^4 *P. berghei* ANKA *gfp*-expressing sporozoite addition, measured by FACS. (**E**) EEF development (GFP intensity) in Huh7 cells, in the three conditions described above 36h post-2 x 10^4 *P. berghei* ANKA *gfp*-expressing sporozoite addition, quantified by FACS. (**F**) Sporozoite infection (EEF/1000 nuclei) of mouse primary hepatocytes isolated from naive mice (control) and mice infected 5 to 7 days previously with *10^6 P. berghei* NK65 iRBCs (PbNK), 48h post-2 x 10^4 *P. berghei* ANKA *gfp*-expressing sporozoite addition, analysed by wide field microscopy. (**G**) EEF development (EEF area) in mouse primary hepatocytes isolated from naive mice (control) and mice infected 5 to 7 days previously with *10^6 P. berghei* NK65 iRBCs (PbNK), 48h post-2 x 10^4 *P. berghei* ANKA *gfp*-expressing sporozoite addition, analysed by confocal microscopy.

fig. S3

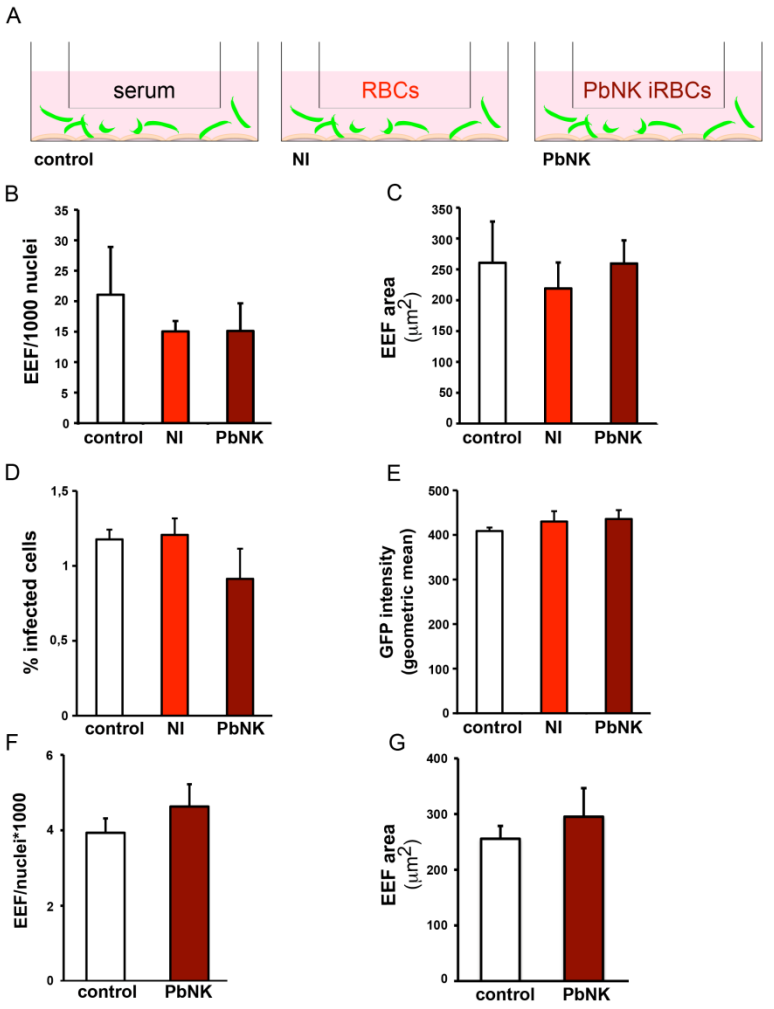
A
serum
RBCs
PbNK iRBCs
control
NI
PbNK
B
EEF/1000 nuclei
control
NI
PbNK
C
EEF area (µm2)
control
NI
PbNK
D
% infected cells
control
NI
PbNK
E
GFP intensity (geometric mean)
control
NI
PbNK
F
EEF/nuclei*1000
control
PbNK
G
EEF area (µm2)
control
PbNK

fig. S4. Microarray data analysis of liver RNA and targeting of hit molecules. (**A**) Venn diagram showing the proportion of differentially expressed (DE) transcripts found in our analysis. Numbers are indicated for each group. (**B**) Heatmap generated from the group of DE transcripts, reflecting the log ratios of each infected category compared to non-infected mice, as indicated at the bottom. Gene Ontology enrichment analysis results for each identified cluster are indicated on the table, ($P<0.05$, Fisher Exact Test One Tail). (BS: blood stage, LS: liver stage, Reinf: re-infection).

fig. S4

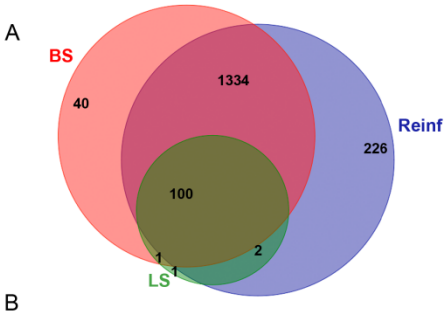

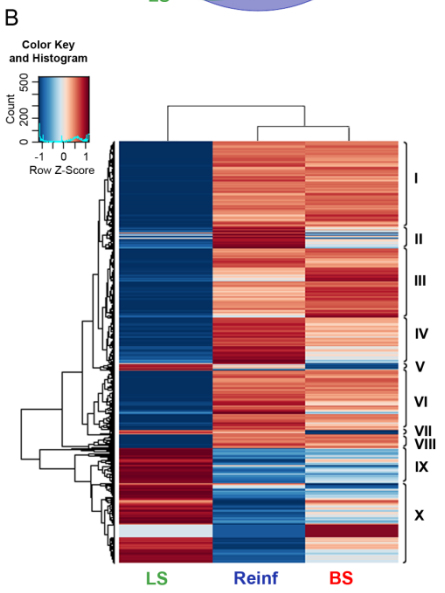

Cluster	GOID	Enriched Term
I	GO:0002376	immune system process
I	GO:0007010	cytoskeleton organization
I	GO:0006691	leukotriene metabolic process
I	GO:0019221	cytokine-mediated signaling pathway
I	GO:0018108	peptidyl-tyrosine phosphorylation
II	GO:0006952	defense response
II	GO:0019221	cytokine-mediated signaling pathway
III	GO:0006323	DNA packaging
III	GO:0051301	cell division
III	GO:0006468	protein amino acid phosphorylation
III	GO:0006270	DNA replication initiation
III	GO:0030705	cytoskeleton-dependent intracellular transport
III	GO:0032663	regulation of interleukin-2 production
IV	GO:0002376	immune system process
IV	GO:0032680	regulation of tumor necrosis factor production
V	GO:0009615	response to virus
V	GO:0006915	apoptosis
VI	GO:0002376	immune system process
VI	GO:0045807	positive regulation of endocytosis
VI	GO:0006334	nucleosome assembly
VI	GO:0006910	phagocytosis, recognition
VI	GO:0032680	regulation of tumor necrosis factor production
VI	GO:0019221	cytokine-mediated signaling pathway
VI	GO:0032956	regulation of actin cytoskeleton organization
VII	na	na
VIII	GO:0006953	acute-phase response
VIII	GO:0045807	positive regulation of endocytosis
VIII	GO:0009615	response to virus
IX	GO:0007586	digestion
IX	GO:0055114	oxidation reduction
IX	GO:0042446	hormone biosynthetic process
IX	GO:0007179	transforming growth factor beta receptor signaling pathway
X	GO:0055114	oxidation reduction
X	GO:0019752	carboxylic acid metabolic process
X	GO:0019835	cytolysis
X	GO:0006957	complement activation, alternative pathway

fig. S5. (**A**) Macrophage and monocyte staining in 50µm liver section 40h post 5 x 10^4 *P. berghei* ANKA *gfp*-expressing sporozoite infection, of naïve mice (control), mice 5 days previously infected with 10^6 iRBCs of *P. berghei* NK65 (PbNK), mice treated with clodronate liposomes 48h prior to sporozoite infection (clodLip control) and mice infected with 10^6 iRBCs of *P. berghei* NK65 and treated with clodronate liposomes 48h prior to sporozoite infection (clodLip PbNK), (Blue = DNA, white = polymerized actin, and red = pan macrophage marker. Bar = 10µm.) (**B**) *Plasmodium* liver load 40h post 5 x 10^4 *P. berghei* ANKA-GFP sporozoite injection into naïve mice (control), and mice infected 5 days previously with 10^6 iRBCs of *P. berghei* NK65 iRBCs (PbNK), preceded 15 days by mock surgery (mock) or splenectomy (splenectom.). (**C**) *Plasmodium* liver load 40h post 5 x 10^4 *P. berghei* ANKA-GFP sporozoite injection into naïve mice (control), and mice infected 11 days previously with 10^6 iRBCs of *P. berghei* NK65 iRBCs (PbNK) using RAGII deficient mice in C57BL/6 background, and naïve mice (control), and mice infected 14 days previously with 10^6 iRBCs of *P. berghei* NK65 iRBCs (PbNK) using BALBscid mice in BALB/c background. (**D**) *Plasmodium* liver load 40h post 5 x 10^4 *P. berghei* ANKA-GFP sporozoite injection into naïve mice (control), and mice infected 5 days previously with 10^6 iRBCs of *P. berghei* NK65 iRBCs (PbNK), using untreated WT mice, mice treated with IFNγ monoclonal antibody 24h prior to sporozoite infection (aIFNγ), mice deficient for IFNγ receptor 1 (IFN-R1-/-), and mice deficient for IFNγ (IFNγ-/-); all in C57BL/6 background. (**E**) *Plasmodium* liver load 40h post 5 x 10^4 *P. berghei* ANKA-GFP sporozoite injection into naïve mice (control), and mice infected 5 days previously with 10^6 iRBCs of *P. berghei* NK65 iRBCs (PbNK), using untreated mice, mice treated with L-NAME or SMT every day for the whole extent of the experiment, all mice in C57BL/6 background, and using WT mice and NOS2 deficient mice (iNOS-/-) in B6.126 background. (**F**) *Plasmodium* liver load 40h post 5 x 10^4 *P. berghei* ANKA-GFP sporozoite injection into naïve mice (control), and mice infected 5 days previously with 10^6 iRBCs of *P. berghei* NK65 iRBCs (PbNK), using mice with different and genotypes, C5a deficient mice treated with C3a antagonist SB 290157 (C5a-/- C3a ant.) in C57BL/10 background, (TCRδ-/-) in B6.129 background, RAGγc deficient compared to RAGII (RAGγc), mastocyte deficient in (wsh-/-), IL-10 deficient (IL-10-/-) and after monoclonal antibody treatment (aTNFα) in C57BL/6 background, all compared to respective background littermates. (*P < 0.05, **P < 0.01, Ttest) Results are expressed as the mean ± s.d. of 3 independent infections each counting with a minimum of 5 mice per group.

fig. S5

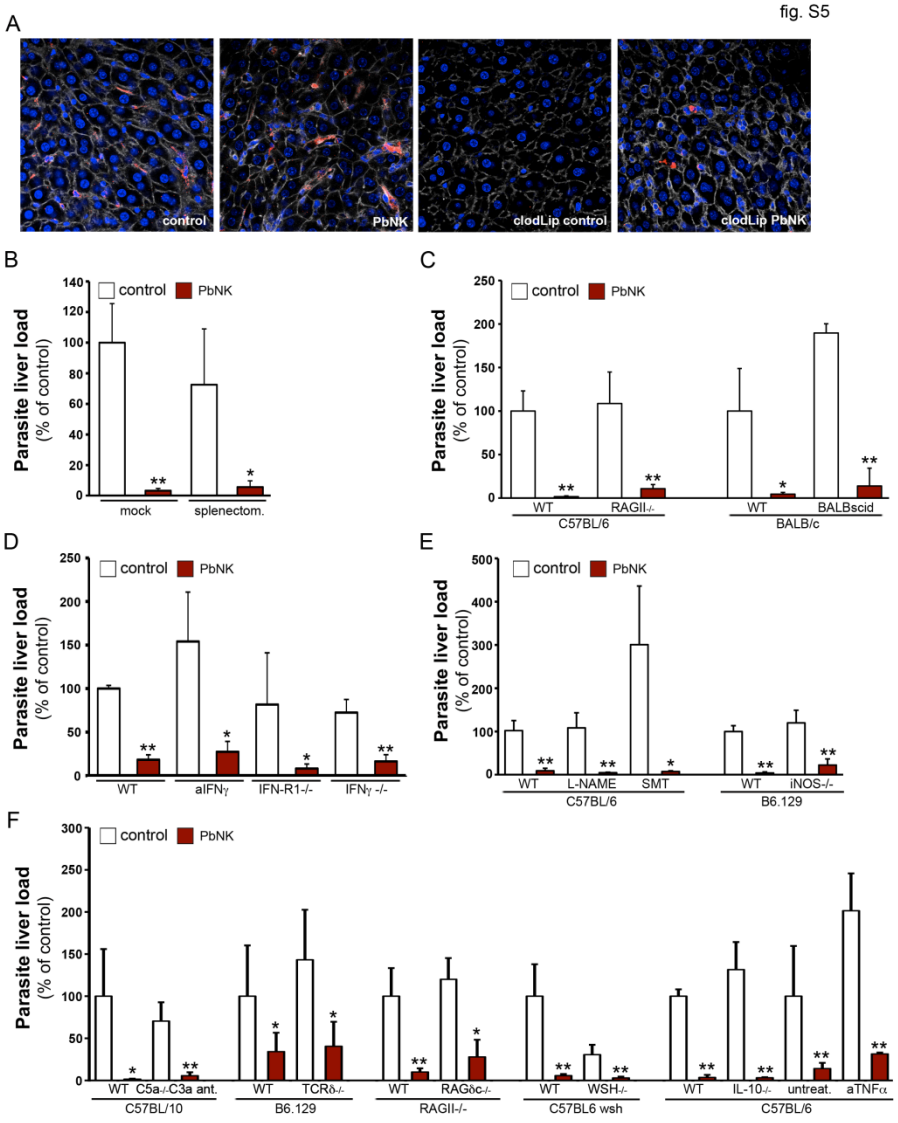
A
control
PbNK
clodLip control
clodLip PbNK
B
Parasite liver load
(% of control)
control
PbNK
mock
splenectom.
C
WT
RAGII-/-
C57BL/6
WT
BALBscid
BALB/c
D
WT
aIFNγ
IFN-R1-/-
IFNγ -/-
E
WT
L-NAME
SMT
C57BL/6
WT
iNOS-/-
B6.129
F
WT
C5a-/-
C3a ant.
C57BL/10
WT
TCRδ-/-
B6.129
WT
RAGδc-/-
RAGII-/-
WT
WSH-/-
C57BL6 wsh
WT
IL-10-/-
untreat.
aTNFα
C57BL/6

fig. S6. Blood stage induced apoptosis in caspase 3-deficient mice. (**A**) Apoptosis in liver sections (16µm) of naïve wild-type C57BL/6 mice (WT control), wild-type C57BL/6 mice infected 6 days previously with 10^6 *P. berghei* NK65 iRBCs (WT PbNK) and caspase3-deficient mice infected 6 days previously with 10^6 *P. berghei* NK65 iRBCs (caspase 3-/- PbNK). (Blue = DNA and green = apoptoctic nuclei; bar =20µm). (**B**) Quantification of apoptotic nuclei in liver sections (16µm) of naïve wild-type C57BL/6 mice (WT control), wild-type C57BL/6 mice infected 6 days previously with 10^6 *P. berghei* NK65 iRBCs (WT PbNK) and caspase3 deficient mice infected 6 days previously with 10^6 *P. berghei* NK65 iRBCs (caspase 3 -/- PbNK) (*P <0.01, Ttest). Results are expressed as the mean ± s.d. of 3 independent infections each counting with a minimum of 5 mice per group.

fig. S6

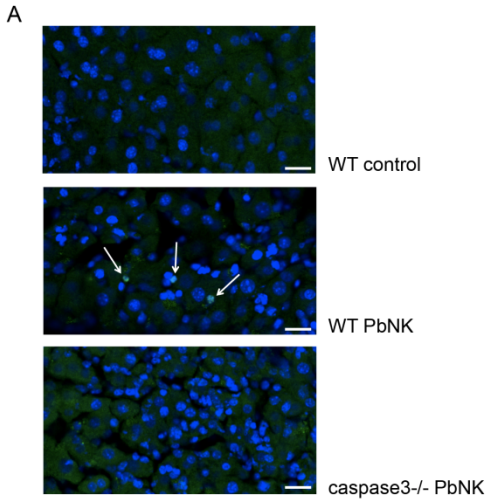
A
WT control
WT PbNK
caspase3-/- PbNK
B
no. Apoptotic nuclei/10000 nuclei
90
80
70
60
50
40
30
20
10
0
*
WT control
WT PbNK
caspase3-/- PbNK

fig. S7. Iron availability and infection. (**A**) Effect of various concentrations of Desferrioxamine (DFO) on *P. berghei* ANKA-GFP EEF development inside Huh7 hepatoma cells, measured by flow cytometry 36h after-2 x 10^4 *P. berghei* ANKA *gfp*-expressing sporozoite addition. The graphs show one representative data set of triplicate samples. (**B**) Area of EEFs inside Huh7 hepatoma cells 36h post-2 x 10^4 *P. berghei* ANKA-GFP sporozoite infection of untreated cells (control), cells treated 24h before infection with DFO and cells treated 24h before infection with Ferric Ammonium Citrate (FAC), (*P <0.01, Ttest). Results are expressed as the mean ± s.d. of 3 independent infections, each measuring the area of 12 EEFs per group.

fig. S7

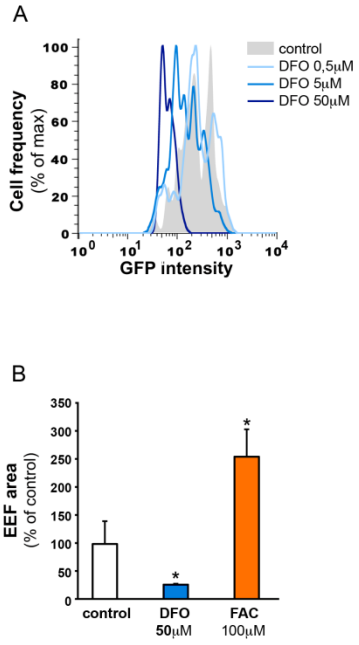
A
Cell frequency
(% of max)
100
80
60
40
20
0
control
DFO 0,5μM
DFO 5μM
DFO 50μM
10^0
10^1
10^2
10^3
10^4
GFP intensity
B
EEF area
(% of control)
350
300
250
200
150
100
50
0
*
*
control
DFO
50μM
FAC
100μM

fig. S8. (**A**) Functional relationship between parasite density and probability of infection. As the level of parasitaemia of an ongoing infection (red line) remains above a critical threshold density, πcrit, the probability of establishing a new blood stage infection (blue line) is extremely low but significantly increases as soon as the parasitaemia level falls below this threshold. (**B**) Acquired immunity as a function of infection history. The probability of infection is dependent on the total number of blood-stage infections experienced by the host and D, which can generally be understood as a proxy for antigenic diversity, where greater D requires more infections to gain protection.

fig. S8

A

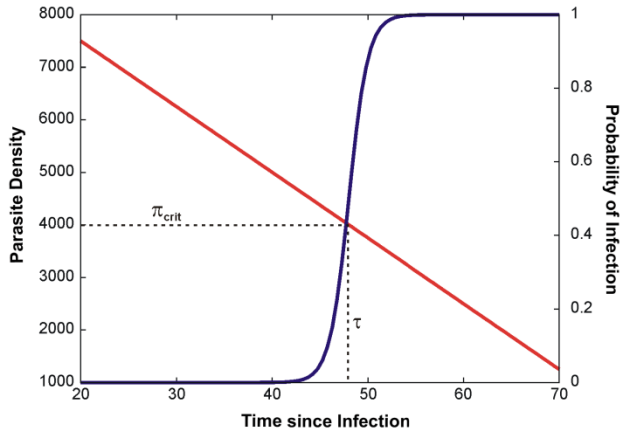
8000
7000
6000
5000
4000
3000
2000
1000
Parasite Density
π_{crit}
τ
1
0.8
0.6
0.4
0.2
0
Probability of Infection
20
30
40
50
60
70
Time since Infection

B

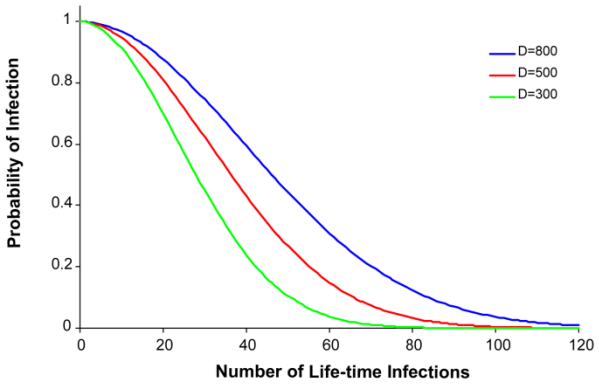
1
0.8
0.6
0.4
0.2
0
Probability of Infection
D=800
D=500
D=300
0
20
40
60
80
100
120
Number of Life-time Infections

fig. S9. Model behaviour under changes in duration of infections. The model was tested under three different assumptions concerning the duration of infection: (i) constant over age (T=100), (ii) decreasing with age (T=100-2*age), or (iii) increasing with age (T=60+2*age). Shown are the age-related annual infection rates (**A**) and multiplicity of infections (**B**) under these assumptions, clearly demonstrating a qualitative invariance of the model's behaviour to the underlying assumption about the period of infection.

fig. S9

A

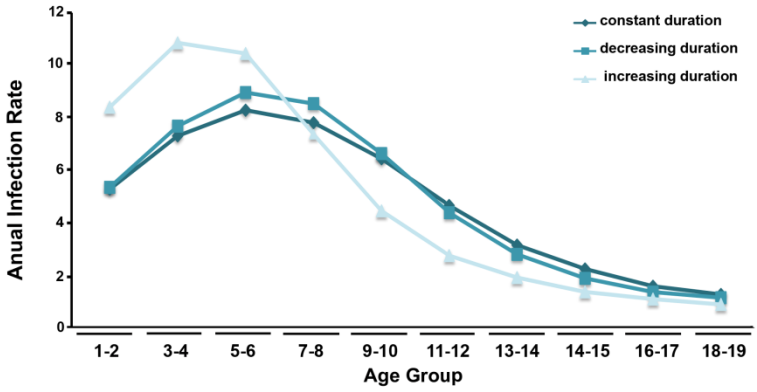
Anual Infection Rate
12
10
8
6
4
2
0
constant duration
decreasing duration
increasing duration
1-2
3-4
5-6
7-8
9-10
11-12
13-14
14-15
16-17
18-19
Age Group

B

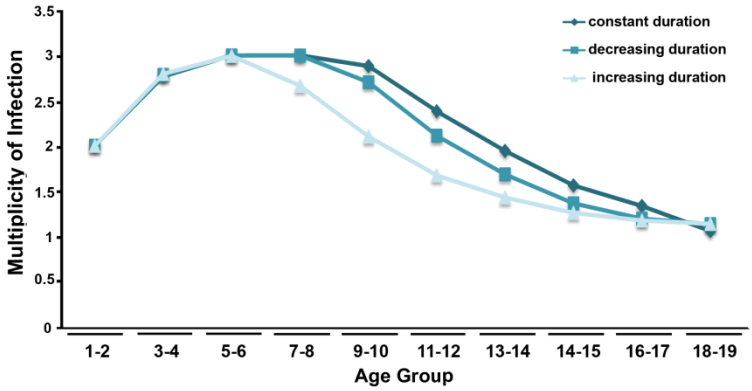
Multiplicity of Infection
3.5
3
2.5
2
1.5
1
0.5
0
constant duration
decreasing duration
increasing duration
1-2
3-4
5-6
7-8
9-10
11-12
13-14
14-15
16-17
18-19
Age Group

Additional Results

Our data strongly points that the observed impairment of secondary liver infection in Plasmodium blood infected mice is promoted by iron redistribution in the liver induced by hepcidin upregulation. However, many other theories were investigated during the course of this work that ultimately led us to propose the iron redistribution mechanism.
Besides the hypothesis mentioned in the main body of the Results chapter (see Results section **Blood stage *Plasmodium* parasites suppress co-infection in the liver***) we have tested several others that we projected during the course of this work. The results presented here serve to further explain the conclusions drawn, and although not included in the previous section were discussed later on this thesis and are of some importance to the conclusions made.*

Serum transfers. Considering the possibility that *Plasmodium* molecules released by iRBCs could affect hepatocytes towards impairment of EEF development, we designed experiments to investigate if the serum of blood infected mice transferred into naïve ones, prior to sporozoite infection, would protect these mice from sporozoite challenge.

Two groups of mice were infected with 10^6 *P. berghei* NK65 iRBCs. One of these groups was then re-infected on day 6 post blood infection (PbNK) and the rest of the mice were sacrificed on the same day to collect blood and produce serum. Serum of every two donor mice was injected to a recipient naïf one (serumPbNK), 2 to 12h prior to 5 x 10^4 *P. berghei* ANKA-GFP sporozoite challenge. Expression of *gfp* was determined to assess liver infection, 40h post sporozoite injection, and compared to control naïve non-transferred mice (control).
It was never observed any effect of the transferred serum on liver infection. Indeed no reduction was observed in the mice that were injected serum

from mice with *Plasmodium* blood stage infection prior to sporozoite challenge (fig. A1).

Cholesterolemia. Numerous molecules involved in lipid metabolism appeared modulated in the liver microarray study performed during this thesis and described in the previous section. Of those molecules several related to cholesterol metabolism, in that context we designed experiments to address cholesterol involvement in the observed reduction of sporozoite infection in re-infected mice.

Blood and livers were collected 40h after 5 x 10^4 *P. berghei* ANKA-GFP sporozoite of naïve mice (control) and mice 4 days previously infected with 10^6 *P. berghei* NK65 iRBCs (PbNK).

Serum was then collected and total cholesterol, HDL- and LDL-cholesterol biochemically determined by DNAtech (INETI, Portugal). No significant differences in either of these values were found between control and re-infected group (fig. A2).

In addition, livers were also collected after perfusion with PBS and a section was used for quantification of cholesterol by fluorometric method with The Amplex® Red Cholesterol Kit Assay (Invitrogen). No significant difference was observed in cholesterol levels control and re-infected mice (fig. A2).

***Toxoplasma* infection effect over *Plasmodium* sporozoite liver infection.** In order to address the dependence and specificity of *Plasmodium* blood stage infection to impose protection from secondary liver challenge by sporozoites, we substituted the primary blood infection by an infection of a related parasite.

Mice bearing a 4-day infection with 10^4 *Toxoplasma gondii* tachizoites (TOXO) or 10^6 *P. berghei* NK65 iRBCs (PbNK) were challenged with 5 x 10^4 *P. berghei* ANKA sporozoites, in parallel with naïve mice (control).

Plasmodium liver infection was monitored 40h post-sporozoite infection by qRT-PCR.

A strong and similar reduction of *Plasmodium* liver infection was found in all previous infected mice compared to naïve ones, regardless of the parasite used for primary infection (fig. A3).

Hepcidin quantification was performed to these same samples and a 4-fold increase was observed in all previous infected mice compared to naïve ones (fig. A3).

All these results are also considered in the general discussion of this thesis.

Effect of secondary sporozoite infection over primary blood infection.

These experiments aimed at further investigating possible interactions of *Plasmodium* blood and liver stages within a single host. We verified what would be the impact of the secondary sporozoite infection over the primary blood stage infection already established at the time of re-infection.

After 5 x 10^4 *P. berghei gfp*-expressing sporozoite infection of mice 4 days previously infected with 10^6 *P. berghei* NK65 iRBCs (Reinf), blood parasitemias were followed by Giemsa staining of thin blood films. Non-reinfected mice 4 days previously infected with *P. berghei* NK65 infected were used as a control group (BS). While non-reinfected mice (BS) died of hyper-parasitemia on day 18 post- *P. berghei* NK65 iRBCs infection, re-infected mice showed increasing parasitaemias until day 20 post- *P. berghei* NK65 iRBCs infection, time when peripheral blood parasites began to decrease and reach zero between days 30 and 35 post infection. Parasitaemias were kept undetectable until day fifty post infection, when all surviving mice were sacrificed by cervical dislocation (fig. A4).

These last results are considered in The next in line *section where future perspectives are proposed.*

fig. A1. *Plasmodium* liver load 40h post 5 x 10^4 *P. berghei* ANKA-GFP sporozoite injection into naïve mice (control), mice infected 5 days previously with 10^6 iRBCs of *P. berghei* NK65 iRBCs (PbNK), and mice injected serum collected from mice infected 5 days previously with 10^6 iRBCs of *P. berghei* NK65 iRBCs, 6h prior to sporozoite infection (serumPbNK). (*P < 0.01, Ttest) Results are expressed as the mean ± s.d. of 3 independent infections each counting with a minimum of 5 mice per group.

fig. A1

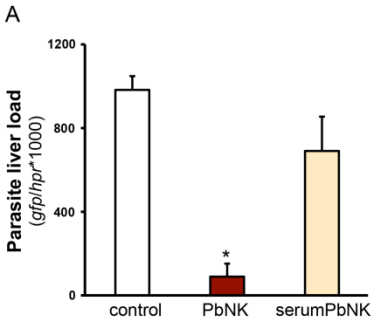
A
Parasite liver load
(gfp/hpr*1000)
1200
800
400
0
*
control
PbNK
serumPbNK

fig. A2. (**A**) *Plasmodium* liver load 40h post 5 x 10^4 *P. berghei* ANKA-GFP sporozoite injection into naïve mice (control), and mice infected 5 days previously with 10^6 iRBCs of *P. berghei* NK65 iRBCs (PbNK). (**B**) Liver cholesterol quantification 40h post 5 x 10^4 *P. berghei* ANKA-GFP sporozoite injection into naïve mice (control), and mice infected 5 days previously with 10^6 iRBCs of *P. berghei* NK65 iRBCs (PbNK) measured by a fluorometric method with The Amplex® Red Cholesterol Kit Assay. (**C**) Serum cholesterol quantificationad 40h post 5 x 10^4 *P. berghei* ANKA-GFP sporozoite injection into naïve mice (control), and mice infected 5 days previously with 10^6 iRBCs of *P. berghei* NK65 iRBCs (PbNK) by a biochemically method performed at DNAtech (INETI, Portugal) measuring total cholesterol, HDL- and LDL-cholesterol respectively. Results are expressed as the mean ± s.d. of 3 independent infections each counting with a minimum of 5 mice per group.

fig. A2

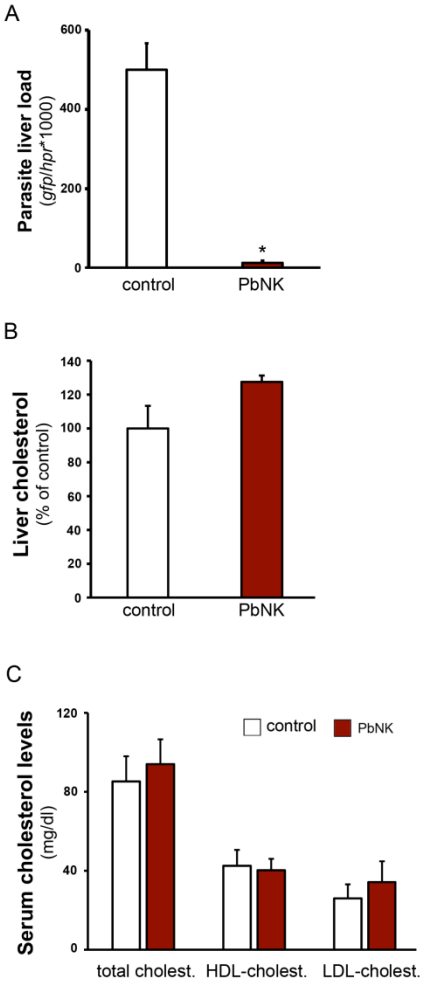
A
Parasite liver load
(gfp/hpr*1000)
600
400
200
0
*
control
PbNK
B
Liver cholesterol
(% of control)
140
120
100
80
60
40
20
0
control
PbNK
C
Serum cholesterol levels
(mg/dl)
120
80
40
0
control
PbNK
total cholest.
HDL-cholest.
LDL-cholest.

fig. A3. (**A**) *Plasmodium* liver load 40h post 5 x 10^4 *P. berghei* ANKA-GFP sporozoite injection into naïve mice (control), mice infected 4 days previously with 10^6 iRBCs of *P. berghei* NK65 iRBCs (PbNK), and mice infected 4 days previously with 10^4 tachizoites of *Toxoplasma gondii* (TOXO), measured by qRT-PCR. (**B**) Relative hepcidin expression levels in the liver 40h post 5 x 10^4 *P. berghei* ANKA-GFP sporozoite injection into naïve mice (control), mice infected 4 days previously with 10^6 iRBCs of *P. berghei* NK65 iRBCs (PbNK), or mice infected 4 days previously with 10^4 tachizoites of *Toxoplasma gondii* (TOXO), measured by qRT-PCR. (*P < 0.01, Ttest) Results are expressed as the mean ± s.d. of 3 independent infections each counting with a minimum of 5 mice per group.

fig. A3

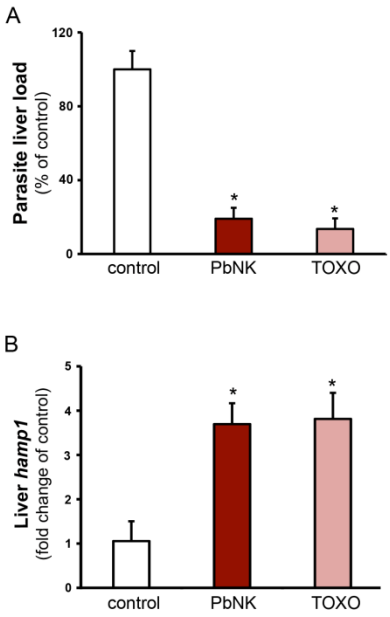
A
Parasite liver load
(% of control)
120
80
40
0
*
*
control
PbNK
TOXO
B
Liver hamp1
(fold change of control)
5
4
3
2
1
0
*
*
control
PbNK
TOXO

fig. A4. (**A**) Peripheral blood parasitaemia after infection with 10^6 iRBCs of *P. berghei* NK65 of non-re-infected mice (BS) and mice re-infected 4 days later with 5 x 10^4 *P. berghei* ANKA *gfp*-expressing sporozoite (Reinf), light grey line shows the time when re-infection occured. (**B**) Survival curve after infection with 10^6 iRBCs of *P. berghei* NK65 of non-re-infected mice (BS) and mice re-infected 4 days later with 5 x 10^4 *P. berghei* ANKA *gfp*-expressing sporozoite (Reinf), light grey intermitent line shows the time when re-infection occured. Results represent 1 of 3 independent infections counting with a minimum of 3 mice per group.

fig. A4

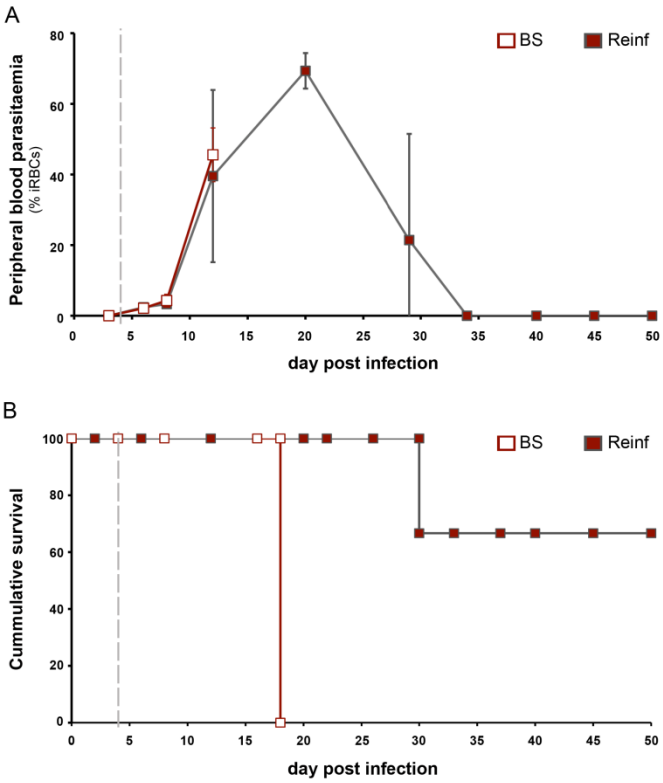
A
BS
Reinf
Peripheral blood parasitaemia
(% iRBCs)
0
20
40
60
80
0
5
10
15
20
25
30
35
40
45
50
day post infection
B
BS
Reinf
Cummulative survival
0
20
40
60
80
100
0
5
10
15
20
25
30
35
40
45
50
day post infection

Discussion

General discussion and conclusions

Although malaria infection is still a major scourge throughout the world, globally extraordinary moves are being made to tackle malaria, involving research, governments, funding agencies and donors, private companies, and civil society towards the common goal of malaria eradication, proposed by Melinda Gates in 2007.

In the 1950's, during the first Global Malaria Eradication Program, there was a significant decline in the number of areas at risk of Plasmodium *transmission [221]. Later, with the emergence of both drug and insecticide resistance in parasite and vector respectively, there was a rebound in the regions where final elimination was not achieved [222].*

Nowadays, with renewed efforts to fight Plasmodium *infection, some goals are being accomplished. Indeed, the latest Malaria Report from WHO states that the number of deaths in Africa decreased by 34000 since the previous report one year before. However, this reduction was primarily attributed to a reduction in the total number of deaths from all causes among children under 5 years of age, mostly as a result of the profound effect on health systems that so many interventions produce [8]. Importantly, the most promising vaccine candidate so far, RTS,S/AS01 has shown around 50% efficacy against clinical malaria disease in a phase III trial in 5 to 17 months old children [223], which although very positive, is still far from the level required to achieve eradication.*

It remains of great importance to learn more about the biology of parasite-host interactions, the determinants of endemicity and transmission dynamics, the social, economic and cultural implications of malaria at household, community and national levels, and the demands made upon health systems in endemic countries. Acknowledging the present situation and increasing our

understanding of the biological features of Plasmodium *infection will allow the development of better future control or eradication strategies.*

Plasmodium *blood stage of infection is the primary target of most therapeutic interventions. New insights on its biology and biochemical pathways provide new ways to target the apicoplast organelles, the invasion or egress processes, the remodelling of the iRBC, or aim at a blood stage vaccine. On the other hand, the liver stage has not been as extensively studied, and as such new discoveries might offer targets for new drugs and vaccine development.*

The aim of the present thesis was to analyse potential interactions between the blood and liver stages of the Plasmodium *parasite within a single host. Indeed, the sequence of events* from mosquito salivary glands towards man's liver and, later, to the blood *are likely to be perturbed in high transmission areas, with new infections occurring in individuals harbouring blood-stage infections. Understanding possible host-pathogen interactions can lead into new insights on* Plasmodium *liver infection, as well as enabling better comprehending of the heterogeneity amongst malaria transmissions when extrapolating to human malaria. The study presented in this thesis focused on the effect of* Plasmodium *iRBCs on the establishment and development of a secondary infection of the liver of a murine model by* Plasmodium *sporozoites, seeking to clarify inter-stage interactions within a single host. What would the impact of such interactions for the re-infected individual be? Furthermore, assuming similar interactions occurred in human malaria, what would their influence at the population-level in regions where transmission rates impose Plasmodium re-infection be?*

Not much research has been done on the interactions of the two stages of Plasmodium *infection occurring within the mammalian host, although one early attempt of addressing this question was initiated in 1939 in a human study [224]. Later, while one mouse study proposes the existence of cross stage protection of blood over liver stage, without existing concomitant infection [169],*

a distinct study indicates that Plasmodium *blood stage infection has an immuno-suppressive effect over the establishment of CD8 mediated immunity against sporozoite infection in mice immunized with irradiated sporozoites [189]. Also, a previous report observes the influence of blood stage* Plasmodium *on sporozoite infection of mouse primary hepatocytes* in vitro *[209].*
Facing the limitation of few publications of previous related work, the present thesis attempted to discuss the obtained results in the light of numerous observations made for each of the two independent stages of Plasmodium *infection.*

Malaria Superinfections. In its endemic settings, *Plasmodium* may often co-exist with other pathogens within the same host. Different pathogens can lead to different outcomes of plasmodial infection, some being part of an antagonistic and others a synergistic interaction with *Plasmodium* (reviewed in [225]). Nevertheless, in regions of high malaria endemicity, a very likely co-infection is unquestionably malaria.
Several reports of *Plasmodium* superinfection describe single individuals hosting more than one *Plasmodium* species, or different genotypes of the same *Plasmodium* species infecting RBCs [177-179]. These mixed infections can be originated from a single infectious bite from one mosquito infected with more than one *Plasmodium* species or genotype, or from consecutive infectious bites [226]. Still, it is well established that superinfection occurs more often in areas of high transmission and, generaly superinfections are more frequently seen in older children that in younger ones [175,181-183].
A number of studies focusing on mixed *Plasmodium* infections, both in human populations and rodent models often present ambiguous results [179]. Nonetheless, common themes discussed are the suppression of mixed infections where one blood parasite will prevail over the others, the oscillatory peaks of infection with no coincidance of the species, or the

general proposal that *P. vivax* helps reduce the severity of *P. falciparum* malaria [179,227,228]. Indeed, until now, studies concerning superinfection have concentrated on interactions between different genotypes or species of *Plasmodium* infecting RBCs. The fact is, however, that in an endemic area any infection starts by an infectious bite, which likely often occurs in individuals already bearing *Plasmodium* blood stage parasites from a previous infection. This event presents an opportunity for interactions between the two stages of *Plasmodium,* inside the same host.

Observations. In order to distinguish *Plasmodium* blood and liver stage parasites, in a single mouse we made use of parasites genetically tagged with GFP or luciferase expression for the sporozoite secondary infection and non-tagged parasites for the primary blood infection.

The present thesis shows that the presence of *Plasmodium* peripheral blood parasitaemia above a certain threshold protects mice from secondary liver infection. Regardless of whether blood stage infection was initiated by blood transfusion or by mosquito bite, a reduction in liver stage infection was always observed in re-infected mice. Regardless of the strain or species of *Plasmodium* used for primary infection, secondary sporozoite infection was always impaired in the liver. Furthermore, this impaired secondary liver infection never produced visible peripheral blood parasitemia, again regardless of the species of *Plasmodium* used for secondary infection and of the number of sporozoites inoculated, either by mosquito bites or through intra-venous injection. These results prompted a number of questions concerning the mechanism leading to this inhibition and its consequences for the individual and the population.

More specific investigations of the phenotype revealed that both the number and the size of the developing liver stages or EEFs were decreased in re-infected mouse livers. The reduction of secondary liver infection was

also dependent on the presence of iRBCs at the time of re-infection. Clearance of RBCs with an anti-malarial drug prior to re-infection abolished the impairment of secondary infection. Moreover, the decrease in liver parasite load was consistently observed from the third day post-blood stage infection, in spite of differences in peripheral blood parasitaemia, indicating that the reduction mechanism was initiated beyond a threshold of iRBCs that was rapidly achieved after primary blood infection.

Quorum sensing and bacteria. Host-pathogen interactions have evolved towards a balance between the roles of both elements that, ideally, ensures the survival of the host and the successful transmission of the pathogen. Many relevant findings on host-pathogen interactions have been obtained for bacterial infections, and host factors were shown to be significant in controlling infections [229,230]. Moreover, bacteria are capable of monitoring their own population by a process called *quorum sensing* through which their density is maintained below potential harmful levels. The same mechanism can be used to control competing bacterial infections in the same host and so protect its niche and ensure transmission. Bacteria sense the accumulation of specific molecules in the environment that increase in the surroundings as their density grows. Beyond a certain threshold, individual bacteria will sense these molecules and trigger gene expression accordingly, promoting a concerted group response through several distinct strategies that include biofilm formation, secretion of virulence factors, motility, conjugation, sporulation, and bioluminescence expression, among others (reviewed in [231-233]).

Could the interaction between *Plasmodium* blood and liver stages be mediated by a quorum sensing-like mechanism? The data presented in this thesis shows that the presence of *Plasmodium* peripheral blood

parasitaemia above a certain threshold protects mice from secondary liver infections in a parasite-dependent fashion. Thus, in a process somewhat akin to *quorum sensing*, liver stage parasites could be responding to molecules released by *Plasmodium* iRBCs and thereby aborting their development. However, the involvement of a possible soluble factor secreted by the blood stage parasites was discarded, as infection of both mouse primary hepatocytes and hepatoma cells by *Plasmodium* sporozoites was not affected when they were co-cultured with iRBCs. Additionally, and contrary to a previous report [209], sporozoite infection was repeatedly found to be similar in primary hepatocytes isolated either from blood-infected or naïve mice, indicating that possible alterations occurring in hepatocytes during blood stage infection reverted when these primary cells were cultured *ex vivo*.

Nevertheless, the complete rejection of the hypothesis that the observed impairment in *Plasmodium* liver infection by malaria blood stage is due to a released molecule by iRBCs is more complex than can be shown by co-culture experiments. *Plasmodium* asexual replication inside the RBC leads to important changes in its shape and content, promoting secretion of a vast array of molecules and iRBC adhesion to the vasculature of certain organs, including the liver [234,235]. Thus, one could hypothesize that the constant secretion of certain molecules would be necessary for the observed protective effect. These molecules might exist in the circulating serum or be concentrated in certain areas of circulatory system, where iRBCs sequester. Still, during the course of this work, several serum transfer experiments were performed under various conditions without ever recapitulating the reduction in infection observed in re-infected mice. Altogether, the present data seems to exclude that a soluble factor released by iRBCs acts directly on hepatocytes preventing full development of sporozoite liver infection.

Liver gene expression during *Plasmodium* blood infection. Since secreted parasite molecules appear not to be directly involved in reduction of liver infection, host molecules were then investigated. Examining the differences in liver transcription between naïve mice (NI), sporozoite infected mice (LS), mice carrying a blood stage infection alone (BS) or after secondary sporozoite infection (Reinf) by genome wide microarray analysis, most of the 1704 transcripts identified were found similarly differentially expressed between the BS and the Reinf groups, while only a limited number of genes were differentially expressed in the LS group. Gene ontology enrichment analysis highlighted immune system processes as up-regulated in both BS and Reinf, while genes involved in oxidation-redox were down-regulated in those two groups. Moreover, genes specifically over-expressed in Reinf appear predominantly to play a role in defence response and TNF regulation. Altogether, this analysis showed that major host alterations occur in gene expression in the liver during malaria blood stage infection.

It is possible that the observed alterations concur to explain the impairment of *Plasmodium* liver stage during an ongoing blood stage infection. However, testing synergies would be complex. Nevertheless inflammation, immune, apoptotic and metabolic genes were found to be differentially expressed in mice with an ongoing blood stage infection, recapitulating numerous previous studies where host responses to *Plasmodium* blood infection have been described (reviewed in [159,210,236-238]).

Immunity. Protection from infection is consensually attributed to immunity, and malaria is not an exception, with strong clinical evidence that *Plasmodium* infections are fought by the immune system. Through different cellular populations and by action of cytokines and chemokines produced by immune cells, the *Plasmodium* host can reduce and even neutralize

infection [159,238,239]. Also, *Plasmodium* is known to manipulate host immunity for its own benefit or to circumvent its actions [240] and thereby prevent its own annihilation, evidencing an extreme adaptation to its host [10]. Hence, part of this work aimed at establishing what the role would be, if any, of immune factors in the observed protection. To that end, we used the presented microarray analysis, which showed great alterations occurring in immunity during blood stage malaria infection, to select the best candidates to be tested.

Infection of erythrocytes by *Plasmodium* parasites is known to have repercussions in several of the host's organs. Bone marrow, spleen, brain, placenta and lungs show cytokine and chemokine enhancement of infiltrates, composed of macrophages, neutrophils, natural killer (NK) cells, gamma/delta (γδ) T cells and both CD4(+) and CD8(+) effector T cells. These changes lead to local vascular and organ disturbances showing that, in addition to parasite-mediated pathology, the host inflammatory response contributes to the development of disease (reviewed in [241]). In addition, the liver is strongly affected by blood stage malaria. The liver is known to enlarge and accumulate hemozoin pigment during *Plasmodium* infection, and it has been reported that it plays an active role in controlling blood-stage infection, as a site of parasite destruction [242]. Also, several cellular changes occur in the liver during blood-stage infection. The livers of *Plasmodium* blood stage-infected mice are characterised by increased numbers of lymphocytes, blasts, monocytes and granulocytes, as well as an increase in cell numbers in the sinusoids and periportal region specifically, completely modifying the architecture of the liver, as we too observed. Additionally, these livers present an increase on both numbers of liver macrophages and their phosphatase activity [234].

Hypothesizing that impaired liver stage development of re-infected mice could be caused by a blood stage-initiated immune response, several

features of the immune system were tested in an attempt to identify any involved.

The protection of re-infected mice was observed to be acquired very rapidly. Protection is achieved in just three days, and the level of protection is maintained, independently of the increasing parasitaemia and time of exposure to blood stage infection. This rapid effect implies that the involvement of the adaptive immunity in the observed protection is unlikely, as production of antibodies or of effector T cells would not be possible in such a short period of time. Furthermore, protection is also quite transient, disappearing straight away after clearance with anti-malarial drugs. Still, the involvement of the adaptive immune system in reducing secondary liver infection was assessed using splenectomised mice, and mice deficient for B and T cells. Expectedly, these experiments provided no support for any role of adaptive immunity in the phenotype observed; re-infected mice were protected from secondary infection regardless of surgery or adaptive immune cell deficiency.

The inflammatory response and the innate immune system were targeted using either genetically deficient mice, depletion methods and/or drug treatments. The results from such experiments show that the impairment of *Plasmodium* liver infection was independent of Kupffer cells and macrophages in the liver, NK or γδ T cells; IFN-γ, TNF-α, NOS, IL-10, IL-6, TLR/MyD88 signalling; the complement system or mastocytes. All the experiments performed, testing a range of immune mediators, provided no support for a role of features of innate immunity or inflammation to the phenotype observed.

Co-operation and redundancy among the innate germline and its encoded receptors allow synergistic responses to infection, allowing appropriate defences against microbes and protecting the host against immune evasion by parasites [243]. Still, it is hard to consider that impairment of liver stage

infection would be under such a synergistic process that would never even produce an intermediate phenotype in at least some of the mouse lines tested, which exhibited deficiency in more than one cellular population (e.g. RAGII/γc mice lack T and B cells as well as NK cells and as such produce very low levels of certain cytokines including IFN-γ).

Host cell survival. Developing sporozoites in the liver are known to modulate cell death of infected hepatocytes. Initially during early development, parasites inhibit apoptosis [244], and later, to egress and colonize the blood, EEFs promote cell death to ease their way out of the hepatocyte [245]. It is also known that *Plasmodium* blood stages increase apoptosis in the liver [210]. Accordingly, the microarray data showed a robust pro-apoptotic stimulus in the livers of mice with an ongoing blood stage infection. This raised the question of whether alterations in the apoptotic status of the liver, due to the presence of blood infection, could impair secondary liver infection. Using caspase 3-deficent mice, we showed that malaria blood stage infection impaired *Plasmodium* liver stage even in the absence of a significantly increased level of apoptosis in the liver. Thus, hepatocyte apoptosis does not explain the observed protection. The stimulus reducing secondary liver infection seems to be stronger than that of caspase 3 deficiency allowing sporozoites to infect better due to the absence of apoptosis.

Nutrient depletion. Prevention from liver secondary infection could be promoted by the absence or deficiency of a nutrient resulting from the ongoing primary blood stage infection. The fact that not only the number, but also the size of EEFs was reduced in the presence of a *Plasmodium* blood infection suggests that some nutrient or growth factor could be limiting *Plasmodium* development in hepatocytes.

The extensive *Plasmodium* proliferation rate inside hepatocytes certainly requires the availability of nutrients for its metabolism and growth, besides sufficient lipids for the synthesis of the large amounts of membranes that must surround the newly formed merozoites at the end of liver stage development. Thus, it was hypothesized that altered nutrient resources in hepatocytes during blood stage infection could be responsible for the impairment of EEF development. Malaria blood stage infection would cause the removal of resources that would in turn impair survival or replication of *Plasmodium* in the liver.

As previously stated, in the enrichment analysis of the microarray data several clusters of differentially expressed genes stood out related to immunity and defence mechanisms. To a lesser extent, metabolic processes, such as the carboxylic acid metabolic process, were highlighted too. In addition, numerous genes involved in metabolic processes were found differentially expressed. These include over 40 genes concerning iron homeostasis and almost 80 genes related with lipid metabolism.

It is known that malaria patients exhibit significant lipid profile abnormalities, such as decreased total cholesterol levels, decreased low (LDL) and high (HDL) density lipoprotein-cholesterol, elevated lactate dehydrogenase, and moderately elevated triglycerides [236,237], strongly suggesting lipid metabolism alterations, possibly caused by malaria blood stage infection. However, what was observed during the course of this work was that the low parasitaemias that were able to induce protection against secondary sporozoite infection produced no changes in cholesterolemia (including LDL-cholesterol and HDL-cholesterol levels), in the serum or in the liver of blood stage-infected mice.

Nevertheless, the possibility that alterations in lipid metabolism during blood stage infection might limit to a certain extent the development of EEFs could not be completely ruled out. More complex experiments would

be needed to verify the involvement of other lipid-related molecules. For instance, transplanting livers from blood-infected to naïve mice just prior to sporozoite infection would theoretically be ideal. Of course other consequences would arise from such an experiment; for example, the inflammatory response associated to the transplant technique could easily mask the object of the experiment.

Iron has received great interest as a nutrient that is vital for pathogen infection of development inside cells (reviewed in [246]). Moreover, a recent clinical trial or iron supplementation to children bellow 5 years of age showed a statistically significant increase in the number of malaria infections in those receiving iron [220]. This observation can be attributed to the known effect of iron on iRBCs [215], but a possible effect on the liver stage of infection cannot be excluded.

Regarding iron related genes that were found altered in the microarray analysis, one stood out for its key role in iron homeostasis. *Hamp1* encodes for hepcidin, a peptide hormone produced in the liver that represents the master regulator of iron homeostasis in humans and other mammals [247].

When hepcidin levels in primarily or secondarily sporozoite-infected mice were analysed, a strong correlation was observed between hepcidin expression in the liver during the blood-stage and protection from secondary liver infection. The increase in hepcidin was shown to be tightly dependent on the presence of iRBCs, promptly raising its levels after a few division cycles of *Plasmodium* in the blood, and being immediately reversed to normal levels after treatment of infected mice with an anti-malarial drug, thereby allowing liver stage infection to grow. Hepcidin was therefore investigated in greater detail as a candidate for explaining the reduced liver infection in re-infected mice.

Hepcidin regulates iron homeostasis by triggering the degradation of the iron exporter protein ferroportin, which is strongly expressed by

enterocytes and macrophages and to a lesser extent, hepatocytes [213,214]. An increase in hepcidin levels therefore inhibits iron uptake through duodenal enterocytes and leads to iron redistribution into macrophages, consequently promoting relative iron depletion in hepatocytes.

Connections between iron availability and *Plasmodium* infection of both red blood cells [215] and hepatocytes [216-218] have previously been reported. This was also observed *in vitro* and *in vivo* for the work gathered in this thesis. Reducing iron availability with iron chelators led to a significant and dose-dependent reduction of *Plasmodium* EEF development whereas iron supplementation increased EEF development. This indicates that if blood stage infection is indeed reducing iron availability inside hepatocytes, than this reduction could account for the reduced liver infection of re-infected mice, and the whole mechanism could be mediated by *hamp* upregulation in the liver.

Liver staining of re-infected mice for ferritin chains, the major intracellular iron storage protein, showed noticeable redistribution of iron to reticuloendothelial cells, consistent with hepcidin activity [214]. Moreover, it was found that increased *hamp* expression during blood stage infection re-distributes iron, promoting its sequestration inside macrophages in the liver and in the spleen. In addition, the level of iron in hepatocytes of blood-infected mice was shown to be reduced, as hipothesized.

Interestingly, a recently performed microarray analysis was consistent with iron availability being important in *Plasmodium* liver stage infection. In *Plasmodium*-infected hepatoma cells, while the expression of the iron exporter protein ferroportin, which is degraded by hepcidin, was significantly reduced, that of the iron receptor DMT1 was significantly increased [66], suggesting that iron acquisition and retention might be important for complete *Plasmodium* development inside its host cells, and manipulated by the infecting liver stage parasite, possibly to potentiate its

resources. This work proposes, on the other hand, that during a blood stage infection liver parasites are no longer able to modulate the iron exporter and receptor due to the presence of a much stronger stimulus induced by the iRBCs. Even only three days post-blood stage infection, hepcidin mRNA levels in the liver are already quite high, so the level of iron in circulation should already be low, promoting depletion of iron from hepatocytes.

Nevertheless, if hepcidin is to be attributed the functional role of decreasing liver infection in re-infected mice, it should affect liver stage infection when introduced in the absence of a blood stage infection. Crucially, hepcidin introduced into mice by administration of *hamp*-expressing adenovirus, prior to sporozoite infection, could alone significantly reduce liver stage infection. This demonstrated that sporozoite infection is impaired by an increase in the iron regulatory hormone, to the same extent that limiting infection through iron negative regulation in hepatocytes was proven in this study and by previous work of others [216]. Thus, increased hepcidin alone is sufficient to protect against the liver stage, even in the absence of the blood stage infection.

Altogether, the presented data showed that an ongoing blood stage infection leads to a rapid increase in liver hepcidin levels, which resultes in a redistribution of iron in infected mice. This limits iron availability in hepatocytes necessary for *Plasmodium* EEF development/replication inside hepatocytes, preventing EEFs from fully developing and therefore preventing the release of new merozoites into the blood-stream, thereby interrupting the cycle of secondary infection and preventing superinfection.

***Plasmodium* co-infection with other pathogens.** In *Plasmodium* endemic areas, people often bear more than one infectious agent at a given time [248]. In order to determine whether other pathogens would lead to similar results as those observed for *Plasmodium* blood stage infection, we used

Toxoplasma, an apicomplexan parasite closely related to *Plasmodium*, for the primary infection.

When challenging mice bearing an infection with *Toxoplasma gondii* tachizoites with *Plasmodium* sporozoites, in parallel with *Plasmodium*-infected mice and compared with control naïve mice we monitored the effect of this other parasite on liver stage malaria infection. Indeed, mice with an ongoing *Toxoplasma* infection exhibited the same level of protection as *Plasmodium* iRBC-infected ones. This result provides evidence that our observation of impaired liver stage development is not genus specific, but rather consistent with induction of hepcidin. Mice infected with *Toxoplasma* show an increase in hepcidin expression in the liver to a similar extent as that observed on *Plasmodium*-infected mice. Iron redistribution should therefore happen for the *Toxoplasma* infection similarly to what was observed for the *Plasmodium* blood stage.

It is likely that some, but not all, infections have a similar effect on establishment and development of secondary liver infection as long as the primary infection leads to an increase of hepcidin expression. However, some pathogens, such as Hepatitis C virus (HCV), are known to suppress hepcidin [249-251]. A non-hepcidin inducing pathogen would be ideal to test and use as a negative control in our study. Murine models for HCV would be of useful to clarify the impact on a non-hepcidin increasing infection over a secondary *Plasmodium* sporozoite infection; unfortunately they are not currently available.

We hypothesize that different outcomes may arise depending on how much hepcidin is induced by any particular type of infection, and/or by the balance of hepcidin induction *versus* other influencing factors. Co-infections probably do not all have the identical effects and, moreover, in regions where malaria is endemic, one of the most likely co-infections is actually malaria itself.

Outcome for the individual. The scenario of secondary malaria challenges in individuals already harbouring blood-stage infections, modelled using a murine system in this thesis, must frequently occur in malaria endemic populations. If the findings for the mouse model were extended to human malaria, would be expected that new liver infections initiated during previous blood ones would be interrupted prompting protection from superinfection. This should prevent infected people with peripheral blood parasitaemias above a certain threshold from having a second circulating parasite to combat. Furthermore, abrogating competition between two *Plasmodium* blood stages sharing the same host, primary *Plasmodium* in the blood protects its niche and tries to ensure transmission to the next infection on a *first come, first served* basis. Or if any merozoite reaches the bloodstream it does so in such a low number or viability status that is never able to compete with the already settled iRBCs population. The host immune system will then have to fight only one circulating parasite, raising its chances of eliminating the circulating iRBCs and clearing infection, thereby increasing its chances of survival. Moreover, it avoids competition between two different parasites in the blood, promoting transmission of the first colonizer. Both host and pathogen gain from the interaction, only the third part, the secondary liver infection is condemned not to succeed.

The speculation that peripheral blood parasitaemia above a threshold prevents successful re-infections and thus superinfection is not in disagreement with the numerous observations of people bearing mixed plasmodium infections, as in humans the liver stage development takes around a week and early very low levels of parasitaemia should not affect secondary liver infections, giving plenty of time for successful re-infcetions to occur and thus promote the observed superinfections.

P. falciparum iRBCs were shown in the work of others to raise hepcidin levels in the urine and serum of naturally and experimentally *Plasmodium* infected humans [212,252,253] and to uphold hepcidin *mRNA* induction in human leukocytes *in vitro* [211]. Therefore, a possible side effect of increased levels of hepcidin induced by blood stage malaria infection could be a significant contribution to acute anaemia associated with clinical malaria and the chronic decrease in haemoglobin levels that occur in individuals living in malaria endemic areas [211,212].

Iron is also known to influence immunity. Specifically, some cells involved in innate immunity have been described to be iron-modulated in the presence of infections, and hepcidin has been implicated in several proposed mechanisms (reviewed in [254]). Therefore, it is tempting to speculate that the effect observed is induced by hepcidin, as demonstrated in the results presented during this work, still without totally excluding some possible involvement of immune response that could also be responding to iron restrictions, although we could not, during this work, demonstrate any role of immune cells in the observed reduction.

Outcome in populations. Re-infections occurring during ongoing blood stage malaria are certainly frequent in endemic settings for *Plasmodium*. Mouse models, although not perfect, have been extensively used in *Plasmodium* research producing a great deal of important discoveries. If it is assumed that the observations produced in this work and presented in this thesis can be extrapolated to what occurs in human malaria, several questions and hypotheses regarding the possible implications of these findings for endemic populations can be raised.

Epidemiological studies from highly endemic areas consistently show that the incidence of infection first increases with age in young children before it declines later presumably as a result of acquired immunity (e.g. [175,183]). At

the same time, the complexity of infection, expressed by the average number of clones per infection, also increases as hosts get older [175,181-183]. Although well known, these facts were never completely elucidated or justified. A previous attempt to explain these observations relied on an apparent biting preference of mosquitoes towards older individuals, where the risk factor would be the increase in body area exposed to anopheline biting as children grow older [219].

The model proposed in this work to explain the same epidemiological observations provides a more parsimonious solution, depending only on the threshold density-dependent inhibitory effect reported here. A simple agent-based model was devised to simulate infection histories in a number of individuals, which were followed over time whilst recording the average annual infection rates as well as the number of co-infecting clones to enable comparison with the well known epidemiological data.

Based on several epidemiological observations, the model assumes that the average parasite density per infection decreases with age [175,181,205]. The probability of an infectious bite leading to a new infection then depends on the level of a current blood-stage infection as well as the host's infection history. Under these minimal assumptions the model correctly predicts an initial increase in infection rates, which subsequently declines as individuals acquire immune protection through repeated exposure, fitting to the expected curves previously observed in several endemic regions. As a result of a higher risk of infection and reduced inhibitory effect in older individuals, the model also predicted an increase in the multiplicity of infection with age, as is observed in endemic sites.

The model was tested under various assumptions regarding the relationship between ongoing blood-stage infection and the probability of superinfection, and was found that no other inhibitory effect, including acquired immunity or premunition could explain the observed data as the

threshold density-dependent inhibitory effect does. Altogether, this means that threshold density-dependent inhibition of new liver stage infections alone can account for the increase in infection risk and complexity of infections in young individuals. Crucially, the results show that this effect is strongly dependent on the transmission intensity and most prominently observed under moderate to high transmission settings, and this too fits malaria field data. Our findings therefore provide an explanation for some of the differences in age-dependent risk of infection within the endemicity spectrum.

This is of particular importance in the first years of age and then might fade away as parasitaemias decline below a certain threshold, allowing superinfection to happen more frequently later in life when adaptive immunity or premunition conferred by a number of infections should already protect the young, at least from severe forms of disease. Indeed, besides knowing that superinfection varies throughout the age of individuals in a population [175,181-183], it has been reported that superinfections have been much more frequently observed among asymptomatic carriers who exhibit lower peripheral blood parasitaemias than in clinical cases [180], and are thus probably below the threshold of protection.

Re-infection of blood-infected individuals is of course much more probable in areas where transmission is medium to high, and in these settings people are known to acquire immunity faster that in areas where transmission rates are low [151,152]. In the light of the present work is tempting to speculate that re-infection too can play a role in naturally acquired immunity.

Naturally acquired immunity to malaria has been largely debated and described for almost one hundred years. It is known that it is dependent on constant exposure to *Plasmodium* and on the degree of exposure. Still the re-infection situation and the great impact that an ongoing blood stage

infection has on a subsequent sporozoite infection has never been taken in consideration to assist explaining it. Developmental problems in EEF growth of re-infected individual might naturally be acting as a live attenuated vaccine, promoting protection in endemic populations. Also, the number of liver infections would be higher than the number of episodes of blood stage infection, possibly explaining why high *Plasmodium* transmission rates associate with faster acquisition of immunity and partial protection from severe disease.

Furthermore, one of the previous studies showing interaction between blood and liver stages presents the possibility that blood stages might suppress immune responses [189]. This result is not in disagreement with the work presented in this thesis, as we show no striking involvement of immune cells in reducing liver infection. Nevertheless, we do not know what would happen after several infections, when acquired immunity would play a stronger role and a possible different interaction could happen between these two stages of *Plasmodium* infection.

The sophisticated lifecycle of *Plasmodium* has resulted from millions of years of parasite/host co-evolution and communication, having broad implications for evolution and human health. Above a critical threshold, *Plasmodium* infection of red blood cells leads to an increase in the level of the host hormone hepcidin, which, by re-distributing iron, protects the parasite niche (and thus the host) from the risk of superinfection. This phenomenon, which acts independently of and in addition to acquired immunity, explains previous epidemiological observations and has important implications for future anti-malarial interventions.

The old concern remains of whether reducing the risk of *Plasmodium* infection will always lead to a decrease in the threat of severe malaria throughout life [187]. Would decreasing the possibility of re-infections in an

endemic area solely favour the community, or would potentially harmful consequences arise from interventions that, rather than eliminating transmission, would decrease it to levels where protection induced by re-infections would no longer exist? It is still not totally clear, but results from the trial of the pre-erythrocytic vaccine trial, RTS,S provide evidence that reducing *Plasmodium* liver load in children led to a significant decrease in severity of disease [223].

Further work towards fully understanding associations between transmission and immunity will be of major importance in defining malaria control interventions and prediction of their outcome over time.

To conclude, during this work a new interaction between Plasmodium *blood and liver stages and its shared host has been identified. Bearing a malaria blood stage infection above a certain threshold prevents the appearance of a* de novo *infection in mice.* Plasmodium *liver stage is impaired and the new infection does not compete for blood infection.*

Our observation that infection of RBCs by Plasmodium *impairs the parasite development inside hepatocytes, mediated by iron deficiency is,* per se*, a significant contribution to understanding the dynamics of acquired protection against malaria infection. Increasing our knowledge of the molecular mechanisms behind the achieved protection in endemic settings will help to better design actions and predict the outcomes from such interventions. .*

The next in line

The work presented in this thesis showed for the first time the impairment that an ongoing Plasmodium *blood stage infection imposes on a secondary liver infection. Besides being an interesting observation on its own and having possible implications on malaria interventions in the field should the same be proved for human* Plasmodium *infection, the results gathered here pave the way for future lines of work, as new questions arise.*

One of the questions raised during the course of this work concerns quorum sensing mechanisms. Would another of its kind impair a sporozoite infection? Liver infection in humans lasts for 5 to 13 days [58], and in highly endemic areas an infected person is likely to be secondarily infected. Although the murine model offers a liver infection of solely 48h, the re-infection scheme could still be attempted. Using once more parasites tagged with different markers, we could observe what effect, if any, would an ongoing liver stage have on a secondary one. While no significant alteration was found in hepcidin expressions levels, in a recently performed microarray analysis in *Plasmodium*-infected hepatoma cells, the expression of the iron exporter protein ferroportin, which is degraded by hepcidin, was significantly reduced and that of the iron receptor DMT1 was significantly increased [66]. This suggests that iron acquisition and retention are manipulated by the infecting liver stage parasite, possibly to potentiate its resources. Therefore, it would be interesting to investigate whether any interactions would arise between competing liver forms and to what extent the mechanisms observed during the work in this thesis would be important for any possible interaction.

On the parasite side, it would be interesting to investigate how iron is required for *Plasmodium* metabolism. In studies with bacteria, iron has been

identified to work as a co-factor for several enzymes (reviewed in[246]). During *Plasmodium* infection, iron has been shown to be of relevance during the blood stage of infection in its iron-sulfur cluster form [255]. Numerous proteins that are central to several cellular processes, such as redox-actions, metabolic catalysis, and sensing of iron and oxygen levels, use these clusters as co-factors. The Apicoplast genome has been involved in assembly of such clusters, but not much is known regarding where the iron-sulfur clusters are used or if they are exported to the RBC cytoplasm or surface. Also during the blood stage of infection, iron is intimately connected to *Plasmodium* through the vast haemoglobin degradation. However, the haemoglobin-derived iron seems not to be required for the parasite heame synthesis (reviewed in [256]).

Not much information is available on the literature regarding the requirements of iron during liver stage infection, although a transcriptome analysis points that iron-sulphur subunit of succinate dehydrogenase is upregulated in sporozoites [257]. Understanding the pathways through which *Plasmodium* utilises iron could provide a basis for testing new prophylactic actions to combat malaria prior to its symptoms or to its radical cure, including combating hypnozoites.

On a different perspective of blood and liver stage interactions within a single host, we preliminarily observed that not only the blood primary infection has an effect on secondary liver challenge, but also the challenge produces alterations on the course of the primary blood infection. Indeed, some experiments were performed in which blood parasitemia from primary infection was followed, in an attempt to identify iRBCs originated from the secondary infection. Although secondary parasitaemia was not detected, we have observed that, in a few situations, primary blood infections were prevented from increasing after the mice were challenged

with sporozoites. Parasitaemias from the primary infection were found to decrease over time until mice fully cleared iRBCs. This result seemed to depend on the level of primary parasitemia at the time of re-infection, probably because the path towards hyper-parasitemia and death could no longer be interrupted if re-infection happened at already high primary parasitaemias. The inter-stage interactions between blood and liver *Plasmodium* within a single host could therefore continue to be studied and provide possible new insights concerning malaria transmission dynamics and disease protection in endemic settings.

Appendix

table S1. Differentially expressed (DE) transcripts organised as toptable (sorted by log odds that a transcript is DE = B column). Cluster Nb corresponds to the clusters found in the non-hierarchical clustering and used for GO enrichment analysis. GO annotation for each transcript is also added, as well as if the transcript detected is a full length or partial or even if it's an EST (expressed sequence tag). All trancripts are signiIicant at p.value adjusted for multiple testing $p<0.05$. Transcript Cluster ID is the Affymetrix accession number. logFC is the log base of the fold change. Grey highlighted rows correspond to genes mentioned in the text.

Affymetrix ID	BS/Non Inf.		LS/Non Inf.		RelNF/Non Inf.		Average	Cluster	Gene	Gene	Gene Ontology (GO)	Transcript
Transcript	logFC	B	logFC	B	logFC	B	expression	Number	Symbol	Title	Description	Classification
10345436	-0,488662795	-6,097090524	-0,825587163	-3,532697959	-1,076411999	-3,117384936	6,217143022		LOC280487	pol polyprotein	---	partial
10345675	-0,601415904	-4,795082462	0,35401	-5,448006231	-1,400368093	0,620039438	5,596311087		Npas2	neuronal PAS domain protein 2	two-component sensor activity /// two-component	full-length
10345762	0,458723039	-6,626551458	0,596520253	-5,34801059	1,502116908	-2,596326751	9,483007998	Cluster II	Il1r1	interleukin 1 receptor, type I	signal transducer activity /// receptor activity ///	full-length
10345824	1,568464859	4,074662933	0,265663926	-5,607002262	1,295822929	1,686074687	5,127333798	Cluster I	Il18rap	interleukin 18 receptor accessory	receptor activity /// transmembrane receptor	full-length
10346168	1,528045861	8,174531437	-0,201671997	-5,425216669	1,529619231	7,753375662	4,854649429		Stat4	signal transducer and activator of	DNA binding /// transcription factor activity ///	full-length
10346191	2,245572797	11,23540134	1,660163087	7,406066781	2,746698753	13,22610923	10,57502395	Cluster VI	Stat1	signal transducer and activator of	DNA binding /// transcription factor activity ///	full-length
10346222	-0,488662795	-6,097090524	-0,825587163	-3,532697959	-1,076411999	-3,117384936	6,217143022		LOC280487	pol polyprotein	---	partial
10346365	1,238860264	-0,384631353	0,009722207	-6,39106834	0,658326799	-4,736829807	4,835880402	Cluster III	Sgol2	shugoshin-like 2 (S. pombe)	chromosome, centromeric region /// condensed	full-length
10346410	-1,305856453	1,39552679	-0,106658749	-6,27740713	-1,639414101	3,314302862	11,56194851		Aox3	aldehyde oxidase 3	aldehyde oxidase activity /// electron carrier	full-length
10346783	1,116786756	0,770029106	0,124253399	-6,206669298	1,164535111	0,791102651	5,177951702		Cd28	CD28 antigen	positive regulation of inflammatory response to	full-length
10346799	1,244777455	5,865333743	-0,020208044	-6,381216662	1,316080191	6,070957486	5,841575758		Icos	inducible T-cell co-stimulator	protein binding /// integral to plasma membrane ///	full-length
10347222	1,009351426	1,168341395	0,326829754	-4,859414166	0,924341947	-0,013352143	8,293681242		---	---	---	est
10347277	-1,090022407	-0,823040232	-0,184213474	-6,096532361	-2,386674567	6,773248621	10,61137768		Igfbp2	insulin-like growth factor binding	regulation of cell growth /// insulin-like growth	full-length
10347291	0,684676664	-3,650414189	-0,094564517	-6,302858742	1,340719157	1,206746426	3,806800288		Il8rb	interleukin 8 receptor, beta	signal transducer activity /// receptor activity ///	full-length
10347335	2,278314362	14,57719563	0,422528475	-2,126773417	2,527775954	15,41483684	8,624475088		Slc11a1	solute carrier family 11 (proton-	transporter activity /// iron ion binding /// transport	full-length
10347928	1,356642952	7,36001555	0,234880094	-4,994067087	1,407440196	7,355674074	5,476680342		---	---	---	partial
10347933	1,560499279	6,143283378	0,187881662	-5,807803663	1,868274434	7,797119961	6,667701127		Sp140 ///	Sp140 nuclear body protein ///	zinc ion binding /// metal ion binding	full-length
10347948	0,918196146	1,354902028	0,505754699	-2,585760485	1,058910266	2,385416972	7,573024817		Sp100	nuclear antigen Sp100	DNA binding /// binding /// protein binding ///	full-length
10348244	1,738001686	9,469374676	0,004353374	-6,391323262	1,688241862	8,692895905	7,214365916	Cluster I	Inpp5d	inositol polyphosphate-5-	inositol or phosphatidylinositol phosphatase	full-length
10348702	-0,50596952	-4,628101337	-0,052503521	-6,357725144	-1,407190544	2,760263873	9,348201241	Cluster X	Agxt	alanine-glyoxylate	catalytic activity /// serine-pyruvate transaminase	full-length
10349661	1,680824552	5,144786193	0,344731087	-5,0546373	2,1352932	7,455580651	5,887134529		5430435G22Rik	RIKEN cDNA 5430435G22 gene	nucleotide binding /// GTP binding /// lysosome ///	full-length
10349968	1,427600734	-0,256316403	0,068122624	-6,364326118	2,314194199	4,136204015	5,932215742		Chi3l1	chitinase 3-like 1	catalytic activity /// hydrolase activity, hydrolyzing	full-length
10350136	1,561697103	8,093157466	-0,06927187	-6,276654408	1,507842033	7,249358357	8,901392019	Cluster I	Csrp1	cysteine and glycine-rich protein 1	protein binding /// nucleus /// zinc ion binding ///	full-length
10350247	1,080375795	1,055258105	0,454354862	-4,033226296	1,244611762	2,057660348	5,607917906		Kif21b	kinesin family member 21B	nucleotide binding /// motor activity /// microtubule	full-length
10350630	1,321470502	2,276906762	0,020093247	-6,387016139	0,848068004	-1,996823983	6,659460595	Cluster III	Fam129a	family with sequence similarity	negative regulation of protein amino acid	full-length
10350733	-0,014113415	-7,278357094	0,16497872	-6,177300387	-1,350982589	0,234568256	9,176120665		Rgs16	regulator of G-protein signaling 16	signal transducer activity /// GTPase activator	full-length
10350838	2,551290618	6,695762609	0,432454803	-5,179335221	2,393876047	5,539023704	7,445096409		2810417H13Rik	RIKEN cDNA 2810417H13 gene	nucleus /// mitochondrion	full-length
10351182	1,485107925	0,586966806	-0,100790127	-6,324957052	2,329459636	4,808263004	6,004016261		Sele	selectin, endothelial cell	binding /// protein binding /// sugar binding /// cell	full-length
10351197	2,334114146	7,154491617	-0,152993339	-6,179350612	2,888676791	9,229972691	6,692433976		Sell	selectin, lymphocyte	binding /// protein binding /// sugar binding ///	full-length
10351206	0,867361333	-1,321676529	0,069243969	-6,332462495	1,370177033	2,501456826	5,60655358	Cluster IV	Selp	selectin, platelet	glycoprotein binding /// binding /// protein binding	full-length
10351293	-0,751052198	-1,808340459	-0,493701816	-3,56027995	-1,287103194	2,689000294	6,018635441		Dpt	dermatopontin	protein binding /// extracellular region ///	full-length
10351380	0,892956567	-1,943854175	-0,269983577	-5,703569557	2,049555665	5,672559586	7,378538886		Ildr2	immunoglobulin-like domain	---	full-length
10351477	1,186634491	-0,272682983	-0,142762829	-6,219802944	1,242948217	-0,218601857	4,006053373	Cluster I	Sh2d1b1	SH2 domain protein 1B1	phosphotyrosine binding /// natural killer cell	full-length
10351509	2,841819489	15,45932015	0,441521476	-2,71974558	3,075590109	16,01124046	8,983862863		Fcgr4	Fc receptor, IgG, low affinity IV	receptor activity /// integral to membrane	full-length
10351603	1,556326916	8,473372975	0,036801279	-6,356666839	1,567628491	8,125526096	6,86342467		Arhgap30	Rho GTPase activating protein 30	molecular_function /// GTPase activator activity ///	full-length
10351644	1,615634983	5,124579543	-0,060886902	-6,34198717	1,737446201	5,515617234	5,609582963		Cd244	CD244 natural killer cell receptor	receptor activity /// protein binding /// external side	full-length
10351658	2,522447918	13,90759518	-0,061766518	-6,298054647	2,512707559	13,46627181	7,006319409	Cluster VI	Cd48	CD48 antigen	protein binding /// plasma membrane /// signal	full-length
10351679	1,394320753	5,462182946	-0,139351858	-6,02873136	1,30283081	4,28572126	6,883782526		Cd84	CD84 antigen	receptor activity /// protein binding /// plasma	full-length
10351691	1,100684335	6,257330663	0,161952271	-5,52191284	0,960231284	4,301727566	4,757971483		Slamf6	SLAM family member 6	receptor activity /// plasma membrane /// integral to	full-length
10351792	1,561576307	10,34337334	0,258436141	-4,377862172	1,720155183	11,07417637	6,657600169		Slamf9	SLAM family member 9	membrane /// integral to membrane	full-length
10351825	1,811187972	10,84318358	-0,251028138	-4,801401858	1,721957093	9,813086611	7,474558649		Tagln2	transgelin 2	muscle development	full-length
10351867	1,072097677	3,083283713	-0,185203377	-5,708429779	0,982535182	1,793274685	5,170416975		Aim2	absent in melanoma 2	protein binding /// nucleus	full-length
10351873	2,28142115	6,700626036	1,029071192	-0,608596332	2,554497554	7,581962168	6,396509508		Pyhin1	pyrin and HIN domain family,	protein binding /// nucleus	full-length
10352344	-1,015213476	2,301230637	-0,448676484	-3,251060095	-2,205925589	10,6731044	8,451798175		---	---	---	predicted
10352439	-1,236846041	5,695558624	-0,092604521	-6,176952776	-1,567998449	8,006570776	6,38606834		Susd4	sushi domain containing 4	membrane /// integral to membrane	full-length
10352548	-0,919126119	0,551804675	-0,095255508	-6,238161762	-1,330436461	3,885246873	8,765617624		Slc30a10	solute carrier family 30, member	plasma membrane /// transport /// ion transport ///	full-length
10352709	1,188215565	0,683735867	-0,102366216	-6,282188557	0,613764117	-4,320271609	5,275984687	Cluster III	Nsl1	NSL1, MIND kinetochore complex	nucleus /// cell cycle /// chromosome segregation	full-length
10353181	-0,68800574	0,532026627	-0,134953538	-5,859787627	-1,547971544	8,910071712	10,62300121		Lactb2	lactamase, beta 2	mitochondrion /// zinc ion binding /// hydrolase	full-length
10353420	1,620406997	3,571632592	0,060811008	-6,354586927	1,496507151	2,336163727	6,817711044		Mcm3	minichromosome maintenance	nucleotide binding /// DNA binding /// ATP binding	full-length
10354003	0,945108111	0,700823085	-0,025335671	-6,381057958	1,067995612	1,492002814	4,89286009		Mgat4a	mannoside	extracellular region /// Golgi apparatus ///	full-length
10354472	1,096688317	4,972609226	-0,320481857	-3,981673445	1,262847229	6,138668628	6,764435211		Gls	glutaminase	neurological control of breathing /// glutaminase	full-length
10354588	1,46491064	10,83786926	-0,317822901	-3,033637799	1,494521959	10,65226473	8,308846166		Stk17b	serine/threonine kinase 17b	nucleotide binding /// protein kinase activity ///	full-length
10354768	1,091393952	3,806670901	0,083653963	-6,231178029	0,815462021	0,486796789	7,973761064		Akr1b3	aldo-keto reductase family 1,	aldehyde reductase activity /// cytoplasm ///	full-length
10355162	1,152675424	1,960371794	0,247095105	-5,556749701	1,014798475	0,361323767	5,673447408		Plekhm3	pleckstrin homology domain	intracellular signaling cascade /// zinc ion binding	full-length
10356020	1,865246671	10,11537985	0,098354227	-6,164735859	1,659987366	8,300379508	6,989028641		Dock10	dedicator of cytokinesis 10	guanyl-nucleotide exchange factor activity /// Rho	full-length
10356082	0,553155346	-3,21849284	0,035106609	-6,369913882	1,099866905	2,08600168	8,757588006	Cluster IV	Plscr1	phospholipid scramblase 1	calcium ion binding /// response to virus ///	full-length
10356248	0,869490439	8,300054267	0,169772364	-4,402490107	1,076243774	10,4037186	4,76004335		C130026I21Rik	RIKEN cDNA C130026I21 gene ///	---	full-length
10356269	0,923575905	-2,532104671	0,075702059	-6,346734144	1,195167635	-0,896646034	6,380586917		A530032D15Rik	RIKEN cDNA A530032D15Rik	---	full-length
10356278	1,135509064	8,92492463	0,256884186	-3,612150977	1,427116847	11,22217422	6,950308132	Cluster IV	Sp110 ///	Sp110 nuclear body protein ///	DNA binding /// binding /// nucleus /// transcription	full-length
10356293	1,29886182	8,832593564	0,40383995	-1,926843486	1,257892917	8,021437883	5,615639076		A630001G21Rik	RIKEN cDNA A630001G21 gene	---	full-length
10356593	-1,108556479	3,457428402	-0,155972915	-5,897857779	-1,477516015	6,219126636	7,862908758		Hes6	hairy and enhancer of split 6	DNA binding /// transcription factor activity ///	full-length
10356762	-0,488662795	-6,097090524	-0,825587163	-3,532697959	-1,076411999	-3,117384936	6,217143022		100043821 ///	predicted gene, 100043821 ///	---	est
10357003	-0,381223971	-6,393638041	0,202990275	-6,134720024	-1,362877505	-0,696793284	6,758321153		Rnf152	ring finger protein 152	protein binding /// zinc ion binding /// metal ion	full-length
10357242	-0,549853945	-4,593855377	0,005344403	-6,391486617	-1,053276575	-0,696939613	11,7567844		Dbi	diazepam binding inhibitor	acyl-CoA binding /// binding /// mitochondrion ///	full-length
10357261	4,526537759	17,07484221	0,233843469	-5,700442254	4,310452098	16,17993199	9,380993706		Marco	macrophage receptor with	receptor activity /// scavenger receptor activity ///	full-length
10357298	-0,488662795	-6,097090524	-0,825587163	-3,532697959	-1,076411999	-3,117384936	6,217143022		100043821 ///	predicted gene, 100043821 ///	---	est
10357332	0,872655299	6,257582797	0,12059409	-5,618529154	1,034816739	7,802282788	10,28407466		Actr3	ARP3 actin-related protein 3	nucleotide binding /// actin binding /// protein	full-length

Affymetrix ID	BS/Non Inf.		LS/Non Inf.		ReINF/Non Inf.		Average	Cluster	Gene	Gene	Gene Ontology (GO)	Transcript
Transcript	logFC	B	logFC	B	logFC	B	expression	Number	Symbol	Title	Description	Classification
10357436	1,963521823	7,583204295	0,066898253	-6,329278606	1,761095853	5,895875753	7,150609625		Mcm6	minichromosome maintenance	nucleotide binding /// DNA binding /// DNA	full-length
10357472	1,269732834	8,768783458	-0,01878545	-6,377311439	2,039226378	13,99596486	6,988309214		Cxcr4	chemokine (C-X-C motif) receptor	patterning of blood vessels /// ameboidal cell	full-length
10357604	1,452698965	5,903257289	-0,016276289	-6,386718335	2,184763448	10,25673191	8,603072906		Ikbke	inhibitor of kappaB kinase epsilon	nucleotide binding /// protein kinase activity ///	full-length
10357875	1,820055808	0,11500494	0,274601404	-6,099217696	1,695533034	-0,845038051	6,818474213		Btg2	B-cell translocation gene 2, anti-	protein binding /// transcription /// regulation of	full-length
10357878	0,963253546	-3,794594483	-0,176076967	-6,244602029	1,735995154	0,187034967	7,161137143	Cluster IV	Adora1	adenosine A1 receptor	adenosine receptor activity, G-protein coupled ///	full-length
10358027	0,664333066	-4,926673837	0,146848774	-6,258821933	1,131375739	-2,232432656	5,272792099		Elf3	E74-like factor 3	DNA binding /// transcription factor activity ///	full-length
10358224	2,579933642	14,87817004	0,173498235	-5,601379677	2,608336334	14,62734008	8,427281409	Cluster VI	Ptprc	protein tyrosine phosphatase,	activation of MAPK activity /// negative regulation	full-length
10358389	1,578881287	3,646778056	0,019463212	-6,387709407	1,208079639	0,568838403	6,440332482		Rgs2	regulator of G-protein signaling 2	signal transducer activity /// GTPase activator	full-length
10358408	0,920727537	-2,083180418	-0,471844374	-4,644021144	1,077097369	-1,198922602	5,267976285		Rgs1	regulator of G-protein signaling 1	signal transducer activity /// GTPase activator	full-length
10358434	2,059111457	11,14202971	0,030870844	-6,369631359	1,993117365	10,32807003	7,00380142		Pla2g4a	phospholipase A2, group IVA	phospholipase activity /// lysophospholipase	full-length
10358454	1,812480084	1,721865529	0,03895128	-6,383256522	2,101723556	2,829483671	10,23263092		Rbm3	RNA binding motif protein 3	nucleotide binding /// nucleic acid binding /// RNA	full-length
10358476	1,379392915	6,202294558	0,139347025	-5,971022388	1,921470187	9,654226163	8,433181645		Prg4	proteoglycan 4 (megakaryocyte	extracellular region	full-length
10359161	1,945498921	12,69735625	0,311962195	-3,730795685	2,047679482	12,89993494	7,781374022		Soat1	sterol O-acyltransferase 1	sterol O-acyltransferase activity /// sterol O-	full-length
10359582	0,763183298	-6,566799093	-0,33640944	-6,250606425	2,239576201	-3,015820247	8,760436618		Fmo2	flavin containing monooxygenase	magnesium ion binding /// monooxygenase activity	full-length
10359593	2,369822837	-4,969049554	0,093358349	-6,38761594	4,832316558	-0,926295075	6,589762045		Fmo3	flavin containing monooxygenase	monooxygenase activity /// flavin-containing	full-length
10359642	-0,488662795	-6,097090524	-0,825587163	-3,532697959	-1,076411999	-3,117384936	6,217143022		100043821 ///	predicted gene, 100043821 ///	---	est
10359890	2,188209014	3,088687425	0,061358334	-6,372806062	1,754502657	0,514259396	5,670234685		Nuf2	NUF2, NDC80 kinetochore	chromosome, centromeric region /// kinetochore ///	full-length
10359970	0,789262932	-2,728299611	0,152339065	-6,159535033	1,054601546	-0,873397667	6,628030778		Nos1ap	nitric oxide synthase 1 (neuronal)	PDZ domain binding /// nitric-oxide synthase	full-length
10360040	1,315938931	6,835291013	-0,063282427	-6,282707146	1,149575594	4,872577046	7,178272194	Cluster I	Fcgr3	Fc receptor, IgG, low affinity III	antibody-dependent cellular cytotoxicity /// positive	full-length
10360070	2,547024871	14,06393917	0,2510721	-4,985737813	2,622844323	14,01947442	10,10560572	Cluster VI	Fcer1g	Fc receptor, IgE, high affinity I,	positive regulation of type IIa hypersensitivity ///	full-length
10360158	2,332627992	14,53317849	0,080131645	-6,188239089	2,310602555	14,03489461	6,714514011		Ly9	lymphocyte antigen 9	protein binding /// cell adhesion /// membrane ///	full-length
10360173	2,252196952	3,221698512	-0,480984069	-5,349661773	2,864306529	5,43212602	5,84719144		Slamf7	SLAM family member 7	receptor activity /// membrane /// integral to	full-length
10360306	2,077551657	9,355413266	-0,197062217	-5,765270951	2,763899434	12,34053829	6,205779542		Slamf8	SLAM family member 8	membrane /// integral to membrane	full-length
10360328	1,347003667	-0,940922403	0,056457287	-6,373757653	2,137773995	3,041491689	10,1167251		Apcs	serum amyloid P-component	calcium ion binding /// sugar binding ///	full-length
10360367	1,151856355	1,81323835	1,178350132	2,484207364	1,7610862	5,960798547	6,198808716		---	---	---	partial
10360370	1,145955613	-3,02483614	0,356977878	-5,852968498	0,637235509	-5,808802792	4,070470875		BC094916	cDNA sequence BC094916	protein binding /// nucleus	full-length
10360373	1,071424452	-2,210477258	1,389919613	0,466021514	1,621751532	0,908252189	4,98433849		---	---	---	partial
10360377	1,647610747	5,456112424	0,886601735	-0,091752475	2,04723578	7,521415775	8,119960418		AI607873	expressed sequence AI607873	---	full-length
10360382	1,758429232	7,172285646	0,947215281	1,155794289	1,978064747	8,116221071	7,764202583		Mnda /// Ifi204	myeloid cell nuclear differentiation	transcription cofactor activity /// protein binding ///	full-length
10360391	0,87578147	-2,242859167	1,022394879	-0,408489897	1,070141006	-1,026252448	7,600846508		Ifi203	interferon activated gene 203	protein binding /// nucleus	full-length
10360406	2,975243539	8,612193504	0,667704224	-3,764111831	3,54843202	10,27631824	6,758379305		Ifi205	interferon activated gene 205	protein binding /// nucleus /// transcription ///	full-length
10360506	1,086485113	4,229990997	0,039557383	-6,352234248	1,050079467	3,448331077	6,251975011	Cluster III	Akt3	thymoma viral proto-oncogene 3	nucleotide binding /// protein kinase activity ///	full-length
10360631	-0,334255269	-6,187614199	-0,029165998	-6,38298082	-1,251190712	0,713158533	10,58090668		Cabc1	chaperone, ABC1 activity of bc1	nucleotide binding /// protein kinase activity /// ATP	full-length
10361065	1,021558326	9,833413408	0,036670075	-6,290455906	1,229659351	11,6238222	7,104265134	Cluster IV	Mfsd7b	major facilitator superfamily	in utero embryonic development /// receptor	full-length
10361091	1,674577616	2,134704173	0,163999254	-6,201950598	2,057733114	3,885549776	6,493619283		Atf3	activating transcription factor 3	DNA binding /// transcription factor activity ///	full-length
10361110	1,093713695	2,102786385	0,144630165	-6,051862863	0,711368331	-2,025103631	5,019566964		Dtl	denticleless homolog (Drosophila)	nucleus /// cytoplasm /// DNA replication ///	full-length
10361133	1,270400628	3,490397665	-0,08169506	-6,284784032	1,615537793	5,718403967	6,621638214		---	---	---	---
10361246	-1,75170692	4,275116517	-1,118186675	0,425096	-2,251807281	6,676837589	7,833937967		G0s2	G0/G1 switch gene 2	cell cycle	full-length
10361375	1,755301447	2,168553775	0,45695988	-5,149253852	1,284054021	-1,063411423	5,455597213	Cluster I	Fbxo5	F-box protein 5	mitotic metaphase /// oocyte maturation /// oocyte	full-length
10361790	1,040729629	0,466361906	0,01122691	-6,390137714	0,731817461	-2,672183103	7,423174497		Fuca2	fucosidase, alpha-L- 2, plasma	catalytic activity /// alpha-L-fucosidase activity ///	full-length
10361807	0,887436856	0,854722358	0,179105892	-5,791389203	1,120879743	2,783145423	5,959132819		Hivep2	human immunodeficiency virus	nucleic acid binding /// DNA binding ///	full-length
10361887	-0,689250152	2,114803956	-0,105101445	-5,942570265	-1,15350809	7,354165131	9,413311509		Perp	PERP, TP53 apoptosis effector	protein binding /// mitochondrion /// Golgi	full-length
10362091	-0,51324539	-5,169196626	-0,162036674	-6,154990654	-1,849444783	4,077323332	7,61060347		Raet1d /// Raet1e	retinoic acid early transcript delta	plasma membrane /// immune response ///	full-length
10362129	0,487609316	-4,263344469	0,179583748	-5,906685703	1,166097385	2,022981371	10,41536753		Vnn3	vanin 3	extracellular space /// plasma membrane ///	full-length
10362138	-1,634332453	2,246424186	-0,24072564	-5,960956874	-1,839373457	3,06586999	9,223019333		Vnn1	vanin 1	acute inflammatory response /// chronic	full-length
10362350	1,209549714	2,180574811	0,11380783	-6,214781546	1,078234223	0,679443774	4,57014725		E430004N04Rik	RIKEN cDNA E430004N04 gene	---	full-length
10362379	-0,740247154	-1,957657115	-0,109991365	-6,219360426	-1,399339963	3,509962107	8,903988682		Echdc1	enoyl Coenzyme A hydratase	catalytic activity /// metabolic process	full-length
10362538	-0,646404854	-3,491254958	-0,173009186	-6,045660615	-1,09355326	0,103497855	5,887827853		Lama4	laminin, alpha 4	blood vessel development /// receptor binding ///	full-length
10362596	1,046466734	0,987280822	-0,086459512	-6,284241421	0,857183867	-1,124638987	7,675973755	Cluster III	Fyn	Fyn proto-oncogene	nucleotide binding /// neuron migration /// neuron	full-length
10362896	1,010778356	-1,943995819	-0,560584606	-4,320939134	0,793963923	-3,775034488	5,84573092	Cluster III	Cd24a	CD24a antigen	response to hypoxia /// cell activation /// regulation	full-length
10362904	-0,610620913	-1,457964983	-0,098446486	-6,16118027	-1,071905703	3,424141321	8,380765767	Cluster X	Rtn4ip1	reticulon 4 interacting protein 1	protein binding /// mitochondrion /// mitochondrion	full-length
10363005	-0,488662795	-6,097090524	-0,825587163	-3,532697959	-1,076411999	-3,117384936	6,217143022		LOC280487	pol polyprotein	---	partial
10363070	3,489822096	9,876060996	0,326670844	-5,727656711	4,126552251	11,45311271	7,562396819		Gp49a	glycoprotein 49 A	membrane /// integral to membrane	full-length
10363082	2,794059814	7,532401052	0,21255272	-6,088575369	3,394983507	9,398446859	7,256798107	Cluster VI	Lilrb4	leukocyte immunoglobulin-like	receptor activity /// plasma membrane /// immune	full-length
10363161	1,591120189	6,88086314	0,100984784	-6,201482788	1,659545777	6,936467473	7,047246907		---	---	---	partial
10363475	1,189894173	-0,770349478	0,351689864	-5,517933047	1,538587996	1,183020383	5,976169472		Prf1	perforin 1 (pore forming protein)	calcium ion binding /// membrane /// integral to	full-length
10363561	-0,488662795	-6,097090524	-0,825587163	-3,532697959	-1,076411999	-3,117384936	6,217143022		100043821 ///	predicted gene, 100043821 ///	---	est
10363669	0,543098373	-5,667227879	-0,340521201	-5,727814419	1,322457655	-1,167289663	8,936570341		Dnajc12	DnaJ (Hsp40) homolog, subfamily	molecular_function /// cellular_component ///	full-length
10364262	2,826728451	16,24887648	-0,079894243	-6,205906576	2,973509212	16,47996796	8,480707392	Cluster VI	Itgb2	integrin beta 2	receptor activity /// binding /// protein binding ///	full-length
10364593	1,863987541	10,26143735	-0,055613942	-6,316406268	1,868118108	9,85939879	7,09953153	Cluster I	Cnn2	calponin 2	actin binding /// calmodulin binding /// actomyosin	full-length
10364950	1,105789686	-4,201914788	-0,14180972	-6,329457361	2,404728971	1,20972625	8,011268438		Gadd45b	growth arrest and DNA-damage-	activation of MAPKK activity /// protein binding ///	full-length
10365482	0,574366458	-0,126839786	-0,060035708	-6,25717396	1,570778565	10,36624007	7,852668869		Timp3	tissue inhibitor of	enzyme inhibitor activity /// protein binding ///	full-length
10366476	-1,354729312	3,504230558	0,050727062	-6,355216601	-2,544360843	10,31164239	8,322779568		Ptprb	protein tyrosine phosphatase,	protein tyrosine phosphatase activity /// receptor	full-length
10366886	1,0240414	4,432962946	0,017081966	-6,383152745	0,931961095	3,008474954	6,416521213		Arhgap9	Rho GTPase activating protein 9	GTPase activator activity /// cellular_component ///	full-length
10367066	-2,265239313	3,66888708	-0,193218274	-6,198425349	-3,269151426	7,370115533	8,30989025	Cluster IX	Sdr9c7	4short chain	catalytic activity /// binding /// cytoplasm ///	full-length
10367634	0,932606492	2,159433981	0,212462986	-5,42106521	1,230785411	4,694440457	6,511553206		Akap12	A kinase (PRKA) anchor protein	protein binding /// cellular_component ///	full-length
10367734	1,014488874	3,420266068	0,268527662	-4,801532655	1,048606128	3,362041571	5,524470178		Ust	uronyl-2-sulfotransferase	Golgi apparatus /// membrane /// integral to	full-length
10367805	1,650803283	4,77429189	0,002199906	-6,391732273	1,59701093	3,992150593	5,474218023		9130014G24Rik	RIKEN cDNA 9130014G24 gene	---	partial
10367816	1,838134186	5,505616267	0,104769138	-6,270527901	1,216782423	0,795283394	5,364307106		---	---	---	predicted
10368144	1,880001717	-0,141165237	0,325852217	-6,029337638	2,899248002	3,73822324	7,20719571		Tnfaip3	tumor necrosis factor, alpha-	DNA binding /// protein binding /// nucleus ///	full-length
10368644	1,707112856	2,090415316	0,200074166	-6,123929484	2,301219589	4,853888231	6,725260485		Fam26f	family with sequence similarity 26,	membrane /// integral to membrane	full-length
10368675	1,372548595	6,2349302	-0,028293408	-6,373609003	1,268834334	4,920684017	8,483214743		Marcks	myristoylated alanine rich protein	actin binding /// protein kinase C binding ///	full-length

Affymetrix ID	BS/Non Inf.		LS/Non Inf.		ReINF/Non Inf.		Average	Cluster	Gene	Gene	Gene Ontology (GO)	Transcript
Transcript	logFC	B	logFC	B	logFC	B	expression	Number	Symbol	Title	Description	Classification
10368713	-0,729881771	-0,051802218	-0,080669603	-6,238910697	-1,369861596	6,035555939	9,257790419		AI317395	expressed sequence AI317395	sugar:hydrogen symporter activity /// plasma	full-length
10368947	1,164132296	2,358447877	0,586831506	-2,514625144	1,728132635	6,244155232	8,448273162		Aim1	absent in melanoma 1	molecular_function /// cellular_component ///	full-length
10369264	-0,664503812	-4,498074544	-0,145277744	-6,233065128	-1,872858588	3,204607579	8,504763706		Oit3	oncoprotein induced transcript 3	calcium ion binding /// nucleus	full-length
10369290	0,797558457	-6,058145688	0,661217888	-5,550172703	2,094584762	-1,7784914	7,882915674		Ddit4	DNA-damage-inducible transcript 4	molecular_function /// cellular_component ///	full-length
10369541	0,902230137	4,111263221	0,068612148	-6,224606006	1,032014275	5,174419469	6,363685635		Hk1	hexokinase 1	nucleotide binding /// catalytic activity ///	full-length
10369615	1,832506603	11,36015098	-0,084495753	-6,177584313	2,036507757	12,20430104	10,03750933		Srgn	serglycin	ossification /// protein binding /// extracellular	full-length
10369815	1,526985135	1,762301183	0,19953856	-6,081041485	0,792120564	-3,710461741	6,320725725	Cluster III	Cdc2a	cell division cycle 2 homolog A (S.	nucleotide binding /// protein kinase activity ///	full-length
10370339	1,197304332	1,141454085	0,138605444	-6,17553227	1,1821282	0,647100424	6,368579705		Trpm2	transient receptor potential cation	receptor activity /// ion channel activity /// calcium	full-length
10370946	1,290354763	7,790552998	0,091132483	-6,117999678	1,364359874	8,011843291	7,401956996		Mobkl2a	MOB1, Mps One Binder kinase	protein binding /// zinc ion binding /// metal ion	full-length
10371054	-0,792592944	6,747548816	-0,312281575	-1,543713231	-1,001532463	9,058771803	9,764962308		Creb3l3	cAMP responsive element binding	DNA binding /// transcription factor activity ///	full-length
10371591	1,18092784	5,150213285	0,116859855	-6,054457252	0,79095565	6,608438401	4,785507696		4930547N16Rik	RIKEN cDNA 4930547N16 gene	DNA binding /// nucleus /// cytoplasm	full-length
10371607	1,782829489	8,375094421	0,233546586	-5,407862883	2,28492287	10,89748787	7,138551976		1200002N14Rik	RIKEN cDNA 1200002N14 gene	lysosome /// autophagy /// apoptosis /// membrane	full-length
10371662	2,900484713	7,616295235	0,218421418	-6,090319858	3,230321953	8,448960992	6,919085471		Spic	Spi-C transcription factor (Spi-	DNA binding /// transcription factor activity ///	full-length
10371796	-0,637584342	-2,786021194	-0,102915726	-6,231268045	-1,151396731	1,806726418	7,347246192		Slc17a8	solute carrier family 17 (sodium-	transporter activity /// L-glutamate transmembrane	full-length
10371846	1,231010175	7,231056845	-0,151037827	-5,667263652	1,233488813	6,822111734	6,894045396		Apaf1	apoptotic peptidase activating	nucleotide binding /// neural tube closure /// protein	full-length
10371970	-0,410972989	-4,248045702	0,078744354	-6,256010746	-1,654345506	7,809346945	10,99451669	Cluster X	Amdhd1	amidohydrolase domain containing	iron ion binding /// cytoplasm /// histidine metabolic	full-length
10372028	-1,058169955	2,398480302	-0,054300529	-6,336309284	-1,483127529	5,633603911	7,615402266		Plxnc1	plexin C1	receptor activity /// membrane /// integral to	full-length
10372177	-0,532103302	-1,529807826	-0,345591142	-3,446203596	-1,067759855	4,779974404	6,702880178		Tmtc2	transmembrane and	binding /// membrane /// integral to membrane	full-length
10372324	-0,524425534	-6,215835438	-0,100929981	-6,35023252	-1,153293513	-3,476009927	7,315046123		Syt1	synaptotagmin I	transporter activity /// calcium ion binding ///	full-length
10372410	1,962854789	14,90729117	-0,075229842	-6,122958795	1,82496027	13,66420586	5,768514647		Glipr1	GLI pathogenesis-related 1	extracellular region /// membrane /// integral to	full-length
10372648	1,64329724	6,325026331	-0,032900656	-6,374366025	1,43231003	4,356750009	10,3580629		Lyz2	lysozyme 2	lysozyme activity /// catalytic activity ///	full-length
10372716	0,920126308	7,341540095	-0,081965306	-5,992443829	1,138885077	9,423468345	10,67557607		Rap1b	RAS related protein 1b	nucleotide binding /// protein binding /// GTP	full-length
10372781	2,105091219	8,900567408	0,352950236	-4,724246551	2,420479379	10,13091087	6,98071657	Cluster VI	Irak3	interleukin-1 receptor-associated	nucleotide binding /// magnesium ion binding ///	full-length
10372831	-0,366265715	-5,705678145	-0,374942938	-4,793464895	-1,06407414	0,231104729	5,863238486		Tbc1d30	TBC1 domain family, member 30	Rab GTPase activator activity /// intracellular ///	partial
10373054	-0,677718443	-0,607918476	-0,254837324	-4,983276414	-1,173153616	4,406199234	5,933289485		Slc26a10	solute carrier family 26, member	transporter activity /// transport /// antiporter activity	partial
10373197	-1,012609869	3,953512817	-0,321656049	-4,019567799	-0,255764436	-5,790502085	9,254078765		Inhbc	inhibin beta-C	hormone activity /// extracellular region /// growth	full-length
10373325	-0,858355708	-0,46298624	-0,071927876	-6,311386459	-1,706323831	6,152539739	7,546581133		Gpr182	G protein-coupled receptor 182	signal transducer activity /// receptor activity /// G-	full-length
10373334	-1,392349111	-4,159252343	-0,354926384	-6,144812829	-3,108649354	1,549614482	11,02856138	Cluster IX	Hsd17b6	hydroxysteroid (17-beta)	catalytic activity /// estradiol 17-beta-	full-length
10373407	1,183128152	4,766522979	-0,135089993	-5,975228098	1,210366106	4,596887709	7,677344106		Mbc2	membrane bound C2 domain	membrane /// integral to membrane	full-length
10374183	-0,488662795	-6,097090524	-0,825587163	-3,532697959	-1,076411999	-3,117384936	6,217143022		100043821 ///	predicted gene, 100043821 ///	---	predicted
10374236	1,082967561	0,108769141	-0,078166782	-6,323746361	1,600189571	3,581772438	6,047462293		Upp1	uridine phosphorylase 1	catalytic activity /// uridine phosphorylase activity	full-length
10374333	1,712968256	10,47807967	0,010290408	-6,388603786	1,990403633	11,85054124	6,025749216	Cluster I	Ikzf1	IKAROS family zinc finger 1	nucleic acid binding /// DNA binding ///	full-length
10374352	-0,488662795	-6,097090524	-0,825587163	-3,532697959	-1,076411999	-3,117384936	6,217143022		100043821 ///	predicted gene, 100043821 ///	---	est
10374842	1,240939914	2,843331599	-0,084037245	-6,286844123	0,825835549	-1,294966867	5,03492856	Cluster III	Ccdc88a	coiled coil domain containing 88A	regulation of protein amino acid phosphorylation ///	full-length
10375065	1,456871655	4,851211078	0,438049206	-3,910302045	1,857819427	7,191718798	5,783462051		Sh3pxd2b	SH3 and PX domains 2B	protein binding /// cytoplasm /// cell communication	full-length
10375083	1,47394103	5,59971414	0,00550984	-6,391255605	1,433739267	4,864753323	6,743067489		Stk10	serine/threonine kinase 10	nucleotide binding /// protein kinase activity ///	full-length
10375145	2,196852134	14,89080491	0,154794919	-5,527258491	2,311834375	15,11137589	7,70870904	Cluster VI	Lcp2	lymphocyte cytosolic protein 2	protein binding /// cytoplasm /// mast cell activation	full-length
10375324	-0,488662795	-6,097090524	-0,825587163	-3,532697959	-1,076411999	-3,117384936	6,217143022		100043821 ///	predicted gene, 100043821 ///	---	est
10375443	1,641451406	10,12203555	0,342129426	-3,525647257	1,753040767	10,47997449	5,628203496		Havcr2	hepatitis A virus cellular receptor 2	receptor activity /// membrane /// integral to	full-length
10375472	1,552143994	2,11048047	0,165447208	-6,168561526	1,134191285	-1,119213371	8,248047736		Timd4	T-cell immunoglobulin and mucin	membrane /// integral to membrane	full-length
10375515	2,163320003	8,343374057	1,0206651	0,87964578	2,878337614	11,31430543	7,98201593		Ifi47 /// Olfr56	interferon gamma inducible protein	endoplasmic reticulum /// defense response ///	full-length
10375704	-0,594441182	-2,772098413	-0,217833598	-5,601141092	-1,482968028	5,271349894	7,589326709		3010026O09Rik	RIKEN cDNA 3010026O09 gene	---	full-length
10376060	1,843935277	6,317100379	0,18700999	-5,959483611	1,93189853	6,42150479	8,934093717	Cluster I	Irf1	interferon regulatory factor 1	DNA binding /// transcription factor activity ///	full-length
10376094	-0,624635402	-3,992569208	-0,0540101	-6,360940626	-1,130227665	-0,109979543	7,852882164		---	---	---	est
10376324	3,58629976	9,882140173	2,107233713	4,067294086	4,783493732	12,90275301	9,063691189		OTTMUSG00000	predicted gene,	---	full-length
10376326	2,423222592	12,94644092	1,803062145	8,835895185	3,056565883	15,29314886	10,25251441		Igtp /// Iigp2	interferon gamma induced GTPase	GTPase activity /// cytosol /// GTPase activity ///	full-length
10376459	0,961331072	6,784603893	0,111535496	-5,786359065	1,00358155	6,850207737	6,438140325		OTTMUSG00000	predicted gene,	---	est
10376868	1,591914123	6,092440238	0,281838315	-5,199372816	1,40095067	4,23908462	6,280057207		Trpv2	transient receptor potential cation	ion channel activity /// cation channel activity ///	full-length
10377265	0,942198022	0,486583777	0,019760394	-6,385516741	1,027666852	0,92710934	5,781217238		Pik3r5	phosphoinositide-3-kinase,	nucleus /// cytoplasm /// membrane /// kinase	full-length
10377405	1,865137577	5,143414988	0,133920715	-6,212208372	1,428693823	1,899420406	6,25133693		Aurkb	aurora kinase B	nucleotide binding /// magnesium ion binding ///	full-length
10377439	0,232662313	-6,99085316	0,415530918	-5,531526463	1,157581454	-2,616593463	6,846480927		Per1	period homolog 1 (Drosophila)	two-component sensor activity /// two-component	full-length
10378068	1,581144999	6,385460143	1,998100913	8,587921138	1,848288823	7,765228547	7,159940547	Cluster V	Xaf1	XIAP associated factor 1	nucleus /// cytoplasm /// mitochondrion ///	full-length
10378216	1,422618765	5,59110259	0,21731545	-5,555746516	1,397747953	4,967898054	5,792143921		Atp2a3	ATPase, Ca++ transporting,	nucleotide binding /// magnesium ion binding ///	full-length
10378385	-1,07461346	-2,778868455	-0,000252509	-6,391790625	-1,442749025	-0,897472939	6,359157411		Spata22	spermatogenesis associated 22	---	full-length
10378572	-0,705770047	-4,803373921	0,23019386	-6,088224483	-1,909553634	2,057567954	10,40341831		Tlcd2	TLC domain containing 2	membrane /// integral to membrane	full-length
10379511	1,966443803	-1,805702183	0,090508217	-6,374345808	3,052353723	1,689273299	6,598362357	Cluster VI	Ccl2	chemokine (C-C motif) ligand 2	G-protein-coupled receptor binding /// cytokine	full-length
10379518	1,133878564	-3,696256706	0,07166272	-6,373371737	1,996043296	0,136329844	6,175795342	Cluster II	Ccl7	chemokine (C-C motif) ligand 7	cytokine activity /// extracellular region ///	full-length
10379530	0,791371974	-3,783133729	-0,015423917	-6,390091529	1,829506656	2,627194333	4,578959959	Cluster II	Ccl12	chemokine (C-C motif) ligand 12	cytokine activity /// extracellular region ///	full-length
10379535	1,584947677	7,125922051	0,107671717	-6,164970074	1,69700124	7,488912684	4,281286028	Cluster I	Ccl8	chemokine (C-C motif) ligand 8	cytokine activity /// extracellular region ///	full-length
10379615	0,821428303	1,539505649	1,055279843	4,374243239	1,192390482	5,060238797	7,57563771		Slfn5	schlafen 5	nucleotide binding /// ATP binding /// nucleus ///	full-length
10379630	2,533280086	8,816292331	0,797448229	-1,856306275	2,862628874	9,837658605	7,890803406		Slfn2	schlafen 2	negative regulation of cell proliferation	full-length
10379633	2,058122405	0,994984416	0,795818624	-4,367711997	2,944921854	4,275221911	5,999187408		Slfn1	schlafen 1	G1/S transition of mitotic cell cycle ///	full-length
10379636	1,616899303	-0,757859217	0,27328985	-6,09189986	2,625558883	3,518960356	5,436920306		Slfn4	schlafen 4	---	full-length
10379646	0,944728061	2,242020862	0,558149814	-1,595456678	1,002172616	2,446667565	5,968986553		Slfn3	schlafen 3	negative regulation of cell proliferation	full-length
10379721	1,189204782	-1,786203663	-0,035181415	-6,384540312	1,322808382	-1,279876661	5,531307805	Cluster I	Ccl4	chemokine (C-C motif) ligand 4	cytokine activity /// protein binding /// extracellular	full-length
10379727	1,730466441	12,55887777	0,150101175	-5,511781817	1,930974581	13,45820118	9,847081292		OTTMUSG00000	predicted gene,	---	full-length
10380566	-0,89420656	3,179791791	0,084601416	-6,175226146	-1,013180753	4,105959481	5,871579626		Phospho1 ///	phosphatase, orphan 1 /// ABI	magnesium ion binding /// molecular_function ///	full-length
10380571	1,703075558	8,768440781	-0,001720336	-6,3917234	1,600568673	7,604699712	6,434065744		Gngt2	guanine nucleotide binding protein	signal transducer activity /// heterotrimeric G-	full-length
10381072	1,40332835	3,727326683	0,328250893	-5,049644893	1,228483902	1,941921279	6,072626386	Cluster III	Cdc6	cell division cycle 6 homolog (S.	nucleotide binding /// chromatin binding /// ATP	full-length
10381387	-1,195230754	-0,362150293	-0,254322056	-5,878686617	-2,371967117	6,267681109	11,83997744		G6pc	glucose-6-phosphatase, catalytic	catalytic activity /// glucose-6-phosphatase activity	full-length
10381514	-0,671256707	-0,689955674	-0,115432964	-6,076654319	-1,373420774	6,175937106	7,372488574		Cd300lg	CD300 antigen like family member	receptor activity /// endosome /// plasma	full-length
10381588	0,800235002	6,950372262	0,071194392	-6,018682223	1,016219219	9,327053297	11,47042852		Grn	granulin	blastocyst hatching /// cytokine activity ///	full-length

Affymetrix ID	BS/Non Inf.		LS/Non Inf.		ReINF/Non Inf.		Average	Cluster	Gene	Gene	Gene Ontology (GO)	Transcript
Transcript	logFC	B	logFC	B	logFC	B	expression	Number	Symbol	Title	Description	Classification
10381708	1,180230383	1,975381799	0,262133753	-5,496949833	1,405109577	3,375636805	5,575184047		Fmnl1	formin-like 1	actin binding /// profilin binding /// cytoplasm ///	full-length
10381809	1,103158855	7,367009489	0,191495566	-4,9859428	1,426749919	9,974346778	7,271567779		Itgb3	integrin beta 3	receptor activity /// integrin binding /// binding ///	full-length
10382106	1,992028991	7,568821326	0,325980552	-5,087704377	2,151038093	8,035907293	6,701270724		Gm885	gene model 885, (NCBI)	extracellular region /// membrane /// integral to	full-length
10382271	-0,277664227	-6,523456235	-0,001800876	-6,391758082	-1,114225444	-0,428514439	7,364389253		Arsg	arylsulfatase G	catalytic activity /// calcium ion binding ///	full-length
10382438	1,34328317	10,67344314	-0,226129352	-4,218138081	1,220631538	9,103606688	7,15321494	Cluster I	Cd300a	CD300A antigen	DNA binding /// receptor activity /// plasma	full-length
10382532	1,055830526	-4,333466296	-0,477270362	-5,693782454	2,024011731	-0,203438738	7,11095152		Slc16a5	solute carrier family 16	---	full-length
10383152	1,418770227	6,507303881	2,192405812	10,50640326	2,044228831	10,37704321	9,644297057		---	---	---	partial
10383168	1,490500526	6,67682517	2,15467087	10,05104298	2,033536025	9,900379192	9,837844354		---	---	---	partial
10383192	1,35905021	4,719314619	2,071940942	8,959127911	2,077220639	9,187727499	8,684434569		---	---	---	partial
10383194	1,391641572	4,789091982	2,024667161	8,580936049	1,948620432	8,223494762	9,864739093		---	---	---	partial
10383196	1,567901683	6,723583211	2,157004688	9,643522439	1,96193122	8,917694279	8,892665308		---	---	---	partial
10383198	1,61574014	6,838241853	2,161775081	9,481035537	2,10055242	9,49118417	9,823970862		---	---	---	partial
10383200	1,574268366	6,124748376	2,206625429	9,33819291	2,039170261	8,707840906	8,952714283		---	---	---	partial
10383202	1,623369752	8,690550066	2,210102957	11,02299423	2,092909436	11,28972542	9,977040214		---	---	---	partial
10383204	1,547985395	7,511593612	2,21166423	10,57872862	2,078258436	10,57039772	9,081417163		---	---	---	partial
10383206	1,579579841	6,825879742	2,344417795	10,39647201	2,236424433	10,49882322	9,365484694		---	---	---	partial
10383208	1,255452005	0,631817021	1,904109723	5,060843454	1,931205565	6,645691756	7,767187752		---	---	---	partial
10383210	1,35328663	6,799857288	2,076120554	10,6630425	2,017349605	11,08972709	9,491558493		---	---	---	partial
10383212	1,460430637	6,40381905	2,183797038	10,13994933	2,125101266	10,38706652	9,905593156		---	---	---	partial
10383214	1,403403128	7,930134961	2,138613293	11,42024444	1,969024763	11,52866311	9,841506825		Rnf213	ring finger protein 213	---	partial
10383233	1,325744716	6,693197561	2,008067158	10,47307902	1,899945089	10,50628882	9,881494571		Rnf213	ring finger protein 213	---	partial
10383395	-0,509778151	-1,397085802	0,024269993	-6,371029983	-1,016118758	4,895077022	10,00298178		Slc25a10	solute carrier family 25	binding /// mitochondrion /// mitochondrial inner	full-length
10383502	1,406111692	4,943938216	0,227526952	-5,556069307	2,262143321	10,0415289	7,173573762		Slc16a3	solute carrier family 16	transporter activity /// plasma membrane ///	full-length
10383556	-0,340877279	-4,87544513	-0,085035956	-6,218597911	-1,007937443	2,787015437	7,137788823		BC032265	cDNA sequence BC032265	kinase activity /// transferase activity	full-length
10383564	-0,61448859	-0,257887293	-0,104022915	-6,054494658	-1,267579849	6,853098886	6,636475529		Fn3k	fructosamine 3 kinase	soluble fraction /// cytosol /// kinase activity ///	full-length
10384154	1,967312651	10,83032492	-0,138384508	-5,943958918	2,050799907	10,90309524	6,403158349		Myo1g	myosin IG	nucleotide binding /// motor activity /// actin binding	full-length
10384373	1,975806708	3,162585665	0,312916632	-5,804256112	1,701763906	1,258214588	5,190272439		Fignl1	fidgetin-like 1	nucleotide binding /// magnesium ion binding ///	full-length
10384378	-0,733861122	-2,131301216	-0,098594134	-6,257001035	-1,119022157	1,08392066	9,164559336	Cluster X	Ddc	dopa decarboxylase	catalytic activity /// aromatic-L-amino-acid	full-length
10384458	3,165962824	14,67055603	0,103335959	-6,203425002	3,752989775	16,27588698	7,875501065		Plek	pleckstrin	intracellular signaling cascade	full-length
10385118	2,180841882	9,945359245	0,294795069	-5,063000387	2,058639798	8,82897407	6,924710381	Cluster I	Dock2	dedicator of cyto-kinesis 2	membrane raft polarization /// establishment of T	full-length
10385236	1,091424672	3,909354003	0,12805245	-6,01465206	0,786205394	0,239389138	8,125265415		Akr1b3	aldo-keto reductase family 1,	aldehyde reductase activity /// cytoplasm ///	full-length
10385248	1,289603378	2,079562322	0,199087121	-5,93484672	1,018511523	-0,496219458	3,892145997		Hmmr	hyaluronan mediated motility	receptor activity /// hyaluronic acid binding ///	full-length
10385391	1,768715548	10,40944604	0,122359588	-5,98683602	2,161546179	12,38634957	6,654200439		Cyfip2	cytoplasmic FMR1 interacting	molecular_function /// protein binding /// cytoplasm	full-length
10385428	1,09630116	9,09056877	0,067982989	-6,1283278	1,17772544	9,510600581	5,80265477	Cluster III	Itk	IL2-inducible T-cell kinase	nucleotide binding /// protein kinase activity ///	full-length
10385500	1,89722396	7,387294162	1,545956735	5,183620549	2,606642781	10,71931804	10,04014577	Cluster VI	Irgm1	immunity-related GTPase family M	nucleotide binding /// GTP binding /// endoplasmic	full-length
10385504	1,570955825	-0,409868479	1,129342508	-2,149194545	1,737524383	0,123854686	5,701314774		EG432555	predicted gene, EG432555	---	full-length
10385507	0,624544378	1,911396748	0,082886949	-6,061980009	1,09839234	7,697454988	4,871835754		---	---	---	predicted
10385513	1,87147335	11,07906977	0,827327434	2,339016976	1,727180237	9,694656539	7,209400817		9930111J21Rik	RIKEN cDNA 9930111J21 gene ///	---	full-length
10385518	4,546315414	16,60680771	1,885822012	6,255855848	5,170872358	17,72414045	9,176843692	Cluster VIII	Tgtp	T-cell specific GTPase	GTPase activity /// GTP binding ///	full-length
10385526	1,814934235	10,68956465	0,779302152	1,781196203	1,687242294	9,391274569	7,152753182		9930111J21Rik	RIKEN cDNA 9930111J21 gene ///	---	full-length
10385533	4,273880337	16,52872138	1,635440815	5,400330775	4,968870374	17,89159697	9,588838281	Cluster VIII	Tgtp	T-cell specific GTPase	GTPase activity /// GTP binding ///	full-length
10385542	-0,070151101	-7,228573715	-0,093014875	-6,303769248	-1,145567281	-0,142437489	6,647123073		Btnl9	butyrophilin-like 9	membrane /// integral to membrane	full-length
10385747	0,609016939	-0,712901442	0,147992268	-5,78034716	1,009216143	3,794825596	6,594592237		Phf15	PHD finger protein 15	protein binding /// zinc ion binding /// metal ion	full-length
10385814	-0,803806754	-0,694799364	-0,222745146	-5,604240096	-1,612201881	5,941651306	5,970543864		Leap2	liver-expressed antimicrobial	extracellular region /// defense response to	full-length
10385872	-1,355691427	6,58797815	-0,36634407	-3,711515267	-0,819101918	0,830814953	7,326963237	Cluster X	Slc22a5	solute carrier family 22 (organic	nucleotide binding /// transporter activity /// ATP	full-length
10385941	0,974132651	1,654862104	-0,079748518	-6,270677366	1,173052781	3,154185805	7,000225866		Tnip1	TNFAIP3 interacting protein 1	nucleus /// cytoplasm	full-length
10386652	-0,996211169	3,930222866	-0,171561116	-5,60218059	-1,353678598	6,951578396	10,68909927	Cluster X	Aldh3a2	aldehyde dehydrogenase family 3,	aldehyde dehydrogenase (NAD) activity ///	full-length
10387536	2,030701703	13,99935585	0,074793699	-6,178372531	2,087236709	13,931892	9,319713129		Cd68	CD68 antigen	lysosome /// endosome /// plasma membrane ///	full-length
10387821	1,371964504	3,117001144	-0,15153186	-6,101819317	1,186375541	1,254658929	5,625007224		Alox12	arachidonate 12-lipoxygenase	arachidonate 12-lipoxygenase activity /// iron ion	full-length
10387890	0,990819115	1,344020075	-0,133899396	-6,086538261	1,183769232	2,738125304	6,997679828	Cluster IV	Cxcl16	chemokine (C-X-C motif) ligand 16	low-density lipoprotein receptor activity ///	full-length
10387985	1,133220648	1,904214037	0,373329116	-4,588198202	1,514570878	4,552171001	6,00226295		A430084P05Rik	RIKEN cDNA A430084P05 gene	membrane /// integral to membrane	full-length
10388254	-0,924423784	-0,066490249	-0,158772845	-6,029782049	-1,082751974	1,02103159	6,99445857	Cluster X	Aspa	aspartoacylase	aminoacylase activity /// nucleus /// cytoplasm ///	full-length
10388545	1,563280718	5,874953765	0,051834398	-6,347719357	2,005928056	8,336088805	6,379464514		Abr	active BCR-related gene	guanyl-nucleotide exchange factor activity /// Rho	full-length
10388834	-0,996006349	3,708003305	-0,119470869	-6,012155086	-1,125839763	4,625815973	5,334581833		Slc13a2	solute carrier family 13 (sodium-	transporter activity /// transport /// ion transport ///	full-length
10388958	1,947611678	14,61597744	0,218921957	-4,465806934	1,900282657	13,9398213	5,944090119		Evi2b /// Evi2a	ecotropic viral integration site 2b ///	membrane /// integral to membrane	full-length
10389134	1,493285921	5,309575499	1,606629716	6,123745662	1,434916318	4,443909464	6,658812368		Slfn9	schlafen 9	nucleus	full-length
10389143	1,186781313	0,751254378	0,809723921	-1,655485832	1,745034567	4,290075812	5,88579375		Slfn8	schlafen 8	---	full-length
10389207	3,716420785	19,3673981	-0,31227799	-3,960604353	3,466792941	18,35100876	8,705297218		Ccl5	chemokine (C-C motif) ligand 5	cytokine activity /// extracellular region ///	full-length
10389222	3,026076712	15,04294057	0,079962802	-6,259577713	3,34017426	15,82161349	9,346184162	Cluster VI	Ccl6	chemokine (C-C motif) ligand 6	cytokine activity /// extracellular region ///	full-length
10389231	3,683332876	5,958010909	0,224943937	-6,241327809	4,214842774	7,077988055	6,760123827		Ccl3	chemokine (C-C motif) ligand 3	cytokine activity /// protein binding /// extracellular	full-length
10389261	0,001174274	-7,279970578	0,072915931	-6,315146967	-1,263014481	2,456286747	7,233731466		OTTMUSG00000	predicted gene,	membrane /// integral to membrane	partial
10389606	1,164228284	-0,712097807	0,167480865	-6,170804287	0,857750529	-3,235842233	5,093231743		Prr11	proline rich 11	---	full-length
10390186	1,294572607	1,131487866	0,101216438	-6,292453201	1,231112258	0,291784605	7,417077977	Cluster III	Abi3	ABI gene family, member 3	molecular_function /// intracellular /// cytoplasm ///	full-length
10390640	1,742359822	6,121824829	-0,137820004	-6,134166337	1,876718523	6,543531527	5,273988617		Ikzf3	IKAROS family zinc finger 3	nucleic acid binding /// DNA binding /// protein	full-length
10390691	-0,803763522	-5,495063916	-0,310089453	-6,101455779	-2,20259578	0,344776126	9,463424518		Nr1d1 /// Thra	nuclear receptor subfamily 1,	DNA binding /// transcription factor activity ///	full-length
10390707	2,774201802	5,731240285	0,261495857	-6,052437602	2,434168612	3,860717015	6,535280504		Top2a	topoisomerase (DNA) II alpha	nucleotide binding /// condensed chromosome ///	full-length
10391207	0,786058486	4,391660712	1,731465742	11,88019373	0,886289086	5,301715261	7,698706802		Dhx58	DEXH (Asp-Glu-X-His) box	nucleotide binding /// nucleic acid binding /// DNA	full-length
10391301	0,777641281	1,722013077	0,280568908	-4,347442513	1,057840044	4,54479799	10,18687501	Cluster II	Stat3	signal transducer and activator of	temperature homeostasis /// eye photoreceptor	full-length
10391461	1,42091858	9,015926383	0,160499497	-5,565966602	1,390575661	8,327973051	5,29610825		Brca1	breast cancer 1	condensed chromosome /// DNA binding ///	full-length
10392142	0,916798156	-0,008067696	-0,444486993	-3,926278691	1,121382105	1,50418196	6,093784094		Cd79b	CD79B antigen	transmembrane receptor activity /// protein binding	full-length
10392522	-0,977191331	-3,073158683	-0,136005362	-6,282258866	-1,354364023	-1,013591263	9,924223409		Abca8a	ATP-binding cassette, sub-family A	nucleotide binding /// ATP binding /// plasma	full-length
10392796	1,168013368	3,311884815	0,108847487	-6,176332493	1,253312408	3,652527883	5,595038043		Cd300lb	CD300 antigen like family member	receptor activity /// plasma membrane /// immune	full-length

Affymetrix ID	BS/Non Inf.		LS/Non Inf.		ReINF/Non Inf.		Average	Cluster	Gene	Gene	Gene Ontology (GO)	Transcript
Transcript	logFC	B	logFC	B	logFC	B	expression	Number	Symbol	Title	Description	Classification
10392808	1,451453647	2,779988711	-0,042090474	-6,37265396	1,215462683	0,642803467	7,657685187	Cluster I	4732429D16Rik	RIKEN cDNA 4732429D16 gene	receptor activity /// plasma membrane /// immune	full-length
10392815	1,711074121	11,98604065	0,076017385	-6,170995216	1,732503323	11,71831981	7,336673965	Cluster I	Cd300a ///	CD300A antigen /// cDNA	DNA binding /// receptor activity /// plasma	full-length
10392825	1,138292597	4,835141703	0,028551094	-6,370801478	1,070260306	3,743326226	6,555058249		RP23-331L12.8	CMRF-35-like molecule 3 ///	molecular_function /// receptor activity ///	full-length
10392834	1,086404843	4,339119619	-0,042103909	-6,346087178	1,103433823	4,091269021	6,607936086		RP23-331L12.8	CMRF-35-like molecule 3 ///	molecular_function /// receptor activity ///	full-length
10392839	2,595166456	14,80435953	0,118924858	-6,01732804	2,777867661	15,22357452	8,049746496	Cluster VI	Cd300e	CD300e antigen	receptor activity /// plasma membrane /// immune	full-length
10392845	2,394464465	5,669463728	0,335926505	-5,670238858	3,218570833	8,671290607	6,547312912	Cluster VI	Cd300lf	CD300 antigen like family member	receptor activity /// protein binding /// plasma	full-length
10393341	1,149121609	4,773528908	0,138608494	-5,928036632	1,322266484	5,92524287	7,661117494		Rhbdf2	rhomboid 5 homolog 2	endoplasmic reticulum /// membrane /// integral to	full-length
10393449	0,773793266	-1,327426713	0,056670133	-6,341897585	1,119473844	1,608358209	6,989372155	Cluster III	Socs3	suppressor of cytokine signaling 3	regulation of cell growth /// regulation of protein	full-length
10393754	1,76581318	15,22034632	0,054534265	-6,206338935	1,962221976	16,07704213	11,50216721	Cluster I	Actg1	actin, gamma, cytoplasmic 1	nucleotide binding /// structural constituent of	full-length
10394054	1,138933719	3,636753121	0,01336199	-6,388100847	0,783656441	-0,392064577	5,983748651		Cd7	CD7 antigen	receptor activity /// immune response ///	full-length
10394068	1,194806982	-0,716258774	0,560962999	-4,358271053	1,124746572	-1,533316933	5,059150181		Sectm1a	secreted and transmembrane 1A	extracellular region /// plasma membrane ///	full-length
10394593	2,213459504	12,79084346	0,450407523	-2,481493959	2,348283286	13,08903361	7,819887087		Fam49a	family with sequence similarity 49,	---	full-length
10394674	-1,78352182	-1,779570122	-1,903208928	-0,608438617	-0,806442524	-5,880105734	8,610149583		---	---	---	partial
10394978	1,422706486	2,329722983	0,154469197	-6,150267775	1,032896095	-0,995206251	7,3537293		Rrm2	ribonucleotide reductase M2	ribonucleoside-diphosphate reductase activity ///	full-length
10395039	0,785167927	-1,769653404	2,097353396	7,791693477	1,424408161	3,340787627	7,435309179		Cmpk2	cytidine monophosphate (UMP-	nucleotide binding /// cytidylate kinase activity ///	full-length
10395259	1,147507637	1,122438025	0,682585815	-2,275930359	2,121606291	7,336951906	9,953764182		Nampt	nicotinamide	cytoplasm /// NAD biosynthetic process ///	full-length
10395273	1,434576677	-1,136793428	1,045593913	-2,586198095	1,882236995	0,894947699	6,321739011		Gdap10	ganglioside-induced differentiation-	---	full-length
10395275	-0,488662795	-6,097090524	-0,825587163	-3,532697959	-1,076411999	-3,117384936	6,217143022		100043821 ///	predicted gene, 100043821 ///	---	est
10395770	0,88012766	2,629449619	0,144009567	-5,824810786	1,044751718	4,03732745	7,199263659		Srp54c ///	signal recognition particle 54C ///	---	full-length
10395780	0,88012766	2,629449619	0,144009567	-5,824810786	1,044751718	4,03732745	7,199263659		Srp54c ///	signal recognition particle 54C ///	---	full-length
10395805	0,857542087	0,778533572	0,190979028	-5,678863099	1,053741675	2,415419716	8,681631134		1700047I17Rik1	RIKEN cDNA 1700047I17 gene 1	---	full-length
10396402	1,071638349	3,567697856	0,12287853	-6,052783996	0,883471046	1,204768584	7,291487619	Cluster III	Prkch	protein kinase C, eta	nucleotide binding /// protein kinase activity ///	full-length
10396919	0,627693376	-4,51854092	0,386769507	-5,236817828	1,480509428	1,34874753	8,8702687		4933426M11Rik	RIKEN cDNA 4933426M11 gene	---	full-length
10397145	-0,785886437	1,715537389	-0,34024313	-3,624202176	-1,405160143	7,65954487	7,820804004	Cluster X	Acot2	acyl-CoA thioesterase 2	carboxylesterase activity /// mitochondrion ///	full-length
10397148	-2,679519424	6,530530195	-0,54174295	-4,770249546	-3,901762127	10,52782823	6,949443915		Acot1	acyl-CoA thioesterase 1	long-chain fatty acid metabolic process ///	full-length
10397346	0,609271995	-4,869318125	0,355101232	-5,495958959	1,020338138	-2,250238417	6,13773868		Fos	FBJ osteosarcoma oncogene	DNA binding /// transcription factor activity ///	full-length
10397359	1,023215347	5,934855567	-0,235162539	-4,539232816	0,959111414	4,78198452	5,964798568		Batf	basic leucine zipper transcription	DNA binding /// transcription factor activity ///	full-length
10397541	0,514786118	-5,27349734	0,016220665	-6,389525982	1,001801681	-1,939870303	9,123939191		Eif1a ///	eukaryotic translation initiation	RNA binding /// translation initiation factor activity	full-length
10397543	0,608812509	-4,836788785	-0,030946735	-6,384367374	1,102969378	-1,607158422	9,157370996		Eif1a ///	eukaryotic translation initiation	RNA binding /// translation initiation factor activity	full-length
10397645	2,130857952	12,58583067	-0,093987929	-6,151396124	2,343083731	13,31014553	6,70528544		Gpr65	G-protein coupled receptor 65	signal transducer activity /// receptor activity /// G-	full-length
10398011	-4,236418831	5,376953055	-0,384729327	-6,094998667	-4,724305998	6,18582556	7,794616807		Serpina4-ps1	serine (or cysteine) peptidase	---	full-length
10398039	3,024887823	13,52453352	0,836000377	0,071615834	3,302049243	14,16722273	8,690266092		Serpina3g ///	serine (or cysteine) peptidase	endopeptidase inhibitor activity /// serine-type	full-length
10398069	0,65095769	-4,996485966	0,17085164	-6,211545304	1,354842259	-0,814721316	11,97186424		Serpina3m	serine (or cysteine) peptidase	endopeptidase inhibitor activity /// serine-type	full-length
10398075	0,748148429	-3,85597004	0,177316848	-6,151647049	1,294419992	-0,27651097	12,42849654		Serpina3n	serine (or cysteine) peptidase	endopeptidase inhibitor activity /// serine-type	full-length
10398267	1,328113799	6,655897573	0,201848204	-5,40605402	1,67139821	8,915702252	7,749627151		Evl	Ena-vasodilator stimulated	actin binding /// protein binding /// profilin binding	full-length
10398299	-0,414113476	-2,189107046	-0,20713247	-4,759823898	-1,042064259	6,336871498	12,00415093		AI132487	expressed sequence AI132487	transporter activity /// binding /// mitochondrion ///	full-length
10398665	1,395080545	6,346715589	-0,31897107	-4,437423227	1,431343308	6,210618629	8,046413842		Tnfaip2	tumor necrosis factor, alpha-	angiogenesis /// multicellular organismal	full-length
10398907	2,196906967	11,39213238	0,287734017	-4,83075924	1,988957712	9,779246239	7,792405489		Pld4	phospholipase D family, member 4	catalytic activity /// phospholipase D activity ///	full-length
10399005	1,842722128	10,4411117	-0,098534411	-6,14552749	1,595845627	8,301758115	7,507792165		Crip1	cysteine-rich protein 1 (intestinal)	zinc ion binding /// metal ion binding	full-length
10399087	2,356759165	5,831690596	0,113892433	-6,299233731	1,671018599	1,738825877	5,411149749		Ncapg2	non-SMC condensin II complex,	inner cell mass cell proliferation /// protein binding	full-length
10399178	1,127067018	0,335031041	0,125455748	-6,222959443	1,071082224	-0,47018502	5,622974669		Cdca7l	cell division cycle associated 7 like	protein binding /// nucleus /// cytoplasm ///	full-length
10399354	-0,366255893	-5,727432216	-0,070370004	-6,329168453	-1,100725263	0,469744695	6,011129199		---	---	---	est
10399360	0,614127492	-3,247146272	0,004575843	-6,391491767	1,037108548	0,461916687	7,695296935		Rhob	ras homolog gene family, member	nucleotide binding /// angiogenesis /// protein	full-length
10399457	1,137965692	5,430766007	0,017209863	-6,383292704	0,838680136	1,770338843	7,990043937		Akr1b3	aldo-keto reductase family 1,	aldehyde reductase activity /// cytoplasm ///	full-length
10399540	1,426207631	8,458097486	0,199326442	-5,268516067	1,260744555	6,585677966	6,026872392		Pqlc3	PQ loop repeat containing	membrane /// integral to membrane	full-length
10399710	1,240784794	-0,157267941	2,363898115	6,433481636	2,023616548	4,32671077	8,643245448	Cluster VII	Rsad2	radical S-adenosyl methionine	catalytic activity /// iron ion binding /// endoplasmic	full-length
10399924	1,740633292	11,10230928	0,00089324	-6,391765136	1,874917551	11,57004594	6,058329615		Pik3cg	phosphoinositide-3-kinase,	inositol or phosphatidylinositol kinase activity ///	full-length
10400023	1,28835144	0,936101917	-0,237037464	-5,88057061	1,13988572	-0,527390172	7,295455465		Tspan13	tetraspanin 13	membrane /// integral to membrane	full-length
10400357	0,708757144	-0,140400459	0,205382859	-5,425680148	1,012749728	2,929153795	7,299846646		Baz1a	bromodomain adjacent to zinc	nuclear chromosome /// protein binding /// nucleus	full-length
10400510	-1,29696058	3,316803279	-0,318007458	-5,028716076	-2,109816912	8,38905659	6,358353593		Clec14a	C-type lectin domain family 14,	binding /// sugar binding /// membrane /// integral	full-length
10400589	1,161950156	-0,53727765	-0,193614134	-6,084822032	0,812132146	-3,428831083	3,987229999		C79407	expressed sequence C79407	---	full-length
10400844	-0,323514574	-4,337820223	-0,046856844	-6,316685667	-1,088399635	5,522330055	11,1221662		Pygl	liver glycogen phosphorylase	nucleotide binding /// catalytic activity ///	full-length
10401160	1,225138039	1,313716903	-0,160927964	-6,104791485	1,228739332	0,963635091	6,56918436		6330442E10Rik	RIKEN cDNA 6330442E10 gene	membrane /// integral to membrane	full-length
10401829	0,595803589	-4,749467229	-0,025635437	-6,386243133	1,097266459	-1,314144536	8,497319048		Eif1a ///	eukaryotic translation initiation	RNA binding /// translation initiation factor activity	full-length
10402268	1,493248649	12,7635069	0,010006908	-6,385967906	1,512831697	12,51011842	10,81436756		Lgmn	legumain	cysteine-type endopeptidase activity /// lysosome	full-length
10402347	1,24179531	9,379263728	0,592324645	1,736052766	1,157023561	8,110260294	6,430070166		Ifi27	interferon, alpha-inducible protein	aging /// response to virus	full-length
10402428	-0,839393488	-0,577386966	0,000339599	-6,391789134	-1,723276604	6,368210274	7,875891223		Serpina12	serine (or cysteine) peptidase	endopeptidase inhibitor activity /// serine-type	full-length
10402585	0,921100346	5,661194202	-0,044298367	-6,302820047	1,339516934	9,599457844	8,611743433		Wars	tryptophanyl-tRNA synthetase	nucleotide binding /// aminoacyl-tRNA ligase	full-length
10402708	1,18918105	0,969065702	0,029781478	-6,381872439	0,655028302	-3,831718517	7,671534298		Ckb	creatine kinase, brain	nucleotide binding /// catalytic activity /// creatine	full-length
10402864	2,412037407	8,105508827	0,014681937	-6,389599134	2,523119293	8,202195067	6,248789458	Cluster VI	Igh /// Igh-6 ///	immunoglobulin heavy chain	activation of MAPK activity /// humoral immune	full-length
10402991	2,399502366	3,94282047	-0,331881645	-5,870341475	2,157094225	2,41403181	6,467209059		---	---	---	partial
10403006	1,620561415	-1,344328757	0,135290938	-6,327309011	0,777842614	-5,545859126	3,798757982		---	---	---	partial
10403009	2,389924278	-0,977717719	-0,691308212	-5,591200369	2,05812809	-2,423139364	5,082742289		---	---	---	full-length
10403011	2,111400194	2,704021211	0,118904277	-6,320955827	1,778406131	0,628485928	3,842409925		---	---	---	partial
10403015	4,337803737	9,685338007	-0,545166827	-5,273574212	4,120459401	8,643590934	6,744391441		---	---	---	partial
10403018	4,21655688	8,942663514	-0,873432448	-3,98083219	3,951374756	7,743953801	7,37883165		---	---	---	partial
10403021	4,287390512	7,729487478	-0,046014356	-6,385402761	3,997255288	6,48350264	5,800215116		---	---	---	partial
10403028	3,752118089	10,65221645	-0,075561169	-6,355007032	3,266736604	8,574404045	4,964840004		---	---	---	partial
10403031	1,92222016	-0,917950971	0,035480886	-6,388269904	1,989601566	-0,968703829	4,68986167		---	---	---	partial
10403034	5,189469753	13,669253	-0,195840125	-6,179949344	5,241060299	13,38871935	7,401476571		Igh	immunoglobulin heavy chain	---	full-length
10403036	1,638535218	-0,450231253	-0,145283652	-6,301570293	1,428014942	-1,881517886	3,831466274		Igh	immunoglobulin heavy chain	---	full-length
10403038	3,048582165	12,45499113	0,123845885	-6,191691887	2,520318938	9,76137894	4,406416528		---	---	---	partial

Affymetrix ID	BS/Non Inf.		LS/Non Inf.		ReINF/Non Inf.		Average	Cluster	Gene	Gene	Gene Ontology (GO)	Transcript
Transcript	logFC	B	logFC	B	logFC	B	expression	Number	Symbol	Title	Description	Classification
10403043	3,894345847	11,19214841	-0,024815067	-6,387748467	3,908256773	10,81170244	7,674871583	Cluster VIII	---	---	---	partial
10403046	0,566215986	-5,515228577	0,011803673	-6,390935091	1,168699793	-2,048141491	3,878503935		---	---	---	partial
10403048	4,330384989	13,11068604	-0,272816451	-5,867690611	4,278419591	12,56065952	7,978757401	Cluster VIII	---	---	---	partial
10403054	3,276720893	10,2179919	-0,033339043	-6,383043153	3,208850097	9,539312284	7,262290059		---	---	---	partial
10403060	3,474690349	12,27257273	-0,044089698	-6,372591976	3,290268835	11,20381827	6,407605945		---	---	---	partial
10403063	4,290722601	11,40701745	-0,062370461	-6,370010917	4,405231237	11,30132205	6,63507977		Igh	immunoglobulin heavy chain	---	full-length
10403069	4,49697847	12,13711639	-0,217895463	-6,123392072	4,354255691	11,33444869	5,151612048		---	---	---	partial
10403073	2,553319795	1,452620719	0,394920598	-5,986090858	2,532027782	0,992309655	3,791517751		---	---	---	partial
10403079	3,862783219	9,268242166	-0,237930472	-6,124018497	3,559129045	7,8684451	6,34304094		---	---	---	partial
10403108	1,178575616	5,298144584	0,116595453	-6,045838055	0,925758752	2,292751768	9,558395208		Hmgn2	high mobility group nucleosomal	chromatin /// DNA binding /// nucleus /// cytoplasm	full-length
10403352	1,26068969	3,913274215	-0,134064248	-6,080144249	1,790123181	7,446241723	7,597721323		Klf6	Kruppel-like factor 6	nucleic acid binding /// DNA binding /// intracellular	full-length
10403743	-1,350960195	4,66877051	-0,69941719	-0,919781683	-1,901696051	8,157441671	6,548072685		Inhba	inhibin beta-A	receptor binding /// hormone activity ///	full-length
10403842	1,463572157	9,408897112	-0,095184702	-6,086984176	1,520993538	9,435594404	5,951190619		Elmo1	engulfment and cell motility 1, ced-	protein binding /// cytoplasm /// cytoskeleton ///	full-length
10403871	1,692428397	8,281319133	0,117035347	-6,106640473	1,713700433	7,995078383	6,294626442		Aoah	acyloxyacyl hydrolase	lipid metabolic process /// lipopolysaccharide	full-length
10403938	1,011035303	3,641839976	0,039051838	-6,35186637	0,792729324	0,792897986	10,80120072	Cluster III	Hist1h2ai ///	histone cluster 1, H2ai /// histone	nucleosome /// DNA binding /// nucleus ///	full-length
10403941	2,656640354	11,07813234	0,233534434	-5,677809695	2,344801224	9,161492735	10,27607897	Cluster VI	Hist1h3i ///	histone cluster 1, H3i /// histone	nucleosome /// DNA binding /// nucleus ///	full-length
10403943	1,120615391	1,549044076	0,203522352	-5,828277997	0,828974157	-1,472093356	7,723914203	Cluster III	Hist1h2bm	histone cluster 1, H2bm	nucleosome /// DNA binding /// nucleus ///	full-length
10403948	1,004053745	0,761116453	-0,088212161	-6,275957082	0,611647463	-3,381911426	9,427372087		LOC665622 ///	H2b histone family member ///	nucleosome /// DNA binding /// nucleus ///	full-length
10403955	1,037873776	3,422236924	0,025148054	-6,376685124	0,797657686	0,415266552	11,02750983	Cluster III	RP23-480B19.10	similar to histone 2a /// histone	nucleosome /// DNA binding /// nucleus ///	full-length
10403957	1,083932352	2,622156242	0,037934599	-6,364773774	0,806643561	-0,548756545	9,955015714	Cluster III	Hist1h4i ///	histone cluster 1, H4i /// histone	nucleosome /// DNA binding /// nucleus ///	full-length
10403978	1,057983377	1,071912872	-0,05369897	-6,350260663	0,67753786	-2,862977282	9,612201009		LOC665622 ///	H2b histone family member ///	nucleosome /// DNA binding /// nucleus ///	full-length
10404026	1,004131759	3,186191256	0,015980321	-6,3855548	0,778642822	0,292649043	11,05200557	Cluster III	Hist1h2ai ///	histone cluster 1, H2ai /// histone	nucleosome /// DNA binding /// nucleus ///	full-length
10404028	2,603618434	10,85407752	0,248023803	-5,589892243	2,304269785	8,970109424	10,36666004	Cluster VI	Hist1h3i ///	histone cluster 1, H3i /// histone	nucleosome /// DNA binding /// nucleus ///	full-length
10404045	1,042313045	3,499200285	0,015822981	-6,385770926	0,79826785	0,449626287	10,84549605	Cluster III	Hist1h2ai ///	histone cluster 1, H2ai /// histone	nucleosome /// DNA binding /// nucleus ///	full-length
10404049	2,749791353	10,85610984	0,264904828	-5,572538312	2,420768202	8,909123131	10,35790962	Cluster VI	Hist1h3i ///	histone cluster 1, H3i /// histone	nucleosome /// DNA binding /// nucleus ///	full-length
10404061	1,060988666	-0,478686811	0,269557393	-5,690363293	0,943211155	-1,757122982	5,224189199	Cluster III	Hist1h2bb	histone cluster 1, H2bb	nucleosome /// DNA binding /// nucleus ///	full-length
10404063	2,178380614	3,680430705	0,057091388	-6,37324649	1,390160901	-0,992441981	4,158456098		Hist1h2ab	histone cluster 1, H2ab	nucleosome /// DNA binding /// nucleus ///	full-length
10404065	2,726411915	11,08407653	0,250747507	-5,613465591	2,416737208	9,218562981	10,49620367	Cluster VI	Hist1h3i ///	histone cluster 1, H3i /// histone	nucleosome /// DNA binding /// nucleus ///	full-length
10404067	1,033673356	3,385528424	0,031752827	-6,367696583	0,784845383	0,272698487	10,22968492	Cluster III	Hist1h4m ///	histone cluster 1, H4m /// histone	nucleosome /// DNA binding /// nucleus ///	full-length
10404069	1,626035492	3,747389607	-0,104516501	-6,279660429	1,1859411	0,215485721	7,752394477		Hist1h1a	histone cluster 1, H1a	nucleosome /// DNA binding /// nucleus ///	full-length
10404097	-0,900095184	2,929042522	0,005478626	-6,390922106	-1,101639355	4,690669101	9,493295348		Slc17a3	solute carrier family 17 (sodium	---	full-length
10404132	-0,897137612	-4,390626389	0,000504039	-6,391789858	-1,653929598	-0,644467084	9,930473069	Cluster X	Cmah	cytidine monophospho-N-	iron ion binding /// cytoplasm /// endoplasmic	full-length
10404152	1,570728718	6,644797174	-0,062726013	-6,318808392	1,744170892	7,427818227	5,893428157		Fam65b	family with sequence similarity 65,	binding	full-length
10404389	1,165804227	4,369368097	-0,258682058	-5,033796989	1,429154956	6,229401636	4,70963077	Cluster IV	Irf4	interferon regulatory factor 4	DNA binding /// transcription factor activity ///	full-length
10404422	0,818703961	1,349662037	0,111271679	-6,082772061	1,222765064	5,160686433	7,079824406		Serpinb6b	serine (or cysteine) peptidase	---	full-length
10404429	1,143220679	3,127847614	0,145216577	-6,010205264	1,517787696	5,818186752	6,642140254		Serpinb9	serine (or cysteine) peptidase	protein binding /// anti-apoptosis	full-length
10404439	0,937929806	0,19623511	0,113369739	-6,199085796	1,212375807	2,284911638	4,997937458		Serpinb9b	serine (or cysteine) peptidase	protein binding /// cytolysis	full-length
10404496	-0,353015577	-5,823868425	-0,08940307	-6,290799673	-1,01561348	-0,244164602	10,21135598	Cluster X	Nqo2	NAD(P)H dehydrogenase, quinone	dihydronicotinamide riboside quinone reductase	full-length
10404606	1,774521878	7,451937686	0,345994823	-4,641714074	1,555228036	5,505739165	9,058640403	Cluster I	Ly86	lymphocyte antigen 86	protein binding /// extracellular region ///	full-length
10404874	-0,778647753	4,735822104	-0,150221369	-5,273121148	-1,013959411	7,31448221	7,084982906		Mylip	myosin regulatory light chain	molecular_function /// binding /// protein binding ///	full-length
10405216	1,677566478	8,248008208	0,053573833	-6,330259197	1,57094802	7,046848368	6,416556822	Cluster I	Syk	spleen tyrosine kinase	nucleotide binding /// activation of MAPK activity ///	full-length
10405587	1,038529572	6,280423137	0,01178464	-6,386231903	1,219639924	7,711946634	9,217578351		Tgfbi	transforming growth factor, beta	protein binding /// extracellular region ///	full-length
10405753	-0,77841468	-2,779502736	-0,030464808	-6,38222512	-1,40252469	1,793414342	11,10209971	Cluster X	Me1	malic enzyme 1, NADP(+)-	catalytic activity /// malic enzyme activity /// malate	full-length
10406407	-0,132794714	-7,17789115	-0,046992785	-6,379220837	-1,401069646	-0,928053055	10,06352336		Arrdc3	arrestin domain containing 3	molecular_function /// cellular_component ///	full-length
10406417	1,605874795	13,36525042	0,007367722	-6,388768671	1,777866237	14,17400532	11,60114828		Actg1	actin, gamma, cytoplasmic 1	nucleotide binding /// structural constituent of	full-length
10406676	-1,141512845	3,74917922	-0,428593424	-3,370723353	-1,448358048	5,968348952	6,521617429		Lhfpl2	lipoma HMGIC fusion partner-like	membrane /// integral to membrane	full-length
10406817	0,530953684	-3,325505291	0,086399273	-6,254219671	1,044105157	1,797532176	7,554511623		Enc1	ectodermal-neural cortex 1	actin binding /// protein binding /// cytoplasm ///	full-length
10406928	2,56849209	17,16581422	0,110748034	-5,894686271	2,826397166	17,91298073	7,022083842	Cluster VI	Cd180	CD180 antigen	receptor activity /// protein binding /// plasma	full-length
10406982	0,643151629	-3,557585931	0,851854434	-0,996312857	1,323500189	1,85478772	5,314655354		Adamts6	a disintegrin-like and	molecular_function /// cellular_component ///	full-length
10407327	2,4935708	4,607925365	-0,330479742	-5,851719965	2,86552595	5,739516162	5,758154418		Emb	embigin	membrane /// integral to membrane	full-length
10407481	1,775358402	11,34963967	-0,110298871	-6,008675967	2,194438508	13,46550743	7,321659514		Pfkp	phosphofructokinase, platelet	nucleotide binding /// magnesium ion binding ///	full-length
10407792	1,517900535	4,38555468	-0,212925213	-5,812571708	1,830979119	6,061363868	6,519176974		Gpr137b-ps ///	G protein-coupled receptor 137B,	molecular_function /// cellular_component ///	full-length
10407803	1,159358544	1,522383585	0,258624353	-5,563763527	1,288877063	2,187174401	6,007661361		Gpr137b	G protein-coupled receptor 137B	molecular_function /// cellular_component ///	full-length
10407985	2,412308373	4,233311296	0,153448223	-6,271724004	3,103360856	6,641294408	4,742868145		Gpr141	G protein-coupled receptor 141	signal transducer activity /// receptor activity /// G-	full-length
10408072	1,010068222	3,503430192	0,03156476	-6,366298409	0,787498501	0,618477156	11,07846573	Cluster III	Hist1h2ai ///	histone cluster 1, H2ai /// histone	nucleosome /// DNA binding /// nucleus ///	full-length
10408074	1,030828203	3,296861972	0,050982006	-6,330548389	0,796721123	0,358431987	10,20357844	Cluster III	Hist1h4m ///	histone cluster 1, H4m /// histone	nucleosome /// DNA binding /// nucleus ///	full-length
10408077	1,28868286	2,58698012	-0,02905779	-6,380638533	0,987583699	-0,325216131	6,156464837	Cluster III	Hist1h2ak	histone cluster 1, H2ak	nucleosome /// DNA binding /// nucleus ///	full-length
10408081	2,812923756	10,96193489	0,184656867	-5,99155171	2,552592512	9,375854526	8,758656865	Cluster VI	Hist1h1b	histone cluster 1, H1b	nucleosome /// DNA binding /// protein binding ///	full-length
10408083	2,649884886	10,95584562	0,243234839	-5,631898033	2,332684904	9,907990185	10,26776855	Cluster VI	Hist1h3i ///	histone cluster 1, H3i /// histone	nucleosome /// DNA binding /// nucleus ///	full-length
10408085	1,018184824	3,369328625	0,020011024	-6,381947355	0,797077252	0,539189499	10,80013262	Cluster III	Hist1h2ai ///	histone cluster 1, H2ai /// histone	nucleosome /// DNA binding /// nucleus ///	full-length
10408092	1,083932352	2,622156242	0,037934599	-6,364773774	0,806643561	-0,548756545	9,955015714	Cluster III	Hist1h4i ///	histone cluster 1, H4i /// histone	nucleosome /// DNA binding /// nucleus ///	full-length
10408094	1,022867933	3,591068061	0,03605511	-6,358838125	0,793267193	0,645735645	10,8471452	Cluster III	RP23-480B19.10	similar to histone 2a /// histone	nucleosome /// DNA binding /// nucleus ///	full-length
10408111	1,012918984	3,362643784	0,021968165	-6,379821143	0,78275691	0,413990572	11,02689464	Cluster III	Hist1h2ai ///	histone cluster 1, H2ai /// histone	nucleosome /// DNA binding /// nucleus ///	full-length
10408118	1,045914804	3,491040544	0,033613183	-6,36489555	0,813642892	0,587064081	10,79949939	Cluster III	Hist1h2ag ///	histone cluster 1, H2ag /// histone	nucleosome /// molecular_function /// DNA binding	full-length
10408200	1,421810245	2,668680891	0,063709336	-6,347161071	1,234249764	0,879564021	7,385365586	Cluster III	Hist1h4f	histone cluster 1, H4f	nucleosome /// DNA binding /// nucleus ///	full-length
10408202	2,674371361	10,21067781	0,217988415	-5,853739131	2,336739279	8,177992903	10,18473722	Cluster VI	Hist1h3i ///	histone cluster 1, H3i /// histone	nucleosome /// DNA binding /// nucleus ///	full-length
10408239	2,689368252	11,19583886	0,2518841	-5,572018029	2,369072959	9,256003265	10,46535703	Cluster VI	Hist1h3i ///	histone cluster 1, H3i /// histone	nucleosome /// DNA binding /// nucleus ///	full-length
10408243	1,06134143	3,663048314	0,094210028	-6,182863685	0,839327786	0,892430554	9,94395126	Cluster III	Hist1h4m ///	histone cluster 1, H4m /// histone	nucleosome /// DNA binding /// nucleus ///	full-length
10408246	2,608984263	10,81349922	0,240695322	-5,641715772	2,297328517	8,86930596	10,36360744	Cluster VI	Hist1h3a ///	histone cluster 1, H3a /// histone	nucleosome /// DNA binding /// nucleus ///	full-length
10408251	-0,2257751	-6,707382349	0,2214465	-5,853433258	-1,183883458	0,66171065	9,185585321		Slc17a4	solute carrier family 17 (sodium	transporter activity /// transport /// ion transport ///	full-length
10408600	1,014257298	1,833239822	-0,129014317	-6,092824855	0,679061019	-2,010586481	8,283333601		Serpinb6a	serine (or cysteine) peptidase	endopeptidase inhibitor activity /// serine-type	full-length
10408693	1,673038375	-3,326360576	-0,367135822	-6,143816796	2,777961747	0,187511219	5,712335758		F13a1	coagulation factor XIII, A1 subunit	protein-glutamine gamma-glutamyltransferase	full-length

Affymetrix ID	BS/Non Inf.			LS/Non Inf.		ReINF/Non Inf.		Average	Cluster	Gene	Gene	Gene Ontology (GO)	Transcript
Transcript	logFC	B		logFC	B	logFC	B	expression	Number	Symbol	Title	Description	Classification
10408838	-0,524174474	-4,823580402		-0,08751202	-6,311645142	-1,679538688	3,772874628	11,37920873	Cluster X	Elovl2	elongation of very long chain fatty	very-long-chain fatty acid metabolic process ///	full-length
10408850	1,068925592	6,055389156		-0,148033571	-5,640923679	1,062705125	5,560992577	7,079941882	Cluster III	Nedd9	neural precursor cell expressed,	regulation of cell growth /// protein binding ///	full-length
10408861	-0,724048852	0,223769085		-0,042286803	-6,346006033	-1,027027005	3,282750419	9,509372748		9530008L14Rik	RIKEN cDNA 9530008L14 gene	membrane /// integral to membrane	full-length
10409240	1,846269208	10,08405799		0,020260726	-6,381842135	2,038492694	10,84060835	6,461892809		Sema4d	sema domain, immunoglobulin	receptor binding /// multicellular organismal	full-length
10409376	1,897247082	8,304814493		0,108437502	-6,194868798	2,158847792	9,402381432	6,988596414		Hk3	hexokinase 3	nucleotide binding /// catalytic activity ///	full-length
10409567	1,862487502	6,317365676		0,178774213	-6,003206374	2,088668809	7,209941214	6,060815846		Tifab	TRAF-interacting protein with	---	full-length
10409866	1,208470232	5,332220193		0,199139508	-5,469044371	0,621620548	-1,513341107	5,914253402		Ctla2b	cytotoxic T lymphocyte-associated	cysteine protease inhibitor activity /// protein	partial
10409876	1,782509988	6,502418331		0,153153368	-6,068572673	1,853597947	6,521443825	6,039876641		Ctla2a	cytotoxic T lymphocyte-associated	molecular_function /// cellular_component ///	full-length
10410452	-1,363159492	-3,494152106		-0,000896818	-6,391788824	-1,761729846	-2,095708147	9,460559388	Cluster IX	Srd5a1	steroid 5 alpha-reductase 1	3-oxo-5-alpha-steroid 4-dehydrogenase activity ///	full-length
10410560	1,081985533	2,452804367		-0,012822341	-6,388788134	0,807327052	-0,666580287	5,630000489		Trip13	thyroid hormone receptor	nucleotide binding /// pachytene /// oocyte	full-length
10410650	-0,926630249	2,300887814		-0,419003046	-3,136384648	-1,09240193	3,615806155	7,123835428		Zfp825	zinc finger protein 825	nucleus /// zinc ion binding /// metal ion binding	full-length
10410927	-0,488662795	-6,097090524		-0,825587163	-3,532697959	-1,076411999	-3,117384936	6,217143022		LOC280487	pol polyprotein	---	partial
10410931	1,729542495	-0,511448571		0,13312081	-6,324653275	2,028486224	0,551234424	5,144738856		Vcan	versican	binding /// calcium ion binding /// sugar binding ///	full-length
10411359	1,792012955	6,978017219		-0,07141986	-6,314801607	1,729926972	6,140992556	6,998276701		Plp2	proteolipid protein 2	membrane /// integral to membrane	full-length
10411595	0,995286333	4,561796084		0,170330472	-5,521789554	1,023057653	4,444672927	6,222896902		Naip2	NLR family, apoptosis inhibitory	nucleotide binding /// intracellular /// apoptosis ///	full-length
10411633	1,216206039	3,137363684		0,223687191	-5,614918129	0,798239658	-1,180420403	4,881047026		Naip1	NLR family, apoptosis inhibitory	nucleotide binding /// intracellular /// apoptosis ///	full-length
10411668	-0,666225565	-2,620722632		-0,216683234	-5,733106596	-1,269379597	2,602566946	7,487831736		Ocln	occludin	structural molecule activity /// protein binding ///	full-length
10411728	1,451033253	1,804600321		0,119610032	-6,265273963	0,9970172	-1,839213113	4,183971695	Cluster III	Cenph	centromere protein H	kinetochore /// kinetochore /// protein binding ///	full-length
10411739	2,488172416	6,804383		-0,196357992	-6,103639215	2,251759816	5,237689133	5,870559277		Ccnb1	cyclin B1	in utero embryonic development /// protein binding	full-length
10412036	-0,45115032	-3,217020777		-0,178401881	-5,59231414	-1,052625319	3,759644386	7,912664386		Apoo /// Apoo-ps	apolipoprotein O /// apolipoprotein	membrane /// integral to membrane	full-length
10412123	1,543574131	9,569308021		0,02091855	-6,377881983	1,504395589	8,832488827	6,384197149		Ncf2	neutrophil cytosolic factor 2	acrosome /// binding /// protein binding ///	full-length
10412211	3,430390235	13,31908536		0,140570235	-6,15684091	3,700117919	13,81842533	6,319758208		Gzma	granzyme A	serine-type endopeptidase activity /// extracellular	full-length
10412218	1,181816292	8,48809159		0,008615211	-6,388436167	1,121690893	7,441785754	5,296097447		Gzmk	granzyme K	serine-type endopeptidase activity /// proteolysis ///	full-length
10412345	1,465779112	9,024957918		-0,249636416	-4,645848949	1,655868631	10,04537423	6,361684057		Parp8	poly (ADP-ribose) polymerase	NAD+ ADP-ribosyltransferase activity /// nucleus	full-length
10412607	-1,390891779	5,89759731		-0,186542311	-5,703454918	-1,901624217	9,11239537	8,903904949		Abhd6	abhydrolase domain containing 6	catalytic activity /// membrane /// integral to	full-length
10413047	2,023844067	7,40783395		-0,105536554	-6,250558974	1,876070715	6,100702814	6,515110578		Plau	plasminogen activator, urokinase	response to hypoxia /// serine-type endopeptidase	full-length
10414163	-0,650084089	-1,517696827		-0,041309231	-6,355975999	-1,022002646	2,19609727	7,170806772		Lrit1	leucine-rich repeat,	protein binding /// endoplasmic reticulum ///	full-length
10414262	2,263078432	10,0681886		-0,162422298	-5,980443354	2,249403484	9,566477115	6,70650711		Ear2	eosinophil-associated,	nucleic acid binding /// nuclease activity ///	full-length
10414360	2,866730502	14,22814816		0,205413917	-5,589846347	3,111773911	14,80785711	8,184513738		Lgals3	lectin, galactose binding, soluble 3	skeletal development /// protein binding /// sugar	full-length
10414548	1,7722049	7,615476489		-0,110031642	-6,185366188	1,597444896	5,984295756	6,257220313		Rnase6	ribonuclease, RNase A family, 6	nucleic acid binding /// nuclease activity ///	full-length
10415052	1,035300964	3,884063216		0,053241695	-6,317947871	1,439530205	7,169420941	8,987358541		Mmp14	matrix metallopeptidase 14	metalloendopeptidase activity /// calcium ion	full-length
10415279	-1,417876186	4,879359713		-0,151605523	-6,01772778	-1,947796403	8,094265501	9,114115085		1110028A07Rik	RIKEN cDNA 1110028A07 gene	endoplasmic reticulum /// membrane /// integral to	full-length
10416023	0,79672943	-5,581003887		0,381567119	-5,972973563	1,911733017	-1,04828725	6,708502695		Scara5	scavenger receptor class A,	scavenger receptor activity /// plasma membrane	full-length
10416037	1,172340705	-2,285815974		-0,130575577	-6,302769279	0,157812195	-7,210773537	4,67100739	Cluster III	Pbk	PDZ binding kinase	nucleotide binding /// protein kinase activity ///	full-length
10416071	-0,862731701	0,370234525		-0,249172111	-5,32468896	-1,072324622	2,082431628	5,70183682		Chrna2	cholinergic receptor, nicotinic,	receptor activity /// nicotinic acetylcholine-activated	full-length
10416334	0,874771103	1,612933129		0,109396373	-6,114949803	1,065961839	3,234381088	6,69580545		Dok2	docking protein 2	MAPKKK cascade /// transmembrane receptor	full-length
10416340	1,081198624	-1,600153237		0,019538754	-6,388948473	0,505563684	-5,723286941	5,335315329		Gfra2	glial cell line derived neurotrophic	receptor activity /// plasma membrane ///	full-length
10416437	0,794454397	6,789689158		-0,127875889	-5,272202635	1,102540119	10,22162057	10,33094596		Lcp1	lymphocyte cytosolic protein 1	ruffle /// phagocytic cup /// actin binding /// calcium	full-length
10416566	1,322241611	9,197014321		0,28737806	-3,688190184	1,163299783	7,256789524	5,869620573		Epsti1	epithelial stromal interaction 1	molecular_function /// cellular_component ///	full-length
10416696	-0,488662795	-6,097090524		-0,825587163	-3,532697959	-1,076411999	-3,117384936	6,217143022		100043821 ///	predicted gene, 100043821 ///	---	est
10416698	-0,488662795	-6,097090524		-0,825587163	-3,532697959	-1,076411999	-3,117384936	6,217143022		100043821 ///	predicted gene, 100043821 ///	---	est
10416700	1,153499881	-0,967828384		0,036114042	-6,381788513	0,454941109	-5,964796962	5,994365929		Pcdh17	protocadherin 17	calcium ion binding /// protein binding /// plasma	full-length
10416837	3,07736229	4,602021016		-0,156371507	-6,309598454	3,595138698	5,920298612	6,674863917		Irg1	immunoresponsive gene 1	propionate catabolic process /// response to	full-length
10417787	1,03790217	4,597224852		0,033164717	-6,35919191	0,963873257	3,380243395	6,872385087		Gng2	guanine nucleotide binding protein	GTPase activity /// signal transducer activity ///	full-length
10418410	1,140518857	5,790194814		0,039110906	-6,345359269	1,282549077	6,704151981	8,09274887	Cluster IV	Prkcd	protein kinase C, delta	nucleotide binding /// protein kinase activity ///	full-length
10418434	0,751164488	0,185850163		0,1290006	-6,009389634	1,098754735	3,565523283	12,51440271		Itih3	inter-alpha trypsin inhibitor, heavy	endopeptidase inhibitor activity /// serine-type	full-length
10418848	1,328702946	3,511998235		0,123193638	-6,170419061	1,081487982	1,031975639	6,231075677		Wdfy4	WD repeat and FYVE domain	---	partial
10418868	1,422117113	2,724279327		0,109568469	-6,259320022	1,004862074	-0,901366629	6,763233079		---	---	---	predicted
10418917	-0,755013901	-0,988783226		-0,140704078	-6,048236209	-1,107546431	2,168480798	8,049869819		2200001I15Rik	RIKEN cDNA 2200001I15 gene	---	full-length
10419082	-0,6305862	1,790460819		-0,025557435	-6,361065288	-1,089073786	7,342468881	10,41096244		5730469M10Rik	RIKEN cDNA 5730469M10 gene	extracellular region	full-length
10419154	1,824621031	9,835061402		-0,003448791	-6,391507718	1,624689193	8,02836958	5,73450307		Ear2 /// Ear1 ///	eosinophil-associated,	nucleic acid binding /// nuclease activity ///	full-length
10419156	2,046706297	6,699734101		-0,002442783	-6,391724781	1,813061987	4,896932944	6,271160705		Ear2 /// Ear1 ///	eosinophil-associated,	nucleic acid binding /// nuclease activity ///	full-length
10419296	1,160290348	2,779568821		-0,000876063	-6,391777978	1,012340426	1,029637081	5,684902209		Wdhd1	WD repeat and HMG-box DNA	DNA binding /// nucleus	full-length
10419323	1,570038014	4,452191649		0,107457158	-6,247385138	1,396478739	2,787233013	5,686657303		Dlgap5	discs, large (Drosophila) homolog-	nucleus /// cytoplasm /// cell cycle /// cell-cell	full-length
10419563	-4,085458832	1,162971677		-3,094252761	-0,608404836	-4,114620294	0,854708968	6,062411127		Rnase1	ribonuclease, RNase A family, 1	nucleic acid binding /// nuclease activity ///	full-length
10419854	1,860609124	11,21372998		0,109706572	-6,05332113	2,135477046	12,44323259	7,533482936		Slc7a8	solute carrier family 7 (cationic	amine transmembrane transporter activity ///	full-length
10420023	-0,581250126	-3,027489904		0,168097551	-5,925138904	-1,113826155	2,0241902	8,178549003		Fam158a	family with sequence similarity	---	full-length
10420198	2,085226247	11,00553043		0,220196085	-5,396477187	1,870699525	9,283001959	6,89746141		Ripk3	receptor-interacting serine-	nucleotide binding /// protein kinase activity ///	full-length
10420308	4,739648816	15,47432623		0,287669311	-5,67388678	5,280516687	16,36105088	7,145009835	Cluster VIII	Gzmb	granzyme B	serine-type endopeptidase activity /// protein	full-length
10420426	1,333050422	-0,877488785		-0,116986967	-6,311886325	0,866736596	-4,056564519	4,420003638		F630043A04Rik	RIKEN cDNA F630043A04 gene	---	full-length
10420483	1,947397729	3,932709116		0,885863718	-2,234253083	2,322103987	5,456833953	5,23748241		Phf11 ///	PHD finger protein 11 /// predicted	---	full-length
10420488	0,952217941	0,999543106		0,757201147	-0,368515922	1,522709011	5,518553136	6,957555637		D14Ertd668e ///	DNA segment, Chr 14, ERATO Doi	DNA binding /// nucleus /// methyltransferase	full-length
10420935	-0,855791201	6,976219728		-0,045933479	-6,252867676	-1,142308166	9,948892794	11,52961769		Ephx2	epoxide hydrolase 2, cytoplasmic	magnesium ion binding /// catalytic activity ///	full-length
10421029	1,292894468	2,541242522		0,229578766	-5,739790672	0,724769138	-2,76271783	5,279592811	Cluster III	Cdca2	cell division cycle associated 2	molecular_function /// cellular_component ///	full-length
10421293	1,071854084	6,256505287		-0,191568099	-5,146468318	1,062085568	5,723218877	6,540193183		Ppp3cc	protein phosphatase 3, catalytic	phosphoprotein phosphatase activity /// iron ion	full-length
10421309	0,227183247	-6,912292179		-0,031222194	-6,384823978	1,024446085	-2,446551362	10,22480952		Slc39a14	solute carrier family 39 (zinc	zinc ion transmembrane transporter activity ///	full-length
10421648	-2,500849101	4,458013489		-0,984584126	-2,79072219	-2,913221775	5,738994633	8,878193232		Slc25a30	solute carrier family 25, member	transporter activity /// binding /// mitochondrion ///	full-length
10421697	1,484596241	6,320152516		0,245565075	-5,299841049	1,981364073	9,266597797	7,938886558		9030625A04Rik	RIKEN cDNA 9030625A04 gene	---	full-length
10422247	-0,488662795	-6,097090524		-0,825587163	-3,532697959	-1,076411999	-3,117384936	6,217143022		LOC280487	pol polyprotein	---	partial
10422493	1,086765034	3,9468177		0,196985869	-5,520065782	1,073495126	3,4024823	5,979377752		Gpr18	G protein-coupled receptor 18	signal transducer activity /// receptor activity /// G-	full-length
10422608	1,359864788	0,278290709		0,083418859	-6,340687954	1,200894381	-1,134943011	6,618715783		Oxct1	3-oxoacid CoA transferase 1	mitochondrion /// metabolic process /// 3-oxoacid	full-length
10422635	-1,626773115	2,936619132		-0,074116017	-6,343219375	-1,908887909	4,2347417	9,704342597		C6	complement component 6	---	full-length

Affymetrix ID	BS/Non Inf.			LS/Non Inf.			RelNF/Non Inf.		Average	Cluster	Gene	Gene	Gene Ontology (GO)	Transcript
Transcript	logFC	B		logFC	B		logFC	B	expression	Number	Symbol	Title	Description	Classification
10422748	-1,011501279	-0,785611259		0,011821303	-6,390333294		-1,153547347	0,000170563	11,49263507	Cluster X	C9	complement component 9	extracellular region /// membrane attack complex	full-length
10422760	2,121215255	7,029865932		0,255835346	-5,713117689		2,025042928	6,064795188	7,013326301	Cluster I	Fyb	FYN binding protein	nucleus /// cytoplasm /// mast cell activation	full-length
10422822	-1,206566678	-2,683148725		-0,20630745	-6,206349742		-2,006593534	1,152124436	10,37370014		Lifr	leukemia inhibitory factor receptor	receptor activity /// hematopoietin/interferon-class	full-length
10423005	-1,268627979	7,644371912		-0,065733874	-6,246618518		-1,654735772	10,36084297	10,05926814		Ugt3a1	UDP glycosyltransferases 3 family,	metabolic process /// glucuronosyltransferase	full-length
10423090	-0,584527936	-0,364574257		-0,046189538	-6,318594351		-1,14144221	6,0795235	10,06168223		Amacr	alpha-methylacyl-CoA racemase	catalytic activity /// mitochondrion /// peroxisome ///	full-length
10424188	1,099818259	0,81327286		0,215750749	-5,827923196		0,849252223	-1,733229611	5,293418537		Mtbp	Mdm2, transformed 3T3 cell	protein binding /// ubiquitin-dependent protein	full-length
10424377	-0,488662795	-6,097090524		-0,825587163	-3,532697959		-1,076411999	-3,117384936	6,217143022		100043821 ///	predicted gene, 100043821 ///	---	predicted
10424400	1,610728559	10,97211977		-0,214528029	-4,881263666		1,531018796	9,939740787	7,262905063		Myc	myelocytomatosis oncogene	B cell apoptosis /// release of cytochrome c from	full-length
10424676	1,052586866	6,445673286		0,70662265	2,558853264		1,134407823	6,877828367	11,9742688		Ly6e	lymphocyte antigen 6 complex,	in utero embryonic development /// plasma	full-length
10424683	0,680433621	-2,168893491		0,180955747	-5,884155585		1,229363994	2,726397924	4,004173444		---	---	---	partial
10424929	-0,998410269	1,88880566		-0,217485487	-5,542763879		-1,582949172	6,464582555	7,827781599		Adck5	aarF domain containing kinase 5	protein kinase activity /// protein serine/threonine	full-length
10425049	0,802535498	4,2800802		1,271031507	8,941546977		1,280955908	9,227511735	11,38494442		Apol9a /// Apol9b	apolipoprotein L 9a ///	---	full-length
10425053	1,729952914	8,949268103		-0,170188032	-5,762671008		1,883960136	9,530800042	6,415382968		Ncf4	neutrophil cytosolic factor 4	protein binding /// cytoplasm /// cell communication	full-length
10425066	1,906754174	6,726485865		-0,222096142	-5,787643546		2,025385409	6,993058303	7,134698146	Cluster VI	Csf2rb	colony stimulating factor 2	receptor activity /// hematopoietin/interferon-class	full-length
10425092	2,280002693	9,931153201		0,314661185	-5,015310279		2,095910028	8,500293091	7,435875071		Cyth4	cytohesin 4	guanyl-nucleotide exchange factor activity /// ARF	full-length
10425161	1,586039166	6,770286803		-0,025656783	-6,379493761		1,262811319	3,793621814	9,472872593		Lgals1	lectin, galactose binding, soluble 1	sugar binding /// galactose binding /// extracellular	full-length
10425321	2,359205695	12,27425151		0,577242047	-1,600399795		2,625105992	13,13843722	7,136738212		Apobec3	apolipoprotein B mRNA editing	nucleus /// cytoplasm /// zinc ion binding ///	full-length
10425410	1,314826364	7,082891176		0,155745747	-5,730231913		1,383186644	7,239569793	5,64960807		Grap2	GRB2-related adaptor protein 2	protein binding	full-length
10425866	1,93690622	8,29320546		0,170449924	-5,935240245		2,00834374	8,286921127	7,008517122		Parvg	parvin, gamma	actin binding /// protein binding /// cytoplasm ///	full-length
10426479	1,202293745	3,566087177		-0,134437048	-6,069095759		1,13784037	2,5816952	7,757515217		Ano6	anoctamin 6	ion channel activity /// chloride channel activity ///	full-length
10426557	-0,664617276	3,666589984		-0,147451612	-5,184896407		-1,012275101	7,999980883	7,948039329		Pfkm	phosphofructokinase, muscle	nucleotide binding /// magnesium ion binding ///	full-length
10426812	-0,78627222	3,822985401		-0,18258336	-5,04568881		-1,457251204	10,50940482	10,78864991	Cluster X	Gpd1	glycerol-3-phosphate	catalytic activity /// glycerol-3-phosphate	full-length
10427035	1,548274755	4,369321786		0,077880269	-6,314560799		1,614198121	4,407623523	6,596011679		Nr4a1	nuclear receptor subfamily 4,	DNA binding /// transcription factor activity ///	full-length
10427336	2,297149129	15,3541954		0,006939591	-6,389948784		2,219440645	14,57756846	7,860930127		Nckap1l	NCK associated protein 1 like	---	full-length
10427389	-0,488662795	-6,097090524		-0,825587163	-3,532697959		-1,076411999	-3,117384936	6,217143022		LOC280487	pol polyprotein	---	partial
10427918	1,647756833	4,706411184		-0,034922552	-6,377142404		1,491600492	3,214037644	6,441586478		Fam105a	family with sequence similarity	---	full-length
10428302	-0,66476758	-3,510747169		-0,447684593	-4,47299739		-1,40431655	2,200637139	7,722891507		Klf10	Kruppel-like factor 10	nucleic acid binding /// DNA binding /// intracellular	full-length
10428534	1,230721493	2,022701269		-0,099879238	-6,263690921		1,492373113	3,622334505	4,545753771		Trps1	trichorhinophalangeal syndrome I	DNA binding /// transcription factor activity ///	full-length
10428536	1,173417702	5,027733779		0,17016661	-5,702411122		1,036177173	3,258060786	5,254332809		Trps1	trichorhinophalangeal syndrome I	DNA binding /// transcription factor activity ///	full-length
10428604	1,024609234	8,174936914		-0,048400533	-6,259554433		0,666046338	2,920149523	7,10136318		Tnfrsf11b	tumor necrosis factor receptor	receptor activity /// protein binding /// extracellular	full-length
10428763	1,186061874	-3,273003811		0,116283731	-6,340629484		0,911263413	-4,841234148	6,009052725		Atad2	ATPase family, AAA domain	nucleotide binding /// ATP binding /// nucleus ///	full-length
10428983	1,547352456	11,61627575		-0,0529457	-6,267778264		1,723037128	12,48585871	8,19133647		Fam49b	family with sequence similarity 49,	---	full-length
10429114	0,843720289	-2,300373089		-0,059888565	-6,355637103		1,14649618	-0,193742168	5,915243503		Tmem71	transmembrane protein 71	membrane /// integral to membrane	full-length
10429128	2,274439678	10,66625231		0,314793578	-4,846605702		2,589163657	11,79410151	7,45697743		Sla	src-like adaptor	protein binding /// cytoplasm /// endosome	full-length
10429520	0,904149481	-0,805158109		-0,155648568	-6,084393203		1,006937077	-0,230461318	6,828532686		Ly6d	lymphocyte antigen 6 complex,	plasma membrane /// membrane /// anchored to	full-length
10429560	2,740088064	10,05264577		0,255904825	-5,71161494		3,816276419	13,58972306	5,42516361		Ly6i	lymphocyte antigen 6 complex,	plasma membrane /// membrane /// anchored to	full-length
10429564	2,792793476	16,13039233		0,936583426	3,783099915		3,147798147	17,14835405	11,10187085		Ly6a	lymphocyte antigen 6 complex,	intracellular /// plasma membrane /// external side	full-length
10429568	3,903071062	18,98967398		0,380013251	-3,477026386		4,237746196	19,59639302	9,071093523		Ly6c1 /// Ly6c2	lymphocyte antigen 6 complex,	external side of plasma membrane	full-length
10429573	3,476367095	17,78210874		0,60820174	-0,585117848		3,847649503	18,5930618	8,008440878		Ly6c1 /// Ly6c2	lymphocyte antigen 6 complex,	external side of plasma membrane	full-length
10429580	2,215200895	1,475479852		-0,362685906	-5,936812267		2,916592948	3,912943175	5,453274242		---	---	---	partial
10429843	0,933719421	0,94340034		0,815581567	0,328018928		1,166511672	2,767214847	7,421057387		Plec1	plectin 1	actin binding /// insoluble fraction /// cytoplasm ///	full-length
10429968	-1,049741368	-3,626065877		0,216135939	-6,194115942		-1,525858686	-1,378619994	10,01580257		---	---	---	---
10430006	-0,495407831	-6,310103402		-0,218492002	-6,196643202		-1,511554154	-1,587997882	9,554130242		Slc39a4	solute carrier family 39 (zinc	zinc ion transmembrane transporter activity ///	full-length
10430174	0,813447524	4,696158923		1,415581923	10,14043318		1,308066779	9,76851272	11,22478343		Apol9a /// Apol9b	apolipoprotein L 9a ///	---	full-length
10430190	1,793706532	6,791595894		0,312972565	-5,094409772		2,754514976	11,43760276	5,561483606		Apol11b ///	apolipoprotein L 11b ///	---	full-length
10430201	0,908113346	4,069556212		0,040095645	-6,335382948		1,016784774	4,892590066	9,663875234		Myh9	myosin, heavy polypeptide 9, non-	microfilament motor activity /// nucleotide binding	full-length
10430302	1,642667929	5,684467469		0,040162886	-6,368582884		1,929517323	7,101505619	6,621200507		Csf2rb2	colony stimulating factor 2	receptor activity /// hematopoietin/interferon-class	full-length
10430344	1,773893886	8,510522376		0,026059524	-6,378125638		2,041793245	9,748070163	6,242377276		Il2rb	interleukin 2 receptor, beta chain	receptor activity /// hematopoietin/interferon-class	full-length
10430372	2,356779373	14,12524268		0,397363153	-2,900269987		2,305409345	13,47082264	8,233053659		Rac2	RAS-related C3 botulinum	nucleotide binding /// GTPase activity /// GTP	full-length
10430883	-1,047927229	-3,528717329		0,379529775	-5,779138658		-1,675249468	-0,451770473	10,36108874		Cyp2d13	cytochrome P450, family 2,	cellular_component	full-length
10430892	-0,267030392	-6,711542289		0,525859136	-4,465499643		-1,205247289	-0,704870828	10,1082096		Pcdhb11	protocadherin beta 11	calcium ion binding /// protein binding /// cell	full-length
10430899	-1,20078454	-1,542695619		0,134669255	-6,281586281		-2,032357736	2,923284374	8,485597411	Cluster IX	Cyp2d40	cytochrome P450, family 2,	---	full-length
10430904	-0,611650983	-2,341066847		-0,010963009	-6,389506336		-1,155953887	2,941862537	10,33625098		---	---	---	partial
10430931	1,786420227	8,269244146		0,22041239	-5,526380937		1,620620088	6,699616855	6,080490153	Cluster I	Nfam1	Nfat activating molecule with ITAM	molecular_function /// transmembrane receptor	full-length
10431546	-0,909327214	-1,776217319		0,18291382	-6,063964627		-1,547981039	2,664256955	8,506278506		Tymp /// Sco2	thymidine phosphorylase /// SCO	phosphorylase activity /// pyrimidine base	full-length
10431872	1,26960455	1,018309237		-0,23140574	-5,881270033		1,147737299	-0,266249765	5,155475309		---	---	---	partial
10431874	1,538111842	9,419460569		-0,043139759	-6,333899359		1,717680682	10,30623093	6,037791985		Slc38a1	solute carrier family 38, member 1	membrane fraction /// plasma membrane ///	full-length
10432511	2,2759967	6,936479599		0,091173195	-6,314569412		1,711152513	3,333622363	6,290527884		Racgap1	Rac GTPase-activating protein 1	GTPase activator activity /// intracellular /// nucleus	full-length
10432636	-0,53183503	-5,387373287		4,32E-05	-6,391790956		-1,018097195	-2,303196747	9,476271372		BC004728	cDNA sequence BC004728	plasma membrane /// membrane /// integral to	full-length
10432640	2,145925805	7,12745468		-0,261422383	-5,68895799		2,094982276	6,418167717	7,135877657		---	---	---	partial
10432652	-2,541275397	0,393581144		-1,61182399	-2,35885849		-2,77506375	0,842114527	7,353592002		Ela1	elastase 1, pancreatic	---	full-length
10432939	-1,415889356	10,91091988		-0,341996978	-2,403031563		-0,590071913	0,792018067	10,84800121	Cluster X	Csad	cysteine sulfinic acid	catalytic activity /// sulfinoalanine decarboxylase	full-length
10432957	1,575497878	6,506125438		-0,205156464	-5,671731085		1,698094196	6,939848612	6,027632194		Itgb7	integrin beta 7	receptor activity /// binding /// protein binding /// cell	full-length
10433101	1,030580787	-2,033582306		0,090472388	-6,332318552		1,596089379	1,364320075	5,661803673		Gpr84	G protein-coupled receptor 84	signal transducer activity /// receptor activity /// G-	full-length
10433735	1,378627975	7,379630497		0,188260762	-5,484326686		1,684348665	9,307476613	6,482743374		Abcc1	ATP-binding cassette, sub-family	nucleotide binding /// transporter activity /// ATP	full-length
10434758	0,580173832	0,525794994		-0,092041411	-6,039331398		1,040674558	6,249793159	9,169413185		St6gal1	beta galactoside alpha 2,6	beta-galactoside alpha-2,6-sialyltransferase	full-length
10434778	1,164211571	1,217438448		1,912801615	6,447257235		1,754136705	5,105514517	9,343740496		Rtp4	receptor transporter protein 4	membrane /// integral to membrane	full-length
10434934	-0,735430377	-3,593990416		-0,286133147	-5,704773775		-1,657121029	2,713407549	9,968215809	Cluster X	Bdh1	3-hydroxybutyrate dehydrogenase,	catalytic activity /// 3-hydroxybutyrate	full-length
10435457	0,733701773	0,471035525		1,05869792	4,408213097		1,26171546	5,700377006	8,942648337		Parp9	poly (ADP-ribose) polymerase	NAD+ ADP-ribosyltransferase activity /// nucleus	full-length
10435497	0,840393984	-4,854990028		0,265618131	-6,113254154		1,439997034	-2,05928526	3,690222975		Stfa2l1 /// Stfa2	stefin A2 like 1 /// stefin A2	endopeptidase inhibitor activity /// cysteine	full-length
10435565	2,118670158	14,63681336		-0,078426115	-6,151882504		2,388575717	15,66108625	8,017027176	Cluster VI	Hcls1	hematopoietic cell specific Lyn	protein binding /// nucleus /// cytoplasm ///	full-length
10435907	1,137228931	7,590647098		0,119600689	-5,818721563		1,131593214	7,099930266	4,37228433		Cd200r1	CD200 receptor 1	receptor activity /// protein binding /// plasma	full-length

Affymetrix ID	BS/Non Inf.		LS/Non Inf.		ReINF/Non Inf.		Average	Cluster	Gene	Gene	Gene Ontology (GO)	Transcript
Transcript	logFC	B	logFC	B	logFC	B	expression	Number	Symbol	Title	Description	Classification
10435982	1,139697524	2,421238288	-0,082183192	-6,282205141	1,333608487	3,662721335	5,016592127	Cluster I	Btla	B and T lymphocyte associated	immune response-regulating cell surface receptor	full-length
10436100	1,483165239	-3,597910256	0,321480112	-6,170924156	2,556185498	0,103284521	4,850677062		Retnlg	resistin like gamma	molecular_function /// cellular_component ///	full-length
10436106	1,609248187	1,952511182	0,019067187	-6,389072194	1,07740903	-1,922040583	5,497935674		C330027C09Rik	RIKEN cDNA C330027C09 gene	binding /// cytoplasm /// membrane /// integral to	full-length
10436978	0,844551139	-4,29407099	-0,115553492	-6,323497693	1,86717129	1,186841856	5,120377719		Cbr3	carbonyl reductase 3	---	full-length
10437224	0,67795618	-5,559988253	2,587550364	4,115099316	1,208721174	-3,140620739	5,972771953		Mx2	myxovirus (influenza virus)	nucleotide binding /// GTPase activity /// GTP	full-length
10437243	1,494147386	7,548485342	0,303145268	-4,489128824	1,192269125	4,550219778	5,505725786		Mefv	Mediterranean fever	actin binding /// protein binding /// intracellular ///	full-length
10437945	1,438997105	1,064231298	0,075313832	-6,347711692	1,328534745	-0,038151357	6,325926571		Mcm4	minichromosome maintenance	nucleotide binding /// DNA binding /// DNA	full-length
10438405	3,793517437	11,51244062	-0,311239036	-5,720525578	3,384348722	9,724402542	7,433082037		Igl-V1 /// Igl	immunoglobulin lambda chain,	antigen binding /// protein binding	full-length
10438415	2,692160172	6,66508726	-0,509884173	-4,91758581	2,783897874	6,620156263	5,557052576		---	---	---	full-length
10438445	1,650281535	11,35443274	-0,090257428	-6,092694159	1,753479806	11,66012571	7,434939334		Klhl6	kelch-like 6 (Drosophila)	protein binding	full-length
10438575	-0,651281857	-4,509626477	-0,276353644	-5,816010114	-1,741230199	2,626230711	10,9737441	Cluster X	Ehhadh	enoyl-Coenzyme A, hydratase/3-	catalytic activity /// 3-hydroxyacyl-CoA	full-length
10438738	1,95955977	-1,819883289	1,224124976	-3,79214633	0,488786556	-6,863029562	7,521272229	Cluster V	Bcl6	B-cell leukemia/lymphoma 6	negative regulation of transcription from RNA	full-length
10438769	-0,609206284	-2,987142496	-0,039229795	-6,367534987	-1,305938773	3,248975228	9,693129707		Cldn1	claudin 1	structural molecule activity /// protein binding ///	full-length
10439058	1,272480571	5,58471622	0,344789341	-4,064409219	1,277104278	5,19957192	5,622702681		Lrrc33	leucine rich repeat containing 33	protein binding /// membrane /// integral to	full-length
10439249	1,225533971	3,703155898	1,552382127	6,288628331	1,732563042	7,166766675	8,945483224		Parp14	poly (ADP-ribose) polymerase	nucleic acid binding /// NAD+ ADP-	full-length
10439312	1,295640362	3,849878185	0,063191162	-6,32575349	1,157028518	2,258181535	6,586548231		Cd86	CD86 antigen	receptor activity /// external side of plasma	full-length
10439404	-1,420205888	5,718266346	-0,583330793	-1,863455399	-1,194287735	3,392406453	5,834661297		100043264	predicted gene, 100043264	---	predicted
10439527	0,986353752	2,09576891	0,225737883	-5,42420748	1,290267116	4,526853121	6,389275095		---	---	---	full-length
10439744	1,193169229	6,178703303	0,021058749	-6,378587814	0,927791694	2,99304501	3,828303882		Cd96	CD96 antigen	protein binding /// cell adhesion /// membrane ///	full-length
10439881	0,670296656	0,064387487	0,251914691	-4,776490916	1,040337068	4,059055892	5,343532932		---	---	---	partial
10439936	1,327683691	0,578624727	0,350405118	-5,449953694	1,936093129	3,996942922	7,028171883		Nfkbiz	nuclear factor of kappa light	nucleus /// transcription /// regulation of	full-length
10440300	0,970398965	2,948684415	0,1248742	-6,013260486	1,136971735	4,230922188	7,762257944		---	---	---	predicted
10440393	1,813030098	7,274848612	0,12383542	-6,156689703	1,988844689	7,924075991	5,972900831		Samsn1	SAM domain, SH3 domain and	phosphotyrosine binding /// cytoplasm	full-length
10440522	1,061569281	7,647075554	0,009812308	-6,387118429	1,306168803	9,665498522	7,442104091		Adamts1	a disintegrin-like and	ovulation from ovarian follicle /// kidney	full-length
10440926	-0,730450912	-1,613874102	-0,379667111	-4,393785977	-1,231441682	2,78551659	6,504875978		Dnajc28	DnaJ (Hsp40) homolog, subfamily	heat shock protein binding	full-length
10440993	0,553798819	-1,620679833	0,058772008	-6,294993536	1,247367826	5,947926272	8,441396538		Rcan1	regulator of calcineurin 1	nucleus /// cytoplasm /// calcium-mediated	full-length
10441003	1,467312988	5,043473827	0,622949423	-2,035383266	1,632652295	5,819753451	5,946737289	Cluster I	Runx1	runt related transcription factor 1	skeletal development /// in utero embryonic	full-length
10441233	1,042584165	-2,008507551	0,966942459	-1,808183612	1,221457362	-1,103928663	5,589674728	Cluster II	Mx1	myxovirus (influenza virus)	nucleotide binding /// GTPase activity /// protein	full-length
10441361	-0,628859043	0,047844825	-0,398622887	-2,585916729	-1,021802147	4,541085297	5,445934645		Tiam2	T-cell lymphoma invasion and	receptor signaling protein activity /// guanyl-	full-length
10441601	1,137106413	4,244098688	0,085218782	-6,225399888	1,218684854	4,585331255	5,804234343		Tagap	T-cell activation Rho GTPase-	---	full-length
10442098	0,9470498	4,262143823	-0,00906041	-6,389035714	1,149402355	6,002258103	4,614580712		Fpr2 /// Fpr3	formyl peptide receptor 2 /// formyl	receptor activity /// signal transducer activity /// G-	full-length
10442606	1,347603682	-0,110750903	0,378821541	-5,473021452	1,155741532	-1,707655103	7,267708466		4930528F23Rik	RIKEN cDNA 4930528F23 gene	---	full-length
10442625	-1,008179153	5,601682035	-0,218639592	-4,802736484	-0,86053821	3,441296404	9,118478135		Igfals	insulin-like growth factor binding	protein binding /// extracellular region /// cell	full-length
10442914	-0,806079874	1,327970344	-0,107640869	-6,094542454	-1,035237931	3,48200314	10,2427874		0610011F06Rik	RIKEN cDNA 0610011F06 gene	---	full-length
10443463	1,116339342	-4,162703907	1,272916374	-2,681979523	1,532028425	-2,548109102	8,267880863	Cluster V	Cdkn1a	cyclin-dependent kinase inhibitor	cyclin-dependent protein kinase holoenzyme	full-length
10443730	1,6752258	8,974323352	0,106839958	-6,118742667	1,650767198	8,367697238	8,447230901		Abcg1	ATP-binding cassette, sub-family	nucleotide binding /// ATP binding /// endosome ///	full-length
10443764	0,88208584	0,127953849	0,268166663	-5,275570726	1,221441554	2,917036825	6,920328836		Slc37a1	solute carrier family 37 (glycerol-3-	---	full-length
10443786	-0,488119484	-4,520128068	0,084788926	-6,292102023	-1,286835541	2,457956343	7,607760304		Pde9a	phosphodiesterase 9A	catalytic activity /// 3',5'-cyclic-nucleotide	full-length
10443836	0,864536336	1,465230914	0,121145583	-6,056092927	1,002230624	2,555497193	5,961292748		Rrp1b	ribosomal RNA processing 1	nucleus /// rRNA processing /// nucleolar	full-length
10443898	-0,564475587	-2,973481986	0,07682544	-6,283677695	-1,046567765	1,779365605	10,62785536	Cluster X	Cyp4f15	cytochrome P450, family 4,	---	full-length
10443980	2,807198761	11,58492488	0,307279841	-5,228752089	3,009101677	11,99783168	6,887715013	Cluster VI	Myo1f	myosin IF	nucleotide binding /// neutrophil mediated	full-length
10444068	1,110043185	9,90380278	0,304817358	-2,139339066	1,262867881	11,01791592	10,50675251	Cluster IV	Tapbp	TAP binding protein	antigen processing and presentation of exogenous	full-length
10444229	1,538799059	2,96358935	-0,022498278	-6,386746025	1,26504782	0,635380733	6,84628491	Cluster I	H2-DMa	histocompatibility 2, class II, locus	antigen processing and presentation of peptide or	full-length
10444236	1,867965994	5,087384876	-0,105858405	-6,280452517	1,691874842	3,585444112	7,196002519	Cluster I	H2-DMb1 /// H2-	histocompatibility 2, class II, locus	antigen processing and presentation of peptide or	full-length
10444244	2,253832491	13,54040651	1,098758596	5,241919839	2,47518143	14,25438161	8,580041007	Cluster VI	Tap1	transporter 1, ATP-binding	nucleotide binding /// transporter activity /// protein	full-length
10444258	1,759586238	11,20261837	0,445329104	-1,966995805	1,807238065	11,10001196	8,799732379	Cluster I	Psmb8	proteasome (prosome, macropain)	endopeptidase activity /// threonine-type	full-length
10444291	1,729824887	0,501948001	0,051561251	-6,379081369	1,529533146	-0,924148656	9,949317767	Cluster I	H2-Ab1	histocompatibility 2, class II	antigen processing and presentation of peptide or	full-length
10444298	1,745536388	0,773882442	0,10836264	-6,333537829	1,388321374	-1,538200176	9,037003517	Cluster I	H2-Eb1	histocompatibility 2, class II	antigen processing and presentation of peptide or	full-length
10444658	1,92353341	13,49327829	0,041243965	-6,324665745	1,949141623	13,25033413	7,841183657		Clic1	chloride intracellular channel 1	ion channel activity /// voltage-gated ion channel	full-length
10444780	1,116713311	8,885819095	0,236922926	-3,903065777	1,209096829	9,397593004	11,90527292	Cluster IV	H2-L /// H2-D1	histocompatibility 2, D region ///	antigen processing and presentation of peptide	full-length
10444814	1,717967204	12,05353506	0,598490967	0,957517097	1,885178339	12,75020032	9,175239684		H2-gs10	MHC class I like protein GS10	---	full-length
10444821	0,939938356	5,917446337	0,159602031	-5,318010524	1,092127239	7,21432325	8,485113558		H2-Q8	histocompatibility 2, Q region locus	antigen processing and presentation of peptide	full-length
10444824	1,958447916	12,37890343	0,686998568	1,251912658	2,100595626	12,80481473	9,3866276		H2-Q6	histocompatibility 2, Q region locus	---	full-length
10444890	0,928000385	-2,199603921	0,028948862	-6,384590474	1,241732482	-0,204161819	5,461780087		Ier3	immediate early response 3	membrane /// integral to membrane	full-length
10444932	1,164149321	6,628000446	0,013307231	-6,385797616	1,303363068	7,506895204	5,881660628		2310014H01Rik	RIKEN cDNA 2310014H01 gene	actin binding /// cytoplasm /// cytoskeleton	full-length
10445112	2,695343423	11,05281754	0,263542537	-5,52294313	3,810465874	14,76184318	6,219396373		Ubd	ubiquitin D	protein modification process /// ubiquitin-	full-length
10445119	1,04391677	6,564373615	0,536043628	0,313442151	1,019416455	5,862735232	6,222411154	Cluster II	H2-M3	histocompatibility 2, M region locus	positive regulation of T cell mediated cytotoxicity	full-length
10445241	1,091650194	5,492444062	0,106449746	-6,043893597	1,335262391	7,375209601	7,61061741		Tnfrsf21	tumor necrosis factor receptor	receptor activity /// protein binding /// apoptosis ///	full-length
10445251	-0,957473618	1,445027622	-0,229031824	-5,462220276	-2,548435268	12,07420049	6,821117462		Gpr110	G protein-coupled receptor 110	signal transducer activity /// receptor activity /// G-	full-length
10445293	2,597943739	6,273633851	0,102181672	-6,325396585	3,414066046	9,034155329	8,39096902		Pla2g7	phospholipase A2, group VII	catalytic activity /// 1-alkyl-2-	full-length
10445558	-0,366454339	-5,097320127	-0,098063851	-6,214061825	-1,162403961	2,924133919	6,614634118		BC048355	cDNA sequence BC048355	nucleus	full-length
10445746	0,806177275	-3,454580589	0,068235373	-6,355879639	1,261100799	-0,528303057	4,565014359		Trem1	triggering receptor expressed on	receptor activity /// membrane /// integral to	full-length
10445753	1,619310014	8,982910475	-0,02521188	-6,375166223	1,968813272	10,88338154	5,481639646		Trem3	triggering receptor expressed on	receptor activity /// protein binding	full-length
10445758	2,202413808	5,551881484	0,157430348	-6,20054181	2,053987135	4,352216969	8,582157902		Treml4	triggering receptor expressed on	receptor activity	full-length
10445767	1,142791353	4,780923528	-0,11186211	-6,08226432	1,162963531	4,553126171	5,391907312		Treml2	triggering receptor expressed on	receptor activity /// plasma membrane ///	full-length
10445774	1,632568301	10,29291321	0,307130971	-3,909793386	1,897367839	11,66636032	6,66909564		B430306N03Rik	RIKEN cDNA B430306N03 gene	receptor activity	full-length
10445953	1,285630581	-1,104195277	0,002144214	-6,3917635	0,681576887	-5,096418656	7,833197683		Emr4	EGF-like module containing,	signal transducer activity /// receptor activity /// G-	full-length
10446074	1,84919339	4,228934577	0,066122449	-6,353639697	1,556929345	2,016450175	5,736139862		Uhrf1	ubiquitin-like, containing PHD and	DNA binding /// protein binding /// nucleus /// DNA	full-length
10446253	2,416270656	16,83445264	0,270581787	-3,739976463	2,548274287	17,10200665	7,212046424	Cluster VI	Vav1	vav 1 oncogene	guanyl-nucleotide exchange factor activity /// Rho	full-length
10446282	1,817628491	3,966384337	0,203117831	-6,045194989	1,429124188	1,106045818	9,015923298		Emr1	EGF-like module containing,	signal transducer activity /// receptor activity /// G-	full-length
10446553	1,696078557	3,73612301	0,15928452	-6,155224252	1,492977432	2,005561634	6,210383606		Epb4.1l3	erythrocyte protein band 4.1-like 3	actin binding /// structural molecule activity ///	full-length
10446763	1,040612358	0,883048197	-0,160040717	-6,034289016	0,820366752	-1,516584123	7,123892691		Lbh	limb-bud and heart	nucleus /// cytoplasm /// transcription /// regulation	full-length

Affymetrix ID	BS/Non Inf.		LS/Non Inf.		RelNF/Non Inf.		Average	Cluster	Gene	Gene	Gene Ontology (GO)	Transcript
Transcript	logFC	B	logFC	B	logFC	B	expression	Number	Symbol	Title	Description	Classification
10446777	-1,314377083	6,496499735	-0,032488626	-6,364445976	-1,967182876	10,82140006	9,002762177		Ehd3	EH-domain containing 3	nucleotide binding /// GTPase activity /// calcium	full-length
10447594	1,077240247	8,639261007	-0,068179549	-6,13734935	0,892801713	6,021598788	9,265479972		Dynlt1	dynein light chain Tctex-type 1	motor activity /// protein binding /// Golgi apparatus	full-length
10447602	1,362442951	8,318672971	-0,056076953	-6,288679699	1,728194691	10,71604293	7,683696716		Ezr	ezrin	uropod /// binding /// protein binding /// cytoplasm	full-length
10448124	1,84971366	12,59073734	0,050281436	-6,299352475	1,872339655	12,32516804	8,589630726		Fpr1	formyl peptide receptor 1	signal transducer activity /// receptor activity /// G-	full-length
10448202	1,474491973	7,365051521	-0,13348706	-5,978127105	1,613011144	7,982870378	10,10265422		Tpm4	tropomyosin 4	podosome /// actin binding /// cytoplasm ///	full-length
10448230	-0,488662795	-6,097090524	-0,825587163	-3,532697959	-1,076411999	-3,117384936	6,217143022		LOC280487	pol polyprotein	---	partial
10448459	0,622563169	-1,870014438	-0,140834804	-5,989796554	1,257347869	4,355249583	7,818047307		Tbc1d24	TBC1 domain family, member 24	GTPase activator activity /// Rab GTPase activator	full-length
10448495	-1,048742287	3,292366096	-0,099381637	-6,169932139	-1,03593091	2,758030804	8,485406504		1600002H07Rik	RIKEN cDNA 1600002H07 gene	---	full-length
10448743	-1,046059865	1,295290595	-0,369021164	-4,568129456	-1,316198435	3,22824763	8,32627698		Fahd1	fumarylacetoacetate hydrolase	magnesium ion binding /// catalytic activity ///	full-length
10448836	-0,628883761	-1,89736954	-0,061295895	-6,315806959	-1,136990017	3,123449747	7,602567725		Tmem204	transmembrane protein 204	plasma membrane /// membrane /// integral to	full-length
10449245	-1,52714552	-0,81982212	-1,364572295	-1,020621308	-1,554591665	-1,007746616	4,234351713		Pdia2	protein disulfide isomerase	protein disulfide isomerase activity	full-length
10449303	1,459481097	7,986613753	0,160025886	-5,72989637	1,521415596	8,041762046	7,468885339	Cluster I	Bak1	BCL2-antagonist/killer 1	leukocyte homeostasis /// B cell homeostasis /// B	full-length
10449452	0,425254568	-6,742409127	0,291791721	-6,139494578	1,50885449	-2,742396815	9,737641753		Fkbp5	FK506 binding protein 5	peptidyl-prolyl cis-trans isomerase activity ///	full-length
10449467	-2,976818582	-0,140743959	-2,251997949	-1,62300943	-3,114758703	-0,09488016	6,862724585	Cluster IX	Clps	colipase, pancreatic	extracellular region /// digestion /// enzyme	full-length
10449661	-1,322487467	-2,808061345	-1,067383792	-3,262600432	-1,344559211	-2,976617171	5,494785472		Tff2	trefoil factor 2 (spasmolytic protein	extracellular region	full-length
10449940	-0,663751654	-5,413127876	-0,037718489	-6,385013037	-1,170424698	-2,913895192	10,43354049		Cyp4f14	cytochrome P450, family 4,	monooxygenase activity /// iron ion binding ///	full-length
10449999	-0,568707892	-4,954648352	-0,124265085	-6,263641049	-1,172172603	-0,806645416	5,728844895	Cluster X	Zfp101	zinc finger protein 101	nucleus /// zinc ion binding /// metal ion binding	full-length
10450038	-1,084090052	5,905961098	0,040502657	-6,335583062	-1,141852127	6,068547082	10,1315938		Angptl4	angiopoietin-like 4	molecular_function /// enzyme inhibitor activity ///	full-length
10450145	2,224036882	10,14892722	0,766885223	-0,419926507	2,232775249	9,766777477	9,552751845	Cluster VI	Psmb9	proteasome (prosome, macropain)	endopeptidase activity /// threonine-type	full-length
10450154	1,781179563	2,565847473	0,142451308	-6,25343954	1,560339179	0,871080556	9,776977452	Cluster I	H2-Aa	histocompatibility 2, class II	antigen processing and presentation of peptide or	full-length
10450374	2,753912984	16,68917607	0,137785926	-5,782590813	3,014837951	17,37761257	7,68058165		D17H6S56E-5	DNA segment, Chr 17, human	viral envelope	full-length
10450444	-0,529028937	-1,236852552	-0,119045341	-5,925283139	-1,062774729	5,209401157	11,07881118		Apom	apolipoprotein M	lipid transporter activity /// extracellular region ///	full-length
10450484	1,864623454	10,67698524	0,295030777	-4,435563708	1,811529301	9,904895662	7,08047346		Aif1	allograft inflammatory factor 1	ruffle /// phagocytic cup /// calcium ion binding ///	full-length
10450496	1,209220542	3,373026756	0,133406239	-6,08840054	1,176595196	2,680858979	6,878429881		Lst1	leukocyte specific transcript 1	cell morphogenesis /// immune response ///	full-length
10450501	1,388657468	-1,69357711	0,127770731	-6,32026928	1,767491387	-0,038330006	6,031594066	Cluster I	Tnf	tumor necrosis factor	negative regulation of transcription from RNA	full-length
10450605	1,051051005	2,006754686	-0,075890648	-6,290500457	1,024801778	1,369728755	10,22799912		Tubb5	tubulin, beta 5	nucleotide binding /// GTPase activity /// structural	full-length
10450694	1,065670646	7,588421198	0,407249012	-1,255608631	1,247634657	9,013140486	10,39271794		H2-T22 /// H2-	histocompatibility 2, T region locus	---	full-length
10450723	1,017640367	3,681471217	0,21419331	-5,29301222	1,199098109	5,060544231	7,350323445		H2-T10	histocompatibility 2, T region locus	---	full-length
10451287	1,114592054	5,548027878	2,074627428	11,36409224	1,731285738	10,26737958	7,168436177	Cluster V	Isg15	ISG15 ubiquitin-like modifier	protein binding /// extracellular region /// cytoplasm	full-length
10451291	-1,672034169	-1,063243468	0,169395974	-6,290202535	-2,528055825	2,383176819	7,648587551		Slc22a7	solute carrier family 22 (organic	transporter activity /// plasma membrane ///	full-length
10451547	1,176487677	6,941068383	0,008923698	-6,389004134	0,937952507	3,967852619	7,000322959		LOC100043385	similar to high mobility group	---	predicted
10451710	1,060420785	1,297030788	-0,086357382	-6,280344749	1,155286951	1,751393194	5,912516755		Rftn1	raftlin lipid raft linker 1	plasma membrane /// membrane	full-length
10451763	1,158463494	8,849173736	0,397086782	-1,265514311	1,573490688	12,07652456	5,862075776	Cluster IV	Satb1	special AT-rich sequence binding	negative regulation of transcription from RNA	full-length
10451818	-0,557483652	-5,641007735	0,185635208	-6,193987114	-1,142967074	-2,395816037	5,900782627		Sult1c2	sulfotransferase family, cytosolic,	lysosome /// sulfotransferase activity ///	full-length
10451860	1,14950815	-1,958999026	-0,041857059	-6,381308529	0,785037415	-4,495987602	6,171729564		Pot1b	protection of telomeres 1B	---	full-length
10451943	-1,292386352	7,402881626	0,070658898	-6,236838815	-0,830772865	2,125779261	8,122545322		2310076L09Rik	RIKEN cDNA 2310076L09 gene	lipid particle	full-length
10451953	0,533754077	-4,939084752	0,219410937	-5,945842178	1,227093599	0,17755241	11,66407445		Lrg1	leucine-rich alpha-2-glycoprotein 1	---	full-length
10452485	1,158274696	6,728270418	-0,017372424	-6,381295007	0,926607147	3,80546563	7,421783188		Rab31	RAB31, member RAS oncogene	nucleotide binding /// GTP binding /// plasma	full-length
10452648	0,909831128	1,699191068	-0,146326532	-5,932436194	1,156704831	3,781208669	6,581575019		Emilin2	elastin microfibril interfacer 2	protein binding /// extracellular region ///	full-length
10452815	0,781862172	2,295412921	0,476011874	-1,355438582	1,492665557	9,119355363	10,54554979		Xdh	xanthine dehydrogenase	catalytic activity /// xanthine dehydrogenase	full-length
10452854	-0,446130636	-3,498379396	-0,06521775	-6,286834203	-1,336961577	6,017332606	6,613266776	Cluster X	Srd5a2	steroid 5 alpha-reductase 2	3-oxo-5-alpha-steroid 4-dehydrogenase activity ///	full-length
10452980	0,340660131	-4,574525934	1,366669388	7,178056379	0,603188415	-1,306160147	7,859384946	Cluster V	Eif2ak2	eukaryotic translation initiation	nucleotide binding /// RNA binding /// double-	full-length
10453026	-0,685062641	-2,399017438	-0,039515203	-6,368558001	-1,005421042	0,370667686	9,892991383		Prkd3	protein kinase D3	nucleotide binding /// protein kinase activity ///	full-length
10453715	1,35016213	2,114359991	0,054259669	-6,359561198	0,958024768	-1,351737691	5,742254083		---	---	---	predicted
10453759	-1,170810218	0,588275263	-0,476649319	-4,339477997	-1,413902429	2,031303689	4,43268366		---	---	---	partial
10453867	0,655264614	-0,748175409	-0,26664891	-4,817654109	1,243094241	5,238921274	6,710269372		Rbbp8	retinoblastoma binding protein 8	G1/S transition of mitotic cell cycle /// blastocyst	full-length
10454015	-0,871376232	1,668428467	0,088286103	-6,206696209	-1,933692664	10,16739805	10,83023706		Ttc39c	tetratricopeptide repeat domain	---	full-length
10454030	-1,206890922	-0,554437758	0,13846418	-6,245033191	-1,341446145	0,016250529	5,323092408		Cabyr	calcium-binding tyrosine-(Y)-	calcium ion binding /// calcium ion binding ///	full-length
10454039	0,672727362	-0,233349604	-0,000740622	-6,391776242	1,369675423	6,734141625	8,525794132		Impact	imprinted and ancient	negative regulation of protein amino acid	full-length
10454198	-0,25571687	-6,726122153	0,149296221	-6,202441512	-1,082621247	-1,339316554	11,0708006		Rnf125	ring finger protein 125	protein binding /// intracellular /// ubiquitin-	full-length
10454286	0,889876374	2,818490152	0,007151272	-6,39030832	1,127503152	4,957484853	7,994471029	Cluster III	Mapre2	microtubule-associated protein,	protein binding /// cytoplasm /// cytoskeleton ///	full-length
10454709	1,453795038	4,123534883	-0,011948442	-6,389808561	0,888271299	-1,012255619	5,56699016		Kif20a	kinesin family member 20A	nucleotide binding /// motor activity /// microtubule	full-length
10454782	1,191071214	-2,197848419	0,387252547	-5,652790303	0,175704232	-7,182433741	6,342220951		Egr1	early growth response 1	negative regulation of transcription from RNA	full-length
10455015	1,47775062	8,801267107	0,254587809	-4,668396143	1,067578069	4,63066707	8,0078		---	---	---	est
10455533	0,868053987	-2,646055581	0,211225323	-6,017591434	1,34779765	0,555832597	8,171033047		Eif1a	eukaryotic translation initiation	RNA binding /// translation initiation factor activity	full-length
10455647	1,28908237	7,802257566	-0,02802723	-6,365287186	1,295906803	7,430902085	6,356141617		Tnfaip8	tumor necrosis factor, alpha-	cytoplasm /// apoptosis	full-length
10455813	1,042615551	1,258528139	-0,207285159	-5,759194567	0,787890443	-1,539186826	6,624766481		Lmnb1	lamin B1	structural molecule activity /// nucleus /// lamin	full-length
10455957	1,228499573	-2,049942331	0,918374836	-3,095310448	1,129406287	-2,917315854	8,233767417		EG546714	predicted gene, EG546714	---	predicted
10455961	0,973753612	5,825855848	0,689825577	2,553688931	1,194675558	7,756570169	11,75968432	Cluster II	Iigp1	interferon inducible GTPase 1	nucleotide binding /// GTPase activity /// GTPase	full-length
10455970	3,272123556	3,106863243	2,366983416	0,556761766	2,39864889	-0,276163304	7,629838105		BC023105	cDNA sequence BC023105	---	full-length
10456005	1,906401481	4,444146892	-0,087041604	-6,327223531	1,660904883	2,565145607	9,479464669	Cluster I	Cd74	CD74 antigen (invariant	protein binding /// lysosome /// late endosome ///	full-length
10456071	1,254429206	1,550943468	0,127525146	-6,209808044	0,92648035	-1,483078306	9,441390094	Cluster III	Csf1r	colony stimulating factor 1 receptor	nucleotide binding /// protein kinase activity ///	full-length
10456357	0,732353659	-0,4544337	0,000659012	-6,391781621	1,051817519	2,605674884	6,103746176		Pmaip1	phorbol-12-myristate-13-acetate-	release of cytochrome c from mitochondria ///	full-length
10456400	1,511840537	9,106229913	-0,023930567	-6,374247237	1,458426761	8,248203534	7,80170063		Tubb6	tubulin, beta 6	nucleotide binding /// GTPase activity /// structural	full-length
10456439	1,038815639	1,456804159	0,043036283	-6,361794384	0,967170909	0,406176038	5,981632074		Cep192	centrosomal protein 192	---	full-length
10456490	1,362927519	3,819536648	-0,144124763	-6,088736815	0,88243054	-0,765061376	4,492004888		---	---	---	partial
10457203	0,887243	-3,311661423	0,448152814	-5,169530402	1,391802431	-0,295499764	7,659872894		---	---	---	---
10457225	1,042965395	3,727663792	0,272724841	-4,754082964	0,935865319	2,191428658	6,629561266	Cluster III	Map3k8	mitogen-activated protein kinase	nucleotide binding /// magnesium ion binding ///	full-length
10457640	1,766205164	12,36880803	-0,045977242	-6,310062738	1,685490718	11,3941297	8,192710744		S100a11	S100 calcium binding protein A11	calcium ion binding /// nucleus /// cytoplasm ///	full-length
10457667	-0,488662795	-6,097090524	-0,825587163	-3,532697959	-1,076411999	-3,117384936	6,217143022		100043821 ///	predicted gene, 100043821 ///	---	predicted
10457733	1,310877363	6,550059153	0,223214134	-5,197133877	1,083995375	3,99633491	5,6671515		B4galt6	UDP-Gal:betaGlcNAc beta 1,4-	magnesium ion binding /// calcium ion binding ///	full-length
10458046	-0,692366194	-2,638876933	-0,228675127	-5,717051552	-1,144826369	1,160379293	6,707875805		D0H4S114	DNA segment, human D4S114	protein binding /// regulation of transforming	full-length

Affymetrix ID	BS/Non Inf.		LS/Non Inf.		ReINF/Non Inf.		Average	Cluster	Gene	Gene	Gene Ontology (GO)	Transcript
Transcript	logFC	B	logFC	B	logFC	B	expression	Number	Symbol	Title	Description	Classification
10458278	2,88946772	11,26483061	0,160347903	-6,088556817	2,726849578	10,1479584	6,174965608		2010001M09Rik	RIKEN cDNA 2010001M09 gene	extracellular region /// cytoplasm /// apoptosis	full-length
10458314	1,820156211	11,07918591	-0,124488953	-5,95013044	2,033083822	11,98239557	7,740144556	Cluster VI	Tmem173	transmembrane protein 173	mitochondrion /// mitochondrial outer membrane ///	full-length
10458340	0,779021062	2,320414196	-0,045037402	-6,322516351	1,044641716	5,049250291	6,079460435		Hbegf	heparin-binding EGF-like growth	angiogenesis /// blastocyst growth /// epidermal	full-length
10458382	1,303677249	4,29049128	0,268385575	-5,22200767	2,250380673	10,17444272	6,276383122	Cluster II	Cd14	CD14 antigen	response to molecule of bacterial origin /// protein	full-length
10458843	-1,027330326	1,619987067	0,070378766	-6,307340577	-1,310938743	3,734443542	6,20611498		Sema6a	sema domain, transmembrane	protein binding /// protein binding /// apoptosis ///	full-length
10459066	1,413742363	2,652464028	0,117368028	-6,240331859	1,541241429	3,149062751	4,994741396		---	---	---	predicted
10459236	-0,942963626	1,381434336	-0,092825411	-6,22677121	-1,19250182	3,376459606	8,709411828		Grpel2	GrpE-like 2, mitochondrial	adenyl-nucleotide exchange factor activity ///	full-length
10459262	-0,960949779	-0,942274679	-0,159489743	-6,114745609	-1,113951862	-0,023249367	7,002665501		Ablim3	actin binding LIM protein family,	actin binding /// cytoplasm /// cytoskeleton	full-length
10459288	1,121728749	0,689450788	0,165160023	-6,076361076	1,639125835	4,149407807	6,297768645		Adrb2	adrenergic receptor, beta 2	regulation of systemic arterial blood pressure by	full-length
10459730	2,004408	7,668119055	-0,195526197	-5,88938663	1,741821677	5,619259765	7,171460388		Me2	malic enzyme 2, NAD(+)-	catalytic activity /// malic enzyme activity /// binding	full-length
10459772	-0,926197054	0,915833683	0,003018151	-6,391624795	-1,24308936	3,491993345	6,56049869		Lipg	lipase, endothelial	catalytic activity /// lipoprotein lipase activity ///	full-length
10460085	0,882051065	5,746516892	-0,012190411	-6,384284576	1,086416057	7,720325926	9,272447403		Cndp2	CNDP dipeptidase 2	carboxypeptidase activity /// cytosol /// proteolysis	full-length
10460146	2,250913326	2,412004711	0,059582889	-6,376941991	2,041796383	1,059745966	6,583268641		---	---	---	full-length
10460237	1,125442816	7,430854889	0,332366426	-2,928025072	1,153976715	7,289873574	8,794796532	Cluster IV	Unc93b1	unc-93 homolog B1 (C. elegans)	toll-like receptor signaling pathway ///	full-length
10460263	-0,478392862	-3,07952269	-0,101029642	-6,142835435	-1,331749178	5,970229776	9,517888132		Acy3	aspartoacylase (aminoacylase) 3	aminoacylase activity /// membrane fraction ///	full-length
10460371	0,898761692	0,497229079	0,119736701	-6,142769834	1,057017722	1,668668494	6,884615332		Ptprcap	protein tyrosine phosphatase,	receptor activity /// plasma membrane ///	full-length
10460738	1,565712565	5,523393684	0,416068478	-4,159825389	1,024589445	0,702085325	5,374752519	Cluster III	Cdca5	cell division cycle associated 5	protein binding /// nucleus /// cytoplasm /// cell	full-length
10460767	0,898531108	-1,671882528	0,296258034	-5,524086354	1,508888154	2,666001465	6,208407445		Batf2	basic leucine zipper transcription	DNA binding /// transcription factor activity ///	full-length
10460833	0,943922605	4,354992011	0,091671677	-6,109206054	1,123645645	5,878419729	8,121066044		Ehd1	EH-domain containing 1	nucleotide binding /// GTPase activity /// calcium	full-length
10461093	1,105770262	10,51195464	0,211369247	-3,765326494	1,197818958	11,04302345	6,680104296		Pla2g16	phospholipase A2, group XVI	cell cycle /// membrane /// integral to membrane ///	full-length
10461558	2,171567819	12,46742094	0,467328335	-2,31169033	2,601261152	14,20921947	8,63452774		Slc15a3	solute carrier family 15, member 3	transporter activity /// lysosome /// transport ///	full-length
10461587	4,986026362	14,12293561	0,308831262	-5,793669366	5,582581523	15,06649976	7,4441669		Ms4a4a	membrane-spanning 4-domains,	---	predicted
10461594	2,764149806	7,858323095	0,27394531	-5,857398646	3,749211828	11,04920377	6,943540494		Ms4a4c	membrane-spanning 4-domains,	---	full-length
10461605	2,486652415	12,07357334	0,130498929	-6,081305996	2,295308095	10,6967029	5,02248326		Ms4a4b	membrane-spanning 4-domains,	integral to plasma membrane	full-length
10461614	3,005638696	13,11957774	0,931254233	0,726433031	3,471796862	14,43011497	8,154908608		Ms4a6c	membrane-spanning 4-domains,	receptor activity /// signal transduction ///	full-length
10461622	3,08140971	16,13744997	0,691568798	0,208163853	3,519260077	17,30465695	7,270745875		Ms4a6b	membrane-spanning 4-domains,	receptor activity /// signal transduction ///	full-length
10461629	0,66855835	-0,432177206	0,279351606	-4,630511398	1,190946775	4,952325326	7,022685378		Ms4a4d	membrane-spanning 4-domains,	receptor activity /// signal transduction ///	full-length
10461636	1,18485248	-1,921413322	0,085748966	-6,350059998	1,620200185	0,333688934	3,924021196		---	---	---	partial
10461721	2,32020093	15,30679273	0,825915541	3,666249959	2,390656823	15,2852448	10,20896729		Mpeg1	macrophage expressed gene 1	membrane /// integral to membrane	full-length
10461723	2,167127194	7,035772671	0,430812048	-4,691492474	2,014024203	5,764240224	6,292205917		4632417K18Rik	RIKEN cDNA 4632417K18 gene	---	full-length
10461728	-1,282115485	7,573415088	-0,096198335	-6,094603805	-1,760492633	10,90386251	10,35804535		EG240549	predicted gene, EG240549	mitochondrion /// acyltransferase activity ///	partial
10461758	-1,732729513	11,64315163	-0,334417932	-3,283600113	-2,025166293	13,09186593	10,6983087		Keg1	kidney expressed gene 1	mitochondrion /// microtubule /// acyltransferase	full-length
10461765	1,440459759	3,217757914	-0,013640667	-6,389569013	1,410298081	2,592934444	6,209711351		Lpxn	leupaxin	cytoplasm /// zinc ion binding /// metal ion binding	full-length
10462390	2,78736912	7,599532313	0,775383673	-3,163467931	3,649312795	10,35956334	7,636047052	Cluster VI	Cd274	CD274 antigen	receptor activity /// protein binding /// plasma	full-length
10462587	1,241155049	1,291163073	0,254200485	-5,718085891	1,136471006	0,099733469	5,633073219		Stambpl1	Stam binding protein like 1	ubiquitin thiolesterase activity /// ubiquitin-	full-length
10462613	1,481593963	3,548550631	1,427163311	3,495300107	2,140806913	7,252784224	7,577183261		Ifit2	interferon-induced protein with	binding	full-length
10462618	1,643328326	3,983910463	2,172402121	6,958525221	2,406819727	7,886113643	8,213695562		Ifit3	interferon-induced protein with	binding	full-length
10462621	1,016066162	-1,484637326	1,556727505	2,789006417	1,831845084	3,672854343	6,558230946		I830012O16Rik	RIKEN cDNA I830012O16 gene	---	full-length
10462623	1,502610045	-1,588776881	3,279459828	6,062178747	2,744289084	3,666860788	9,156570455		Ifit1	interferon-induced protein with	binding	full-length
10462632	1,211612221	-0,646460284	0,084111167	-6,338830602	0,89008632	-3,205491742	4,435083209	Cluster III	Kif20b	kinesin family member 20B	nucleotide binding /// motor activity /// microtubule	full-length
10462796	1,949836308	5,330300999	0,168039	-6,126082081	1,688314515	3,337025651	5,591551463		Kif11	kinesin family member 11	nucleotide binding /// motor activity /// microtubule	full-length
10462866	1,698659084	2,283098604	0,005554961	-6,391569759	1,475073982	0,529925732	4,599056155		Cep55	centrosomal protein 55	cell cycle /// mitosis /// cell division	full-length
10462973	1,552265653	0,62779366	0,125931711	-6,295661154	1,779368023	1,555252371	5,511968544	Cluster I	Hells	helicase, lymphoid specific	nucleotide binding /// urogenital system	full-length
10463005	-1,459398902	-4,001793044	-0,870568473	-5,070524843	-3,129780099	1,457991661	5,52921232	Cluster IX	Cyp2c55	cytochrome P450, family 2,	monooxygenase activity /// iron ion binding ///	full-length
10463027	-0,983422604	-2,75436647	-0,17209444	-6,201753452	-1,279543596	-1,123991437	11,96096848	Cluster X	Cyp2c29	cytochrome P450, family 2,	monooxygenase activity /// iron ion binding ///	full-length
10463068	0,202965545	-6,768781974	-0,00677407	-6,391213266	1,008750636	-0,352968694	10,93024361		Ptp4a1 ///	protein tyrosine phosphatase 4a1	phosphoprotein phosphatase activity /// protein	full-length
10463070	1,851418807	12,17021593	0,219214337	-4,926429659	2,094441463	13,23135304	8,300668322		Entpd1	ectonucleoside triphosphate	magnesium ion binding /// calcium ion binding ///	full-length
10463355	1,896568656	4,348092119	-0,093226557	-6,318303974	2,015494634	4,597023092	7,335570164		Scd2	stearoyl-Coenzyme A desaturase	stearoyl-CoA 9-desaturase activity /// iron ion	full-length
10463551	-3,778744336	0,657105352	0,081357533	-6,384930272	-7,195495181	7,104959929	9,731111606		Elovl3	elongation of very long chain fatty	endoplasmic reticulum /// fatty acid biosynthetic	full-length
10463599	0,962307916	0,594554029	-0,03889199	-6,367971666	1,330756305	3,444241594	7,444765308	Cluster IV	Nfkb2	nuclear factor of kappa light	follicular dendritic cell differentiation /// germinal	full-length
10464298	-5,019751004	0,498481042	-3,975832135	-0,801956694	-5,217591789	0,488279426	5,901841059	Cluster IX	Pnlip	pancreatic lipase	extracellular region /// lipid catabolic process ///	full-length
10464313	-4,298474148	0,315037232	-3,268070107	-1,240065595	-4,503162864	0,375957815	5,221192186		Pnliprp1	pancreatic lipase related protein 1	catalytic activity /// triacylglycerol lipase activity ///	full-length
10464328	-2,432258263	-0,908025131	-1,693042019	-2,687408316	-2,223599598	-1,931458134	5,520067273	Cluster IX	Pnliprp2	pancreatic lipase-related protein 2	catalytic activity /// triacylglycerol lipase activity ///	full-length
10464560	1,16299988	4,050699056	-0,097901372	-6,189758525	1,073422767	2,789021084	7,189839358		Aldh3b1	aldehyde dehydrogenase 3 family,	aldehyde dehydrogenase [NAD(P)+] activity ///	full-length
10464704	0,907255821	4,686385504	0,074167598	-6,177971817	1,066498292	6,07916918	8,301217309	Cluster III	Adrbk1	adrenergic receptor kinase, beta 1	nucleotide binding /// regulation of the force of	full-length
10465059	1,096519691	4,612765503	-0,085178679	-6,200944504	1,08448577	4,073277639	5,421677934		Ctsw	cathepsin W	cysteine-type endopeptidase activity /// proteolysis	full-length
10465342	-1,030317076	-3,660503511	-0,036995235	-6,385763289	-1,210736937	-2,949198917	10,69867225	Cluster X	Tm7sf2	transmembrane 7 superfamily	endoplasmic reticulum /// steroid biosynthetic	full-length
10465587	1,693444407	10,16831283	0,141495409	-5,831405298	1,660797507	9,506948997	7,135438697		Fermt3	fermitin family homolog 3	podosome /// protein binding /// cytoplasm ///	full-length
10465726	1,266580355	-1,923794803	-0,035823943	-6,385403647	1,48012551	-1,030583758	5,451900449		BC014805	cDNA sequence BC014805	---	full-length
10465734	1,234841551	-2,295982004	0,116043769	-6,328475035	0,964728751	-4,065823039	5,546187899		AB056442	cDNA sequence AB056442	---	full-length
10465742	-1,652954084	-0,511806952	-0,241430159	-6,153243457	-1,879630775	0,266971906	10,67638585		C730048C13Rik	RIKEN cDNA C730048C13 gene	---	full-length
10465764	-1,549367591	-0,972624885	-0,211213408	-6,204957696	-1,688484504	-0,593303224	11,5481997		C730048C13Rik	RIKEN cDNA C730048C13 gene	---	full-length
10465861	1,420603863	1,488995167	0,049373406	-6,37052516	1,092265265	-1,21461469	5,742649765	Cluster III	Incenp	inner centromere protein	chromosome, centromeric region /// chromosome,	full-length
10465895	-0,388577034	-6,39511119	0,019503233	-6,389465314	-1,35490416	-0,912751916	11,49938431	Cluster X	Fads2	fatty acid desaturase 2	stearoyl-CoA 9-desaturase activity /// iron ion	full-length
10465912	1,2510891	7,293768951	0,178868904	-5,416912513	1,01190233	4,457976935	6,334800086		Fen1	flap structure specific	magnesium ion binding /// DNA binding /// catalytic	full-length
10466008	0,047934143	-7,212090541	-0,099807486	-6,109104588	-1,209288871	5,748787635	10,90647859		Dak	dihydroxyacetone kinase 2	nucleotide binding /// glycerone kinase activity ///	full-length
10466127	1,636619087	11,47631202	0,257247423	-4,222471216	1,933210124	13,05105344	11,34075692		AW112010	expressed sequence AW112010	---	full-length
10466130	1,964495058	4,084074589	0,099449656	-6,317541531	2,015519363	3,946387798	7,008094963		Ms4a8a	membrane-spanning 4-domains,	receptor activity /// signal transduction ///	full-length
10466172	1,203360755	0,750695256	0,059652656	-6,354770095	1,217319074	0,489085458	4,431061248		Ms4a1	membrane-spanning 4-domains,	receptor activity /// signal transduction ///	full-length
10466200	1,132298365	6,563814791	0,030523931	-6,358896858	1,546320833	9,794466161	4,694239761		Ms4a7	membrane-spanning 4-domains,	---	full-length
10466210	3,112205938	14,63853373	0,555739886	-2,325161784	3,99165371	17,14472217	7,628667648		Ms4a6d	membrane-spanning 4-domains,	receptor activity /// signal transduction ///	full-length
10466410	1,013903475	1,988581452	0,026857268	-6,378115492	1,620792135	6,674923436	6,044552992		Psat1	phosphoserine aminotransferase 1	catalytic activity /// phosphoserine transaminase	full-length

Affymetrix ID	BS/Non Inf.		LS/Non Inf.		RelNF/Non Inf.		Average	Cluster	Gene	Gene	Gene Ontology (GO)	Transcript
Transcript	logFC	B	logFC	B	logFC	B	expression	Number	Symbol	Title	Description	Classification
10466606	1,902520436	12,56719753	-0,140914062	-5,737640384	1,823147699	11,64457879	7,761414524		Anxa1	annexin A1	phospholipase inhibitor activity /// calcium ion	full-length
10466659	1,039093665	2,367084033	0,153630164	-5,947712245	1,752882487	7,73923103	8,279388205		Gda	guanine deaminase	zinc ion binding /// guanine deaminase activity ///	full-length
10466938	1,234924516	7,454948	0,484304433	-1,15410145	1,209748799	6,783236747	5,987491074		5033414D02Rik	RIKEN cDNA 5033414D02 gene	membrane /// integral to membrane	full-length
10467136	2,23139962	4,464153385	-0,181187222	-6,189017938	3,193009273	8,131547955	5,842932533		Ch25h	cholesterol 25-hydroxylase	cholesterol 25-hydroxylase activity ///	full-length
10467162	-0,485973925	-1,878965891	-0,057457006	-6,279743793	-1,085659013	5,465672875	11,72353271		Pank1	pantothenate kinase 1	nucleotide binding /// pantothenate kinase activity	full-length
10467258	1,743792282	8,304126921	-0,034522795	-6,36784749	2,16151098	10,42488712	6,773575795		Myof	myoferlin	protein binding /// nucleus /// plasma membrane ///	full-length
10467380	-1,227459889	4,630282756	-0,203845706	-5,559771897	-1,534317983	6,727543129	11,11372254	Cluster IX	Cyp2c67	cytochrome P450, family 2,	---	full-length
10467390	-0,679323982	0,318456085	-0,081922589	-6,194780819	-1,017023863	3,974182851	11,78690644	Cluster X	Cyp2c40 ///	cytochrome P450, family 2,	monooxygenase activity /// iron ion binding ///	full-length
10467470	1,314609753	3,088273489	-0,034192431	-6,375454433	1,417669415	3,478550281	6,273448877		Aldh18a1	aldehyde dehydrogenase 18	catalytic activity /// glutamate 5-kinase activity ///	full-length
10467578	0,586541882	-0,449422514	0,104218207	-6,036816321	1,011810868	4,573310485	9,749611344		Pik3ap1	phosphoinositide-3-kinase adaptor	transmembrane receptor protein tyrosine kinase	full-length
10467637	1,281091776	6,161719347	0,200794235	-5,428309076	0,936677504	2,340316923	5,487164912		Arhgap19	Rho GTPase activating protein 19	molecular_function /// GTPase activator activity ///	full-length
10467784	-0,666140936	-0,651284599	-0,108035018	-6,108207919	-1,496857138	7,313804516	6,937847078	Cluster X	4833409A17Rik	RIKEN cDNA 4833409A17 gene	electron carrier activity /// carotenoid biosynthetic	full-length
10467897	-1,098497015	-3,519599384	-0,103969431	-6,347909421	-1,871648582	0,123379608	11,70373801	Cluster X	Cyp2c44	cytochrome P450, family 2,	molecular_function /// cellular_component ///	full-length
10467979	-1,299861662	-6,223951391	0,064296005	-6,389060274	-4,964946688	0,730997934	11,72412214	Cluster IX	Scd1	stearoyl-Coenzyme A desaturase	stearoyl-CoA 9-desaturase activity /// iron ion	full-length
10468239	1,628226296	-2,491945685	0,181851542	-6,307403634	1,876323788	-1,769586517	8,201952358		Cyp17a1	cytochrome P450, family 17,	monooxygenase activity /// steroid 17-alpha-	full-length
10468487	-0,488662795	-6,097090524	-0,825587163	-3,532697959	-1,076411999	-3,117384936	6,217143022		LOC280487	pol polyprotein	---	partial
10468893	0,821631407	2,505914089	0,236738381	-4,809370592	1,045313051	4,666078602	7,679715771		Csf2ra	colony stimulating factor 2	receptor activity /// hematopoietin/interferon-class	full-length
10468898	1,355226248	3,363232707	0,096979944	-6,262641606	1,41530759	3,414444433	5,403412983	Cluster I	Lax1	lymphocyte transmembrane	plasma membrane /// immune response ///	full-length
10469127	-0,488662795	-6,097090524	-0,825587163	-3,532697959	-1,076411999	-3,117384936	6,217143022		100043821 ///	predicted gene, 100043821 ///	---	est
10469151	-1,09904051	3,683538683	-0,358697252	-4,011651557	-1,84718356	9,185510864	6,211024708		Itih5	inter-alpha (globulin) inhibitor H5	endopeptidase inhibitor activity /// serine-type	full-length
10469255	1,043544068	5,214728599	-0,114549611	-5,974501882	0,863400911	2,750628656	5,998005878	Cluster III	Prkcq	protein kinase C, theta	nucleotide binding /// magnesium ion binding ///	full-length
10469322	2,502514974	15,4271181	-0,208275089	-5,111702718	2,610121959	15,54949623	10,17853404		Vim	vimentin	structural molecule activity /// protein binding ///	full-length
10469358	-0,334914628	-5,778514205	0,004215786	-6,391530788	-1,191121203	1,910282519	8,790619309		Mrc1	mannose receptor, C type 1	receptor activity /// transmembrane receptor	full-length
10469559	-0,553455971	-1,947956292	0,036076356	-6,358158882	-1,237654348	5,371693234	7,279968357	Cluster X	Msrb2	methionine sulfoxide reductase B2	protein-methionine-R-oxide reductase activity ///	full-length
10469695	1,515625389	10,31404439	0,069668518	-6,212716695	1,554868245	10,19164936	6,152865308		Apbb1ip	amyloid beta (A4) precursor	cytoplasm /// cytoskeleton /// plasma membrane ///	full-length
10469786	0,164780482	-6,74866932	-0,063986309	-6,310895518	1,147040946	3,095557268	4,385367898	Cluster IV	Il1f9	interleukin 1 family, member 9	cytokine activity /// interleukin-1 receptor binding ///	full-length
10469816	1,162612069	4,476102537	0,083360068	-6,232796699	2,104332738	10,94604248	6,901085021	Cluster II	Il1rn	interleukin 1 receptor antagonist	receptor activity /// interleukin-1 receptor binding ///	full-length
10470175	-1,151736031	0,248149205	0,19826752	-6,002416157	-0,969368416	-1,542616087	4,642760215		Lcn13	lipocalin 13	transporter activity /// binding /// extracellular	full-length
10470555	1,351323335	2,125680621	0,508036617	-4,044562247	1,057040467	-0,539325351	6,21651426		Gbgt1	globoside alpha-1,3-N-	Golgi apparatus /// carbohydrate metabolic	full-length
10471555	-0,320794681	-5,196116014	-0,215564303	-5,396313475	-1,110891505	3,567156219	6,960526538		Angptl2	angiopoietin-like 2	receptor binding /// extracellular region /// signal	full-length
10471929	1,471319367	6,2574927	0,216651746	-5,520648774	1,355851953	4,90748036	5,27143872		Arhgap15	Rho GTPase activating protein 15	GTPase activator activity /// protein binding ///	full-length
10472162	-0,354201633	-6,229096622	-0,035024645	-6,380942152	-1,023118894	-1,677103861	8,278362786	Cluster X	Gpd2	glycerol phosphate dehydrogenase	glycerol-3-phosphate dehydrogenase activity ///	full-length
10472501	1,386446546	2,792861378	0,062918096	-6,344909272	1,908121919	5,862240339	8,272018868		Lass6	LAG1 homolog, ceramide	DNA binding /// transcription factor activity ///	full-length
10472782	0,962237676	5,638324812	-0,070126044	-6,190085999	1,07699999	6,49487946	8,604974033		Hat1	histone aminotransferase 1	histone acetyltransferase activity /// protein binding	full-length
10472820	1,67427159	2,524216297	-0,348339332	-5,515396952	1,718186251	2,390939912	6,683535679	Cluster I	Itga6	integrin alpha 6	receptor activity /// integrin binding /// calcium ion	full-length
10473022	1,840878591	9,516247438	-0,215327435	-5,437928037	1,762595863	8,568949184	7,444680794		Plp2	proteolipid protein 2	membrane /// integral to membrane	full-length
10473125	3,040177509	14,96289202	0,082566369	-6,254106968	3,15719443	15,02883799	7,736763775		Itga4	integrin alpha 4	fibronectin binding /// blood vessel remodeling ///	full-length
10473356	0,889473419	2,783997756	0,603111285	-0,212655311	1,195175187	5,5804509	9,298366494		Ube2l6	ubiquitin-conjugating enzyme E2L	ubiquitin-protein ligase activity /// protein binding ///	full-length
10473809	2,276347359	13,17978987	0,156697321	-5,763880538	2,333451637	13,07123598	6,887271262	Cluster VI	Sfpi1	SFFV proviral integration 1	DNA binding /// transcription factor activity /// RNA	full-length
10474223	-0,653317953	-1,906825879	-0,048673356	-6,347400731	-1,00339428	1,451262269	5,983055728	Cluster X	Cd59b	CD59b antigen	negative regulation of activation of membrane	full-length
10474700	1,429393917	4,546001536	0,003900972	-6,391554785	2,114859009	8,614663777	6,760881527	Cluster II	Thbs1	thrombospondin 1	structural molecule activity /// calcium ion binding	full-length
10474769	1,694252799	4,254073872	-0,098473107	-6,29101682	1,274127459	0,934172217	5,8795331		Bub1b	budding uninhibited by	nucleotide binding /// kinetochore /// kinetochore ///	full-length
10474825	1,348332924	3,233275253	0,359960564	-4,827029422	0,961176156	-0,414379405	5,259583211		D2Ertd750e	DNA segment, Chr 2, ERATO Doi	protein binding /// cellular_component /// nucleus	full-length
10474875	2,069323413	4,951738572	0,277640499	-5,80497004	1,502060139	1,2016752	4,718535857		Casc5	cancer susceptibility candidate 5	nucleus	full-length
10474984	1,2537303	1,476734591	0,180259208	-6,038038947	0,727392292	-3,223205407	4,684452844	Cluster III	Nusap1	nucleolar and spindle associated	mitotic sister chromatid segregation /// cytokinesis	full-length
10475378	-0,758797377	-0,851628764	-0,417484698	-3,809338771	-1,031414275	1,574031397	5,976881303		Casc4	cancer susceptibility candidate 4	membrane /// integral to membrane	full-length
10475487	1,968727263	6,901889108	0,045331301	-6,366327642	2,488236245	9,22045879	5,869697832		Slc28a2	solute carrier family 28 (sodium-	nucleoside binding /// nucleoside:sodium	full-length
10475517	0,768308943	-3,806840117	0,073828972	-6,350962746	1,990038234	3,7825673	4,850709738		AA467197	expressed sequence AA467197	nucleus	full-length
10475866	0,993393233	1,646458463	-0,21287927	-5,605477779	1,411874532	4,946074487	6,546310036	Cluster IV	Bcl2l11	BCL2-like 11 (apoptosis facilitator)	peripheral to membrane of membrane fraction ///	full-length
10475990	1,321651003	-0,222691502	0,063259436	-6,363944852	1,824248664	2,472712141	8,843556456		Slc20a1	solute carrier family 20, member 1	receptor activity /// inorganic phosphate	full-length
10476021	2,609838095	14,0693225	0,222477963	-5,311369005	2,451237167	12,92864886	8,821230176	Cluster VI	Sirpa	signal-regulatory protein alpha	protein binding /// integral to plasma membrane ///	full-length
10476395	-1,466583564	3,417241497	-0,080949703	-6,313858329	-2,024070395	6,576874324	6,897514685	Cluster IX	Bmp2	bone morphogenetic protein 2	ossification /// osteoblast differentiation ///	full-length
10476399	-0,488662795	-6,097090524	-0,825587163	-3,532697959	-1,076411999	-3,117384936	6,217143022		100043821 ///	predicted gene, 100043821 ///	---	est
10476590	-0,80652864	-3,250836903	-0,479307348	-4,726232494	-1,094123552	-1,417422763	5,756261639		Macrod2	MACRO domain containing 2	---	full-length
10476945	1,612151193	9,761750156	0,076682808	-6,216996184	1,845031353	10,9457588	5,580810296		Cst7	cystatin F (leukocystatin)	endopeptidase inhibitor activity /// cysteine	full-length
10477187	2,287114466	5,354366738	0,230379833	-6,029966973	1,792698443	2,322244512	5,948502264		Tpx2	TPX2, microtubule-associated	nucleus /// aster /// spindle microtubule /// protein	full-length
10477250	2,337438242	13,59489776	0,14689577	-5,82747763	2,58673914	14,39972479	7,648146316		Hck	hemopoietic cell kinase	nucleotide binding /// protein kinase activity ///	full-length
10477717	1,653046945	5,644478407	-0,172927881	-5,982425501	2,180939091	8,424264226	6,496627531	Cluster VI	Procr	protein C receptor, endothelial	receptor activity /// centrosome /// immune	full-length
10478048	0,910169562	1,570409737	0,154463421	-5,894999431	1,806274412	8,716186554	11,83996246	Cluster IV	Lbp	lipopolysaccharide binding protein	lipopolysaccharide binding /// macrophage	full-length
10478326	-1,08985098	0,287600729	-0,155512263	-6,119442073	-1,514611201	3,141173401	9,253589467		Sgk2	serum/glucocorticoid regulated	nucleotide binding /// protein kinase activity ///	full-length
10478572	1,009483165	2,70305541	-0,075123091	-6,268622741	0,73987763	-0,611736451	5,26826722	Cluster III	Ube2c	ubiquitin-conjugating enzyme E2C	ubiquitin-protein ligase activity /// ATP binding ///	full-length
10478746	-0,488662795	-6,097090524	-0,825587163	-3,532697959	-1,076411999	-3,117384936	6,217143022		100043821 ///	predicted gene, 100043821 ///	---	est
10478897	1,545188129	11,84018457	-0,054856567	-6,253329124	1,830065027	13,44745795	8,576595502		Ptpn1	protein tyrosine phosphatase, non-	phosphoprotein phosphatase activity /// protein	full-length
10479154	1,127171583	2,725645939	0,080661788	-6,277319369	1,395153147	4,598200105	6,209895047		Tubb1	tubulin, beta 1	nucleotide binding /// structural constituent of	full-length
10479811	-1,156750889	0,163185123	-0,034842992	-6,379743713	-1,229963918	0,357956207	6,78419562		Mcm10	minichromosome maintenance	nucleus /// DNA replication /// zinc ion binding ///	full-length
10479950	0,986305057	6,708816978	-0,095438479	-5,970120481	1,089400784	7,430600981	7,407963305		Cugbp2	CUG triplet repeat, RNA binding	nucleotide binding /// nucleic acid binding /// RNA	full-length
10479979	1,003945769	-1,348297151	0,010880811	-6,39069996	0,755072263	-3,579009726	5,958785638		---	---	---	est
10480090	-1,059367462	1,903077506	-0,329063689	-4,76536529	-1,724280797	6,784493083	6,294424228	Cluster IX	Itga8	integrin alpha 8	metanephros development /// metanephros	full-length
10480347	1,783493623	9,407880442	0,082159487	-6,237088808	1,741157007	8,690982313	7,739346798		Pip4k2a	phosphatidylinositol-5-phosphate	nucleotide binding /// ATP binding /// kinase	full-length
10480432	1,007256885	1,945022711	-0,115663072	-6,141665516	0,571942453	-3,061366811	3,970897341	Cluster III	Mastl	microtubule associated	nucleotide binding /// protein kinase activity ///	full-length
10480714	0,745906467	-0,495507262	-0,06252931	-6,311930644	1,10793801	2,905329345	7,444314595		Uap1l1	UDP-N-acetylglucosamine	metabolic process /// transferase activity ///	full-length
10480725	-0,62017123	-2,226247105	0,05694818	-6,330124557	-1,28025693	4,058936142	7,975430416		BC029214	cDNA sequence BC029214	---	full-length

Affymetrix ID	BS/Non Inf.		LS/Non Inf.		ReINF/Non Inf.		Average	Cluster	Gene	Gene	Gene Ontology (GO)	Transcript
Transcript	logFC	B	logFC	B	logFC	B	expression	Number	Symbol	Title	Description	Classification
10480751	-0,812513081	-2,822787455	0,008191352	-6,391164137	-1,372146758	1,095958329	11,33875798	Cluster X	C8g	complement component 8, gamma	transporter activity /// binding /// extracellular	full-length
10481164	1,499911038	8,188441124	0,351713205	-3,730003063	1,742438361	9,531294595	6,712015649		Slc2a6	solute carrier family 2 (facilitated	sugar:hydrogen symporter activity /// transport ///	full-length
10481278	-4,618514149	0,287678602	-3,508298616	-1,267319969	-4,5741576	-0,156064067	5,646560443		Cel	carboxyl ester lipase	carboxylesterase activity /// cholinesterase activity	full-length
10481435	-0,452658511	-2,880627858	0,080315205	-6,203816408	-1,830777349	10,73973843	10,25468932		Ccbl1	cysteine conjugate-beta lyase 1	catalytic activity /// cytoplasm /// transaminase	full-length
10481627	5,422026923	16,25269912	0,280252088	-5,789664209	6,199083402	17,43109168	10,24787587	Cluster VIII	Lcn2	lipocalin 2	transporter activity /// binding /// extracellular	full-length
10481634	-1,394724484	10,51124781	-0,812888691	4,498990842	-1,003010376	6,20383801	9,762130228		Slc25a5	solute carrier family 25	binding /// calcium ion binding /// mitochondrion ///	full-length
10482059	1,297382784	4,655290928	-0,141591016	-6,017572196	1,349124346	4,666306011	6,611375033		Ggta1	glycoprotein galactosyltransferase	Golgi apparatus /// carbohydrate metabolic	full-length
10482517	0,789310287	5,266841605	0,738696992	4,726737769	1,119984884	8,889017575	8,655197278		Nmi	N-myc (and STAT) interactor	cytoplasm	full-length
10482802	3,133753561	14,05353684	-0,110863888	-6,192840249	3,30678609	14,2982301	5,945448866		Cytip	cytohesin 1 interacting protein	protein binding /// cytoplasm /// endosome /// cell	full-length
10482929	1,213924445	8,128884811	0,196392235	-4,999120725	1,953828402	13,37519537	6,740579655		Ly75	lymphocyte antigen 75	receptor activity /// binding /// sugar binding ///	full-length
10483110	0,651924901	2,049059179	1,159482111	8,031769564	0,689270922	2,21736966	8,971028461	Cluster V	Ifih1	interferon induced with helicase C	nucleotide binding /// nucleic acid binding /// DNA	full-length
10483161	-0,488662795	-6,097090524	-0,825587163	-3,532697959	-1,076411999	-3,117384936	6,217143022		100043821 ///	predicted gene, 100043821 ///	---	est
10483249	0,969727763	-1,539572481	0,142184462	-6,204401998	1,34629822	0,946266159	5,693007346		Galnt3	UDP-N-acetyl-alpha-D-	polypeptide N-acetylgalactosaminyltransferase	full-length
10483381	1,14346345	3,620088485	0,117881209	-6,113738456	1,306362724	4,652829378	6,686791978		Stk39	serine/threonine kinase 39,	nucleotide binding /// protein kinase activity ///	full-length
10483698	1,036669508	1,720432057	0,146225288	-6,034092405	1,002733837	1,015235206	6,286672412		Wipf1	WAS/WASL interacting protein	actin binding /// cytoplasm /// cytoskeleton /// actin	full-length
10484261	0,22264535	-6,629486176	0,088032791	-6,288362416	1,042231506	0,231202691	5,663838342		Cerkl /// Itga4	ceramide kinase-like /// integrin	kinase activity /// fibronectin binding /// blood	full-length
10484307	1,042377068	2,290352498	-0,288250174	-4,975611444	1,097056524	2,414553571	5,909022108		Frzb	frizzled-related protein	protein binding /// extracellular region ///	full-length
10484355	-0,488662795	-6,097090524	-0,825587163	-3,532697959	-1,076411999	-3,117384936	6,217143022		100043821 ///	predicted gene, 100043821 ///	---	est
10485355	-0,488662795	-6,097090524	-0,825587163	-3,532697959	-1,076411999	-3,117384936	6,217143022		100043821 ///	predicted gene, 100043821 ///	---	predicted
10485405	2,19778607	12,63192896	0,1808263	-5,585504399	2,198175872	12,22320785	7,166124152		Cd44	CD44 antigen	ureteric bud branching /// healing during	full-length
10485963	1,579041319	1,859263967	0,091158953	-6,328738677	1,314221035	-0,232820621	6,046620223		Arhgap11a	Rho GTPase activating protein	molecular_function /// GTPase activator activity ///	full-length
10486061	1,636580761	6,955332487	0,021141737	-6,383690769	1,653159083	6,640092414	6,740774706		Rasgrp1	RAS guanyl releasing protein 1	guanyl-nucleotide exchange factor activity ///	full-length
10486396	1,544583646	7,535214006	0,055232564	-6,323524553	1,517356346	6,895712777	7,53213852		Ehd4	EH-domain containing 4	nucleotide binding /// GTPase activity /// calcium	full-length
10487208	2,132013634	6,930580439	0,175232161	-6,073086876	2,564921095	8,663711398	5,431067874		Atp8b4	ATPase, class I, type 8B, member	molecular_function /// cellular_component ///	full-length
10487238	1,075451275	3,878158087	0,291828522	-4,600700831	1,250490616	5,116706739	7,029848773		Hdc	histidine decarboxylase	catalytic activity /// histidine decarboxylase activity	full-length
10487340	1,346288104	0,60358664	-0,02421615	-6,38705662	0,958127153	-2,488644529	5,605997001	Cluster III	Ncaph	non-SMC condensin I complex,	mitotic cell cycle /// nucleus /// cytoplasm /// cell	full-length
10487480	1,85170374	0,410289633	0,076209028	-6,368060649	1,421994546	-2,09797532	4,969871344		Bub1	budding uninhibited by	nucleotide binding /// chromosome, centromeric	full-length
10487577	1,470184246	2,880917356	0,239751447	-5,801636967	0,857762945	-2,261287653	5,496666163		Ckap2l	cytoskeleton associated protein 2-	---	full-length
10487588	1,487458904	5,010420229	-0,269352787	-5,34984473	1,200556517	2,307039784	6,472466881	Cluster I	Il1a	interleukin 1 alpha	fever /// cytokine activity /// interleukin-1 receptor	full-length
10487823	0,937000816	2,825210048	0,596289547	-0,666297485	1,030714293	3,421336319	7,743666614		Siglec1	sialic acid binding Ig-like lectin 1,	protein binding /// sugar binding /// extracellular	full-length
10487894	0,902658979	-1,604711239	-0,076041071	-6,330375242	1,023294616	-0,931563301	6,155330075		Rassf2	Ras association (RalGDS/AF-6)	protein binding /// cell cycle /// signal transduction	full-length
10488010	-0,985082535	7,929494214	-0,045525343	-6,270308424	-1,17629024	9,596205036	11,02519548	Cluster X	Hao1	hydroxyacid oxidase 1, liver	catalytic activity /// (S)-2-hydroxy-acid oxidase	full-length
10488378	0,820779523	-2,828105627	-0,015823979	-6,389502661	1,16943537	-0,459226653	7,368731101		Thbd	thrombomodulin	receptor activity /// transmembrane receptor	full-length
10488382	2,196648792	10,05072932	-0,000321767	-6,391789206	2,338103101	10,36782719	7,864071105		Cd93	CD93 antigen	receptor activity /// binding /// calcium ion binding	full-length
10488797	-1,046676771	7,314904487	-0,061737616	-6,21445487	-1,313048792	9,55646174	10,10297225		Pxmp4	peroxisomal membrane protein 4	molecular_function /// cellular_component ///	full-length
10489107	2,190013447	17,10455946	0,694088519	4,071162841	2,58830289	18,63870009	9,489867642		Samhd1	SAM domain and HD domain, 1	catalytic activity	full-length
10489127	1,72691417	7,035595823	0,140457505	-6,073955682	1,661165552	6,157245534	6,766258985		Rbl1	retinoblastoma-like 1 (p107)	negative regulation of transcription from RNA	full-length
10489204	1,210349338	7,898924156	-0,114845951	-5,896990548	1,73056493	11,72345347	10,21912957		Tgm2	transglutaminase 2, C polypeptide	protein-glutamine gamma-glutamyltransferase	full-length
10489343	-1,020362697	4,925927418	-0,49598417	-1,204491305	-0,961320444	3,8534758	6,188048357		---	---	---	full-length
10489705	0,893820493	2,197492168	0,173000991	-5,671609089	1,653667376	8,631553115	8,015016919		Slc13a3	solute carrier family 13 (sodium-	transporter activity /// membrane fraction ///	full-length
10489721	-0,488662795	-6,097090524	-0,825587163	-3,532697959	-1,076411999	-3,117384936	6,217143022		100043821 ///	predicted gene, 100043821 ///	---	est
10489784	1,129847105	4,776458203	0,000922482	-6,391768928	0,921190013	2,195474417	6,89857238		Prex1	phosphatidylinositol-3,4,5-	guanyl-nucleotide exchange factor activity /// Rho	full-length
10489850	0,781538063	1,524650904	0,870342109	2,999385161	1,204230603	5,715675467	8,090565356		Znfx1	zinc finger, NFX1-type containing 1	transcription factor activity /// nucleus /// regulation	full-length
10490104	1,11031877	4,199328841	0,182073611	-5,637317234	0,875473487	1,340698654	6,092918514	Cluster III	Aurka	aurora kinase A	nucleotide binding /// mitotic cell cycle /// protein	full-length
10490150	2,167278677	11,68300406	1,565366321	7,543765647	3,203619306	15,90162988	8,144558527		Zbp1	Z-DNA binding protein 1	DNA binding /// left-handed Z-DNA binding /// RNA	full-length
10490302	-1,099140789	-3,03707422	-0,66495656	-4,566146086	-1,038667667	-3,635738217	5,113174204		2810021G02Rik	RIKEN cDNA 2810021G02 gene	nucleus /// zinc ion binding /// metal ion binding	partial
10490736	1,05939643	2,203802441	-0,10776939	-6,184421694	0,954374037	0,799740609	6,492394904		Rgs19	regulator of G-protein signaling 19	signal transducer activity /// protein binding ///	full-length
10490815	0,626273718	-5,384865984	0,444880703	-5,394918177	1,58816708	-0,04577535	3,719220959		EG545500	predicted gene, EG545500	---	predicted
10490838	-0,090906679	-7,264961319	-0,366572097	-6,157150685	-1,853971946	-3,124483211	7,159613852		Fabp5	fatty acid binding protein 5,	transporter activity /// binding /// cytoplasm ///	full-length
10490903	1,594708433	8,007296943	-0,071260628	-6,276639307	1,723753448	8,490839003	5,829475019		Car13	carbonic anhydrase 13	carbonate dehydratase activity /// one-carbon	full-length
10490913	-1,427361545	-4,399947827	-0,038265739	-6,389270431	-2,21013299	-2,039857731	12,88593209		Car3	carbonic anhydrase 3	carbonate dehydratase activity /// cytoplasm ///	full-length
10491171	-0,126651563	-6,914563058	-0,004285614	-6,391371083	-1,157099333	3,935191732	11,46663293		Slc2a2	solute carrier family 2 (facilitated	transporter activity /// sugar:hydrogen symporter	full-length
10491820	-0,881621768	-1,342150972	-0,16465323	-6,075180347	-1,215368197	1,120574566	7,371326175		---	---	---	partial
10491825	-1,023493694	-0,755477346	-0,289789207	-5,582842608	-1,457525049	2,154534068	8,294847327		3110057O12Rik	RIKEN cDNA 3110057O12 gene	extracellular region	full-length
10492091	-1,406083063	1,778749749	-0,339470485	-5,384489922	-0,920394222	-2,214397792	6,991975435		Smad9	MAD homolog 9 (Drosophila)	transcription factor activity /// protein binding ///	full-length
10492306	-1,538005023	5,152888223	-0,369577344	-4,617708703	-2,525921069	10,51328669	8,146746129		Sucnr1	succinate receptor 1	signal transducer activity /// receptor activity /// G-	full-length
10492330	-0,987700718	0,727339732	-0,066443367	-6,324116146	-1,1803411	2,076567839	7,270819935		P2ry1	purinergic receptor P2Y, G-protein	signal transducer activity /// receptor activity /// G-	full-length
10492335	1,390197359	5,989864168	0,064238671	-6,304739568	1,428579417	5,87115285	6,825175127		Rap2b	RAP2B, member of RAS	nucleotide binding /// GTP binding /// intracellular	full-length
10492355	-1,972058483	-2,398509281	-0,019475285	-6,391108652	-2,555377739	-0,723329521	7,707558343		Mme	membrane metallo endopeptidase	metalloendopeptidase activity /// proteolysis ///	full-length
10492709	-1,10420078	4,755080807	0,102439929	-6,114352213	-0,547543446	-2,176818813	6,746506592		Accn5	amiloride-sensitive cation channel	ion channel activity /// sodium channel activity ///	full-length
10492964	2,054120144	8,480746272	0,32839555	-4,953293619	1,955428375	7,46931784	10,52916924		Cd5l	CD5 antigen-like	scavenger receptor activity /// extracellular region	full-length
10493267	1,379408241	6,291817394	0,108063175	-6,131506904	1,310039654	5,278431511	6,586090015	Cluster III	Arhgef2	rho/rac guanine nucleotide	cell morphogenesis /// guanyl-nucleotide exchange	full-length
10493382	-0,214911884	-6,658169959	0,010809969	-6,39018176	-1,72812515	5,573660868	10,44931984		Pklr	pyruvate kinase liver and red blood	magnesium ion binding /// catalytic activity ///	full-length
10493494	-0,376055168	-5,598076293	0,34861437	-4,960545672	-1,063046077	0,32077515	5,781147173		OTTMUSG00000	predicted gene,	---	est
10493565	0,549360285	-2,203700476	1,17638093	5,065378109	0,959920239	2,332170282	7,961050431	Cluster V	Adar	adenosine deaminase, RNA-	DNA binding /// left-handed Z-DNA binding /// RNA	full-length
10493812	0,999658342	-1,20553094	-0,086885369	-6,319455893	1,225937422	0,190172335	4,931077818		S100a4	S100 calcium binding protein A4	calcium ion binding /// identical protein binding	full-length
10493820	2,296802396	6,484542299	-0,079777326	-6,338016921	2,390666549	6,514419374	6,401541876		S100a6	S100 calcium binding protein A6	calcium ion binding /// protein binding /// cell cycle	full-length
10493831	1,758579557	-2,514106685	0,147641968	-6,344279803	2,93520884	1,430012164	5,334916203		S100a8	S100 calcium binding protein A8	calcium ion binding /// chemotaxis	full-length
10493990	1,777697873	11,85901845	-0,070688835	-6,218009453	1,746375887	11,22758032	8,438467007		S100a11	S100 calcium binding protein A11	calcium ion binding /// nucleus /// cytoplasm ///	full-length
10494085	-1,504956893	5,847725171	0,013048054	-6,388782566	-1,838775915	7,730653007	11,44435794		Selenbp2	selenium binding protein 2	nucleus /// cytoplasm /// transport /// selenium	full-length
10494200	0,905656274	5,004684097	-0,062057027	-6,232017507	1,023967446	5,962479367	7,887207167		Cdc42se1	CDC42 small effector 1	molecular_function /// cytoplasm /// cytoskeleton ///	full-length
10494271	1,805060349	14,41137887	0,31312555	-2,607897327	1,846231506	14,29088649	10,85415198		Ctss	cathepsin S	cysteine-type endopeptidase activity /// lysosome	full-length

Affymetrix ID	BS/Non Inf.		LS/Non Inf.		RelNF/Non Inf.		Average	Cluster	Gene	Gene	Gene Ontology (GO)	Transcript
Transcript	logFC	B	logFC	B	logFC	B	expression	Number	Symbol	Title	Description	Classification
10494402	2,39627033	9,825098051	0,148761463	-6,093725107	2,03263627	7,448767931	9,772640277		Hist2h3c1 ///	histone cluster 2, H3c1 /// histone	nucleosome /// DNA binding /// nucleus ///	full-length
10494405	2,652913096	10,42586529	0,201708481	-5,904442389	2,316343401	8,383221114	10,25997666	Cluster VI	Hist1h3i ///	histone cluster 1, H3i /// histone	nucleosome /// DNA binding /// nucleus ///	full-length
10494407	1,226955146	3,266511383	-0,032853118	-6,373882845	1,167441713	2,347156158	5,686962689		Hist2h2bb	histone cluster 2, H2bb	nucleosome /// DNA binding /// nucleus ///	full-length
10494428	-1,194767303	5,006952945	-0,505645951	-2,07561042	-1,658245952	8,351119618	10,42168866		Txnip	thioredoxin interacting protein	enzyme inhibitor activity /// protein binding ///	full-length
10494978	2,203143558	13,42807981	0,264158951	-4,584654698	2,342397764	13,75701655	5,656789039	Cluster VI	Ptpn22	protein tyrosine phosphatase, non-	phosphoprotein phosphatase activity /// protein	full-length
10495054	0,976844801	3,873447258	-0,06495891	-6,269029634	1,311118981	6,747761519	7,902039064		Rhoc	ras homolog gene family, member	nucleotide binding /// protein binding /// GTP	full-length
10495186	0,824301174	-0,711695591	-0,115664347	-6,181346497	1,107906276	1,628782911	4,109839783		AI504432	expressed sequence AI504432	---	full-length
10495405	1,453969597	7,105962576	-0,085669757	-6,221004679	1,456067497	6,690657404	6,478906338		Slc25a24	solute carrier family 25	binding /// calcium ion binding /// mitochondrion ///	full-length
10495518	-0,693274171	-1,359419813	-0,218146885	-5,534314175	-1,184343633	3,268898491	5,681527449		Olfm3	olfactomedin 3	protein binding /// extracellular region ///	full-length
10495896	0,913129916	3,2571604	-0,041265788	-6,340999143	1,002827644	3,846864386	6,846953768	Cluster III	Camk2d	calcium/calmodulin-dependent	G1/S transition of mitotic cell cycle /// nucleotide	full-length
10495967	1,354234742	0,827011826	0,124588025	-6,263104704	2,381974553	6,396731559	9,040940457		Tifa	TRAF-interacting protein with	protein binding /// cellular_component /// I-kappaB	full-length
10495993	0,07569608	-7,261208423	-0,183283114	-6,284979671	-1,709707887	-1,633310084	9,219813751	Cluster X	Elovl6	ELOVL family member 6,	mitochondrion /// endoplasmic reticulum /// fatty	full-length
10496077	-0,67019505	-3,573502718	-0,106317566	-6,271527148	-1,062430195	-0,590630599	10,90189143		Agxt2l1	alanine-glyoxylate	molecular_function /// catalytic activity ///	full-length
10496167	-0,488662795	-6,097090524	-0,825587163	-3,532697959	-1,076411999	-3,117384936	6,217143022		100043821 ///	predicted gene, 100043821 ///	---	est
10496204	1,695650222	6,139390726	0,185005073	-5,908723217	1,361047196	3,291607718	4,443752023		Cenpe	centromere protein E	nucleotide binding /// chromosome, centromeric	full-length
10496251	-0,964290777	0,643438373	-0,040767926	-6,365454611	-1,248245797	2,803508045	8,534815189	Cluster X	Bdh2	3-hydroxybutyrate dehydrogenase,	molecular_function /// catalytic activity /// 3-	full-length
10496336	-0,488662795	-6,097090524	-0,825587163	-3,532697959	-1,076411999	-3,117384936	6,217143022		100043821 ///	predicted gene, 100043821 ///	---	est
10496462	-2,21497949	6,256828344	-0,345880155	-5,420028583	-3,223494496	10,2348597	7,204933661		Adh6-ps1	alcohol dehydrogenase 6 (class	---	est
10496466	-0,759348365	-2,771787547	-0,068934639	-6,340368337	-1,321410999	1,461886207	11,20726209	Cluster X	Adh4	alcohol dehydrogenase 4 (class II),	NADPH:quinone reductase activity /// alcohol	full-length
10496539	2,854213321	11,02144562	0,816850256	-1,248233075	3,400255208	12,69614175	6,761024783	Cluster VI	Gbp5	guanylate binding protein 5	nucleotide binding /// GTPase activity /// GTP	full-length
10496555	2,232860934	4,746793524	0,547898981	-4,665511057	1,816516982	2,146092557	7,126066346	Cluster I	Gbp5 /// Gbp1	guanylate binding protein 5 ///	nucleotide binding /// GTPase activity /// GTP	full-length
10496569	2,50615924	12,81241891	1,39531857	5,93746963	3,280003354	15,59183685	9,502672628		Gbp6	guanylate binding protein 6	---	full-length
10496580	2,963882834	14,66561321	1,709195653	7,808379768	3,884613508	17,41547932	8,949500648	Cluster VI	Gbp3	guanylate binding protein 3	nucleotide binding /// GTPase activity /// GTP	full-length
10496592	4,090107564	18,46460104	0,80005463	0,810977844	5,239747688	20,78971155	9,041489013		Gbp2	guanylate binding protein 2	nucleotide binding /// GTPase activity /// GTP	full-length
10496771	0,848295535	2,894500613	-0,439878336	-2,029693971	1,082847048	5,122465238	5,288206063		Mcoln2	mucolipin 2	ion channel activity /// transport /// ion transport ///	full-length
10496872	0,105441508	-7,212869645	-0,204146665	-6,14943201	-1,106771509	-2,561390092	8,108222395		Eltd1	EGF, latrophilin seven	signal transducer activity /// receptor activity /// G-	full-length
10497265	1,602293919	5,711770862	-0,267726559	-5,383800038	0,494901118	-4,472099734	7,062811718		Fabp4	fatty acid binding protein 4,	cytokine production /// transporter activity ///	full-length
10497327	-0,488662795	-6,097090524	-0,825587163	-3,532697959	-1,076411999	-3,117384936	6,217143022		100043821 ///	predicted gene, 100043821 ///	---	est
10497337	-0,909425065	-2,044823179	0,003249056	-6,391692323	-1,295446196	0,554801464	8,53776767		Car1	carbonic anhydrase 1	carbonate dehydratase activity /// cytoplasm ///	full-length
10497349	3,177987358	16,22771721	0,122437546	-6,051802313	3,061177538	15,43834905	6,195426107	Cluster VI	Sirpb1	signal-regulatory protein beta 1	plasma membrane /// intracellular signaling	full-length
10497356	3,011856328	11,32795434	0,121350449	-6,228470576	2,885852617	10,39333336	5,796150474	Cluster VI	Sirpb1	signal-regulatory protein beta 1	plasma membrane /// intracellular signaling	full-length
10497358	3,492406805	18,42353986	0,105331108	-6,081046627	3,489397154	18,11994854	6,414803454	Cluster VIII	Sirpb1	signal-regulatory protein beta 1	plasma membrane /// intracellular signaling	full-length
10497364	3,115699732	15,50284029	0,150886028	-5,923354235	3,061396461	14,92783868	6,01226361	Cluster VI	Sirpb1	signal-regulatory protein beta 1	plasma membrane /// intracellular signaling	full-length
10497372	1,89567073	4,12352216	0,049689596	-6,371655078	1,749368544	2,857209446	5,741104927		381484	predicted gene, 381484	---	full-length
10497381	-2,114348761	5,626499526	-0,093957814	-6,316215326	-1,434157113	1,128976174	10,75370078	Cluster IX	Cyp7b1	cytochrome P450, family 7,	monooxygenase activity /// iron ion binding ///	full-length
10497463	-5,918705204	0,641683144	-4,25687709	-1,378526399	-6,077101567	0,518385455	6,084062008		Cpb1	carboxypeptidase B1 (tissue)	carboxypeptidase activity /// cellular_component ///	full-length
10497548	0,686323484	-2,357796721	0,022018952	-6,384508938	1,022029263	0,559279836	8,355804269		Fndc3b	fibronectin type III domain	molecular_function /// cellular_component ///	full-length
10497831	2,804679494	7,016382663	0,18197643	-6,188390261	2,297682686	4,335728394	6,331291008		Ccna2	cyclin A2	female pronucleus /// male pronucleus /// protein	full-length
10498273	0,869754459	2,314938236	0,050207653	-6,322796602	1,30343628	6,303905314	8,183470017		Tm4sf1	transmembrane 4 superfamily	membrane /// integral to membrane	full-length
10498345	1,066422262	4,229505024	0,272322896	-4,687337086	0,97528667	2,864787964	4,774033721		Gpr171	G protein-coupled receptor 171	signal transducer activity /// receptor activity /// G-	full-length
10498350	1,131973359	5,387571302	0,211953089	-5,212993655	1,429854563	7,642674968	6,095436896		P2ry14	purinergic receptor P2Y, G-protein	signal transducer activity /// receptor activity /// G-	full-length
10498367	2,132316749	13,66321598	0,364085565	-3,041337603	2,140804027	13,3120143	7,910850404		P2ry13	purinergic receptor P2Y, G-protein	signal transducer activity /// receptor activity /// G-	full-length
10498802	0,669237012	-1,206828645	0,033740049	-6,367370069	1,118959786	3,244980393	7,92779443		Rapgef2	Rap guanine nucleotide exchange	guanyl-nucleotide exchange factor activity ///	full-length
10498871	-0,605416875	-3,802506755	-0,06519525	-6,340476276	-1,342345369	2,163252426	7,266984278		Tmem144	transmembrane protein 144	membrane /// integral to membrane	full-length
10498992	1,583734252	-0,268014801	0,125626294	-6,316382077	2,732048746	4,806417864	7,358903429	Cluster VI	Tlr2	toll-like receptor 2	response to molecule of fungal origin /// cell	full-length
10499639	1,148444861	9,917073815	0,270258628	-3,013270299	0,864936844	6,160745658	6,857180033	Cluster III	Cks1b	CDC28 protein kinase 1b	cell cycle /// cyclin-dependent protein kinase	full-length
10499811	-0,749912186	2,62979437	-0,057855458	-6,26135351	-1,425125635	9,45449093	6,81371053		Npr1	natriuretic peptide receptor 1	guanylate cyclase activity /// guanylate cyclase	full-length
10499861	0,868392203	-4,938878727	-0,27630983	-6,120893481	1,434833506	-2,467125706	5,006318676	Cluster IV	S100a9	S100 calcium binding protein A9	calcium ion binding /// leukocyte chemotaxis ///	full-length
10500021	-0,598605127	-3,71104111	-0,116727782	-6,21945157	-1,130448477	0,758197305	7,36619145		Cgn	cingulin	molecular_function /// motor activity /// tight	full-length
10500276	1,057230924	0,318808766	0,085514942	-6,302409849	0,930891964	-1,12261383	5,871618035		BC028528	cDNA sequence BC028528	extracellular region	full-length
10500283	-0,907628246	-4,034302332	0,079343894	-6,360762027	-1,294123849	-2,099228282	8,846132989		Car14	carbonic anhydrase 14	carbonate dehydratase activity /// one-carbon	full-length
10500333	1,030054002	2,660153709	0,093375732	-6,21134251	0,814047726	0,008541734	8,643694391	Cluster III	Hist2h4	histone cluster 2, H4	nucleosome /// DNA binding /// nucleus ///	full-length
10500335	1,965315954	12,35784153	0,413768311	-2,495672213	2,240771132	13,51299659	7,979055521	Cluster VI	Fcgr1	Fc receptor, IgG, high affinity I	antibody-dependent cellular cytotoxicity /// positive	full-length
10500360	-1,885245988	8,309156029	-0,743437323	-0,580718924	-1,816723786	7,441634124	4,675005969		---	---	---	partial
10500527	-0,488662795	-6,097090524	-0,825587163	-3,532697959	-1,076411999	-3,117384936	6,217143022		LOC280487	pol polyprotein	---	partial
10500529	0,592712485	-4,913433487	0,485607835	-4,759637517	1,026958256	-2,083890297	5,754704695		Phgdh	3-phosphoglycerate	catalytic activity /// phosphoglycerate	full-length
10500534	-1,831290894	9,614677766	-0,187486015	-5,636986015	-2,109315358	10,87414346	5,600527943	Cluster IX	Hsd3b4	hydroxy-delta-5-steroid	catalytic activity /// 3-beta-hydroxy-delta5-steroid	full-length
10500539	-1,831290894	9,614677766	-0,187486015	-5,636986015	-2,109315358	10,87414346	5,600527943	Cluster IX	Hsd3b4	hydroxy-delta-5-steroid	catalytic activity /// 3-beta-hydroxy-delta5-steroid	full-length
10500545	-4,466250581	3,95255621	-0,253834241	-6,300573029	-7,01891522	8,684451519	7,804054556	Cluster IX	Hsd3b5	hydroxy-delta-5-steroid	catalytic activity /// 3-beta-hydroxy-delta5-steroid	full-length
10500547	-0,95787231	-0,844089045	0,031123829	-6,380689317	-1,959163729	5,960366863	7,922376311	Cluster X	Hsd3b2	hydroxy-delta-5-steroid	catalytic activity /// 3-beta-hydroxy-delta5-steroid	full-length
10500555	-0,562984572	0,220804405	-0,060260284	-6,239372205	-1,209782032	7,962405831	10,16184924	Cluster X	Hsd3b3	hydroxy-delta-5-steroid	catalytic activity /// 3-beta-hydroxy-delta5-steroid	full-length
10500677	2,090561007	8,903773752	-0,225180639	-5,650019446	2,13372695	8,7132887	6,463473438		Cd2	CD2 antigen	protein binding /// extracellular region /// cell	full-length
10501020	3,521425603	-1,533829062	-0,041952741	-6,390533951	5,760785238	2,581837839	5,868352879		Chi3l3	chitinase 3-like 3	catalytic activity /// hydrolase activity, hydrolyzing	full-length
10501063	2,419626469	17,92752791	0,102709477	-5,840760185	2,700752331	18,82897692	9,652832945		Cd53	CD53 antigen	membrane /// integral to membrane	full-length
10501199	-0,452464254	-4,72662594	-0,089243804	-6,274955869	-1,248243828	2,441176362	9,638588832		Gstm7	glutathione S-transferase, mu 7	glutathione transferase activity /// cytoplasm ///	full-length
10501456	1,003786545	7,133918013	-0,052857943	-6,254365475	1,113846405	7,916344738	6,437975495		---	---	---	partial
10501494	-7,078706891	0,898707182	-5,408247963	-0,750617638	-7,182894401	0,664028756	6,181829707		Amy2 /// Amy2-1	amylase 2, pancreatic /// amylase	extracellular space /// carbohydrate metabolic	full-length
10501500	-5,513863339	0,455552363	-4,040526292	-1,388772766	-5,519387062	0,102692609	7,891640469		Amy2 /// Amy2-1	amylase 2, pancreatic /// amylase	extracellular space /// carbohydrate metabolic	full-length
10501511	-5,513863339	0,455552363	-4,040526292	-1,388772766	-5,519387062	0,102692609	7,891640469		Amy2 /// Amy2-1	amylase 2, pancreatic /// amylase	extracellular space /// carbohydrate metabolic	full-length
10501522	-5,513863339	0,455552363	-4,040526292	-1,388772766	-5,519387062	0,102692609	7,891640469		Amy2 /// Amy2-1	amylase 2, pancreatic /// amylase	extracellular space /// carbohydrate metabolic	full-length
10501533	-5,513863339	0,455552363	-4,040526292	-1,388772766	-5,519387062	0,102692609	7,891640469		Amy2 /// Amy2-1	amylase 2, pancreatic /// amylase	extracellular space /// carbohydrate metabolic	full-length
10501608	2,4940662	19,29720036	0,433103612	0,477316281	3,028660203	21,04402626	9,103576726		Vcam1	vascular cell adhesion molecule 1	protein binding /// plasma membrane /// cell	full-length

Affymetrix ID	BS/Non Inf.		LS/Non Inf.		ReINF/Non Inf.		Average	Cluster	Gene	Gene	Gene Ontology (GO)	Transcript
Transcript	logFC	B	logFC	B	logFC	B	expression	Number	Symbol	Title	Description	Classification
10501832	-0,703728821	0,564580179	-0,051410778	-6,314784419	-1,169113603	5,424733821	11,62599751		Abcd3	ATP-binding cassette, sub-family	nucleotide binding /// protein binding /// ATP	full-length
10502042	1,158938931	-0,961024221	0,282475121	-5,811032686	2,272198614	5,319585729	5,743961452		Alpk1	alpha-kinase 1	protein serine/threonine kinase activity /// ATP	partial
10502050	1,264153495	1,019324424	0,163111565	-6,130843877	2,508329387	8,03877974	6,481018994		Alpk1	alpha-kinase 1	protein serine/threonine kinase activity /// ATP	partial
10502052	1,217642889	1,649460101	0,357928319	-4,983309158	2,229917526	7,862130479	5,809516172		Alpk1	alpha-kinase 1	protein serine/threonine kinase activity /// ATP	partial
10502214	-1,441490785	5,831756425	0,018890704	-6,384939041	-1,955023762	8,947756	7,63025315	Cluster IX	Cyp2u1	cytochrome P450, family 2,	monooxygenase activity /// iron ion binding ///	full-length
10502359	1,047123585	2,10660925	-0,17456406	-5,859242112	1,165342151	2,803463997	5,329258129		Dapp1	dual adaptor for phosphotyrosine	protein binding /// cytoplasm /// phosphoinositide	full-length
10502791	1,72980546	6,460096346	2,451059069	9,703244267	2,538556691	10,54772542	8,922873303		Ifi44	interferon-induced protein 44	cytoplasm	full-length
10503098	1,12087455	9,16649602	0,22657926	-4,002854203	1,267462966	10,2001285	8,740269781	Cluster IV	Lyn	Yamaguchi sarcoma viral (v-yes-1)	nucleotide binding /// protein kinase activity ///	full-length
10503107	1,210883621	-1,479176424	0,441200848	-5,297594013	1,123371753	-2,34224208	5,745856049		6330407A03Rik	RIKEN cDNA 6330407A03 gene	---	est
10503259	0,71075106	-3,502199062	0,833572592	-1,766163267	1,74806222	3,810376611	11,11612948		Trp53inp1	transformation related protein 53	nucleus /// nucleolus /// cytoplasm /// apoptosis ///	full-length
10503264	0,80018273	-0,546093189	0,085283575	-6,264695021	1,145722462	2,463499391	4,370066467	Cluster III	Ccne2	cyclin E2	nucleus /// DNA replication initiation /// cell cycle ///	full-length
10504132	1,154501975	7,682119763	0,190441677	-5,045321599	1,457848711	10,01149842	7,441514734	Cluster IV	Ccl19	chemokine (C-C motif) ligand 19	cytokine activity /// extracellular region ///	full-length
10504159	1,263902377	8,541210455	0,179068296	-5,22511788	1,620040715	11,0681254	7,744442309	Cluster I	Ccl19	chemokine (C-C motif) ligand 19	cytokine activity /// extracellular region ///	full-length
10504188	1,247460392	8,028118294	0,208877483	-4,933193894	1,606075678	10,59785731	7,671031933	Cluster I	Ccl19	chemokine (C-C motif) ligand 19	cytokine activity /// extracellular region ///	full-length
10504450	1,374237537	4,30695401	0,163359013	-5,97646688	1,727983013	6,45557898	7,325054622		Glipr2	GLI pathogenesis-related 2	extracellular region /// Golgi apparatus ///	full-length
10504470	1,036813654	1,216806165	0,070051692	-6,316137341	0,934969897	-0,105357499	5,18571552		Melk	maternal embryonic leucine zipper	nucleotide binding /// protein kinase activity ///	full-length
10504755	1,104173149	4,215796045	0,068890641	-6,276610206	0,987961819	2,624518467	5,731324865		---	---	---	full-length
10504957	1,659106466	2,727341358	0,058664783	-6,363646175	1,356978648	0,377861056	5,874075936		Smc2	structural maintenance of	nucleotide binding /// protein binding /// ATP	full-length
10505237	-1,835456143	4,209594875	-0,020626952	-6,388025909	-2,309321443	6,359789196	5,641677358		---	---	---	partial
10505240	-1,824042215	5,875474533	-0,041646578	-6,37085449	-2,241176931	7,825299864	9,654945202		---	---	---	partial
10505246	-1,078396876	4,186598597	0,104751531	-6,117513776	-1,433196039	6,968534361	8,770093611		---	---	---	partial
10505249	-1,549320269	9,311143631	-0,03645657	-6,351725658	-1,691131542	9,92352641	5,308936508		---	---	---	partial
10505252	-2,094043322	5,89526118	-0,448497692	-4,764433154	-1,594250883	2,514799143	3,537291186		---	---	---	partial
10505254	-1,059310095	3,931112576	0,056436624	-6,31188146	-1,465305959	7,159891437	9,178442497		---	---	---	partial
10505258	-1,078396876	4,186598597	0,104751531	-6,117513776	-1,433196039	6,968534361	8,770093611		---	---	---	partial
10505261	-1,79069742	2,923489377	-0,042707013	-6,378478522	-2,502056727	6,178757378	7,536035166		---	---	---	partial
10505266	-3,260832218	10,46882506	0,268415779	-5,820240386	-3,300730203	10,1868863	5,050715117		---	---	---	est
10505268	-3,327199141	7,375661503	-0,048566695	-6,380674121	-5,272031533	12,41781227	8,809710765		---	---	---	partial
10505445	3,697345251	9,006854527	0,309899347	-5,92472881	4,563266905	11,08752886	7,292208797	Cluster VIII	Orm3	orosomucoid 3	regulation of immune system process ///	full-length
10505451	4,048123888	15,39771843	1,293573101	2,72557464	4,248471717	15,59205888	10,43849224	Cluster VIII	Orm2	orosomucoid 2	regulation of immune system process ///	full-length
10505465	1,552349619	7,385950892	0,272769147	-4,950720894	1,492149387	6,49569411	7,211583109		6330416G13Rik	RIKEN cDNA 6330416G13 gene	membrane /// integral to membrane	full-length
10505517	1,392360012	6,537298422	-0,100535701	-6,160479341	1,426285119	6,383264745	6,489037468	Cluster I	Tlr4	toll-like receptor 4	production of nitric oxide during acute	full-length
10505954	-0,743684646	-2,765931967	-0,140287766	-6,172245692	-1,749566145	4,627333442	7,457666882		Tek	endothelial-specific receptor	nucleotide binding /// protein kinase activity ///	full-length
10506301	-0,551928794	-4,927852319	-0,671589256	-3,242641346	-1,197141023	-0,313610272	5,054139309		Lepr	leptin receptor	receptor activity /// transmembrane receptor	full-length
10506424	1,722933002	13,56979114	0,048152883	-6,276686095	1,90506514	14,3644255	11,58666251		Actg1	actin, gamma, cytoplasmic 1	nucleotide binding /// structural constituent of	full-length
10506470	0,514724911	-4,544929581	-0,090965599	-6,28975042	1,208573121	1,248189754	6,842369458		1700024P16Rik	RIKEN cDNA 1700024P16 gene	---	full-length
10507112	1,21282565	0,449480157	-0,200612267	-6,015644977	0,979151645	-1,692920505	4,433124852		Stil	Scl/Tal1 interrupting locus	cytoplasm /// multicellular organismal development	full-length
10507143	-1,749302798	2,676270202	-0,086035231	-6,337981857	-1,199526858	-1,184359761	11,48058243	Cluster IX	Cyp4a12a	cytochrome P450, family 4,	monooxygenase activity /// iron ion binding ///	full-length
10507152	-1,745882186	1,760001157	-0,03744113	-6,383226571	-1,029173176	-2,94100677	11,35715876	Cluster IX	Cyp4a12b	cytochrome P450, family 4,	---	full-length
10507163	-1,586173966	3,300594136	-0,293690082	-5,581814352	-1,754581961	3,969444523	10,53782732	Cluster IX	Cyp4a10 ///	cytochrome P450, family 4,	monooxygenase activity /// iron ion binding ///	full-length
10507171	-1,600555938	3,737808648	-0,374337247	-5,047580779	-2,050260901	6,065245149	9,30165601		---	---	---	full-length
10507177	-1,399312885	3,408950784	-0,305666633	-5,269435753	-1,905806228	6,415111324	11,10098751		---	---	---	full-length
10507551	-0,40913542	-5,92499634	-0,305761199	-5,621297102	-1,479917185	1,513741854	6,674353081		2610528J11Rik	RIKEN cDNA 2610528J11 gene	membrane /// integral to membrane	full-length
10507594	0,786247657	0,275984507	0,038333276	-6,359479728	1,126266754	3,448712353	8,348748867		Slc2a1	solute carrier family 2 (facilitated	transporter activity /// sugar:hydrogen symporter	full-length
10508074	1,224172216	6,893819036	-0,020582181	-6,378220938	1,49815728	8,829003226	5,43016219	Cluster I	Csf3r	colony stimulating factor 3 receptor	receptor activity /// hematopoietin/interferon-class	full-length
10508392	0,604579188	-2,876945203	-0,021402613	-6,384193892	1,219722557	2,792559373	8,305394404	Cluster IV	Rnf19b	ring finger protein 19B	protein binding /// ubiquitin-dependent protein	partial
10508465	1,096159238	4,341455092	-0,232706909	-5,144035353	1,054121205	3,503736076	8,892038057		Marcksl1	MARCKS-like 1	calmodulin binding /// positive regulation of cell	full-length
10508651	1,428246488	3,639934544	0,235488087	-5,700699127	1,350735328	2,645887997	9,082184175		Sdc3	syndecan 3	cytoskeletal protein binding /// membrane ///	full-length
10508663	2,131432829	12,71215782	0,105314161	-6,085221306	2,134207432	12,31774639	9,94727218		Laptm5	lysosomal-associated protein	lysosome /// transport /// membrane /// integral to	full-length
10508686	-0,665065811	1,579804889	-0,168309635	-5,333158024	-1,172566728	7,333785404	7,831642648	Cluster X	Mecr	mitochondrial trans-2-enoyl-CoA	catalytic activity /// binding /// nucleus ///	full-length
10508734	1,227089815	0,659518197	-0,232228884	-5,881836148	1,771007031	3,979533479	5,783498594		Ptafr	platelet-activating factor receptor	lipopolysaccharide binding /// cytokine production	full-length
10508772	2,069788983	9,938298853	0,238854654	-5,398122014	2,214170121	10,31473025	7,027859568		Fgr	Gardner-Rasheed feline sarcoma	nucleotide binding /// protein kinase activity ///	full-length
10508800	0,598241802	-6,186061261	0,814571297	-4,537040434	1,471048151	-2,678610145	11,35434024		LOC433762	hypothetical gene LOC433762	---	full-length
10508992	-0,759562274	-1,346786733	-0,091376155	-6,258688238	-1,029124337	0,949563308	7,571644761		Paqr7	progestin and adipoQ receptor	receptor activity /// steroid binding /// lipid binding	full-length
10509063	0,724057015	-2,401637236	0,367700106	-4,802581025	2,273292831	8,570711406	7,107333145		Il22ra1	interleukin 22 receptor, alpha 1	receptor activity /// membrane /// integral to	full-length
10509071	0,21334721	-6,73984086	0,012148726	-6,390010416	1,676198354	4,493302054	6,851812466		9130219A07Rik	RIKEN cDNA 9130219A07 gene	---	est
10509122	-0,909022103	3,927889361	-0,277369326	-4,183375808	-1,164514333	6,26844788	5,384640604		Cnr2	cannabinoid receptor 2	signal transducer activity /// receptor activity /// G-	full-length
10510172	2,229784039	9,906739667	0,087552928	-6,269238428	2,028331702	8,351731187	7,271841256		Hmgb2	high mobility group box 2	DNA binding /// nucleus /// chromosome	full-length
10510221	0,485100034	-6,389974587	0,883388894	-3,875778153	1,46718775	-2,00126656	8,886326633		LOC433762	hypothetical gene LOC433762	---	full-length
10510580	0,931184299	3,274063665	-0,216429932	-5,163590948	1,324086867	6,765598218	5,815692187		Tnfrsf9	tumor necrosis factor receptor	receptor activity /// protein binding /// membrane ///	full-length
10511703	0,842047827	-4,430517514	-0,003120657	-6,391743419	2,072713533	1,95990597	8,18134533	Cluster II	Ripk2	receptor (TNFRSF)-interacting	nucleotide binding /// protein kinase activity ///	full-length
10511779	1,265676598	0,112535437	0,049124964	-6,372024497	1,00674632	-2,081660998	5,780640819		Atp6v0d2	ATPase, H+ transporting,	transport /// ion transport /// hydrogen ion	full-length
10512067	0,676696165	1,73026268	1,371760957	8,96247481	0,718724378	1,940262323	8,862401896	Cluster V	Ddx58	DEAD (Asp-Glu-Ala-Asp) box	nucleotide binding /// nucleic acid binding /// RNA	full-length
10512322	1,263902377	8,541210455	0,179068296	-5,22511788	1,620040715	11,0681254	7,744442309	Cluster I	Ccl19	chemokine (C-C motif) ligand 19	cytokine activity /// extracellular region ///	full-length
10512372	1,291507809	7,537817358	0,193786292	-5,283885262	1,664054368	10,10468174	7,658796508	Cluster I	Ccl19	chemokine (C-C motif) ligand 19	cytokine activity /// extracellular region ///	full-length
10512463	-0,488662795	-6,097090524	-0,825587163	-3,532697959	-1,076411999	-3,117384936	6,217143022		LOC280487	pol polyprotein	---	partial
10512774	1,182610633	8,414833724	0,033051201	-6,34326183	1,370280674	9,730311245	5,985724094		Coro2a	coronin, actin binding protein 2A	actin binding	full-length
10512886	1,173904512	-1,050748677	0,197090762	-6,11571038	2,207433522	4,729970638	7,992343589		Acnat2	acyl-coenzyme A amino acid N-	peroxisome /// lipid metabolic process /// fatty acid	full-length
10513512	-0,844587145	-0,920512729	-0,110923385	-6,216009249	-1,048139723	0,621945711	12,84287633		Apobec3 ///	apolipoprotein B mRNA editing	nucleus /// cytoplasm /// zinc ion binding ///	full-length
10513514	-1,147172821	2,711931858	-0,005847025	-6,39120667	-1,206132765	2,829548276	4,692947639		Mup5	major urinary protein 5	transporter activity /// binding /// pheromone	full-length
10513529	-1,469449186	3,032749596	0,030041371	-6,3817994	-1,926975685	5,575148705	12,2411669		Mup3	major urinary protein 3	transporter activity /// binding /// pheromone	full-length
10513538	-2,889917101	5,623844043	-0,048292435	-6,38105518	-3,246053694	6,520896268	8,974474653		OTTMUSG00000	predicted gene,	extracellular region	full-length

Affymetrix ID	BS/Non Inf.		LS/Non Inf.		RelNF/Non Inf.		Average	Cluster	Gene	Gene	Gene Ontology (GO)	Transcript
Transcript	logFC	B	logFC	B	logFC	B	expression	Number	Symbol	Title	Description	Classification
10513884	-0,62443526	-2,965486101	0,344831351	-4,805185009	-1,097474683	1,267175796	7,723190895		Tle1	transducin-like enhancer of split 1,	negative regulation of transcription from RNA	full-length
10514763	-1,037911163	-0,634430218	0,01096071	-6,390556991	-1,181121869	0,142731399	11,5893039	Cluster X	C8a	complement component 8, alpha	molecular_function /// extracellular region ///	full-length
10514912	-1,315696234	-4,81168371	0,016194844	-6,391350085	-1,800609574	-3,472423852	8,863544694	Cluster IX	Dio1	deiodinase, iodothyronine, type I	thyroxine 5'-deiodinase activity /// endoplasmic	full-length
10515187	-1,240374971	-2,380161726	-0,301128197	-5,990012881	-0,958789494	-4,181687463	12,02813561	Cluster X	Cyp4a14	cytochrome P450, family 4,	monooxygenase activity /// iron ion binding ///	full-length
10515201	-0,996936139	4,826747692	-0,180027879	-5,386393476	-1,081831399	5,315395436	7,389424209	Cluster X	Cyp4b1	cytochrome P450, family 4,	monooxygenase activity /// iron ion binding ///	full-length
10515257	1,119811724	2,298966831	0,212421331	-5,685271006	0,99340464	0,74349973	5,418414643		Rad54l	RAD54 like (S. cerevisiae)	nucleotide binding /// double-strand break repair	full-length
10515431	1,465222473	2,740900943	-0,015062334	-6,389401103	0,957056365	-1,519888442	5,34577183		Kif2c	kinesin family member 2C	nucleotide binding /// motor activity /// microtubule	full-length
10515836	2,379249664	6,022861486	-0,29400008	-5,790342268	2,251547677	4,974301413	5,796594912		Ccnb1	cyclin B1	in utero embryonic development /// protein binding	full-length
10515943	0,864970913	0,44763327	-0,124975421	-6,102940461	1,106779099	2,464167249	5,713036622		Ctps	cytidine 5'-triphosphate synthase	catalytic activity /// CTP synthase activity ///	full-length
10516620	1,694389687	10,30249984	0,17363347	-5,548707385	1,631536235	9,42277261	6,394918544	Cluster I	Lck	lymphocyte protein tyrosine kinase	nucleotide binding /// protein kinase activity ///	full-length
10516735	0,844041879	2,642137936	-0,178133083	-5,47222708	1,037530701	4,432913267	9,019065674		Tinagl1	tubulointerstitial nephritis antigen-	cysteine-type endopeptidase activity ///	full-length
10516956	1,858736245	6,418412888	-0,107797797	-6,244664402	2,006934796	6,87173106	6,090713256		Smpdl3b	sphingomyelin phosphodiesterase,	sphingomyelin phosphodiesterase activity ///	full-length
10516966	2,588968761	13,53671939	0,652643701	-0,632349967	2,54579908	12,93558707	8,051175654		BC013712	cDNA sequence BC013712	---	full-length
10517141	1,23425791	5,998878361	0,175339373	-5,611325978	0,999460328	3,254150911	9,388291567		Hmgn2	high mobility group nucleosomal	chromatin /// DNA binding /// nucleus /// cytoplasm	full-length
10517165	2,787284002	18,36674901	0,219309129	-4,541756331	2,738496887	17,87476476	8,028379154		Cd52	CD52 antigen	plasma membrane /// membrane /// anchored to	full-length
10517169	2,193709969	13,20535468	0,046292769	-6,329843826	2,018337369	11,80268499	8,758177898		Sh3bgrl3	SH3 domain binding glutamic acid-	nucleus /// cytoplasm	full-length
10517508	1,651673624	8,970014699	0,235731943	-5,128491345	1,432561982	6,867746858	9,798965194	Cluster I	C1qb	complement component 1, q	extracellular region /// immune response ///	full-length
10517513	1,507213702	8,506541118	0,052136359	-6,316437191	1,292978497	6,287599556	9,943914586	Cluster I	C1qc	complement component 1, q	extracellular region /// immune response ///	full-length
10517517	1,212081704	7,093635038	0,222952128	-4,896702241	1,022916741	4,737124599	9,768256547		C1qa	complement component 1, q	extracellular region /// immune response ///	full-length
10517573	-4,020076475	1,066526237	-2,973625016	-0,858394294	-4,008993513	0,667138621	6,621416685		Ela3	elastase 3, pancreatic	---	full-length
10518050	-3,462694365	0,080181744	-2,766466163	-1,073853751	-3,639056473	0,167433849	7,239245988		RP23-395H4.4	elastase 2A	serine-type endopeptidase activity /// extracellular	full-length
10518069	1,032631446	2,817935154	0,124612889	-6,065833001	1,781728953	8,522600898	9,351403993		Efhd2	EF hand domain containing 2	calcium ion binding /// protein binding	full-length
10518350	2,266408038	10,83301824	0,066612813	-6,311296172	2,108056996	9,541218936	7,879824932		Hmgb2	high mobility group box 2	DNA binding /// nucleus /// chromosome	full-length
10518352	2,305347254	11,33655404	0,088733747	-6,242364556	2,129224781	9,96217178	7,783047024		Hmgb2	high mobility group box 2	DNA binding /// nucleus /// chromosome	full-length
10518455	1,149284052	10,08963719	0,158852677	-4,978083181	1,141937937	9,583810891	7,168895658		Agtrap	angiotensin II, type I receptor-	receptor activity /// angiotensin type II receptor	full-length
10518570	1,019036746	10,22361508	0,043540111	-6,23909302	0,934764796	8,766580599	9,276692013		Pgd	phosphogluconate dehydrogenase	catalytic activity /// phosphogluconate	full-length
10518686	1,598758802	6,732289463	0,157290799	-5,954639732	1,637992202	6,580544325	6,972624099	Cluster I	Pik3cd	phosphatidylinositol 3-kinase	B cell homeostasis /// inositol or	full-length
10518927	1,400873284	8,28010289	-0,141049576	-5,801686501	1,594007211	9,377134244	6,135767054		Kcnab2	potassium voltage-gated channel,	ion channel activity /// voltage-gated ion channel	full-length
10519060	1,280019499	5,704153807	0,276476088	-4,788489348	1,509543732	7,168188277	7,730143514	Cluster I	Tnfrsf14	tumor necrosis factor receptor	receptor activity /// protein binding /// external side	full-length
10519497	1,612248779	4,610940813	0,158806933	-6,087735569	2,742829652	10,35014798	11,48310367		Steap4	STEAP family member 4	catalytic activity /// binding /// iron ion binding ///	full-length
10519527	0,730722662	-1,602351296	-0,143838886	-6,063157346	1,033933813	1,049471296	6,373375195		Abcb1a	ATP-binding cassette, sub-family B	nucleotide binding /// ATP binding /// transport ///	full-length
10519717	0,37182779	-4,442789469	0,000194516	-6,391790027	1,04205853	3,272067154	4,362042281		Sema3a	sema domain, immunoglobulin	regulation of heart rate /// extracellular region ///	full-length
10519983	2,559961142	14,76732355	0,181043256	-5,538450955	2,834605182	15,58208948	7,423864822		Fgl2	fibrinogen-like protein 2	receptor binding /// extracellular region /// signal	full-length
10520483	-0,719422639	0,989909267	-0,012106436	-6,38729102	-1,070196998	4,697527603	9,704759092		D5Wsu178e	DNA segment, Chr 5, Wayne State	magnesium ion binding ///	full-length
10521090	1,149787559	1,430180708	-0,200974652	-5,880304315	1,006486824	-0,172834659	6,16234815		Tacc3	transforming, acidic coiled-coil	microtubule cytoskeleton organization and	full-length
10521337	1,03364227	0,883496568	0,129384459	-6,152746917	1,417694582	3,687566613	6,22716218		Rgs12	regulator of G-protein signaling 12	---	full-length
10521667	1,72978259	1,622385566	0,034205403	-6,384708897	2,722079638	6,069471593	5,474908448		Bst1	bone marrow stromal cell antigen 1	catalytic activity /// NAD+ nucleosidase activity ///	full-length
10521678	1,204890737	9,303623405	-0,140772408	-5,471227047	1,437007397	10,97736657	9,432181133	Cluster I	Cd38	CD38 antigen	catalytic activity /// NAD+ nucleosidase activity ///	full-length
10521731	1,842467326	3,565849461	0,071592056	-6,351957807	1,413759053	0,524882839	4,927158736		Ncapg	on-SMC condensin I complex,	molecular_function /// cellular_component ///	full-length
10521984	1,306492635	6,084672192	0,085704366	-6,214648796	1,238071405	5,050327263	6,284279642		G6pd2	glucose-6-phosphate	catalytic activity /// glucose-6-phosphate	full-length
10522182	0,965086759	1,910631568	0,145967491	-5,966689617	1,208073108	3,844019491	5,991735453		Rhoh	ras homolog gene family, member	nucleotide binding /// GTP binding /// intracellular	full-length
10522368	1,902127558	3,048195535	0,267211383	-5,934821793	1,476881222	0,185042244	7,547637514		Npal1	NIPA-like domain containing 1	---	full-length
10522742	-0,488662795	-6,097090524	-0,825587163	-3,532697959	-1,076411999	-3,117384936	6,217143022		LOC280487	pol polyprotein	---	partial
10522788	1,096315453	1,15583001	0,018632389	-6,38703845	0,779611118	-2,077684168	4,170000416		Stap1	signal transducing adaptor family	SH3/SH2 adaptor activity /// protein binding ///	full-length
10523095	-0,699819598	-3,66432302	-0,083681321	-6,325346272	-1,27783002	0,522530708	10,19779127		Afm	afamin	molecular_function /// cellular_component ///	full-length
10523111	-0,68798233	2,864128156	-0,177800734	-5,005357588	-1,168898563	8,392738412	9,124755368		---	---	---	partial
10523128	2,353735697	11,28112705	-0,085021066	-6,261217696	2,727384639	12,62536763	6,480180031		Ppbp	pro-platelet basic protein	extracellular region	full-length
10523134	1,130537193	3,025673457	-0,068952728	-6,303520605	1,234365862	3,547113811	5,506924025	Cluster I	Pf4	platelet factor 4	cytokine activity /// extracellular region ///	full-length
10523151	1,082928599	-4,536493553	0,103410703	-6,361719771	1,603644197	-2,56625509	7,962662087	Cluster IV	Cxcl1	chemokine (C-X-C motif) ligand 1	cytokine activity /// extracellular region ///	full-length
10523156	0,445510488	-5,259017323	0,139755294	-6,169261462	1,208245062	0,911598792	4,36961213	Cluster IV	Cxcl2	chemokine (C-X-C motif) ligand 2	cytokine activity /// extracellular region ///	full-length
10523245	-0,869709305	0,940314761	-0,139619593	-5,998605986	-1,313227857	4,80516275	7,063521405		Gm1381	gene model 1381, (NCBI)	---	full-length
10523451	1,259124401	1,277238776	-0,03563931	-6,378280844	0,982456416	-1,271665933	7,232306715		Anxa3	annexin A3	phospholipase inhibitor activity /// calcium ion	full-length
10523468	1,036774594	3,116865653	-0,084789021	-6,231203812	0,936646446	1,682861701	6,677464425	Cluster III	Bmp2k	BMP2 inducible kinase	nucleotide binding /// protein kinase activity ///	full-length
10523766	1,120194244	5,999778219	0,182684333	-5,381709458	1,126915596	5,639521387	8,080128587		Lrrc8c	leucine rich repeat containing 8	protein binding /// membrane /// integral to	full-length
10524169	1,134241686	1,327770778	0,153076663	-6,088332218	0,619546808	-3,669983154	5,088754071		Pole	polymerase (DNA directed),	nucleotide binding /// nucleic acid binding /// DNA	full-length
10524460	-0,042359731	-7,274444876	0,147026509	-6,326833914	-1,682937912	-1,977483509	8,085762867	Cluster X	Acacb	acetyl-Coenzyme A carboxylase	---	full-length
10524621	1,64443359	9,983793594	1,402923774	7,772469496	2,492736703	14,52549431	8,316851404	Cluster VI	Oasl2	2'-5' oligoadenylate synthetase-like	2'-5'-oligoadenylate synthetase activity /// RNA	full-length
10524631	1,271140494	-0,051774318	2,041081748	4,881689944	1,824955646	3,084365489	8,774205986		Oasl1	2'-5' oligoadenylate synthetase-like	transferase activity /// nucleotidyltransferase	full-length
10524698	-2,604987434	-0,190074515	-1,911155236	-1,861118206	-2,565794715	-0,666942502	5,713268427		Pla2g1b	phospholipase A2, group IB,	phospholipase A2 activity /// receptor binding ///	full-length
10525158	0,259411308	-6,429619395	1,291466177	2,979334035	0,260451854	-6,531576988	4,836230779	Cluster V	Oas1b	2'-5' oligoadenylate synthetase 1B	RNA binding /// ATP binding /// immune response	full-length
10525591	1,131437489	-0,668457903	0,002403372	-6,391741441	0,633610339	-4,653466407	4,412665271	Cluster III	Kntc1	kinetochore associated 1	nucleus /// cytoplasm /// cell cycle /// mitosis /// cell	full-length
10526277	-0,567420247	-6,278300017	0,309217192	-6,085983944	-1,314966798	-3,358485219	8,797389512	Cluster X	Mlxipl	MLX interacting protein-like	negative regulation of transcription from RNA	full-length
10526459	1,117017361	9,325944193	0,401653873	-0,627230216	1,118510335	8,909997343	6,120885384		Rasa4	RAS p21 protein activator 4	GTPase activator activity /// intracellular ///	full-length
10526783	1,39751038	1,903074128	0,252567471	-5,793929465	1,636013896	3,120635891	4,399725004		BC055004	cDNA sequence BC055004	---	full-length
10527012	1,20701124	4,307187051	0,10906417	-6,148555619	1,169268777	3,548658099	7,039741206	Cluster X	Lfng	LFNG O-fucosylpeptide 3-beta-N-	ovarian follicle development /// Golgi apparatus ///	full-length
10527425	-0,488662795	-6,097090524	-0,825587163	-3,532697959	-1,076411999	-3,117384936	6,217143022		LOC280487	pol polyprotein	---	partial
10527441	1,327024459	7,971451129	0,034531634	-6,352750331	1,360513138	7,83070935	9,890346488		Arpc1b	actin related protein 2/3 complex,	actin binding /// cytoplasm /// cytoskeleton ///	full-length
10527638	1,935186461	6,057292723	0,00074991	-6,391784733	2,034933053	6,202042595	7,912935821		Alox5ap	arachidonate 5-lipoxygenase	leukotriene metabolic process /// enzyme activator	full-length
10527940	1,607056921	9,894421419	-0,140605516	-5,806170852	1,39390809	7,778445317	6,259755396		Pftk1	PFTAIRE protein kinase 1	nucleotide binding /// protein kinase activity ///	full-length
10528102	-0,838941192	-1,718208883	-0,108900387	-6,251119721	-1,42968	2,755096583	12,28757905		Crot	carnitine O-octanoyltransferase	peroxisome /// lipid metabolic process /// fatty acid	full-length
10528165	-0,488662795	-6,097090524	-0,825587163	-3,532697959	-1,076411999	-3,117384936	6,217143022		LOC280487	pol polyprotein	---	partial
10528205	-0,488662795	-6,097090524	-0,825587163	-3,532697959	-1,076411999	-3,117384936	6,217143022		100043821 ///	predicted gene, 100043821 ///	---	est

Affymetrix ID	BS/Non Inf.		LS/Non Inf.		ReINF/Non Inf.		Average	Cluster	Gene	Gene	Gene Ontology (GO)	Transcript
Transcript	logFC	B	logFC	B	logFC	B	expression	Number	Symbol	Title	Description	Classification
10528207	1,199865519	3,122942178	-0,124069006	-6,136657803	1,145415435	2,241629194	9,935285488	Cluster I	Cd36	CD36 antigen	receptor activity /// protein binding /// transport ///	full-length
10528480	2,297230659	13,35734635	0,134572421	-5,917481776	2,472209076	13,82980929	9,26226561		EG625174	predicted gene, EG625174	---	predicted
10529264	-0,656355279	-3,56120771	-0,202113835	-5,948032636	-1,677421809	4,115313893	7,174509154		Spon2	spondin 2, extracellular matrix	protein binding /// extracellular region ///	full-length
10529689	0,961939528	8,121719782	-0,076697433	-6,025217488	1,024087467	8,426305883	9,664797798		Wdr1	WD repeat domain 1	actin binding /// cytoplasm /// cytoskeleton ///	full-length
10530059	-0,797257189	-2,590421481	-0,299741634	-5,518635894	-1,037694172	-0,919880198	6,49544829		2310045A20Rik	RIKEN cDNA 2310045A20 gene	binding /// membrane /// integral to membrane	full-length
10530145	2,138883209	12,69568451	-0,216623487	-5,194784516	2,260975394	12,94993209	5,812565331	Cluster VI	Tlr1	toll-like receptor 1	receptor activity /// transmembrane receptor	full-length
10530319	1,505208549	2,838926792	0,119000901	-6,249295992	1,669163969	3,521566452	7,123079465		Atp8a1	ATPase, aminophospholipid	nucleotide binding /// magnesium ion binding ///	full-length
10530615	-0,702213504	0,105841257	-0,208181113	-5,330869611	-1,189715885	5,078107354	8,948758429		Ociad2	OCIA domain containing 2	mitochondrion /// mitochondrial inner membrane ///	full-length
10530692	-0,732808555	-5,338901469	-0,125577288	-6,327619373	-2,089464883	1,167683614	8,556329294		Kdr	kinase insert domain protein	nucleotide binding /// angiogenesis /// ovarian	full-length
10531041	-1,404877858	-0,54126263	-0,045070416	-6,380158629	-1,605974095	0,283412934	11,71327095		Ugt2b1	UDP glucuronosyltransferase 2	transferase activity /// transferase activity,	full-length
10531061	-1,258891651	4,644726328	-0,726748129	-0,111938819	-1,499099422	6,183889502	6,53193895		Ugt2b37	UDP glucuronosyltransferase 2	mitochondrial inner membrane /// transferase	full-length
10531073	-1,470261681	8,067553359	-0,456169947	-2,341268608	-1,366076756	6,777528605	9,469183318		Ugt2b38	UDP glucuronosyltransferase 2	transferase activity /// transferase activity,	full-length
10531111	2,542718608	-6,095023149	-0,037514606	-6,391515629	6,912661483	-1,642527878	5,737288701		Sult1e1	sulfotransferase family 1E,	estrone sulfotransferase activity /// steroid binding	full-length
10531126	4,331377006	11,78363841	-0,554428007	-4,80297856	3,942546604	10,23702165	6,407936852		Igj	immunoglobulin joining chain	antigen binding /// humoral immune response	full-length
10531370	2,187735235	14,86611267	0,023616533	-6,370204362	2,509249521	16,08938075	8,100304438		Naaa	N-acylethanolamine acid amidase	molecular_function /// cytoplasm /// lysosome ///	full-length
10531407	4,230603993	13,3164919	0,558497386	-4,29308072	4,796607967	14,40701864	9,559737964		Cxcl9	chemokine (C-X-C motif) ligand 9	cytokine activity /// extracellular region ///	full-length
10531415	3,284129055	5,845560629	1,275170985	-2,147104625	4,005126507	7,706551685	9,175392777	Cluster VI	Cxcl10	chemokine (C-X-C motif) ligand 10	cytokine activity /// extracellular region ///	full-length
10531610	0,98385874	-0,57829419	0,380557814	-4,900875215	1,247119393	1,21164673	7,826576476		Rasgef1b	RasGEF domain family, member	molecular_function /// guanyl-nucleotide exchange	full-length
10531724	3,319720646	14,79925329	0,970168557	1,452632206	3,657079648	15,55435614	7,425699956		Plac8	placenta-specific 8	molecular_function /// cellular_component ///	full-length
10531737	0,984070218	4,771663021	0,101573771	-6,049083512	1,175057297	6,34732289	7,263779614		Hpse	heparanase	magnesium ion binding /// calcium ion binding ///	full-length
10531919	-0,631746848	1,954017921	-0,152766819	-5,348052982	-1,011321636	6,651337276	10,49195738	Cluster X	Hsd17b11	hydroxysteroid (17-beta)	catalytic activity /// estradiol 17-beta-	full-length
10531952	1,37351566	-2,54142828	-0,064450839	-6,377030186	0,769732376	-5,571127626	5,61889919		Abcg3	ATP-binding cassette, sub-family	ATP binding /// transport /// membrane /// integral	full-length
10531972	2,349572989	9,844674668	0,607825287	-2,525618466	2,931001638	12,0634303	7,959047606		5830443L24Rik	RIKEN cDNA 5830443L24 gene	---	full-length
10531980	2,245776889	7,377351891	1,013104077	-0,159453106	3,321957416	11,59482549	8,008903549		BC057170	cDNA sequence BC057170	---	full-length
10531987	3,001872053	15,28462841	1,531899181	7,144571613	3,583991093	16,96410669	8,549475557		Gbp4	guanylate binding protein 4	molecular_function /// cellular_component ///	full-length
10531994	2,58480368	9,202894426	2,083055304	6,584028558	3,330253664	11,80189986	10,81659213		Mpa2l /// Gbp10	macrophage activation 2 like ///	molecular_function /// cellular_component ///	full-length
10532019	2,299860249	5,418681624	0,698528732	-3,649504623	3,045127192	8,229421318	8,974694434		EG634650 ///	predicted gene, EG634650 ///	---	full-length
10532711	1,367416175	5,33692343	0,148763246	-5,97291717	1,355700108	4,816796094	6,539748262		Cmklr1	chemokine-like receptor 1	signal transducer activity /// receptor activity /// G-	full-length
10532744	1,956270544	13,1953109	0,021228792	-6,375379787	1,787402847	11,70904145	7,154404705	Cluster I	Selplg	selectin, platelet (p-selectin) ligand	protein binding /// sugar binding /// plasma	full-length
10532857	1,078725368	5,566797827	0,106280071	-6,032250173	1,018985849	4,507585858	7,832323581		Gltp	glycolipid transfer protein	cytoplasm /// transport /// lipid transport ///	full-length
10532896	1,310288639	8,811469981	0,099528839	-6,017946032	1,097963601	6,314889252	5,337949623		2610524H06Rik	RIKEN cDNA 2610524H06 gene	---	full-length
10533213	0,718674826	-2,156746735	0,552797754	-3,024190516	1,557288695	4,698341638	5,978388153		Oas3 /// Oit3	2'-5' oligoadenylate synthetase 3	calcium ion binding /// nucleus	full-length
10533246	1,620768242	11,31870212	1,277637728	8,088600327	1,959525872	13,17069218	7,334970652		Oas1a /// Oas1g	2'-5' oligoadenylate synthetase 1A	2'-5'-oligoadenylate synthetase activity /// double-	full-length
10533256	0,979266296	-0,309686024	0,682697834	-2,265786012	1,350371736	2,36042009	6,862800256		Oas1a	2'-5' oligoadenylate synthetase 1A	2'-5'-oligoadenylate synthetase activity /// double-	full-length
10533304	0,898563536	3,861867055	0,87661583	3,894930495	1,237655444	7,035459343	9,482743221		Trafd1	TRAF type zinc finger domain	molecular_function /// protein binding ///	full-length
10533720	0,847900592	-3,293404715	0,359663356	-5,501237865	1,155932277	-1,434072446	5,068292115		Gpr109a	G protein-coupled receptor 109A	purinergic nucleotide receptor activity /// signal	full-length
10534202	1,497221117	8,562128128	0,159620749	-5,703104428	1,637319588	9,189512321	7,310640225	Cluster I	Ncf1	neutrophil cytosolic factor 1	leukocyte mediated cytotoxicity /// protein binding	full-length
10534303	0,837551527	1,353029814	-0,198276659	-5,496011516	1,117886985	3,924167835	5,509498245	Cluster IV	Lat2	linker for activation of T cells	plasma membrane /// immune response ///	full-length
10534456	1,030326699	5,922588357	0,114693982	-5,907766368	1,031717746	5,510187318	6,781889841		Hip1	huntingtin interacting protein 1	protein binding /// cytoplasm /// Golgi apparatus ///	full-length
10534667	1,711306691	-5,047851074	0,255508404	-6,33445769	3,460607591	-1,161170389	6,658070615		Serpine1	serine (or cysteine) peptidase	serine-type endopeptidase activity ///	full-length
10534909	1,367097702	11,01569862	0,297753313	-2,934592916	1,512096737	11,80063875	6,816630375		---	---	---	partial
10534927	1,79706072	7,910552567	-0,107863203	-6,188827792	1,727961831	7,019979011	7,540054851		Pilra	paired immunoglobin-like type 2	receptor activity /// protein binding /// signal	full-length
10534935	1,116518393	-0,737309763	0,009959055	-6,390931916	1,063662256	-1,459862694	7,080462816		Pilrb1	paired immunoglobin-like type 2	molecular_function /// cellular_component ///	full-length
10535065	1,112697062	2,638786069	0,131079012	-6,091150333	1,31405468	3,991355168	5,800175541		Adap1	ArfGAP with dual PH domains 1	---	full-length
10535331	-0,288362471	-5,687197354	-0,011275371	-6,389109456	-1,205415178	3,942936602	6,194322943	Cluster X	Mmd2	monocyte to macrophage	receptor activity /// membrane /// integral to	full-length
10535669	-0,608036357	-2,903560265	-0,407347783	-4,138117913	-1,381125838	4,010612152	9,169198597	Cluster X	Cyp3a41a ///	cytochrome P450, family 3,	monooxygenase activity /// iron ion binding ///	full-length
10535683	-0,632854784	-2,475649941	-0,413194425	-3,987630172	-1,419620522	4,578521391	9,095289311	Cluster X	Cyp3a41a ///	cytochrome P450, family 3,	monooxygenase activity /// iron ion binding ///	full-length
10535698	-0,717689038	-3,602766572	-0,668484276	-3,198004033	-1,694113113	3,184049697	7,28328377	Cluster X	Cyp3a44	cytochrome P450, family 3,	molecular_function /// cellular_component ///	full-length
10535704	-0,474377149	-3,845469686	-0,316725946	-4,689234303	-1,302848347	4,342360616	12,01243072	Cluster X	Cyp3a11	cytochrome P450, family 3,	monooxygenase activity /// iron ion binding ///	full-length
10536908	-0,987355742	4,198048371	-0,233094982	-4,916189967	-1,200393353	5,954835806	7,309902618		Tspan33	tetraspanin 33	membrane /// integral to membrane	full-length
10537014	-4,267138497	0,23996627	-3,169580791	-1,458238224	-4,468419067	0,296300514	5,496844338		Cpa2	carboxypeptidase A2, pancreatic	carboxypeptidase activity ///	full-length
10537051	-5,125330544	0,707598472	-3,680291178	-1,340797733	-5,183349316	0,443975037	6,939805354		Cpa1	carboxypeptidase A1	carboxypeptidase activity ///	full-length
10537146	1,301238411	-0,188406708	-0,411773695	-5,266625185	0,642846731	-4,946503886	6,151940185		Akr1b8	aldo-keto reductase family 1,	aldehyde reductase activity /// cytoplasm ///	full-length
10537318	0,805299667	-3,050053128	-0,04989012	-6,369779401	1,410595253	1,105937084	7,940098086		Trim24	tripartite motif-containing 24	DNA binding /// protein binding /// intracellular ///	full-length
10537410	1,564634357	5,185007785	0,171468505	-5,977959798	1,55295223	4,678547621	6,604190282		Tbxas1	thromboxane A synthase 1,	prostaglandin biosynthetic process ///	full-length
10537627	-2,497038611	-1,033031987	-1,631618451	-3,108408462	-2,599142403	-1,038058382	5,773280136	Cluster IX	Prss2	protease, serine, 2	serine-type endopeptidase activity /// calcium ion	full-length
10537634	-2,131670239	-2,310482206	-1,809623313	-2,604242905	-2,350799642	-1,903448881	4,452451047		Try4	trypsin 4	molecular_function /// cellular_component ///	full-length
10537638	-3,204437387	-3,002784426	-2,299598663	-3,928435871	-3,397947448	-2,90033889	5,589625497		Try10	trypsin 10	---	full-length
10537645	-1,518424462	-1,715262595	-1,201381581	-2,540331568	-1,599057217	-1,634943686	4,756948756		EG386551	predicted gene, EG386551	---	full-length
10537650	-2,628866431	2,045346863	-1,910450754	-0,236794553	-2,590407041	1,510460278	5,796098436		Prss1 ///	protease, serine, 1 (trypsin 1) ///	---	full-length
10538126	1,302693065	5,979621458	0,030313669	-6,36964317	1,318089389	5,684835714	8,709321434		Gimap4	GTPase, IMAP family member 4	nucleotide binding /// GTP binding	full-length
10538135	1,493718804	5,135227609	0,058407606	-6,338087828	1,419631119	4,152539987	5,382631459		Gimap7	GTPase, IMAP family member 7	---	full-length
10538150	0,891902187	4,426075359	0,064630248	-6,230894838	1,009913526	5,384984887	9,403364187		Tmem176a	transmembrane protein 176A	membrane /// integral to membrane	full-length
10538187	1,757590118	1,924235445	-0,059336325	-6,369875724	2,2816099	4,254548426	5,536182891		Gpnmb	glycoprotein (transmembrane) nmb	integrin binding /// integral to plasma membrane ///	full-length
10538290	1,230180721	0,792611219	0,18076346	-6,070752888	2,035729863	5,657787245	9,046165486		Snx10	sorting nexin 10	protein binding /// transport /// cell communication	full-length
10538459	-0,490805719	-0,175182728	-0,178178144	-4,944530153	-1,159475539	8,55508039	9,383372307		Aqp1	aquaporin 1	transporter activity /// integral to plasma	full-length
10538590	1,227329012	6,210918115	1,272159264	6,537075251	2,133543007	12,31792119	8,770870552		---	---	---	partial
10538753	1,183873423	0,463386368	0,174701207	-6,089758324	2,05540792	5,799515633	7,979313772		---	---	---	predicted
10538791	1,348206365	0,482216258	0,000702213	-6,391787102	1,613719912	1,826959842	4,748716527		Tnip3	TNFAIP3 interacting protein 3	---	full-length
10538832	1,344891412	2,195535295	-0,014109919	-6,389553538	1,147378575	0,287996827	7,095652374		Mad2l1	MAD2 mitotic arrest deficient-like 1	mitotic sister chromatid segregation ///	full-length
10538868	1,867623301	5,382874151	0,120156856	-6,240972118	1,558145676	2,994215302	6,736994596		---	---	---	partial
10538871	5,180824847	12,3400242	-0,722970889	-4,387550686	5,024076841	11,55768214	6,993904357		---	---	---	full-length

Affymetrix ID	BS/Non Inf.		LS/Non Inf.		ReINF/Non Inf.		Average	Cluster	Gene	Gene	Gene Ontology (GO)	Transcript
Transcript	logFC	B	logFC	B	logFC	B	expression	Number	Symbol	Title	Description	Classification
10538880	5,465986878	11,21222467	0,200778498	-6,258348998	5,009546027	9,745014202	5,388562803		---	---	---	full-length
10538882	3,988322749	11,17756693	-0,316665081	-5,794057073	3,651164433	9,696808996	5,779626007		---	---	---	partial
10538887	1,626032565	3,617536967	0,281128253	-5,638770491	1,383600257	1,558271453	5,188283669		---	---	---	partial
10538903	3,639446982	12,77814982	0,037286782	-6,378155642	3,693791535	12,54637505	6,017442376		Igk /// Igk-V28	immunoglobulin kappa chain	---	full-length
10538921	5,269700073	15,59175001	-0,27031826	-5,860634049	5,083949316	14,80356768	6,848396715		---	---	---	full-length
10538924	2,549728485	6,651355601	0,189171847	-6,143014222	2,516680072	6,071233287	5,567036555		---	---	---	full-length
10538929	3,110082959	10,52112339	0,314539229	-5,540449177	2,87837111	9,169452172	5,505147768		---	---	---	partial
10538936	1,19400107	0,82780394	0,198078472	-5,982348674	1,513947047	2,79369738	5,022714438		---	---	---	partial
10538965	-1,079913289	-5,033685353	-0,12306488	-6,35808042	-2,406340289	-0,315421076	12,48429525		Fabp1	fatty acid binding protein 1, liver	chromatin binding /// transporter activity /// binding	full-length
10538979	1,884386723	9,972051814	-0,121350677	-6,063792712	1,839722786	9,25627372	6,290456288	Cluster I	Cd8b1	CD8 antigen, beta chain 1	protein binding /// protein binding /// immune	full-length
10538993	2,435200159	13,96637883	0,175840779	-5,611633089	2,683781324	14,72361739	6,704989056	Cluster VI	Cd8a	CD8 antigen, alpha chain	T cell mediated immunity /// protein binding ///	full-length
10539135	2,400092038	11,15146765	0,17657177	-5,87748213	2,67392062	12,02407116	6,904038347	Cluster VI	Capg	capping protein (actin filament),	actin binding /// extracellular region /// nucleus ///	full-length
10539143	-1,340049279	2,087067645	-0,262969315	-5,6677477	-1,118071821	-0,009589508	10,96438438	Cluster X	Retsat	retinol saturase (all trans retinol	nuclear outer membrane /// endoplasmic reticulum	full-length
10539194	-2,284685173	-3,42404642	-1,659263665	-4,152818098	-2,407475335	-3,370867754	3,852161108		Reg2	regenerating islet-derived 2	binding /// sugar binding	full-length
10539200	-4,303455637	1,600038646	-3,009234867	-0,866034307	-4,353565683	1,329317359	5,49493167		Reg1	regenerating islet-derived 1	binding /// sugar binding /// growth factor activity	full-length
10539739	0,392861777	-6,614629902	0,004629884	-6,391696126	1,091395763	-3,570269893	5,757768105		Asprv1	aspartic peptidase, retroviral-like 1	aspartic-type endopeptidase activity /// proteolysis	full-length
10539894	-0,650547635	-0,798878414	-0,107371017	-6,108277628	-1,427635017	6,833139186	8,810296483		Mgll	monoglyceride lipase	catalytic activity /// carboxylesterase activity ///	full-length
10540531	-0,488662795	-6,097090524	-0,825587163	-3,532697959	-1,076411999	-3,117384936	6,217143022		LOC280487	pol polyprotein	---	partial
10541129	-0,488662795	-6,097090524	-0,825587163	-3,532697959	-1,076411999	-3,117384936	6,217143022		100043821 ///	predicted gene, 100043821 ///	---	est
10541301	0,961304696	-2,19626656	-0,132619405	-6,252270477	1,730598394	2,64949218	7,714486184		Tuba8	tubulin, alpha 8	nucleotide binding /// microtubule cytoskeleton	full-length
10541307	1,467594006	-0,214646847	2,673612272	5,932332763	2,212753053	3,406596545	8,88341955	Cluster VII	Usp18	ubiquitin specific peptidase 18	ubiquitin thiolesterase activity /// ubiquitin-	full-length
10541555	2,499316029	10,30599854	0,155515002	-6,067786757	2,647846219	10,56891475	7,575845904		Clec4a1	C-type lectin domain family 4,	receptor activity /// sugar binding /// membrane ///	full-length
10541564	2,181030312	9,109689713	0,1864162	-5,898599431	2,215501568	8,863505426	6,366280056		Clec4a3	C-type lectin domain family 4,	receptor activity /// sugar binding /// membrane ///	full-length
10541587	1,444384594	1,635042984	-0,133708857	-6,237945857	1,777871	3,365023917	5,251275153	Cluster I	Clec4a2	C-type lectin domain family 4,	binding /// sugar binding /// membrane fraction ///	full-length
10541605	3,189066798	15,81100189	-0,078259397	-6,261469908	3,51025235	16,55909848	7,65980052	Cluster VI	Clec4n	C-type lectin domain family 4,	binding /// sugar binding /// immune response ///	full-length
10541614	1,109455582	-5,10538896	0,041497601	-6,388286718	2,278539289	-1,159767644	4,781095005		Clec4d	C-type lectin domain family 4,	receptor activity /// binding /// sugar binding ///	full-length
10542040	0,901244144	3,338800073	0,38183743	-2,954799517	1,049267358	4,56925432	6,417619661		Parp11	poly (ADP-ribose) polymerase	NAD+ ADP-ribosyltransferase activity /// nucleus	full-length
10542112	-2,07804802	4,645552	-0,203021174	-6,090713373	-2,180427736	4,756135804	7,128489478		Clec2h	C-type lectin domain family 2,	receptor activity /// transmembrane receptor	full-length
10542120	1,120788223	4,433712224	-0,091156361	-6,189470102	1,052270773	3,338048578	5,933644672		Clec2i	C-type lectin domain family 2,	receptor activity /// transmembrane receptor	full-length
10542164	2,35175771	14,82393968	0,264471009	-4,40401917	2,337216866	14,36964127	7,545243188	Cluster VI	Clec12a	C-type lectin domain family 12,	receptor activity /// binding /// sugar binding ///	full-length
10542214	1,516059884	10,06961699	-0,124661121	-5,856932687	1,117500275	6,061358825	4,557232756		Klrd1	killer cell lectin-like receptor,	receptor activity /// sugar binding /// external side	full-length
10542340	0,565619751	-4,624754503	-0,027730843	-6,384159308	1,035620454	-1,128372678	8,44670565		8430419L09Rik	RIKEN cDNA 8430419L09 gene	membrane /// integral to membrane	full-length
10542355	1,003654338	1,919552154	-0,099480336	-6,205455339	1,348751322	4,630097236	6,521056009		Emp1	epithelial membrane protein 1	membrane /// integral to membrane /// cell growth	full-length
10542691	1,025578115	2,207117181	0,098672132	-6,205868442	0,893499504	0,490746467	6,072193196		Lrmp	lymphoid-restricted membrane	cytoplasm /// endoplasmic reticulum /// membrane	full-length
10542714	-0,53528605	-3,27098776	-0,089568939	-6,243781831	-1,054075729	1,901768801	8,168015426		Lyrm5	LYR motif containing 5	---	full-length
10542738	-0,890912817	1,703082563	-0,139112812	-5,95759342	-1,14581209	3,91033086	7,204707642		Rassf8	Ras association (RalGDS/AF-6)	signal transduction	full-length
10542880	-1,375223082	4,267789579	-0,338205364	-4,786839349	-0,66782887	-2,632884327	9,964710237		4833442J19Rik	RIKEN cDNA 4833442J19 gene	cytoplasm /// protein amino acid methylation ///	full-length
10542911	1,079647187	2,472015403	1,608997563	6,728283017	1,44022008	5,157220072	7,052902858		Samd9l	sterile alpha motif domain	---	partial
10542981	1,238308257	10,29823471	0,058069712	-6,206008381	1,220068834	9,692568448	8,15037344		Gmfg	glia maturation factor, gamma	actin binding /// intracellular /// growth factor	full-length
10543017	-1,285060644	3,216926915	-0,320377271	-5,01097749	-1,544289163	4,79244192	7,211177926		Pdk4	pyruvate dehydrogenase kinase,	two-component sensor activity /// protein histidine	full-length
10543029	-0,488662795	-6,097090524	-0,825587163	-3,532697959	-1,076411999	-3,117384936	6,217143022		100043821 ///	predicted gene, 100043821 ///	---	est
10543239	1,307003194	7,071950037	0,315425551	-4,008410902	1,056870174	4,245455478	6,238678328		Tcfec	transcription factor EC	DNA binding /// nucleus /// transcription ///	full-length
10543253	-0,957457964	1,351978779	-0,329854988	-4,62396308	-1,412002318	5,02157503	6,002353325		Wnt2	wingless-related MMTV integration	signal transducer activity /// receptor binding ///	full-length
10543859	1,06808906	3,594018587	0,093379958	-6,191578884	0,780765571	0,106582191	8,015701646		Akr1b3	aldo-keto reductase family 1,	aldehyde reductase activity /// cytoplasm ///	full-length
10544133	0,860848168	5,293252462	0,984498908	6,705128829	1,207183487	8,777079634	9,529086139		Parp12	poly (ADP-ribose) polymerase	nucleic acid binding /// NAD+ ADP-	full-length
10544273	1,467855131	-2,781289098	0,097065519	-6,364533782	2,251458378	0,256643696	4,744979894		Clec5a	C-type lectin domain family 5,	binding /// sugar binding /// immune response ///	full-length
10544326	-5,217479134	0,318080899	-3,889176018	-1,374968279	-5,415118037	0,293705121	5,941530118		2210010C04Rik	RIKEN cDNA 2210010C04 gene	---	full-length
10544333	-4,878951629	0,972249168	-3,47444622	-1,202145618	-4,722345848	0,300049573	6,493015577		1810049H19Rik	RIKEN cDNA 1810049H19 gene	---	full-length
10544342	-1,38815449	-1,72743561	-0,728523783	-4,411818003	-1,35057967	-2,234486931	4,815866665		Prss1 ///	protease, serine, 1 (trypsin 1) ///	molecular_function /// cellular_component ///	full-length
10544588	1,731553396	4,693833281	0,230709479	-5,837980586	1,850440197	5,008816977	5,495834857		Gimap3	GTPase, IMAP family member 3	nucleotide binding /// GTP binding ///	full-length
10544596	0,968846906	8,1034998	0,089860184	-5,90203911	1,195967696	10,17072248	11,70921069		Tmem176b	transmembrane protein 176B	nucleus /// membrane /// integral to membrane ///	full-length
10544687	-0,604483826	-5,406329366	-0,538575583	-4,903868304	-1,593278246	0,242569203	5,002401673	Cluster X	Cycs	cytochrome c, somatic	iron ion binding /// soluble fraction ///	full-length
10544891	1,025416337	4,637222806	0,009665117	-6,388927238	1,22465331	6,209636014	6,968012409	Cluster IV	Nod1	nucleotide-binding oligomerization	nucleotide binding /// protein binding /// ATP	full-length
10544932	-0,653466925	-5,158829795	-0,071934036	-6,362366881	-1,170351566	-2,308200474	12,68889334		Inmt	indolethylamine N-	cytoplasm /// methyltransferase activity ///	full-length
10545009	-0,617852807	0,277821372	-0,171312774	-5,420694359	-1,038331881	5,201375074	6,597642054		Pigy	phosphatidylinositol glycan anchor	glycosylphosphatidylinositol-N-	full-length
10545135	0,84733356	0,736241415	0,02925264	-6,37386436	1,035456607	2,31267373	4,458958344	Cluster III	Il12rb2	interleukin 12 receptor, beta 2	receptor activity /// hematopoietin/interferon-class	full-length
10545173	3,947470398	7,801508509	-0,557541792	-5,358604934	3,720881824	6,681115109	6,432806415		Igk	immunoglobulin kappa chain	---	full-length
10545175	3,620822916	8,241599792	-0,308968869	-5,965273281	3,281235567	6,659968092	6,231359876		Igk	immunoglobulin kappa chain	---	full-length
10545177	4,879720774	10,83500356	0,119157671	-6,336102844	4,709271098	9,983840733	7,217148335		---	---	---	partial
10545180	1,074493296	-2,877055952	-0,297561424	-5,942624841	1,349984679	-1,550618893	4,450322808		---	---	---	partial
10545184	4,191205765	8,606774533	-0,123172733	-6,336381583	4,075828648	7,844903835	6,884540295		---	---	---	full-length
10545187	3,745234598	8,964745556	-0,002711172	-6,391755095	3,757547634	8,571050279	6,15812255		Gm1502	gene model 1502, (NCBI)	---	full-length
10545190	1,771286472	0,467813679	-0,442069489	-5,562220678	2,09947135	1,714082791	3,456652557		---	---	---	partial
10545194	3,867655173	10,72826563	0,095303268	-6,336092389	3,719663176	9,835291039	6,023863757		---	---	---	partial
10545196	4,160253065	10,36000369	-0,363278562	-5,763098015	3,976279146	9,391801095	7,375811418		Igk-C	immunoglobulin kappa chain,	---	full-length
10545198	4,551976092	10,88341315	-0,39911229	-5,702970414	4,540179008	10,42712775	7,399256472		EG667683	predicted gene, EG667683	---	full-length
10545202	2,20524159	2,627054912	-0,297440105	-6,001326385	2,270085476	2,525371094	4,78550929		---	---	---	partial
10545205	2,555751768	7,184218082	-0,299616722	-5,732270449	2,92231295	8,32118	5,109260646		---	---	---	partial
10545208	4,683603411	12,78002111	-0,269056119	-5,976175647	4,45067736	11,75915313	7,10385586		---	---	---	partial
10545210	1,712350878	2,991919333	0,151545569	-6,208487051	1,709491429	2,571970291	5,931006451		---	---	---	partial
10545212	1,863756755	4,62818496	-0,33032819	-5,452527459	1,982773015	4,892185849	4,683602111		---	---	---	partial
10545215	3,244106044	10,38276562	0,009459353	-6,391051874	3,194680603	9,771288313	4,792748626		Igk /// Igk-V28	immunoglobulin kappa chain	---	full-length

Affymetrix ID	BS/Non Inf.		LS/Non Inf.		ReINF/Non Inf.		Average	Cluster	Gene	Gene	Gene Ontology (GO)	Transcript
Transcript	logFC	B	logFC	B	logFC	B	expression	Number	Symbol	Title	Description	Classification
10545220	3,027746412	4,491449461	0,042847291	-6,385506023	3,204628174	4,697114334	5,141271856		Igk	immunoglobulin kappa chain	---	full-length
10545231	3,897572662	9,962044365	-0,247288641	-6,073699401	3,422563822	7,990392171	5,820163332		---	---	---	partial
10545233	1,092155898	-2,803208422	0,15332421	-6,270647235	1,619744565	-0,075596745	4,946801393		---	---	---	partial
10545235	1,939304416	3,215096736	0,407074977	-5,383556219	1,626172128	1,048579795	4,300834653		---	---	---	partial
10545237	2,288284333	1,719962738	0,053323282	-6,381761579	1,961022612	-0,099138606	3,962047183		---	---	---	partial
10545239	4,170547499	5,23678536	-0,281548291	-6,230142657	3,683430676	3,459091894	5,823827454		---	---	---	partial
10545242	1,509432217	-0,047831693	0,188549028	-6,196971991	1,434633628	-0,830530102	4,436658207		---	---	---	full-length
10545247	3,880419068	7,368772861	0,00822767	-6,391556488	3,840305739	6,81570426	6,248249711		---	---	---	partial
10545249	1,638620534	2,99591071	-0,031258189	-6,383152041	1,841074001	3,824357974	3,952005986		---	---	---	partial
10545436	-1,020814267	6,472473968	-0,308102506	-3,24258128	-1,141375519	7,33312383	7,592659834		Elmod3	ELMO/CED-12 domain containing	cytoskeleton /// phagocytosis	full-length
10545479	2,138600799	11,17809679	0,058970851	-6,316682596	2,272557253	11,48366456	8,999598868	Cluster VI	Tmsb10	thymosin, beta 10	actin binding /// actin monomer binding ///	full-length
10545588	1,801270758	8,571242381	0,111060397	-6,152802051	2,172406423	10,36842405	6,76182383		Hk2	hexokinase 2	nucleotide binding /// catalytic activity ///	full-length
10545623	0,865563697	-1,422367337	-0,131906242	-6,183498324	1,001157838	-0,565173289	6,128726582		Dok1	docking protein 1	MAPKKK cascade /// transmembrane receptor	full-length
10545742	-1,262267066	6,295356771	-0,151973174	-5,792769671	-1,47294725	7,652241658	5,716105068		Cd207	CD207 antigen	binding /// sugar binding /// integral to plasma	full-length
10545771	-1,015849432	1,948688093	-0,14610234	-6,003346222	-0,945650414	0,869556877	6,269596666		Cyp26b1	cytochrome P450, family 26,	cell fate determination /// iron ion binding /// male	full-length
10545874	-1,574658459	3,619608938	-0,142176525	-6,17746049	-2,143981708	6,639828486	7,877041429		Cml5	camello-like 5	gastrulation with mouth forming second ///	full-length
10545877	-1,086524626	1,891220449	0,185996876	-5,854124247	-0,70464353	-2,199757932	6,35389523		Cml4	camello-like 4	gastrulation with mouth forming second /// late	full-length
10545891	-0,978154133	-1,635021031	-0,023643906	-6,386752383	-1,843285697	3,939729123	8,452101051		Cml1	camello-like 1	gastrulation with mouth forming second ///	full-length
10546010	1,635190038	8,144417129	-0,068944804	-6,286765593	1,684284427	8,059143678	6,707468188		Arhgap25	Rho GTPase activating protein 25	molecular_function /// GTPase activator activity ///	full-length
10546163	1,288021587	2,258804717	-0,119583093	-6,216734934	1,043585432	-0,119013389	6,699560963	Cluster III	Mcm2	minichromosome maintenance	nucleotide binding /// DNA binding /// DNA	full-length
10546450	1,065107497	-0,771954957	0,085123692	-6,323751221	1,065189689	-1,10545746	6,447167751		Adamts9	a disintegrin-like and	endopeptidase activity /// proteinaceous	full-length
10546685	1,433205157	12,14808823	-0,150233284	-5,220133995	2,160202195	16,57691024	7,646366775		Eif4e3	eukaryotic translation initiation	RNA binding /// translation initiation factor activity	full-length
10547177	1,743317735	10,51655172	0,033728367	-6,358595718	1,53666394	8,585771749	7,000275126		Rassf4	Ras association (RalGDS/AF-6)	protein binding /// cell cycle /// signal transduction	full-length
10547641	1,178969056	6,847315807	-0,135551767	-5,790542253	1,353094389	8,021651358	5,643649959		Slc2a3	solute carrier family 2 (facilitated	transporter activity /// sugar:hydrogen symporter	full-length
10547657	1,158355624	1,025588383	0,089549919	-6,296772474	1,01208364	-0,553993921	7,087393376		C3ar1	complement component 3a	signal transducer activity /// receptor activity /// G-	full-length
10547664	2,488361682	-1,858207141	-0,1142466	-6,374674161	3,589701885	0,91120557	4,753343963	Cluster VI	Clec4e	C-type lectin domain family 4,	binding /// sugar binding /// immune response ///	full-length
10547769	1,113049516	6,395094568	-0,043980596	-6,323354762	1,196052103	6,792625377	8,685361709	Cluster I	Ptpn6	protein tyrosine phosphatase, non-	phosphotyrosine binding /// negative regulation of	full-length
10547943	1,454027551	2,297393466	-0,093718068	-6,306184191	0,919697143	-2,088356342	6,472423361	Cluster III	Ncapd2	non-SMC condensin I complex,	condensed chromosome /// condensed	full-length
10547976	0,993934567	3,160914864	0,201633614	-5,454445162	1,513566669	7,438343214	8,050597381	Cluster IV	Tapbpl	TAP binding protein-like	endoplasmic reticulum /// microsome /// plasma	full-length
10547985	1,016971327	2,270108072	-0,083415872	-6,254448167	0,933686289	1,041672949	4,92446595		Cd27	CD27 antigen	receptor activity /// transmembrane receptor	full-length
10548105	0,884921887	2,260098887	-0,091799574	-6,173910438	1,152650781	4,659582653	8,904855359		Ccnd2	cyclin D2	protein binding /// nucleus /// cell cycle /// cell	full-length
10548333	1,081289891	1,478771999	0,058296918	-6,340841512	1,324606035	3,145379991	4,718214576		Cd69	CD69 antigen	binding /// sugar binding /// external side of plasma	full-length
10548345	1,113955594	9,336334446	0,231152774	-3,836939526	0,88228811	6,177127447	4,607908797		Klrk1	killer cell lectin-like receptor	stimulatory C-type lectin receptor signaling	full-length
10548375	1,933835241	10,19085679	-0,287587648	-4,756791274	2,229314335	11,46596917	6,920833395	Cluster VI	Clec7a	C-type lectin domain family 7,	opsonin binding /// zymosan binding /// zymosan	full-length
10548385	0,329061223	-6,25747062	-0,015525362	-6,38939143	1,112665967	-0,519086245	3,836599121	Cluster IV	Olr1	oxidized low density lipoprotein	receptor activity /// low-density lipoprotein receptor	full-length
10548409	1,209790687	2,98417177	0,133889943	-6,10780664	0,922783042	-0,029248186	4,454207527		Klrc1	killer cell lectin-like receptor	receptor activity /// external side of plasma	full-length
10548552	1,704290842	5,400526595	0,254376487	-5,616474318	1,692015875	4,895178356	6,089857864		Klra2	killer cell lectin-like receptor,	receptor activity /// binding /// protein binding ///	full-length
10548563	0,203174376	-6,786084379	-0,023791213	-6,384932638	1,002515371	-0,568825628	10,90138827		Ptp4a1	protein tyrosine phosphatase 4a1	phosphoprotein phosphatase activity /// protein	full-length
10548892	2,376679407	13,06583452	-0,129994987	-5,995776758	2,571755739	13,60155074	8,391525411		Arhgdib	Rho, GDP dissociation inhibitor	Rho GDP-dissociation inhibitor activity /// GTPase	full-length
10548931	-0,928498126	1,814184681	0,130000611	-6,032653398	-1,102888231	3,179813467	5,992259881		Slc15a5	solute carrier family 15, member 5	transporter activity /// transport /// oligopeptide	full-length
10548978	-3,253879463	-2,716360147	-0,069520509	-6,388883525	-5,712868154	1,631655564	9,441043394		Slco1a1	solute carrier organic anion	transporter activity /// membrane fraction ///	full-length
10549079	-0,327349507	-2,842953112	-0,138947076	-5,372483723	-1,112731197	8,733601432	11,10601146		Gys2	glycogen synthase 2	catalytic activity /// glycogen (starch) synthase	full-length
10549842	-0,56813921	-4,512811354	-0,11814695	-6,248933813	-1,01888337	-1,093179714	5,358407993		Zfp667	zinc finger protein 667	nucleic acid binding /// DNA binding /// intracellular	full-length
10550102	1,272753686	2,731013103	-0,012670289	-6,389554025	0,938080243	-0,540920962	6,371335232	Cluster III	Lig1	ligase I, DNA, ATP-dependent	nucleotide binding /// DNA binding /// DNA ligase	full-length
10550332	1,456915823	10,57295684	-0,276091475	-3,78048223	1,600253118	11,27102857	6,554242928		Slc1a5	solute carrier family 1 (neutral	transport /// dicarboxylic acid transport /// neutral	full-length
10550509	1,40668621	4,023298817	0,034538332	-6,374443301	1,776642398	6,206743046	6,613428384	Cluster I	Pglyrp1	peptidoglycan recognition protein 1	cytokine activity /// protein binding /// extracellular	full-length
10550574	1,011821926	0,986606585	0,166845321	-5,973699243	0,648851727	-2,91261629	8,536770809		Dmpk	dystrophia myotonica-protein	nucleotide binding /// magnesium ion binding ///	full-length
10550877	1,154006695	6,61333711	-0,054370879	-6,290974995	1,314843607	7,697330521	6,257940699		Kcnn4	potassium intermediate/small	ion channel activity /// voltage-gated potassium	full-length
10550906	1,423959823	2,284566113	-0,16407417	-6,12276362	1,996032658	5,508024134	6,352374772		Plaur	plasminogen activator, urokinase	receptor activity /// extracellular region /// plasma	full-length
10551009	2,152247786	11,29932053	0,06618156	-6,296615201	2,327133813	11,81417332	8,970687919	Cluster VI	Tmsb10	thymosin, beta 10	actin binding /// actin monomer binding ///	full-length
10551185	1,525739803	9,086396447	-0,037132841	-6,350530888	1,521563027	8,621544912	7,811191209	Cluster I	Tgfb1	transforming growth factor, beta 1	skeletal development /// tolerance induction to self	full-length
10551197	1,995448437	-1,745835255	-0,000722319	-6,391789872	1,265578975	-4,70000345	6,721180265		Cyp2b10	cytochrome P450, family 2,	monooxygenase activity /// iron ion binding ///	full-length
10551218	5,094542089	9,700679465	0,004543228	-6,391729327	4,788458311	8,533791914	6,912699648		Cyp2b9	cytochrome P450, family 2,	monooxygenase activity /// iron ion binding ///	full-length
10551226	1,338785124	-1,004945906	-0,272812694	-5,984675181	2,229569033	3,468696504	11,50531954		Cyp2a4 ///	cytochrome P450, family 2,	monooxygenase activity /// iron ion binding ///	full-length
10551282	0,984463127	-0,341392145	-0,18194532	-5,999130654	1,560037462	3,783532525	11,23443618		LOC100047728	similar to Cytochrome P450 2A5	---	predicted
10551531	-3,482734292	1,798098074	-2,474934989	-0,597595526	-3,384344021	1,134666603	6,484586453		Sycn	syncollin	exocytosis /// membrane /// cytoplasmic vesicle	full-length
10551666	1,063651251	3,704322634	-0,091060417	-6,195746577	1,151246088	4,145266506	6,094338234	Cluster III	Map4k1	mitogen-activated protein kinase	nucleotide binding /// protein kinase activity ///	full-length
10551836	-1,079398091	1,737468547	-0,136579557	-6,101425793	-1,374376285	3,839536377	6,174343215		Cox7a1	cytochrome c oxidase, subunit VIIa	cytochrome-c oxidase activity /// mitochondrion ///	full-length
10551883	2,082306122	11,63513967	0,096046518	-6,167482684	1,867245844	9,908789997	8,116751475		Tyrobp	TYRO protein tyrosine kinase	protein binding /// membrane /// integral to	full-length
10552406	3,605802648	16,36720527	-0,028292351	-6,376967424	3,835114939	16,72594633	7,137538368		Nkg7	natural killer cell group 7 sequence	membrane /// integral to membrane	full-length
10552546	-2,132805047	0,290142955	-1,223982521	-2,983733431	-2,867613478	2,797506766	5,835915508		Klk1b5 /// Klk1	kallikrein 1-related peptidase b5 ///	serine-type endopeptidase activity /// proteolysis ///	full-length
10552587	-0,693389413	-1,609011899	-0,363548055	-4,36158272	-1,005078555	1,273315084	5,152680447		Klk1b21 ///	kallikrein 1-related peptidase b21	serine-type endopeptidase activity /// extracellular	full-length
10552613	-1,075721965	-4,656093775	-0,090825569	-6,369504832	-2,766459413	1,896174721	6,697389197		Klk1b4	kallikrein 1-related pepidase b4	serine-type endopeptidase activity /// receptor	full-length
10552672	-0,569360621	-0,202201149	-0,027033339	-6,364260018	-1,063185731	5,782636617	9,587106689	Cluster X	0610012D14Rik	RIKEN cDNA 0610012D14 gene	catalytic activity /// binding /// NADP catabolic	full-length
10552697	1,147404179	4,083421498	-0,066036355	-6,295995792	1,508764369	6,735004348	6,218809944		Napsa	napsin A aspartic peptidase	aspartic-type endopeptidase activity /// proteolysis	full-length
10553274	4,231593123	13,79603473	1,644106897	3,267471496	4,826383706	14,95683786	10,89707688	Cluster VIII	Saa2	serum amyloid A 2	lipid transporter activity /// protein binding ///	full-length
10553324	1,44739001	10,40683442	0,214947019	-4,707807574	1,344638146	9,100266006	7,837450989		Tmem86a	transmembrane protein 86A	membrane /// integral to membrane	full-length
10553521	-0,651089912	-2,780971932	0,071244537	-6,317421422	-1,12518984	1,380540731	8,112004398		Gas2	growth arrest specific 2	cytoplasm /// cytoskeleton /// apoptosis /// cell	full-length
10554269	0,989542952	2,409342316	-0,182421479	-5,708627637	1,440710909	6,078915615	9,287571596		Abhd2	abhydrolase domain containing 2	carboxylesterase activity /// response to wounding	full-length
10554445	2,126659625	1,305808035	-0,183271077	-6,266894329	1,48416195	-2,100941116	5,587346463		Prc1	protein regulator of cytokinesis 1	cytokinesis /// nucleus /// cytoplasm /// spindle ///	full-length
10554574	1,473720448	6,217605425	0,152003768	-5,952613654	1,42197675	5,383846925	8,031510374		Tm6sf1	transmembrane 6 superfamily	membrane /// integral to membrane	full-length
10554667	1,995925785	9,722000893	-0,094785121	-6,218695357	1,700754938	7,400410652	5,529158116		Tmc3	transmembrane channel-like gene	membrane /// integral to membrane	full-length

Affymetrix ID	BS/Non Inf.		LS/Non Inf.		ReINF/Non Inf.		Average	Cluster	Gene	Gene	Gene Ontology (GO)	Transcript
Transcript	logFC	B	logFC	B	logFC	B	expression	Number	Symbol	Title	Description	Classification
10554752	-1,521891648	13,59095004	-0,111325866	-5,639038417	-1,565327165	13,52693787	8,212983056	Cluster IX	Nox4	NADPH oxidase 4	cell morphogenesis /// iron ion binding ///	full-length
10554789	1,477290767	7,004389845	0,097815822	-6,180534884	1,531562769	6,990565117	11,65407239		Ctsc	cathepsin C	cysteine-type endopeptidase activity /// lysosome	full-length
10554938	-1,427258619	7,568391889	-0,717048873	0,851460429	-0,73273188	0,109889385	7,236328263		Rab30	RAB30, member RAS oncogene	nucleotide binding /// GTP binding /// plasma	full-length
10555297	1,020711768	-0,690698792	-0,012246979	-6,390219234	0,41184225	-5,818791331	5,231612306		Kcne3	potassium voltage-gated channel,	ion channel activity /// voltage-gated ion channel	full-length
10555389	1,422158403	8,165149409	-0,144747098	-5,800543804	1,251518363	6,247067877	9,020985141		Ucp2	uncoupling protein 2	transporter activity /// binding /// mitochondrion ///	full-length
10555695	1,185301859	-0,195874552	-0,151502415	-6,194600494	0,66700294	-4,377226874	7,942038136		Rrm1	ribonucleotide reductase M1	nucleotide binding /// catalytic activity ///	full-length
10556076	-0,082431454	-7,128672087	0,006296502	-6,390919007	-1,216702095	4,271852027	7,480336181		Olfml1	olfactomedin-like 1	---	full-length
10556113	1,870826501	1,923754905	0,024549358	-6,388475562	2,156432708	2,979553764	10,31657437		Rbm3	RNA binding motif protein 3	nucleotide binding /// nucleic acid binding /// RNA	full-length
10556266	0,976488054	-0,831164458	-0,207286714	-5,932782303	1,233556491	0,890500461	6,618218245		Wee1	WEE 1 homolog (S. pombe)	nucleotide binding /// magnesium ion binding ///	full-length
10556297	1,422324293	0,480335542	0,027788845	-6,38635303	1,756048809	2,136278228	6,971825707		Adm	adrenomedullin	hormone activity /// extracellular region /// heart	full-length
10556463	-0,533290905	-4,460906832	0,061729221	-6,34617116	-1,002127656	-0,610427559	7,729134391		Arntl	aryl hydrocarbon receptor nuclear	protein import into nucleus, translocation /// two-	full-length
10556491	1,367068804	4,757496088	-0,110235936	-6,181007357	1,294420151	3,743401298	6,035223049		Far1	fatty acyl CoA reductase 1	catalytic activity /// binding /// peroxisome /// lipid	full-length
10556718	-0,94454829	5,222880281	-0,18888513	-5,098173173	-1,060518968	6,106292125	4,198809029	Cluster X	Acsm2	acyl-CoA synthetase medium-	nucleotide binding /// magnesium ion binding ///	full-length
10557156	1,596533156	4,900610636	-0,231587245	-5,71687089	1,23407194	1,772270399	6,111169413		Plk1	polo-like kinase 1 (Drosophila)	nucleotide binding /// protein kinase activity ///	full-length
10557177	1,456905662	3,603600124	0,229483816	-5,762277206	1,194176888	1,181546842	6,865538424		Prkcb	protein kinase C, beta	nucleotide binding /// protein kinase activity ///	full-length
10557300	-0,451514055	-6,883706377	0,200074203	-6,313992841	-1,698664839	-3,369918685	10,16455178		Aqp8	aquaporin 8	transporter activity /// integral to plasma	full-length
10557342	1,709032774	6,46979585	-0,066305321	-6,324941081	2,084829622	8,354575214	5,500078996		Il21r	interleukin 21 receptor	receptor activity /// transmembrane receptor	full-length
10557591	2,264311061	6,947032734	0,20401139	-6,0096209	2,373930848	7,063120002	8,022686726	Cluster VI	Itgal	integrin alpha L	magnesium ion binding /// immunological synapse	full-length
10557862	2,902894071	8,77960763	-0,017250545	-6,389448449	3,707068077	11,2660564	6,611231517	Cluster VI	Itgam	integrin alpha M	opsonin binding /// opsonin binding /// receptor	full-length
10557895	1,988131165	5,96098942	-0,228548999	-5,873503408	1,755887389	4,15183735	5,605603664	Cluster I	Itgax	integrin alpha X	magnesium ion binding /// receptor activity ///	full-length
10558159	-1,734631321	-0,308581976	-0,918384221	-3,698450692	-1,584966198	-1,391899799	7,52125894		Dmbt1	deleted in malignant brain tumors	blastocyst development /// inner cell mass cell	full-length
10558769	1,102944728	7,420735129	0,293431153	-3,455853204	1,534709747	10,90592798	9,193924249		Ifitm1	interferon induced transmembrane	somitogenesis /// anterior/posterior pattern	full-length
10558961	0,649858755	-2,72707557	-0,136054216	-6,119287897	1,253185665	2,562208838	9,546806135		Tspan4	tetraspanin 4	protein binding /// membrane /// integral to	full-length
10559207	2,629630822	12,50528627	-0,302338275	-4,929534021	2,443469467	11,21230507	7,780481748		Lsp1	lymphocyte specific 1	actin binding /// signal transducer activity ///	full-length
10559446	1,519439627	6,594175256	-0,349609597	-4,34155494	1,842959652	8,414895062	7,118440949	Cluster I	Lilrb3	leukocyte immunoglobulin-like	B cell homeostasis /// receptor activity /// cytokine	full-length
10559454	1,954483762	9,770911013	-0,047270742	-6,346073036	1,885174336	8,910691498	7,616675208		Pira6 /// Pira11 ///	paired-Ig-like receptor A6 ///	receptor activity	full-length
10559467	2,26042485	10,20783018	0,018338144	-6,386237448	2,405262108	10,5224867	7,167265355		Lilrb3 /// Pira11 ///	leukocyte immunoglobulin-like	B cell homeostasis /// receptor activity /// cytokine	full-length
10559478	0,962402552	-2,541971057	0,082366752	-6,342825483	1,038680081	-2,303792674	4,641826028		Pira11 /// Pira3 ///	paired-Ig-like receptor A11 ///	receptor activity	full-length
10559486	2,074623104	10,24418575	0,157433037	-5,920343057	2,298638164	11,04398681	6,891761136		Lair1	leukocyte-associated Ig-like	receptor activity /// plasma membrane ///	full-length
10560131	-1,210852231	-2,234522053	-0,00930185	-6,391358341	-2,007000473	1,756988801	11,11210444		2810007J24Rik	RIKEN cDNA 2810007J24 gene	transferase activity	full-length
10560242	1,553544974	2,05719126	-0,24522134	-5,916881493	2,450593209	6,600151566	6,340460568		C5ar1	complement component 5a	signal transducer activity /// receptor activity /// G-	full-length
10561104	1,090845657	2,145105046	0,065273864	-6,320118777	1,159256242	2,366831714	7,993092339		Axl	AXL receptor tyrosine kinase	nucleotide binding /// protein kinase activity ///	full-length
10561212	-1,359348463	2,282731428	-0,121882688	-6,227609699	-1,756596636	4,59635977	6,869244968	Cluster IX	Ltbp4	latent transforming growth factor	binding /// calcium ion binding /// protein binding ///	full-length
10562096	-0,676901261	-0,031191382	-0,074230389	-6,240564116	-1,112077297	4,564742589	8,790791689		Tmem147	transmembrane protein 147	membrane /// integral to membrane	full-length
10562169	0,752259566	-2,266763285	0,052136435	-6,356989548	1,427399868	3,094905248	12,07359576		Hamp	hepcidin antimicrobial peptide	hormone activity /// extracellular region /// cellular	full-length
10562192	2,431143474	14,04423238	-0,072748699	-6,249054763	2,378242355	13,3892215	8,511915673		Fxyd5	FXYD domain-containing ion	ion channel activity /// transport /// ion transport ///	full-length
10562563	0,910785281	4,067807565	0,021390963	-6,375785285	1,009882233	4,782340146	6,152697254	Cluster III	Ccne1	cyclin E1	cyclin-dependent protein kinase holoenzyme	full-length
10562637	2,746447753	7,836127016	-0,063204719	-6,36193252	2,419523639	5,93823877	6,150578498		Ccnb1	cyclin B1	in utero embryonic development /// protein binding	full-length
10562720	2,046875368	9,740517083	0,46950103	-3,22013828	2,30809334	10,74657569	8,050192967		Siglece	sialic acid binding Ig-like lectin E	receptor activity /// receptor signaling protein	full-length
10563178	1,173121541	8,287286764	-0,060305149	-6,232503048	1,16029006	7,724832677	6,558505195	Cluster I	Cd37	CD37 antigen	positive regulation of immunoglobulin production	full-length
10563441	1,772961735	8,852920249	0,010213921	-6,389561909	2,183331887	10,90463498	7,849129923		Emp3	epithelial membrane protein 3	membrane /// integral to membrane /// cell growth	full-length
10563597	4,007478807	11,80545596	0,847655806	-2,73308582	5,205372499	14,50838653	9,567851952	Cluster VIII	Saa3	serum amyloid A 3	lipid transporter activity /// extracellular region ///	full-length
10563602	0,383073325	-3,86605996	0,196204279	-5,343552436	1,255272175	6,284731258	11,45169954		Saa4	serum amyloid A 4	lipid transporter activity /// extracellular region ///	full-length
10563611	3,799359435	8,139212188	1,884045371	1,156400555	4,635045588	10,06601669	9,443243247	Cluster VIII	Saa1 /// Saa2	serum amyloid A 1 /// serum	lipid transporter activity /// protein binding ///	full-length
10563766	1,188174559	1,214464212	0,378376891	-4,891419197	0,946957862	-1,15373998	5,648022165		EG639116	predicted gene, EG639116	---	predicted
10564631	1,064097142	2,206766916	0,109202709	-6,180683712	1,647755488	6,557961765	7,442117782		Slco3a1	solute carrier organic anion	transporter activity /// integral to plasma	full-length
10565018	2,042997062	13,48671116	0,023514217	-6,372399432	2,191080163	13,9193052	8,155987333		Iqgap1	IQ motif containing GTPase	GTPase activator activity /// Ras GTPase activator	full-length
10565598	-0,488662795	-6,097090524	-0,825587163	-3,532697959	-1,076411999	-3,117384936	6,217143022		100043821 ///	predicted gene, 100043821 ///	---	est
10565609	0,666624543	-4,701266542	0,401022074	-5,367815831	-1,401322398	-0,106790866	9,432551632		Thrsp	thyroid hormone responsive	nucleus	full-length
10565727	0,096649126	-7,263946294	0,135581025	-6,360989645	2,287224356	-1,877639108	8,210278955		Tsku	tsukushin	protein binding /// extracellular region	full-length
10565815	-0,79017821	2,605171744	-0,043826816	-6,324367663	-1,012834563	4,856357004	7,460872958		---	---	---	partial
10565910	-1,058232268	0,78108637	-0,09980445	-6,257923222	-0,587393088	-3,898346854	7,035716077		Plekhb1	pleckstrin homology domain	Golgi membrane /// photoreceptor outer segment	full-length
10565958	1,181014202	7,953311355	-0,049832356	-6,289956736	1,568587761	10,89447534	6,13666484		P2ry6	pyrimidinergic receptor P2Y, G-	signal transducer activity /// receptor activity /// G-	full-length
10565994	1,703157686	-2,276138611	0,777455738	-5,035495268	1,343662017	-4,000121975	6,265680221		Art2b	ADP-ribosyltransferase 2b	NAD(P)+-protein-arginine ADP-ribosyltransferase	full-length
10566050	2,039599425	16,2300615	0,507635237	1,139335763	2,098140795	16,20395601	8,29913843		Il18bp	interleukin 18 binding protein	extracellular region	full-length
10566205	-1,02628318	-3,33211446	-1,022875925	-2,585612338	-1,537553549	-0,718804323	9,290583912		Dub2a	deubiquitinating enzyme 2a	ubiquitin thiolesterase activity /// ubiquitin-specific	full-length
10566326	1,27047279	4,335815651	1,525684589	6,338196343	1,445346288	5,344975495	8,234077767		Trim12	tripartite motif-containing 12	protein binding /// intracellular /// cytoplasm /// zinc	full-length
10566333	0,925378923	5,322879603	1,047902123	6,634719537	1,124458778	7,122328659	7,643176504		9230105E10Rik	RIKEN cDNA 9230105E10 gene	/// zinc ion binding /// metal ion binding /// protein	full-length
10566346	1,164459081	-0,086963458	1,260653278	1,183493086	1,341955519	0,845040549	6,354233761		9230105E10Rik	RIKEN cDNA 9230105E10 gene	zinc ion binding /// metal ion binding	full-length
10566358	1,672719508	9,953264368	1,573616131	8,675752337	1,956450413	11,40013736	8,880907825		Trim30	tripartite motif-containing 30	DNA binding /// protein binding /// intracellular ///	full-length
10566366	0,862117914	-1,086470961	1,848450782	6,510871502	1,499344747	3,826346219	6,954639752		AI451617	expressed sequence AI451617	zinc ion binding /// metal ion binding	full-length
10566571	2,015762239	8,177826088	1,177736938	2,653028045	2,394134934	9,78497485	7,150740907		---	---	---	partial
10566574	2,573775802	14,78012787	1,58528115	8,527865073	3,002805171	16,20088858	8,837129981		Gvin1	GTPase, very large interferon	nucleotide binding /// GTP binding /// nucleus ///	full-length
10566578	2,320623234	11,95029597	1,411432527	6,091811646	2,689087005	13,29741414	7,907652068		---	---	---	partial
10566583	1,962889178	10,10431478	0,544400366	-1,971505706	2,239474659	11,25430137	6,811766162		EG668139	predicted gene, EG668139	---	est
10566585	2,216831725	12,61924638	1,19873079	5,493181613	2,700311575	14,55843689	6,465554543		---	---	---	partial
10566934	0,927594691	-0,464337125	-0,167316469	-6,027507661	1,0269406	0,075466825	8,595759076		Lyve1	lymphatic vessel endothelial	receptor activity /// transmembrane receptor	full-length
10567355	0,723097802	-1,958132564	0,21275853	-5,740641734	1,191278829	2,079137564	5,31099488		Gprc5b	G protein-coupled receptor, family	signal transducer activity /// receptor activity /// G-	full-length
10567366	-2,756771512	-1,481551733	-1,645878884	-3,795966311	-2,761773629	-1,783168099	4,698983407		Gp2	glycoprotein 2 (zymogen granule	extracellular region /// plasma membrane ///	full-length
10567394	-1,466515558	5,457974812	-0,143275415	-6,044682836	-1,969461384	8,438314365	6,107730106		---	---	---	partial
10567580	2,334282223	11,10716057	0,189490087	-5,775230493	2,268863418	10,34270665	8,155888604		Igsf6	immunoglobulin superfamily,	membrane /// integral to membrane	full-length
10567825	1,697079536	12,12660444	-0,082721721	-6,120708313	2,029589093	13,84965263	6,37311917	Cluster VI	Lat	linker for activation of T cells	immunological synapse /// receptor signaling	full-length

Affymetrix ID	BS/Non Inf.		LS/Non Inf.		ReINF/Non Inf.		Average	Cluster	Gene	Gene	Gene Ontology (GO)	Transcript
Transcript	logFC	B	logFC	B	logFC	B	expression	Number	Symbol	Title	Description	Classification
10568024	2,936625877	16,99416919	-0,081623491	-6,186863521	3,026322846	17,00194338	7,666034216	Cluster VI	Coro1a	coronin, actin binding protein 1A	immunological synapse /// actin binding ///	full-length
10568050	0,964348837	7,280129971	-0,093918315	-5,922078594	1,130249648	8,711626208	10,57895066		Aldoa	aldolase A, fructose-bisphosphate	catalytic activity /// fructose-bisphosphate aldolase	full-length
10568115	0,727738642	2,835747443	-0,143170365	-5,556668118	1,286146669	8,827448242	8,519490787		Mvp	major vault protein	cytoplasm /// ribonucleoprotein complex	full-length
10568150	1,31910702	3,477877554	0,323563955	-4,989977385	1,003227782	0,367157237	5,361638752		Kif22	kinesin family member 22	nucleotide binding /// chromatin /// DNA binding ///	full-length
10568165	-3,579254408	1,394986327	-2,71492353	-0,414696414	-3,468951207	0,719661611	5,119558762		1810010M01Rik	RIKEN cDNA 1810010M01 gene	sugar binding /// extracellular region	full-length
10568174	1,057084388	3,615748265	-0,139492564	-5,942634714	1,410682199	6,40422423	5,941662575	Cluster IV	Spn	sialophorin	response to protozoan /// negative regulation of	full-length
10568202	1,202205635	3,25106577	0,073495508	-6,299249768	1,26703111	3,398794236	6,39487364	Cluster III	set/01	septin 1	nucleotide binding /// protein binding /// GTP	full-length
10568355	0,81762988	1,04699209	-0,088090936	-6,20768866	1,248278417	5,053513414	5,689599012		Pycard	PYD and CARD domain containing	cysteine-type endopeptidase activity /// protein	full-length
10568502	-1,377804224	-1,367528615	-0,907143772	-3,280314894	-1,323270595	-1,989328488	4,58460422		Cuzd1	CUB and zona pellucida-like	protein binding /// cell cycle /// cell adhesion ///	full-length
10568534	-0,488662795	-6,097090524	-0,825587163	-3,532697959	-1,076411999	-3,117384936	6,217143022		100043821 ///	predicted gene, 100043821 ///	---	est
10568714	2,305490808	6,229562359	0,103140737	-6,306677397	1,917213703	3,75452049	6,288998887		Mki67	antigen identified by monoclonal	chromosome, centromeric region /// condensed	full-length
10568731	-1,157134337	-2,549366519	-1,79257992	1,564200412	-0,389999925	-6,644170383	4,061080795		---	---	---	---
10569020	2,295357295	7,338453665	0,199108027	-6,01271929	2,225064418	6,546045977	6,391430144		Ifitm6	interferon induced transmembrane	integral to membrane	full-length
10569102	1,630031385	8,700835618	1,618719345	8,188775075	2,121904933	11,41614346	9,761425048	Cluster VI	Irf7	interferon regulatory factor 7	DNA binding /// transcription factor activity ///	full-length
10569168	-0,27608831	-6,649786554	0,097613414	-6,31164991	-1,134287641	-1,038163273	9,713838521		Slc25a22	solute carrier family 25	transporter activity /// binding /// mitochondrion ///	full-length
10569504	1,320110788	5,201303899	-0,058829001	-6,321300138	1,190022039	3,644137964	5,49246579		Tnfrsf23	tumor necrosis factor receptor	receptor activity /// protein binding /// plasma	full-length
10569646	1,315356324	-1,72792574	0,03072577	-6,387199047	0,778407193	-4,978915833	8,65021619	Cluster III	Ccnd1	cyclin D1	cyclin-dependent protein kinase holoenzyme	full-length
10569656	0,948502913	4,987700059	0,107697182	-5,963490092	1,017441076	5,348458066	6,858076398		Tpcn2	two pore segment channel 2	ion channel activity /// voltage-gated ion channel	full-length
10569707	1,097125844	7,604693653	-0,172097962	-5,177398293	1,041336698	6,566480025	8,098896359		Myadm	myeloid-associated differentiation	membrane /// integral to membrane	full-length
10569823	-0,500664845	-5,333765492	0,143744417	-6,212716093	-1,310729239	0,379730915	6,002014582		C330021F23Rik	RIKEN cDNA C330021F23 gene	---	full-length
10569877	1,363851524	-1,534171492	-0,134805541	-6,30583988	1,877324041	0,871720013	5,427011323		1810033B17Rik	RIKEN cDNA 1810033B17 gene	---	full-length
10569890	1,229114054	9,690567487	0,421153749	-0,757421906	1,393553842	10,76156788	8,186660791		Aida	axin interactor, dorsalization	protein binding /// multicellular organismal	full-length
10570201	1,415147689	4,184122329	0,202489355	-5,81103585	2,159936578	8,591274577	7,103869424		Atp11a	ATPase, class VI, type 11A	nucleotide binding /// magnesium ion binding ///	full-length
10570434	1,288892481	8,700405724	0,010303883	-6,387608637	1,701830707	11,58616462	8,009019487		Ifitm1	interferon induced transmembrane	somitogenesis /// anterior/posterior pattern	full-length
10570516	1,055426457	2,531663204	-0,034572065	-6,368529115	1,393865867	5,1101362	5,345884845		Kbtbd11	kelch repeat and BTB (POZ)	protein binding	full-length
10570741	0,82074073	-4,755559576	-0,279885532	-6,053187767	1,197062342	-2,999170265	5,698761457	Cluster IV	Defb1	defensin beta 1	extracellular region /// defense response ///	full-length
10571353	-0,786875151	-1,800032056	-0,046168078	-6,36342326	-1,108540972	0,760941782	6,44495606		6430573F11Rik	RIKEN cDNA 6430573F11 gene	metabolic process /// methyltransferase activity ///	full-length
10571467	-0,851288191	-2,934068636	-0,107692629	-6,297124774	-1,0050332	-2,085521085	5,135357867		Pdgfrl	platelet-derived growth factor	extracellular region	full-length
10571560	-0,820605476	-0,861132884	-0,20605097	-5,762673116	-1,045951751	0,940980823	4,766269446		Mtnr1a	melatonin receptor 1A	signal transducer activity /// receptor activity /// G-	full-length
10571653	1,484903434	11,12355499	-0,067440408	-6,191838441	1,647874316	11,94917416	11,25135463		Actg1	actin, gamma, cytoplasmic 1	nucleotide binding /// structural constituent of	full-length
10571657	-0,898437649	3,774642629	-0,217125767	-4,957173292	-1,572468215	9,770228294	12,26350583		Acsl1	acyl-CoA synthetase long-chain	magnesium ion binding /// catalytic activity /// long-	full-length
10571870	2,1660213	10,56469354	-0,000878644	-6,391776221	1,944828899	8,852722552	7,816133841		Hmgb2	high mobility group box 2	DNA binding /// nucleus /// chromosome	full-length
10571891	-1,011472727	2,048971034	-0,136889676	-6,039866342	-1,16043877	3,061795481	9,276019657		Aadat	aminoadipate aminotransferase	catalytic activity /// mitochondrion /// transaminase	full-length
10571984	1,206350869	6,613270595	2,061132524	11,42846226	1,216813538	6,281791409	6,93792394		Ddx60	DEAD (Asp-Glu-Ala-Asp) box	---	full-length
10572130	1,272495458	7,969791284	-0,315345704	-3,56679605	1,562378322	9,969947953	8,882638026	Cluster I	Lpl	lipoprotein lipase	catalytic activity /// lipoprotein lipase activity ///	full-length
10572445	1,927095013	13,75689922	0,083724618	-6,108390781	1,840766804	12,81223116	6,176396948		Lrrc25	leucine rich repeat containing 25	molecular_function /// protein binding ///	full-length
10572747	1,361457919	6,914622087	-0,018454617	-6,382935596	1,35718919	6,44694994	9,158382093		Tpm4	tropomyosin 4	podosome /// actin binding /// cytoplasm ///	full-length
10572897	3,036385549	10,56187205	0,181931781	-6,077909688	3,771312644	12,73340048	9,916885271		Hmox1	heme oxygenase (decyclizing) 1	heme oxygenase (decyclizing) activity /// iron ion	full-length
10572906	1,40915828	1,353655958	0,094768544	-6,314687073	1,305920204	0,266896996	6,735054999	Cluster III	Mcm5	minichromosome maintenance	nucleotide binding /// DNA binding /// ATP binding	full-length
10573261	2,023993028	6,493652228	0,049562639	-6,364965465	1,782584126	4,63361828	6,487735301		Asf1b	ASF1 anti-silencing function 1	chromatin /// nucleus /// chromatin assembly or	full-length
10573747	1,072119104	3,038392793	0,118845734	-6,104001343	1,011865488	2,044673282	6,637704975		Adcy7	adenylate cyclase 7	magnesium ion binding /// adenylate cyclase	full-length
10573865	0,598241802	-6,186061261	0,814571297	-4,537040434	1,471048151	-2,678610145	11,35434024		LOC433762	hypothetical gene LOC433762	---	full-length
10573939	1,669668792	7,661391044	0,20954169	-5,581158576	1,486922888	5,891162953	6,762544118		Lpcat2	lysophosphatidylcholine	calcium ion binding /// endoplasmic reticulum ///	full-length
10574023	3,230663828	5,277827034	1,56538796	-1,002613442	4,399314522	8,412765748	11,06260202		Mt2	metallothionein 2	cellular zinc ion homeostasis /// nitric oxide	full-length
10574027	2,177833598	1,877305594	0,937955367	-3,574091649	3,273161254	5,83903369	11,47718211		Mt1	metallothionein 1	copper ion binding /// lysosome /// cytosol ///	full-length
10574098	1,405643455	5,120012094	1,027576558	2,266919856	1,598108131	6,144212318	7,536384407		---	---	---	predicted
10574102	1,131814074	4,396099723	0,976087739	3,191274672	1,399812503	6,359044025	8,077742135		---	---	---	predicted
10574104	1,623911316	7,431082697	1,206804933	4,326201891	1,825704851	8,372477306	7,179411789		Nlrc5	NLR family, CARD domain	---	partial
10574133	0,808193905	-0,12334535	0,631819291	-1,387184456	1,090495398	2,356378041	6,643898551		---	---	---	predicted
10574135	1,597083603	4,158338918	1,190551163	1,658516751	1,922102983	5,797794345	6,264940751		---	---	---	predicted
10574137	1,353420921	5,541135783	0,998203614	2,693046624	1,513226287	6,383392515	7,34922217		---	---	---	predicted
10574139	1,326458199	4,961181163	0,830920005	0,786073881	1,356789862	4,789746181	6,678549157		---	---	---	predicted
10574141	1,218715219	5,653507891	0,766855346	1,353592975	1,182768309	4,892365848	7,082576626		---	---	---	predicted
10574143	1,156878964	1,694146524	0,552884607	-3,163188726	1,206426522	1,721163796	5,737667443		---	---	---	predicted
10574145	1,695629671	4,603911797	1,033255947	0,290666544	1,796824611	4,82386263	6,577996629		---	---	---	---
10574149	1,953811894	7,796369561	1,474959854	4,781401289	2,166848881	8,581612859	8,43450932		---	---	---	predicted
10574151	1,145269654	1,79117031	0,770040946	-1,009889521	1,386446307	3,3564062	7,164818717		---	---	---	---
10574157	1,518835677	6,859488335	1,199876876	4,440605206	1,740651185	8,017124287	7,861920593		---	---	---	---
10574159	1,394070924	5,488908497	1,165908873	3,833393085	1,771116714	7,816273045	7,806328846		---	---	---	predicted
10574161	0,825130519	3,172802917	0,623777015	0,979911837	1,034954352	5,223927408	7,872669586		---	---	---	predicted
10574163	1,219108958	4,78896865	0,755728311	0,568989492	1,385664549	5,801148202	6,334122499		---	---	---	partial
10574350	-0,806377793	1,175036659	-0,064162026	-6,288003502	-1,305911366	5,871005272	7,111573176		Mmp15	matrix metallopeptidase 15	metalloendopeptidase activity /// calcium ion	full-length
10574432	-0,488662795	-6,097090524	-0,825587163	-3,532697959	-1,076411999	-3,117384936	6,217143022		100043821 ///	predicted gene, 100043821 ///	---	predicted
10574434	-0,488662795	-6,097090524	-0,825587163	-3,532697959	-1,076411999	-3,117384936	6,217143022		100043821 ///	predicted gene, 100043821 ///	---	est
10574471	1,112040662	4,882303381	-0,03435892	-6,359697017	0,975437572	3,049439322	8,386159746		Cmtm3	CKLF-like MARVEL	cytokine activity /// extracellular space ///	full-length
10574488	-0,861275668	-0,109750158	-0,191176235	-5,803602389	-1,276013733	3,347399122	6,663429754		4833426J09Rik	RIKEN cDNA 4833426J09 gene	magnesium ion binding /// phosphoprotein	full-length
10574498	-0,7737782	-1,941909866	-0,36267449	-4,846787778	-1,65748767	4,898805968	10,97506209		Ces6	carboxylesterase 6	---	full-length
10574511	-0,917963404	-1,253970713	-0,336821874	-5,223667478	-1,237247507	1,011362901	4,828648789		BC015286	cDNA sequence BC015286	---	partial
10574524	-1,172249139	0,312160015	-0,444225429	-4,671334223	-1,742967382	3,892166062	8,040426254		Ces2	carboxylesterase 2	---	full-length
10574532	-0,950006372	-1,189546979	-0,208400083	-5,942559926	-1,425663356	2,14745542	10,55367563		Ces2	carboxylesterase 2	---	full-length
10574545	-0,90557559	2,127845151	-0,009239098	-6,389703303	-1,575531229	7,824288339	10,93279401		Ces5	carboxylesterase 5	---	full-length
10574607	-1,158294348	2,20157457	0,018261248	-6,386733625	-1,57375082	5,064847167	11,99954944		EG13909	predicted gene, EG13909	carboxylesterase activity /// endoplasmic reticulum	full-length

Affymetrix ID	BS/Non Inf.		LS/Non Inf.		ReINF/Non Inf.		Average	Cluster	Gene	Gene	Gene Ontology (GO)	Transcript
Transcript	logFC	B	logFC	B	logFC	B	expression	Number	Symbol	Title	Description	Classification
10574617	-1,834191613	5,237764299	-0,355856574	-5,16438228	-2,135989514	6,54126211	6,242408521		BC026374	cDNA sequence BC026374	carboxylesterase activity /// extracellular region ///	full-length
10574976	1,000579753	3,35146952	0,020942815	-6,380665243	0,691225186	-0,587720547	7,407612094		Pla2g15	phospholipase A2, group XV	phosphatidylcholine-sterol O-acyltransferase	full-length
10574985	0,895817867	2,791983347	0,253398291	-4,783041984	1,344614463	6,858705973	5,175531643		Slc7a6	solute carrier family 7 (cationic	plasma membrane /// transport /// amino acid	full-length
10575052	-0,680392424	-3,791011825	-0,044788904	-6,372486717	-1,393293487	1,394009511	8,404381915		Cdh1	cadherin 1	trophectodermal cell differentiation /// calcium ion	full-length
10575153	-0,748635678	1,407162055	-0,113659168	-6,0039872	-1,120603407	5,25221234	11,05118996	Cluster X	Cyb5b	cytochrome b5 type B	iron ion binding /// mitochondrion /// mitochondrial	full-length
10575249	-0,827200011	1,126185817	-0,150209376	-5,873764582	-1,193859429	4,521324665	6,607033861		Txnl4b	thioredoxin-like 4B	nucleus /// spliceosome /// mRNA processing ///	full-length
10575685	-1,529206522	-1,807930684	-0,145557737	-6,3175522	-3,476618305	5,77224222	10,69239738		Nudt7	nudix (nucleoside diphosphate	magnesium ion binding /// acetyl-CoA hydrolase	full-length
10575799	1,477968765	3,270583137	-0,026214354	-6,383920973	1,618546016	3,8299015	6,765863962	Cluster I	Plcg2	phospholipase C, gamma 2	phosphoinositide	full-length
10575833	-0,585077318	-0,048675578	-0,0271899	-6,364478337	-1,210969997	7,169440538	10,94267882	Cluster X	Hsd17b2	hydroxysteroid (17-beta)	catalytic activity /// estradiol 17-beta-	full-length
10576034	2,145282996	12,66443503	0,037610855	-6,352698196	2,494087842	14,05168067	7,82006381	Cluster VI	Irf8	interferon regulatory factor 8	DNA binding /// transcription factor activity ///	full-length
10576332	0,29651147	-5,708458601	-0,26411089	-5,148870551	1,15831078	3,137749244	4,689227248		Tubb3	tubulin, beta 3	nucleotide binding /// GTPase activity /// structural	full-length
10576774	-2,026572183	-0,612608243	0,058255737	-6,382605896	-2,254701884	-0,036315876	10,23722857		Clec4g	C-type lectin domain family 4,	binding /// sugar binding /// membrane /// integral	full-length
10576883	1,445690953	0,899673806	-0,369975509	-5,443662341	1,127321275	-1,587692279	4,813250483		Shcbp1	Shc SH2-domain binding protein 1	protein binding /// SH2 domain binding	full-length
10577190	1,375382906	2,66326166	-0,144045693	-6,151902225	1,190870074	0,850201802	7,359067777		Rasa3	RAS p21 protein activator 3	GTPase activator activity /// intracellular ///	full-length
10577315	1,341175455	5,591540818	0,187664054	-5,6831357	2,414387567	12,08294063	6,001770719	Cluster II	Angpt2	angiopoietin 2	angiogenesis /// receptor binding /// vascular	full-length
10577641	-0,87177066	-3,072014003	0,146976607	-6,231639326	-1,178893724	-1,211726616	8,670180353		1810011O10Rik	RIKEN cDNA 1810011O10 gene	apoptosis	full-length
10577792	1,654872847	11,60916901	0,204477768	-4,938230095	1,758395223	11,91699234	7,15828819		Plekha2	pleckstrin homology domain-	phosphatidylinositol binding /// nucleus ///	full-length
10578222	-0,470616275	-5,382448721	-0,293487924	-5,609147228	-1,222282078	0,174799384	7,796455455		Dlc1	deleted in liver cancer 1	neural tube closure /// heart morphogenesis ///	full-length
10578264	1,640294037	11,3524916	0,130249039	-5,776948067	1,892815275	12,64741578	8,633579254	Cluster I	Msr1	macrophage scavenger receptor 1	receptor activity /// scavenger receptor activity ///	full-length
10578352	1,066303587	4,224903579	0,107239801	-6,096187866	1,378102438	6,685645578	12,39986284		Fgl1	fibrinogen-like protein 1	receptor binding /// extracellular region /// signal	full-length
10578539	1,230504724	2,700802037	-0,042114779	-6,365553167	1,126221196	1,418055363	8,035927094		Slc25a4	solute carrier family 25	transporter activity /// binding /// mitochondrion ///	full-length
10578690	1,055850881	-0,218172613	0,128460762	-6,213770044	0,612179691	-4,244010128	4,799082738		Neil3	nei like 3 (E. coli)	DNA binding /// damaged DNA binding /// DNA-	full-length
10579199	-0,750218242	-2,578682891	-0,033584736	-6,378501512	-1,160097033	0,610910369	7,968760882		Slc25a42	solute carrier family 25, member	binding /// mitochondrion /// mitochondrial inner	full-length
10579347	2,679637727	15,98076274	0,211547155	-5,122072756	2,639602338	15,44635457	10,04021138	Cluster VI	Ifi30	interferon gamma inducible protein	lysosome /// disulfide oxidoreductase activity ///	full-length
10579636	1,201350066	0,803016747	0,060442383	-6,353231916	1,147061348	0,015198705	5,402361328		Cyp4f18	cytochrome P450, family 4,	monooxygenase activity /// iron ion binding ///	full-length
10579649	-1,464044998	8,590614004	-0,223768842	-5,04255229	-1,74453969	10,24371234	5,408798782		Cib3	calcium and integrin binding family	molecular_function /// cellular_component ///	full-length
10579659	1,23702252	5,694064821	0,173979203	-5,663833666	0,986115368	2,80713826	9,376018221		Hmgn2	high mobility group nucleosomal	chromatin /// DNA binding /// nucleus /// cytoplasm	full-length
10579812	0,926110624	3,013489897	-0,104846457	-6,093290438	1,266082515	6,027715515	7,390672217		Ednra	endothelin receptor type A	patterning of blood vessels /// response to hypoxia	full-length
10580033	1,20634148	3,404173199	0,075020409	-6,29326352	1,075030286	1,81732981	8,99859634		Cd97	CD97 antigen	signal transducer activity /// receptor activity ///	full-length
10580457	0,733519296	0,218247683	0,228778529	-5,200343868	1,22761383	5,080994497	8,691842419		N4bp1	NEDD4 binding protein 1	nucleus	full-length
10580649	-1,539150481	5,885981728	-0,018761119	-6,385805794	-2,080518735	8,964902167	10,119366		Es22	esterase 22	carboxylesterase activity /// endoplasmic reticulum	full-length
10580663	-1,073190656	-1,144066149	-0,007423292	-6,391323154	-1,351097767	0,500043682	11,33425658		AU018778	expressed sequence AU018778	carboxylesterase activity /// hydrolase activity	full-length
10580875	-0,580841635	1,078252732	-0,277353799	-3,476290254	-1,076809651	7,314405415	8,091762939		Gtl3	gene trap locus 3	---	full-length
10581009	-0,488662795	-6,097090524	-0,825587163	-3,532697959	-1,076411999	-3,117384936	6,217143022		100043821 ///	predicted gene, 100043821 ///	---	est
10581355	-4,542293816	-0,495573668	-3,525998106	-1,723803267	-4,658286126	-0,624479278	6,929591845		Ctrl	chymotrypsin-like	protein binding /// proteolysis /// peptidase activity	full-length
10581378	1,493759605	11,3400529	0,232306775	-4,302426109	1,61370749	11,84456263	8,846517091		Psmb10	proteasome (prosome, macropain)	endopeptidase activity /// threonine-type	full-length
10581479	1,085082778	-1,390837056	0,206308541	-6,067875962	1,244635495	-0,601934228	5,694608326		Smpd3	sphingomyelin phosphodiesterase	Golgi cis cisterna /// magnesium ion binding ///	full-length
10581538	1,494678423	-2,871036386	-0,219909863	-6,261570901	2,299000145	0,157159792	7,064339982		Nqo1	NAD(P)H dehydrogenase, quinone	NAD(P)H dehydrogenase (quinone) activity ///	full-length
10581813	2,237409527	12,97783522	0,920882873	3,157367477	2,550343665	14,13122199	7,21010936		Mlkl	mixed lineage kinase domain-like	protein kinase activity /// ATP binding /// protein	full-length
10581882	-5,004382372	0,674203021	-3,970793859	-0,647615756	-5,612058432	1,389447816	7,502971004	Cluster IX	Ctrb1	chymotrypsinogen B1	serine-type endopeptidase activity /// extracellular	full-length
10582162	1,295477601	6,024127081	-0,20239225	-5,455354505	1,308548533	5,70982988	7,437038421		Cotl1	coactosin-like 1 (Dictyostelium)	actin binding /// protein binding ///	full-length
10582275	0,68315794	1,362832746	0,081367546	-6,152528269	1,085227754	5,873296254	6,896369202		Slc7a5	solute carrier family 7 (cationic	cytoplasm /// plasma membrane /// transport ///	full-length
10582303	2,285554665	17,11726658	-0,019714681	-6,371322717	2,271416644	16,71428779	8,843436086		Cyba	cytochrome b-245, alpha	iron ion binding /// cytoplasm /// mitochondrion ///	full-length
10582337	1,020307857	1,65438095	0,262316316	-5,286635379	1,004171351	1,117039186	6,36809758		Fam38a	family with sequence similarity 38,	---	partial
10582464	1,199615142	-3,390475435	1,755185887	-0,025388451	1,413787051	-2,619564211	5,005265228		---	---	---	est
10582626	-0,676574658	1,172751357	-0,228418314	-4,740456248	-1,002560291	4,867458052	7,493270746		Abcb10	ATP-binding cassette, sub-family B	nucleotide binding /// transporter activity /// ATP	full-length
10582862	1,222470381	2,24033804	-0,267919357	-5,474982597	1,655054482	5,067971887	6,311637224		Sp140	Sp140 nuclear body protein	zinc ion binding /// metal ion binding	full-length
10582868	0,804972257	5,516120857	0,181768883	-4,707994889	1,03585264	7,995200852	6,321503972		---	---	---	partial
10582874	1,356642952	7,36001555	0,234880094	-4,994067087	1,407440196	7,355674074	5,476680342		---	---	---	partial
10582983	-0,488662795	-6,097090524	-0,825587163	-3,532697959	-1,076411999	-3,117384936	6,217143022		LOC280487	pol polyprotein	---	partial
10582985	1,83640695	8,497859179	0,265975955	-5,185358347	1,99554366	9,049086232	6,589406381		Casp1	caspase 1	response to hypoxia /// cysteine-type	full-length
10582997	1,46415044	5,130505833	-0,011850775	-6,389482726	1,75225527	6,745887094	6,092347803		Casp4	caspase 4, apoptosis-related	cysteine-type endopeptidase activity /// protein	full-length
10583044	0,203809229	-6,754921395	0,002935269	-6,391680363	1,240774804	1,663332639	5,622822041		Mmp13	matrix metallopeptidase 13	metalloendopeptidase activity /// calcium ion	full-length
10583056	0,530989199	-2,407817915	0,145362625	-5,888961031	1,43600108	6,809808106	5,511252115		Mmp12	matrix metallopeptidase 12	metalloendopeptidase activity /// calcium ion	full-length
10583100	1,247746673	-5,001454639	0,05705446	-6,38625962	1,904813075	-3,096011019	4,376221325		Mmp8	matrix metallopeptidase 8	metalloendopeptidase activity /// calcium ion	full-length
10583112	1,258192923	-1,520867517	0,263929517	-6,012121355	0,890001159	-4,036879745	5,324367202		Mmp27	matrix metallopeptidase 27	---	partial
10583519	1,851682626	3,89999952	-0,098407512	-6,31272847	2,39341564	6,341427781	7,677904151	Cluster VI	Icam1	intercellular adhesion molecule 1	immunological synapse /// T cell antigen	full-length
10583669	2,151568257	12,70687032	0,128441279	-5,949412856	2,207489168	12,60412595	7,791693047		AB124611	cDNA sequence AB124611	membrane /// integral to membrane	full-length
10583870	1,330915761	-4,440336891	0,013796504	-6,391420524	2,681825352	0,037288177	6,258045271		Bmper	BMP-binding endothelial regulator	protein binding /// extracellular region /// negative	full-length
10584271	-0,589085755	-5,281902793	0,019358883	-6,38933924	-1,462556703	0,036875979	6,966441469		Tmem218	transmembrane protein 218	membrane /// integral to membrane	full-length
10584628	1,520712284	3,806357442	0,382696148	-4,841564515	1,61002456	4,008474308	6,698572593	Cluster I	Thy1	thymus cell antigen 1, theta	angiogenesis /// plasma membrane /// external	full-length
10584634	0,485342848	-6,746328365	0,092083336	-6,372297993	1,982067339	-1,768627673	7,158435914		Usp2	ubiquitin specific peptidase 2	ubiquitin thiolesterase activity /// cytoplasm ///	full-length
10584674	1,221922053	5,19540903	-0,153054869	-5,85535902	1,181556338	4,400808769	7,547774796		Mcam	melanoma cell adhesion molecule	protein binding /// plasma membrane /// cell	full-length
10584787	0,904677482	-5,817492058	0,166290952	-6,33813466	1,705408089	-3,356615122	5,59374359		Treh	trehalase (brush-border membrane	alpha,alpha-trehalase activity /// plasma	full-length
10584821	1,443063802	2,867208652	0,003480746	-6,391656128	1,590938443	3,488283413	5,454738536	Cluster I	Cd3d	CD3 antigen, delta polypeptide	receptor activity /// transmembrane receptor	full-length
10585276	1,46357122	6,525526381	0,003646418	-6,391511158	1,642884787	7,433198817	6,177629544		Pou2af1	POU domain, class 2, associating	DNA binding /// protein binding /// nucleus ///	full-length
10585331	-0,664898554	-1,739176038	-0,327581749	-4,622016821	-1,228916275	3,582868655	5,508108427		Exph5	exophilin 5	protein binding /// cellular_component ///	full-length
10585467	-0,631083144	-3,232791509	-0,230129491	-5,709152998	-1,649581456	4,978295451	8,586940969		C630028N24Rik	RIKEN cDNA C630028N24 gene	cytoplasm /// kinase activity /// transferase activity	full-length
10585555	1,065143891	3,719904493	-0,045379804	-6,342539867	0,974896806	2,385931335	5,726911091	Cluster III	Pstpip1	proline-serine-threonine	cytokinesis /// stress fiber /// actin binding ///	full-length
10585699	-0,015406095	-7,279563877	-0,286137044	-6,249445561	-1,760242463	-3,474400242	7,313333192		Fabp5	fatty acid binding protein 5,	transporter activity /// binding /// cytoplasm ///	full-length
10585932	2,11538302	11,25623822	0,171432219	-5,762362661	2,266552922	11,66160735	8,401558094		Pkm2	pyruvate kinase, muscle	magnesium ion binding /// catalytic activity ///	full-length
10585956	1,62005939	0,80805939	-0,247381889	-6,04466064	1,264457099	-1,655579774	5,997082669		---	---	---	partial

Affymetrix ID	BS/Non Inf.		LS/Non Inf.		ReINF/Non Inf.		Average	Cluster	Gene	Gene	Gene Ontology (GO)	Transcript
Transcript	logFC	B	logFC	B	logFC	B	expression	Number	Symbol	Title	Description	Classification
10585970	1,6398608	3,084281195	0,325493824	-5,503952756	1,555845978	2,141892749	7,198381975		---	---	---	partial
10585972	1,408902632	-0,075941997	0,000699054	-6,391787869	1,388663586	-0,550693098	5,683544686		---	---	---	partial
10585974	1,768309339	2,407438962	0,491673121	-4,931884511	1,874293025	2,605759066	5,514269818		---	---	---	partial
10585976	1,476646777	0,589578284	0,082792926	-6,346075173	1,334115339	-0,6645658	5,982576166		---	---	---	partial
10585978	1,15660176	-1,162714526	0,252165925	-5,944981638	0,974799579	-2,726063407	5,441697123		---	---	---	partial
10585980	1,178632391	0,391971766	-0,105991278	-6,279718113	1,036783586	-1,065134839	4,939331813		---	---	---	partial
10585982	1,767472613	1,817051336	0,461710107	-5,219018557	1,743954683	1,300412082	6,724500364		---	---	---	partial
10585986	1,663494069	2,93374179	0,172558536	-6,144004239	1,436132852	1,070486461	6,695883966		---	---	---	partial
10585988	1,460649028	2,597696769	0,049954082	-6,366110446	1,315756934	1,166878296	6,476252894		---	---	---	partial
10585990	1,328506137	1,457195247	-0,06986571	-6,343518407	1,136434334	-0,350058304	6,739393638		---	---	---	---
10585992	1,550959979	1,826181674	0,038216283	-6,380335099	1,499847097	1,115253644	6,257063528		Myo9a	myosin IXa	nucleotide binding /// motor activity /// actin binding	partial
10586448	3,20401101	6,613024551	0,59256279	-4,990493443	2,903237993	5,065572295	6,232502426		2810417H13Rik	RIKEN cDNA 2810417H13 gene	nucleus /// mitochondrion	full-length
10586744	1,816520889	10,68801248	-0,042204085	-6,342583063	1,757269528	9,864861444	7,855565497		Anxa2	annexin A2	angiogenesis /// stress fiber /// phospholipase	full-length
10586863	-0,488662795	-6,097090524	-0,825587163	-3,532697959	-1,076411999	-3,117384936	6,217143022		LOC280487	pol polyprotein	---	partial
10587077	-1,857341369	4,227483312	-0,628483225	-3,647475521	-2,345978358	6,423511955	6,717095775	Cluster IX	Onecut1	one cut domain, family member 1	liver development /// regulation of cell-matrix	full-length
10587082	-2,086301328	-0,444605055	-1,265734776	-3,127503402	-1,552078566	-2,97658102	7,460401236	Cluster IX	Onecut1	one cut domain, family member 1	liver development /// regulation of cell-matrix	full-length
10587107	0,958353112	2,636334161	0,06733435	-6,283286413	1,313783841	5,645483336	5,094367196		Myo5a	myosin Va	microfilament motor activity /// nucleotide binding	full-length
10587284	-0,193755905	-7,110517737	0,075143704	-6,366629432	-1,747058466	-0,082110897	11,81302491	Cluster X	Elovl5	ELOVL family member 5,	endoplasmic reticulum /// fatty acid biosynthetic	full-length
10587323	0,560706733	-2,168773762	-0,199769468	-5,507404468	1,160016816	4,170450425	10,55981074		Gsta1 /// Gsta2	///glutathione S-transferase, alpha 1	glutathione transferase activity /// glutathione	full-length
10587331	0,564292247	-2,094186866	-0,183814667	-5,629660793	1,151686627	4,1353949	10,50164458		Gsta1 /// Gsta2	///glutathione S-transferase, alpha 1	glutathione transferase activity /// glutathione	full-length
10587339	0,470591597	-3,784622356	-0,181016217	-5,761893042	1,087496305	2,620335511	10,23057276		Gsta1 /// Gsta2	///glutathione S-transferase, alpha 1	glutathione transferase activity /// glutathione	full-length
10587683	2,113804778	11,96069987	0,202084703	-5,431345705	2,579828647	13,92517008	5,847751887	Cluster VI	Bcl2a1a ///	B-cell leukemia/lymphoma 2	B cell homeostasis /// protein binding /// cytoplasm	full-length
10587690	1,693747441	10,56698699	0,093438521	-6,124508871	2,224635615	13,40609814	5,860841243		Bcl2a1a ///	B-cell leukemia/lymphoma 2	B cell homeostasis /// protein binding /// cytoplasm	full-length
10587792	0,587952065	-0,730558264	-0,132895302	-5,861615827	1,01181343	4,182024136	9,303039621	Cluster IV	Plscr1	phospholipid scramblase 1	calcium ion binding /// response to virus ///	full-length
10587871	-0,601586956	-4,197567195	-0,032147527	-6,38090548	-1,236609233	0,68311506	10,27198573		Paqr9	progestin and adipoQ receptor	receptor activity /// membrane /// integral to	full-length
10588479	0,872329847	2,464739828	0,266863299	-4,645705145	1,011245986	3,608013346	5,845226262	Cluster II	Tlr9	toll-like receptor 9	receptor activity /// transmembrane receptor	full-length
10588577	-1,104097352	-0,897488473	-0,960635901	-1,275700278	-0,312196457	-6,583992686	7,097158297		Cish	cytokine inducible SH2-containing	regulation of cell growth /// protein binding ///	full-length
10588691	-0,60355476	-2,673100803	0,210482693	-5,651064739	-1,006267549	1,19076628	8,536694605		Hyal1	hyaluronoglucosaminidase 1	catalytic activity /// hyaluronoglucosaminidase	full-length
10588883	-0,717394298	3,834761337	-0,120684815	-5,648804359	-1,189243277	9,189144141	9,623753513	Cluster X	Amt	aminomethyltransferase	aminomethyltransferase activity /// cytoplasm ///	full-length
10589350	1,011792171	9,355506537	0,621217154	4,063258276	1,088344429	9,793164094	9,250151899		Shisa5	shisa homolog 5 (Xenopus laevis)	nucleus /// nuclear envelope /// endoplasmic	full-length
10589511	-0,355154471	-3,882172103	0,045332332	-6,321899272	-1,019988257	4,760066063	9,265309811	Cluster X	Scap	SREBF chaperone	protein binding /// protein binding /// endoplasmic	full-length
10589535	1,096511574	6,964250895	0,126979899	-5,770363446	0,559308871	-0,405660184	4,385120426		Ngp	neutrophilic granule protein	molecular_function /// extracellular region ///	full-length
10589884	1,504106887	1,715153024	0,187280086	-6,111669164	1,505568063	1,339914705	4,892258091		Bcl2a1c	B-cell leukemia/lymphoma 2	apoptosis	full-length
10589974	-0,488662795	-6,097090524	-0,825587163	-3,532697959	-1,076411999	-3,117384936	6,217143022		100043821 ///	predicted gene, 100043821 ///	---	est
10590365	-1,112052635	6,956953342	-0,292259408	-3,693227733	-1,610874853	10,90884318	7,11945231		Vipr1	vasoactive intestinal peptide	signal transducer activity /// receptor activity /// G-	full-length
10590381	-0,815495504	2,730762244	-0,196894068	-5,194362567	-1,050333028	5,045949646	6,805033857		Vipr1	vasoactive intestinal peptide	signal transducer activity /// receptor activity /// G-	full-length
10590438	-1,309109412	0,459072038	-0,181870862	-6,123635421	-2,091103501	4,856158601	6,056554873		C730027P07Rik	RIKEN cDNA C730027P07 gene	extracellular region	full-length
10590494	1,460783429	3,428239502	0,056091493	-6,353879394	0,98866721	-0,700054324	5,024740685		Kif15	kinesin family member 15	nucleotide binding /// motor activity /// microtubule	full-length
10590631	2,555080759	10,22388559	-0,227377469	-5,754057726	2,350490552	8,800780332	5,939069689	Cluster VI	Ccr2	chemokine (C-C motif) receptor 2	signal transducer activity /// receptor activity /// G-	full-length
10590635	1,9159098	10,11404502	-0,278271725	-4,841580237	1,941415595	9,842923739	7,409304466		Ccr5	chemokine (C-C motif) receptor 5	signal transducer activity /// receptor activity /// G-	full-length
10590844	-0,904960351	3,772062842	-0,238041793	-4,724810176	-1,038283567	4,857407495	9,378083354		9030420J04Rik	RIKEN cDNA 9030420J04 gene	---	full-length
10590860	-0,864870202	2,443384819	-0,060733054	-6,28737327	-1,005998032	3,621912266	8,465370604		9030420J04Rik	RIKEN cDNA 9030420J04 gene	---	full-length
10591773	1,239993481	6,103303693	0,158689824	-5,740079088	1,002234508	3,331654332	9,406909534		Hmgn2	high mobility group nucleosomal	chromatin /// DNA binding /// nucleus /// cytoplasm	full-length
10591781	1,866435709	2,332913984	0,054320821	-6,374120949	0,771347804	-4,573352898	5,06924241	Cluster III	Anln	anillin, actin binding protein	cytokinesis /// actin binding /// nucleus ///	full-length
10592067	1,144100049	0,986816435	-0,084938827	-6,304820975	0,706985295	-3,148222273	7,472838342		Fli1	Friend leukemia integration 1	DNA binding /// transcription factor activity ///	full-length
10592201	0,949853886	-0,309837415	-0,129334847	-6,174142216	1,168349401	1,223832557	5,093078598		Chek1	checkpoint kinase 1 homolog (S.	DNA damage checkpoint /// DNA damage	full-length
10592515	1,07161533	2,833704008	-0,275143323	-5,028764409	1,189275012	3,524586088	6,086010422		Ubash3b	ubiquitin associated and SH3	nucleus /// cytoplasm	full-length
10592535	1,017370632	5,635823152	0,011872693	-6,386541775	1,321741263	8,233092608	6,17404018		Sorl1	sortilin-related receptor, LDLR	receptor activity /// lipid transporter activity /// lipid	full-length
10592734	1,153962071	3,426954201	0,317298224	-4,689205932	1,297221529	4,275219372	7,170514512		Cbl	Casitas B-lineage lymphoma	signal transducer activity /// calcium ion binding ///	full-length
10593015	3,014608224	15,62493976	0,257166531	-5,011064887	3,054704404	15,41322081	6,740589291		Cd3g	CD3 antigen, gamma polypeptide	receptor activity /// transmembrane receptor	full-length
10593024	1,662642464	10,40307918	0,337998876	-3,531891228	1,631219098	9,747135514	6,406061801	Cluster I	Cd3e	CD3 antigen, epsilon polypeptide	immunological synapse /// positive regulation of T	full-length
10593050	1,560310176	9,482709168	-0,019791665	-6,379780658	1,470962961	8,35189499	6,431904833		Il10ra	interleukin 10 receptor, alpha	receptor activity /// membrane /// integral to	full-length
10593123	1,11296738	-0,125857871	-0,046221357	-6,370347832	0,931744765	-1,902624577	7,076061326		Tagln	transgelin	cytoplasm /// cytoskeleton organization and	full-length
10593198	-1,00211678	0,276048855	-0,178470018	-5,973424221	-1,102954644	0,794434027	7,819183718		Fam55b	family with sequence similarity 55,	---	full-length
10593219	0,666527554	-5,629420569	0,023533454	-6,389515081	1,319612949	-2,609377186	9,593443895		Nnmt	nicotinamide N-methyltransferase	cytoplasm /// nicotinamide N-methyltransferase	full-length
10593332	-0,63607921	-0,513362526	-0,008947177	-6,389538422	-1,510326579	8,152316221	8,24546996	Cluster X	Bco2	beta-carotene oxygenase 2	iron ion binding /// intracellular /// carotene	full-length
10593776	1,333150064	-4,680644435	0,09516658	-6,376032097	2,872558823	0,156877688	6,80627797		Nrg4	neuregulin 4	extracellular region /// plasma membrane ///	full-length
10594251	2,073804861	3,679913011	0,291994411	-5,876923031	1,550656314	0,385059722	5,952961445		Kif23	kinesin family member 23	nucleotide binding /// ATP binding	full-length
10594426	1,125948016	2,021160026	0,065956951	-6,324752013	0,96114853	0,136310047	4,701121671	Cluster III	Zwilch	Zwilch, kinetochore associated,	kinetochore /// molecular_function /// cell cycle ///	full-length
10594540	1,524446666	10,5511892	-0,15063484	-5,572880243	1,771546028	11,92552771	7,107017195		Plekho2	pleckstrin homology domain	---	full-length
10594645	1,582848021	9,279665923	0,008206193	-6,389850625	1,602785643	8,996489915	8,323701767		Rab8b	RAB8B, member RAS oncogene	nucleotide binding /// protein binding /// GTP	full-length
10594774	1,466087193	5,663956329	-0,078514389	-6,281595826	0,734888916	-1,485122457	6,203055383	Cluster III	Ccnb2	cyclin B2	in utero embryonic development /// membrane	full-length
10594798	1,352648817	-0,825177368	1,4836631	0,564021425	0,707374995	-5,017369709	4,265582919		---	---	---	est
10595148	0,448038371	-4,191597849	-0,225160449	-5,491783568	1,122470639	2,646722838	10,34448914		Gsta1 /// Gsta2	///glutathione S-transferase, alpha 1	glutathione transferase activity /// glutathione	full-length
10595480	-0,732382103	-3,155815129	-0,0428403	-6,372819131	-1,343804567	1,390286124	11,19179137	Cluster X	Me1	malic enzyme 1, NADP(+)-	catalytic activity /// malic enzyme activity /// malate	full-length
10595633	1,826881323	10,77219643	0,154169072	-5,762541958	2,348422238	13,35501925	6,628729039		Bcl2a1a ///	B-cell leukemia/lymphoma 2	B cell homeostasis /// protein binding /// cytoplasm	full-length
10597239	-0,5838209	-5,213036196	-0,067480123	-6,360318669	-1,101684094	-2,040243395	7,108688951		Pth1r	parathyroid hormone 1 receptor	skeletal development /// ossification ///	full-length
10597258	-0,238565645	-5,260245793	0,06337906	-6,231524825	-1,120080883	6,769709548	7,348380142		Tmie	transmembrane inner ear	sensory perception of sound /// membrane ///	full-length
10597279	0,875481751	-1,930433223	0,180340355	-6,062010866	1,035350108	-0,940104584	6,636806527		Ccrl2	chemokine (C-C motif) receptor-	signal transducer activity /// receptor activity /// G-	full-length
10597461	1,273547417	9,427617421	0,103761688	-5,918210871	1,365242481	9,825119252	6,417640539		Cmtm7	CKLF-like MARVEL	cytokine activity /// extracellular space ///	full-length
10597592	-1,794214656	-3,534871712	-0,082467267	-6,381470342	-3,036118043	0,037979568	10,22115761		Acaa1b	acetyl-Coenzyme A	---	full-length
10597648	0,562269729	-1,734812423	0,098631588	-6,138261639	1,009189258	3,276376293	8,832675135	Cluster IV	Myd88	myeloid differentiation primary	response to molecule of fungal origin /// MyD88-	full-length

Affymetrix ID	BS/Non Inf.		LS/Non Inf.		RelNF/Non Inf.		Average	Cluster	Gene	Gene	Gene Ontology (GO)	Transcript
Transcript	logFC	B	logFC	B	logFC	B	expression	Number	Symbol	Title	Description	Classification
10597743	1,146003705	-0,230650522	-0,136783048	-6,220858457	0,869636254	-2,683689674	6,298475147		Cx3cr1	chemokine (C-X3-C) receptor 1	signal transducer activity /// receptor activity /// G-	full-length
10598004	1,140055244	-1,658488077	0,337932586	-5,67929761	1,47575061	0,154090193	3,605482505	Cluster IV	Ccr1	chemokine (C-C motif) receptor 1	signal transducer activity /// receptor activity /// G-	full-length
10598013	1,9159098	10,11404502	-0,278271725	-4,841580237	1,941415595	9,842923739	7,409304466		Ccr5	chemokine (C-C motif) receptor 5	signal transducer activity /// receptor activity /// G-	full-length
10598057	-1,599678722	3,16099454	-0,27873557	-5,687349679	-1,077285705	-0,952417706	6,584171712		---	---	---	full-length
10598175	1,84724539	6,089206942	-0,009494922	-6,39068755	1,639207706	4,326945456	6,166346746		Ear2 /// Ear1 ///	eosinophil-associated,	nucleic acid binding /// nuclease activity ///	full-length
10598612	-0,755430343	1,492499399	-0,113009677	-6,008477602	-1,194278095	5,970543829	10,93510976	Cluster X	Otc	ornithine transcarbamylase	urea cycle /// ornithine carbamoyltransferase	full-length
10598863	-0,620642586	-5,107383221	0,003554391	-6,391708884	-1,010671297	-2,86101392	11,80786913		Rgn	regucalcin	calcium ion binding /// nucleus /// cytoplasm ///	full-length
10599120	1,941700448	10,24234074	0,15949635	-5,842908838	2,058497896	10,51298076	6,429167252		Dock11	dedicator of cytokinesis 11	guanyl-nucleotide exchange factor activity /// Rho	full-length
10599487	1,140980011	7,301257995	0,042383631	-6,321039046	0,986487009	5,206794859	6,140603316		Sash3	SAM and SH3 domain containing 3	positive regulation of immunoglobulin production	full-length
10600122	-1,433929497	1,63614647	-0,442214999	-4,86095387	-0,825105621	-3,173530517	4,639575726		Xlr3b /// Xlr3a ///	X-linked lymphocyte-regulated 3B	---	full-length
10600836	2,136234111	12,59448237	0,138642485	-5,881471936	2,332296741	13,23373327	9,421055792		Msn	moesin	uropod /// binding /// cytoplasm /// cytoskeleton ///	full-length
10600852	1,442165658	5,794775752	0,395830323	-3,939065263	1,539670331	6,110978795	5,544133758		---	---	---	full-length
10601011	1,346304961	3,363619533	-0,196105956	-5,872700832	0,923780892	-0,635525602	4,186452861		Kif4	kinesin family member 4	nucleotide binding /// DNA binding /// motor activity	full-length
10601303	-0,442696009	-5,05645191	-0,319724382	-5,17330785	-1,130519668	0,869003	4,980927194		Chic1	cysteine-rich hydrophobic domain	molecular_function /// cellular_component ///	full-length
10601312	-0,407471925	-6,206780863	0,154067342	-6,23139807	-1,469494271	0,280799559	6,190381414		ENSMUSG00000	predicted gene,	---	est
10601385	2,694283129	11,03530586	0,071150649	-6,324494055	2,806677966	11,10123819	7,145522504		Tlr13	toll-like receptor 13	receptor activity /// transmembrane receptor	full-length
10601421	1,799506357	5,993778379	0,018485336	-6,387458198	1,849144787	5,874800985	5,263667464		A630033H20Rik	RIKEN cDNA A630033H20 gene	signal transducer activity /// receptor activity /// G-	full-length
10601581	0,802288959	3,558902322	1,051126547	6,486161121	1,096507068	6,61792581	7,464083813		EG245575	predicted gene, EG245575	---	est
10601705	1,086159009	2,742681497	0,205352506	-5,629835031	0,719584968	-1,407555969	4,282998783		Cenpi	centromere protein I	chromosome, centromeric region /// nucleus ///	full-length
10601878	-0,709635844	-2,549617074	-0,353856984	-4,911205941	-1,076736512	0,475026556	4,664689074		Tceal1	transcription elongation factor A	translation elongation factor activity /// protein	full-length
10602372	-1,90465327	3,104168308	-0,055860154	-6,370963753	-2,861078779	7,215786728	9,087483377		Alas2	aminolevulinic acid synthase 2,	catalytic activity /// 5-aminolevulinate synthase	full-length
10602739	1,268880384	8,739230733	-0,00244091	-6,391547131	1,340352794	8,955886174	7,546610259		Acot9	acyl-CoA thioesterase 9	carboxylesterase activity /// mitochondrion ///	full-length
10602840	1,415497323	8,07369547	-0,296345381	-4,223525112	1,48752649	8,224603928	6,538639347		Sh3kbp1	SH3-domain kinase binding protein	protein binding /// cytoplasm /// cytoskeleton ///	full-length
10603023	1,057906314	1,700075709	0,061298604	-6,330275379	1,227667931	2,814427958	6,284787024		---	---	---	est
10603051	2,10574055	7,274987604	0,150832869	-6,133690305	2,003895529	6,270591571	5,839276754		Ap1s2	adaptor-related protein complex 1,	protein binding /// Golgi apparatus /// coated pit ///	full-length
10603182	-0,626070906	-2,979360399	-0,189427885	-5,875210866	-1,005667151	0,398140376	5,556964725		Arhgap6	Rho GTPase activating protein 6	GTPase activator activity /// Rho GTPase activator	full-length
10603346	1,640935018	6,844658767	0,034848028	-6,370337649	1,662839771	6,566217795	7,047096878		Plp2	proteolipid protein 2	membrane /// integral to membrane	full-length
10603469	1,75129656	1,447138507	0,049058673	-6,378086038	2,027444229	2,522249632	10,09729143		Rbm3	RNA binding motif protein 3	nucleotide binding /// nucleic acid binding /// RNA	full-length
10603549	-0,488662795	-6,097090524	-0,825587163	-3,532697959	-1,076411999	-3,117384936	6,217143022		100043821 ///	predicted gene, 100043821 ///	---	est
10603551	2,348410859	15,4206588	0,313929435	-3,503557037	2,644555768	16,43050597	9,96949981		Cybb	cytochrome b-245, beta	ion channel activity /// voltage-gated ion channel	full-length
10603803	-0,488662795	-6,097090524	-0,825587163	-3,532697959	-1,076411999	-3,117384936	6,217143022		LOC280487	pol polyprotein	---	partial
10603860	1,572862994	9,656322094	0,201149425	-5,24243163	1,463783018	8,372273592	9,327615765	Cluster I	Cfp	complement factor properdin	extracellular region /// immune response ///	full-length
10604393	1,606692364	5,730692578	-0,152180488	-6,049258987	1,642357438	5,551785659	5,86890507		ENSMUSG00000	predicted gene,	---	full-length
10604713	1,241563186	3,506204625	-0,035081777	-6,370930816	1,050292755	1,398835748	5,87872755		Arhgef6	Rac/Cdc42 guanine nucleotide	molecular_function /// guanyl-nucleotide exchange	full-length
10604763	1,348731927	8,787998136	0,036211512	-6,34407391	1,307431851	7,988151547	9,612194625		Arpc1b	actin related protein 2/3 complex,	actin binding /// cytoplasm /// cytoskeleton ///	full-length
10604922	0,385023417	-3,821399984	-0,089895268	-6,155659675	1,005127728	3,83829998	9,092456637		BC023829	cDNA sequence BC023829	---	full-length
10604996	-1,590028689	1,215820492	-0,501952069	-4,914214493	-0,913800389	-3,443114576	4,93450208		Xlr3a /// Xlr3b ///	X-linked lymphocyte-regulated 3A	---	full-length
10605007	-1,351500699	0,938373702	-0,545731625	-4,234562836	-0,74137891	-3,871771558	4,788588524		Xlr3b /// Xlr3a ///	X-linked lymphocyte-regulated 3B	---	full-length
10605256	1,967516635	10,18583129	-0,298403805	-4,700466366	2,116546905	10,63107294	8,841183335		Flna	filamin, alpha	actin binding /// protein kinase C binding /// protein	full-length
10605338	2,151634022	11,68565898	-0,00315093	-6,391558935	2,091145993	10,92398439	8,250294662	Cluster I	G6pdx	glucose-6-phosphate	cytokine production /// angiotensin mediated	full-length
10605392	-0,9406814	-1,447558895	0,168971364	-6,105996026	-1,231568053	0,507698279	7,95645788	Cluster X	F8	coagulation factor VIII	copper ion binding /// calcium ion binding ///	full-length
10605465	0,766916155	1,073383087	-0,048400134	-6,327675598	1,092092932	4,312824434	7,419095524		Prkx	protein kinase, X-linked	nucleotide binding /// protein kinase activity ///	full-length
10605711	1,358617225	4,318155759	-0,221156598	-5,632267613	1,522300563	5,155943257	5,349618038		Pdk3	pyruvate dehydrogenase kinase,	two-component sensor activity /// protein histidine	full-length
10606016	3,007203022	15,68104904	-0,048056134	-6,337447836	3,151624743	15,86242894	8,451119842	Cluster VI	Il2rg	interleukin 2 receptor, gamma	receptor activity /// hematopoietin/interferon-class	full-length
10606058	1,829297628	10,41515309	0,00704491	-6,390494702	1,82537758	9,961725969	6,904253681		Cxcr3	chemokine (C-X-C motif) receptor	signal transducer activity /// receptor activity /// G-	full-length
10606389	1,29246205	-1,715605831	0,325276788	-5,877856046	1,070140116	-3,291557057	6,547321226		Gm379	gene model 379, (NCBI)	---	predicted
10606609	1,094145054	-2,640633085	-0,271722069	-6,001873049	0,542342422	-5,954910103	5,147382982		Tspan6	tetraspanin 6	membrane /// integral to membrane	full-length
10606694	1,353600518	7,960271777	-0,135923326	-5,834549067	1,406457587	7,976947413	5,619798995		Btk	Bruton agammaglobulinemia	nucleotide binding /// protein kinase activity ///	full-length
10606714	0,870023297	1,879252839	0,139390648	-5,919537435	1,04836931	3,401492535	7,600325744		Gla	galactosidase, alpha	catalytic activity /// hydrolase activity, hydrolyzing	full-length
10607429	-0,488662795	-6,097090524	-0,825587163	-3,532697959	-1,076411999	-3,117384936	6,217143022		LOC280487	pol polyprotein	---	partial
10607865	2,261002621	10,69651563	0,099544895	-6,216558988	2,110968857	9,449428899	10,05651212		Tmsb4x	thymosin, beta 4, X chromosome	actin binding /// protein binding /// nucleus ///	full-length
10607868	1,467902197	8,79670545	0,305383041	-4,012898471	1,142536438	5,459812405	5,577972487		Tlr8	toll-like receptor 8	receptor activity /// transmembrane receptor	full-length
10607870	1,249120355	5,951246017	0,265667492	-4,770377685	1,397622577	6,810227315	5,68741911	Cluster IV	Tlr7	toll-like receptor 7	single-stranded RNA binding /// receptor activity ///	full-length

Bibliography

1 Cox, F. E. History of human parasitology. *Clin Microbiol Rev* **15**, 595-612 (2002).

2 Nerlich, A. G., Schraut, B., Dittrich, S., Jelinek, T. & Zink, A. R. Plasmodium falciparum in ancient Egypt. *Emerg Infect Dis* **14**, 1317-1319 (2008).

3 Hawass, Z. *et al.* Ancestry and pathology in King Tutankhamun's family. *JAMA* **303**, 638-647, doi:303/7/638 (2010)

4 Pappas, G., Kiriaze, I. J. & Falagas, M. E. Insights into infectious disease in the era of Hippocrates. *Int J Infect Dis* **12**, 347-350, doi:S1201-9712(07)00212-3 (2008).

5 Cunha, C. B. & Cunha, B. A. Brief history of the clinical diagnosis of malaria: from Hippocrates to Osler. *J Vector Borne Dis* **45**, 194-199 (2008).

6 Gallup, J. L. & Sachs, J. D. The economic burden of malaria. *Am J Trop Med Hyg* **64**, 85-96 (2001).

7 English, M. & Newton, C. R. Malaria: pathogenicity and disease. *Chem Immunol* **80**, 50-69 (2002).

8 WHO. World Malaria Report 2009. *WHO press* (2009).

9 Sachs, J. D. Report of the Commission on Macroeconomics and Health. *Macroeconomics and health: investing in health for economic development.* **Geneva, World Health Organization** (2001).

10 Okamoto, N. The mother of all parasites. *Future Medicine* **3**, 5, doi:10.2217/17460913.3.4.391 (2008).

11 Cox-Singh, J. *et al.* Plasmodium knowlesi malaria in humans is widely distributed and potentially life threatening. *Clin Infect Dis* **46**, 165-171, doi:10.1086/524888 (2008).

12 Jongwutiwes, S., Putaporntip, C., Iwasaki, T., Sata, T. & Kanbara, H. Naturally acquired Plasmodium knowlesi malaria in human, Thailand. *Emerg Infect Dis* **10**, 2211-2213 (2004).

13 Ng, O. T. *et al.* Naturally acquired human Plasmodium knowlesi infection, Singapore. *Emerg Infect Dis* **14**, 814-816 (2008).

14 Prugnolle, F. *et al.* African great apes are natural hosts of multiple related malaria species, including Plasmodium falciparum. *Proc Natl Acad Sci U S A* **107**, 1458-1463, doi:0914440107 (2010)

15 Levine, D. *The protozoan phylum Apicomplexa*. Vol. 2 (1988).

16 Martinsen, E. S., Perkins, S. L. & Schall, J. J. A three-genome phylogeny of malaria parasites (Plasmodium and closely related genera): evolution of life-history traits and host switches. *Mol Phylogenet Evol* **47**, 261-273, doi:S1055-7903(07)00399-5 (2008).

17 Escalante, A. A., Freeland, D. E., Collins, W. E. & Lal, A. A. The evolution of primate malaria parasites based on the gene encoding cytochrome b from the linear mitochondrial genome. *Proc Natl Acad Sci U S A* **95**, 8124-8129 (1998).

18 Coatney, G. R. The simian malarias: zoonoses, anthroponoses, or both? *Am J Trop Med Hyg* **20**, 795-803 (1971).

19 Escalante, A. A. & Ayala, F. J. Phylogeny of the malarial genus Plasmodium, derived from rRNA gene sequences. *Proc Natl Acad Sci U S A* **91**, 11373-11377 (1994).

20 Rich, S. M. *et al.* The origin of malignant malaria. *Proc Natl Acad Sci U S A* **106**, 14902-14907, doi:0907740106 (2009).

21 Snewin, V. A., Longacre, S. & David, P. H. Plasmodium vivax: older and wiser? *Res Immunol* **142**, 631-636 (1991).

22 Marsh, K. *et al.* Indicators of life-threatening malaria in African children. *N Engl J Med* **332**, 1399-1404 (1995).

23 Allison, A. C. Protection afforded by sickle-cell trait against subtertian malareal infection. *Br Med J* **1**, 290-294 (1954).

24 Kwiatkowski, D. P. How malaria has affected the human genome and what human genetics can teach us about malaria. *Am J Hum Genet* **77**, 171-192, doi:S0002-9297(07)62909-7 (2005).

25 Bruce-Chuvatt, L. J. Alphonse Laveran's discovery 100 years ago and today's global fight against malaria. *J R Soc Med* **74**, 531-536 (1981).

26 Ross, R. The role of the mosquito in the evolution of the malarial parasite: the recent researches of Surgeon-Major Ronald Ross, I.M.S. 1898. *Yale J Biol Med* **75**, 103-105 (2002).

27 Shortt, H. E. & Garnham, P. C. Pre-erythrocytic stage in mammalian malaria parasites. *Nature* **161**, 126 (1948).

28 Amino, R. *et al.* Quantitative imaging of Plasmodium transmission from mosquito to mammal. *Nat Med* **12**, 220-224, doi:nm1350 (2006).

29 Amino, R. *et al.* Imaging malaria sporozoites in the dermis of the mammalian host. *Nat Protoc* **2**, 1705-1712, doi:nprot.2007.120 (2007).

30 Kebaier, C. & Vanderberg, J. P. Re-ingestion of Plasmodium berghei sporozoites after delivery into the host by mosquitoes. *Am J Trop Med Hyg* **75**, 1200-1204, doi:75/6/1200 [pii] (2006).

31 King, C. A. Cell motility of sporozoan protozoa. *Parasitol Today* **4**, 315-319, doi:0169-4758(88)90113-5 [pii] (1988).

32 Dobrowolski, J. M. & Sibley, L. D. Toxoplasma invasion of mammalian cells is powered by the actin cytoskeleton of the parasite. *Cell* **84**, 933-939, doi:S0092-8674(00)81071-5 [pii] (1996).

33 Meissner, M., Schluter, D. & Soldati, D. Role of Toxoplasma gondii myosin A in powering parasite gliding and host cell invasion. *Science* **298**, 837-840, doi:10.1126/science.1074553 (2002).

34 Wetzel, D. M., Hakansson, S., Hu, K., Roos, D. & Sibley, L. D. Actin filament polymerization regulates gliding motility by apicomplexan parasites. *Mol Biol Cell* **14**, 396-406, doi:10.1091/mbc.E02-08-0458 (2003).

35 Menard, R. Gliding motility and cell invasion by Apicomplexa: insights from the Plasmodium sporozoite. *Cell Microbiol* **3**, 63-73, doi:cmi97 [pii] (2001).

36 Opitz, C. & Soldati, D. 'The glideosome': a dynamic complex powering gliding motion and host cell invasion by Toxoplasma gondii. *Mol Microbiol* **45**, 597-604, doi:3056 [pii] (2002).

37 Robson, K. J., Naitza, S., Barker, G., Sinden, R. E. & Crisanti, A. Cloning and expression of the thrombospondin related adhesive protein gene of Plasmodium berghei. *Mol Biochem Parasitol* **84**, 1-12, doi:S0166-6851(96)02774-0 [pii] (1997).

38 Rogers, W. O., Rogers, M. D., Hedstrom, R. C. & Hoffman, S. L. Characterization of the gene encoding sporozoite surface protein 2, a protective Plasmodium yoelii sporozoite antigen. *Mol Biochem Parasitol* **53**, 45-51 (1992).

39 Sidjanski, S. & Vanderberg, J. P. Delayed migration of Plasmodium sporozoites from the mosquito bite site to the blood. *Am J Trop Med Hyg* **57**, 426-429 (1997).

40 Amino, R., Thiberge, S., Shorte, S., Frischknecht, F. & Menard, R. Quantitative imaging of Plasmodium sporozoites in the mammalian host. *C R Biol* **329**, 858-862, doi:S1631-0691(06)00189-2 (2006).

41 Amino, R. *et al.* Host cell traversal is important for progression of the malaria parasite through the dermis to the liver. *Cell Host Microbe* **3**, 88-96, doi:S1931-3128(08)00002-4 (2008).

42 Ishino, T., Yano, K., Chinzei, Y. & Yuda, M. Cell-passage activity is required for the malarial parasite to cross the liver sinusoidal cell layer. *PLoS Biol* **2**, E4, doi:10.1371/journal.pbio.0020004 (2004).

43 Ishino, T., Chinzei, Y. & Yuda, M. A Plasmodium sporozoite protein with a membrane attack complex domain is required for breaching the liver sinusoidal cell layer prior to hepatocyte infection. *Cell Microbiol* **7**, 199-208, doi:CMI447 (2005).

44 Kariu, T., Ishino, T., Yano, K., Chinzei, Y. & Yuda, M. CelTOS, a novel malarial protein that mediates transmission to mosquito and vertebrate hosts. *Mol Microbiol* **59**, 1369-1379, doi:MMI5024 (2006).

45 Bhanot, P., Schauer, K., Coppens, I. & Nussenzweig, V. A surface phospholipase is involved in the migration of plasmodium sporozoites through cells. *J Biol Chem* **280**, 6752-6760, doi:M411465200 (2005).

46 Chakravarty, S. *et al.* CD8+ T lymphocytes protective against malaria liver stages are primed in skin-draining lymph nodes. *Nat Med* **13**, 1035-1041, doi:nm1628 (2007).

47 Thiberge, S. *et al.* In vivo imaging of malaria parasites in the murine liver. *Nat Protoc* **2**, 1811-1818, doi:nprot.2007.257 (2007).

48 Nussenzweig, V. & Nussenzweig, R. S. Circumsporozoite proteins of malaria parasites. *Bull Mem Acad R Med Belg* **144**, 493-504 (1989).

49 Pancake, S. J., Holt, G. D., Mellouk, S. & Hoffman, S. L. Malaria sporozoites and circumsporozoite proteins bind specifically to sulfated glycoconjugates. *J Cell Biol* **117**, 1351-1357 (1992).

50 Sinnis, P. The malaria sporozoite's journey into the liver. *Infect Agents Dis* **5**, 182-189 (1996).

51 Frevert, U. *et al.* Intravital observation of Plasmodium berghei sporozoite infection of the liver. *PLoS Biol* **3**, e192, doi:04-PLBI-RA-0927R2 (2005).

52 Pradel, G. & Frevert, U. Malaria sporozoites actively enter and pass through rat Kupffer cells prior to hepatocyte invasion. *Hepatology* **33**, 1154-1165, doi:S0270-9139(01)12578-4 (2001).

53 Mota, M. M. *et al.* Migration of Plasmodium sporozoites through cells before infection. *Science* **291**, 141-144, doi:10.1126/science.291.5501.141 (2001).

54 Coppi, A. *et al.* Heparan sulfate proteoglycans provide a signal to Plasmodium sporozoites to stop migrating and productively invade host cells. *Cell Host Microbe* **2**, 316-327, doi:S1931-3128(07)00248-X (2007).

55 Mota, M. M., Hafalla, J. C. & Rodriguez, A. Migration through host cells activates Plasmodium sporozoites for infection. *Nat Med* **8**, 1318-1322, doi:10.1038/nm785 (2002).

56 Carrolo, M. *et al.* Hepatocyte growth factor and its receptor are required for malaria infection. *Nat Med* **9**, 1363-1369, doi:10.1038/nm947 (2003).

57 Muller, H. M. *et al.* Thrombospondin related anonymous protein (TRAP) of Plasmodium falciparum binds specifically to sulfated glycoconjugates and to HepG2 hepatoma cells suggesting a role for this molecule in sporozoite invasion of hepatocytes. *EMBO J* **12**, 2881-2889 (1993).

58 Prudencio, M., Rodriguez, A. & Mota, M. M. The silent path to thousands of merozoites: the Plasmodium liver stage. *Nat Rev Microbiol* **4**, 849-856, doi:nrmicro1529 (2006).

59 Tarun, A. S. *et al.* A combined transcriptome and proteome survey of malaria parasite liver stages. *Proc Natl Acad Sci U S A* **105**, 305-310, doi:0710780104 (2008).

60 Silvie, O., Goetz, K. & Matuschewski, K. A sporozoite asparagine-rich protein controls initiation of Plasmodium liver stage development. *PLoS Pathog* **4**, e1000086, doi:10.1371/journal.ppat.1000086 (2008).

61 van Dijk, M. R. *et al.* Genetically attenuated, P36p-deficient malarial sporozoites induce protective immunity and apoptosis of infected liver cells. *Proc Natl Acad Sci U S A* **102**, 12194-12199, doi:0500925102 (2005).

62 Mueller, A. K. *et al.* Plasmodium liver stage developmental arrest by depletion of a protein at the parasite-host interface. *Proc Natl Acad Sci U S A* **102**, 3022-3027, doi:0408442102 (2005).

63 Yu, M. *et al.* The fatty acid biosynthesis enzyme FabI plays a key role in the development of liver-stage malarial parasites. *Cell Host Microbe* **4**, 567-578, doi:S1931-3128(08)00368-5 (2008).

64 Vaughan, A. M. *et al.* Type II fatty acid synthesis is essential only for malaria parasite late liver stage development. *Cell Microbiol* **11**, 506-520, doi:CMI1270 (2009).

65 Falae, A. *et al.* The role of Plasmodium berghei cGMP dependent protein kinase in late liver stage development. *J Biol Chem*, doi:M109.070367 (2009).

66 Albuquerque, S. S. *et al.* Host cell transcriptional profiling during malaria liver stage infection reveals a coordinated and sequential set of biological events. *BMC Genomics* **10**, 270, doi:1471-2164-10-270 (2009).

67 Yalaoui, S. *et al.* Hepatocyte permissiveness to Plasmodium infection is conveyed by a short and structurally conserved region of the CD81 large extracellular domain. *PLoS Pathog* **4**, e1000010, doi:10.1371/journal.ppat.1000010 (2008).

68 Rodrigues, C. D. *et al.* Host scavenger receptor SR-BI plays a dual role in the establishment of malaria parasite liver infection. *Cell Host Microbe* **4**, 271-282, doi:S1931-3128(08)00231-X (2008).

69 Prudencio, M. *et al.* Kinome-wide RNAi screen implicates at least 5 host hepatocyte kinases in Plasmodium sporozoite infection. *PLoS Pathog* **4**, e1000201, doi:10.1371/journal.ppat.1000201 (2008).

70 Singh, A. P. *et al.* Plasmodium circumsporozoite protein promotes the development of the liver stages of the parasite. *Cell* **131**, 492-504, doi:S0092-8674(07)01198-1 (2007).

71 Sturm, A. & Heussler, V. Live and let die: manipulation of host hepatocytes by exoerythrocytic Plasmodium parasites. *Med Microbiol Immunol* **196**, 127-133, doi:10.1007/s00430-007-0044-3 (2007).

72 Baer, K., Klotz, C., Kappe, S. H., Schnieder, T. & Frevert, U. Release of hepatic Plasmodium yoelii merozoites into the pulmonary microvasculature. *PLoS Pathog* **3**, e171, doi:07-PLPA-RA-0376 (2007).

73 Stiene-Martin, E. A., Lotspeich-Steininger, C. A., Koepke, J. A. (Schwabbauer, M.). *Clinical Hematology: Principles, Procedures, Correlations. 2nd Edition. (The Erythrocytes)*. 57-72 (Lippencott-Raven Pubishers, 1998).

74 Maier, A. G., Cooke, B. M., Cowman, A. F. & Tilley, L. Malaria parasite proteins that remodel the host erythrocyte. *Nat Rev Microbiol* **7**, 341-354, doi:nrmicro2110 (2009).

75 Holder, A. A. *et al.* Malaria parasites and erythrocyte invasion. *Biochem Soc Trans* **22**, 291-295 (1994).

76 Sanders, P. R. *et al.* Distinct protein classes including novel merozoite surface antigens in Raft-like membranes of Plasmodium falciparum. *J Biol Chem* **280**, 40169-40176, doi:M509631200 (2005).

77 van Dijk, M. R. *et al.* A central role for P48/45 in malaria parasite male gamete fertility. *Cell* **104**, 153-164, doi:S0092-8674(01)00199-4 [pii] (2001).

78 Desimone, T. M. *et al.* Cooperativity between Plasmodium falciparum adhesive proteins for invasion into erythrocytes. *Mol Microbiol*, doi:MMI6667 (2009).

79 Triglia, T. *et al.* Apical membrane antigen 1 plays a central role in erythrocyte invasion by Plasmodium species. *Mol Microbiol* **38**, 706-718, doi:mmi2175 [pii] (2000).

80 Treeck, M. *et al.* Functional analysis of the leading malaria vaccine candidate AMA-1 reveals an essential role for the cytoplasmic domain in the invasion process. *PLoS Pathog* **5**, e1000322, doi:10.1371/journal.ppat.1000322 (2009).

81 Miller, L. H., Hudson, D. & Haynes, J. D. Identification of Plasmodium knowlesi erythrocyte binding proteins. *Mol Biochem Parasitol* **31**, 217-222 (1988).

82 Rayner, J. C., Galinski, M. R., Ingravallo, P. & Barnwell, J. W. Two Plasmodium falciparum genes express merozoite proteins that are related to Plasmodium vivax and Plasmodium yoelii adhesive proteins involved in host cell selection and invasion. *Proc Natl Acad Sci U S A* **97**, 9648-9653, doi:10.1073/pnas.160469097 (2000).

83 Duraisingh, M. T. *et al.* Phenotypic variation of Plasmodium falciparum merozoite proteins directs receptor targeting for invasion of human erythrocytes. *EMBO J* **22**, 1047-1057, doi:10.1093/emboj/cdg096 (2003).

84 Gilberger, T. W., Thompson, J. K., Reed, M. B., Good, R. T. & Cowman, A. F. The cytoplasmic domain of the Plasmodium falciparum ligand EBA-175 is essential for invasion but not protein trafficking. *J Cell Biol* **162**, 317-327, doi:10.1083/jcb.200301046 (2003).

85 Maier, A. G. *et al.* Plasmodium falciparum erythrocyte invasion through glycophorin C and selection for Gerbich negativity in human populations. *Nat Med* **9**, 87-92, doi:10.1038/nm807 (2003).

86 Stubbs, J. *et al.* Molecular mechanism for switching of P. falciparum invasion pathways into human erythrocytes. *Science* **309**, 1384-1387, doi:309/5739/1384 (2005).

87 Triglia, T., Duraisingh, M. T., Good, R. T. & Cowman, A. F. Reticulocyte-binding protein homologue 1 is required for sialic acid-dependent invasion into human erythrocytes by Plasmodium falciparum. *Mol Microbiol* **55**, 162-174, doi:MMI4388 (2005).

88 Aikawa, M., Rabbege, J. R., Udeinya, I. & Miller, L. H. Electron microscopy of knobs in Plasmodium falciparum-infected erythrocytes. *J Parasitol* **69**, 435-437 (1983).

89 Keeley, A. & Soldati, D. The glideosome: a molecular machine powering motility and host-cell invasion by Apicomplexa. *Trends Cell Biol* **14**, 528-532, doi:10.1016/j.tcb.2004.08.002(2004).

90 Ward, G. E., Miller, L. H. & Dvorak, J. A. The origin of parasitophorous vacuole membrane lipids in malaria-infected erythrocytes. *J Cell Sci* **106 (Pt 1)**, 237-248 (1993).

91 McPherson, R. A., Donald, D. R., Sawyer, W. H. & Tilley, L. Proteolytic digestion of band 3 at an external site alters the erythrocyte membrane organisation and may facilitate malarial invasion. *Mol Biochem Parasitol* **62**, 233-242 (1993).

92 Ginsburg, H. Some reflections concerning host erythrocyte-malarial parasite interrelationships. *Blood Cells* **16**, 225-235 (1990).

93 Ball, E. G., Mc, K. R. & et al. Studies on malarial parasites; chemical and metabolic changes during growth and multiplication in vivo and in vitro. *J Biol Chem* **175**, 547-571 (1948).

94 Sherman, I. W. Amino acid metabolism and protein synthesis in malarial parasites. *Bull World Health Organ* **55**, 265-276 (1977).

95 Sherman, I. W. Transport of amino acids and nucleic acid precursors in malarial parasites. *Bull World Health Organ* **55**, 211-225 (1977).

96 Sherman, I. W., Ting, I. P. & Tanigoshi, L. Plasmodium lophurae: glucose-1-14C nd glucose-6-14C catabolism by free plasmodia and duckling host erythrocytes. *Comp Biochem Physiol* **34**, 625-639 (1970).

97 McCormick, G. J. Amino acid transport and incorporation in red blood cells of normal and Plasmodium knowlesi-infected rhesus monkeys. *Exp Parasitol* **27**, 143-149 (1970).

98 Rosenthal, P. J. & Meshnick, S. R. Hemoglobin catabolism and iron utilization by malaria parasites. *Mol Biochem Parasitol* **83**, 131-139, doi:S0166-6851(96)02763-6 [pii] (1996).

99 Gluzman, I. Y. *et al.* Order and specificity of the Plasmodium falciparum hemoglobin degradation pathway. *J Clin Invest* **93**, 1602-1608, doi:10.1172/JCI117140 (1994).

100 Goldberg, D. E., Slater, A. F., Cerami, A. & Henderson, G. B. Hemoglobin degradation in the malaria parasite Plasmodium falciparum: an ordered process in a unique organelle. *Proc Natl Acad Sci U S A* **87**, 2931-2935 (1990).

101 Omara-Opyene, A. L. *et al.* Genetic disruption of the Plasmodium falciparum digestive vacuole plasmepsins demonstrates their functional redundancy. *J Biol Chem* **279**, 54088-54096, doi:M409605200 (2004).

102 Liu, J., Gluzman, I. Y., Drew, M. E. & Goldberg, D. E. The role of Plasmodium falciparum food vacuole plasmepsins. *J Biol Chem* **280**, 1432-1437, doi:M409740200 (2005).

103 Hiller, N. L. *et al.* A host-targeting signal in virulence proteins reveals a secretome in malarial infection. *Science* **306**, 1934-1937, doi:306/5703/1934 (2004).

104 Crabb, B. S. *et al.* Targeted gene disruption shows that knobs enable malaria-infected red cells to cytoadhere under physiological shear stress. *Cell* **89**, 287-296, doi:S0092-8674(00)80207-X [pii] (1997).

105 Glenister, F. K., Coppel, R. L., Cowman, A. F., Mohandas, N. & Cooke, B. M. Contribution of parasite proteins to altered mechanical properties of malaria-infected red blood cells. *Blood* **99**, 1060-1063 (2002).

106 Benting, J., Mattei, D. & Lingelbach, K. Brefeldin A inhibits transport of the glycophorin-binding protein from Plasmodium falciparum into the host erythrocyte. *Biochem J* **300 (Pt 3)**, 821-826 (1994).

107 Marti, M., Good, R. T., Rug, M., Knuepfer, E. & Cowman, A. F. Targeting malaria virulence and remodeling proteins to the host erythrocyte. *Science* **306**, 1930-1933, doi:306/5703/1930 (2004).

108 de Koning-Ward, T. F. *et al.* A newly discovered protein export machine in malaria parasites. *Nature* **459**, 945-949, doi:nature08104 (2009).

109 Russo, I. *et al.* Plasmepsin V licenses Plasmodium proteins for export into the host erythrocyte. *Nature* **463**, 632-636, doi:nature08726 (2010)

110 Boddey, J. A. *et al.* An aspartyl protease directs malaria effector proteins to the host cell. *Nature* **463**, 627-631, doi:nature08728 (2010)

111 Lanzer, M., Wickert, H., Krohne, G., Vincensini, L. & Braun Breton, C. Maurer's clefts: a novel multi-functional organelle in the cytoplasm of Plasmodium falciparum-infected erythrocytes. *Int J Parasitol* **36**, 23-36, doi:S0020-7519(05)00345-0 (2006).

112 Langreth, S. G., Jensen, J. B., Reese, R. T. & Trager, W. Fine structure of human malaria in vitro. *J Protozool* **25**, 443-452 (1978).

113 Trager, W., Rudzinska, M. A. & Bradbury, P. C. The fine structure of Plasmodium falciparum and its host erythrocytes in natural malarial infections in man. *Bull World Health Organ* **35**, 883-885 (1966).

114 Blisnick, T., Vincensini, L., Barale, J. C., Namane, A. & Braun Breton, C. LANCL1, an erythrocyte protein recruited to the Maurer's clefts during Plasmodium falciparum development. *Mol Biochem Parasitol* **141**, 39-47, doi:S0166-6851(05)00046-0 (2005).

115 Marti, M., Baum, J., Rug, M., Tilley, L. & Cowman, A. F. Signal-mediated export of proteins from the malaria parasite to the host erythrocyte. *J Cell Biol* **171**, 587-592, doi:jcb.200508051 (2005).

116 Wickert, H. *et al.* Evidence for trafficking of PfEMP1 to the surface of P. falciparum-infected erythrocytes via a complex membrane network. *Eur J Cell Biol* **82**, 271-284 (2003).

117 Aikawa, M. Studies on falciparum malaria with atomic-force and surface-potential microscopes. *Ann Trop Med Parasitol* **91**, 689-692 (1997).

118 Luse, S. A. & Miller, L. H. Plasmodium falciparum malaria. Ultrastructure of parasitized erythrocytes in cardiac vessels. *Am J Trop Med Hyg* **20**, 655-660 (1971).

119 Biggs, B. A. *et al.* Antigenic variation in Plasmodium falciparum. *Proc Natl Acad Sci U S A* **88**, 9171-9174 (1991).

120 Roberts, D. J. *et al.* Rapid switching to multiple antigenic and adhesive phenotypes in malaria. *Nature* **357**, 689-692, doi:10.1038/357689a0 (1992).

121 Berendt, A. R., Ferguson, D. J. & Newbold, C. I. Sequestration in Plasmodium falciparum malaria: sticky cells and sticky problems. *Parasitol Today* **6**, 247-254, doi:0169-4758(90)90184-6 [pii] (1990).

122 Scherf, A., Lopez-Rubio, J. J. & Riviere, L. Antigenic variation in Plasmodium falciparum. *Annu Rev Microbiol* **62**, 445-470, doi:10.1146/annurev.micro.61.080706.093134 (2008).

123 Lyon, J. A. & Haynes, J. D. Plasmodium falciparum antigens synthesized by schizonts and stabilized at the merozoite surface when schizonts mature in the presence of protease inhibitors. *J Immunol* **136**, 2245-2251 (1986).

124 Arastu-Kapur, S. *et al.* Identification of proteases that regulate erythrocyte rupture by the malaria parasite Plasmodium falciparum. *Nat Chem Biol* **4**, 203-213, doi:nchembio.70 (2008).

125 Wickham, M. E., Culvenor, J. G. & Cowman, A. F. Selective inhibition of a two-step egress of malaria parasites from the host erythrocyte. *J Biol Chem* **278**, 37658-37663, doi:10.1074/jbc.M305252200 (2003).

126 Yeoh, S. *et al.* Subcellular discharge of a serine protease mediates release of invasive malaria parasites from host erythrocytes. *Cell* **131**, 1072-1083, doi:S0092-8674(07)01403-1 (2007).

127 Pang, X. L., Mitamura, T. & Horii, T. Antibodies reactive with the N-terminal domain of Plasmodium falciparum serine repeat antigen inhibit cell proliferation by agglutinating merozoites and schizonts. *Infect Immun* **67**, 1821-1827 (1999).

128 Dvorak, J. A., Miller, L. H., Whitehouse, W. C. & Shiroishi, T. Invasion of erythrocytes by malaria merozoites. *Science* **187**, 748-750 (1975).

129 Silvestrini, F., Alano, P. & Williams, J. L. Commitment to the production of male and female gametocytes in the human malaria parasite Plasmodium falciparum. *Parasitology* **121 Pt 5**, 465-471 (2000).

130 Mair, G. R. *et al.* Regulation of sexual development of Plasmodium by translational repression. *Science* **313**, 667-669, doi:313/5787/667 (2006).

131 Billker, O., Shaw, M. K., Margos, G. & Sinden, R. E. The roles of temperature, pH and mosquito factors as triggers of male and female gametogenesis of Plasmodium berghei in vitro. *Parasitology* **115 (Pt 1)**, 1-7 (1997).

132 Billker, O. *et al.* Identification of xanthurenic acid as the putative inducer of malaria development in the mosquito. *Nature* **392**, 289-292, doi:10.1038/32667 (1998).

133 Sinden, R. E. & Croll, N. A. Cytology and kinetics of microgametogenesis and fertilization in Plasmodium yoelii nigeriensis. *Parasitology* **70**, 53-65 (1975).
134 Janse, C. J., Van der Klooster, P. F., Van der Kaay, H. J., Van der Ploeg, M. & Overdulve, J. P. Rapid repeated DNA replication during microgametogenesis and DNA synthesis in young zygotes of Plasmodium berghei. *Trans R Soc Trop Med Hyg* **80**, 154-157 (1986).
135 Han, Y. S., Thompson, J., Kafatos, F. C. & Barillas-Mury, C. Molecular interactions between Anopheles stephensi midgut cells and Plasmodium berghei: the time bomb theory of ookinete invasion of mosquitoes. *EMBO J* **19**, 6030-6040, doi:10.1093/emboj/19.22.6030 (2000).
136 Sinden, R. E. Gametocytogenesis in Plasmodium spp., and observations on the meiotic division. *Ann Soc Belg Med Trop* **65 Suppl 2**, 21-33 (1985).
137 Nacer, A., Walker, K. & Hurd, H. Localisation of laminin within Plasmodium berghei oocysts and the midgut epithelial cells of Anopheles stephensi. *Parasit Vectors* **1**, 33, doi:1756-3305-1-33 (2008).
138 Thathy, V. *et al.* Levels of circumsporozoite protein in the Plasmodium oocyst determine sporozoite morphology. *EMBO J* **21**, 1586-1596, doi:10.1093/emboj/21.7.1586 (2002).
139 Sinden, R. E. & Strong, K. An ultrastructural study of the sporogonic development of Plasmodium falciparum in Anopheles gambiae. *Trans R Soc Trop Med Hyg* **72**, 477-491 (1978).
140 Menard, R. *et al.* Circumsporozoite protein is required for development of malaria sporozoites in mosquitoes. *Nature* **385**, 336-340, doi:10.1038/385336a0 (1997).
141 Vanderberg, J. & Rhodin, J. Differentiation of nuclear and cytoplasmic fine structure during sporogonic development of Plasmodium berghei. *J Cell Biol* **32**, C7-10 (1967).
142 Aly, A. S. & Matuschewski, K. A malarial cysteine protease is necessary for Plasmodium sporozoite egress from oocysts. *J Exp Med* **202**, 225-230, doi:jem.20050545 (2005).
143 Sidjanski, S. P., Vanderberg, J. P. & Sinnis, P. Anopheles stephensi salivary glands bear receptors for region I of the circumsporozoite protein of Plasmodium falciparum. *Mol Biochem Parasitol* **90**, 33-41, doi:S0166-6851(97)00124-2 [pii] (1997).
144 Wengelnik, K. *et al.* The A-domain and the thrombospondin-related motif of Plasmodium falciparum TRAP are implicated in the invasion process of mosquito salivary glands. *EMBO J* **18**, 5195-5204, doi:10.1093/emboj/18.19.5195 (1999).
145 Kariu, T., Yuda, M., Yano, K. & Chinzei, Y. MAEBL is essential for malarial sporozoite infection of the mosquito salivary gland. *J Exp Med* **195**, 1317-1323 (2002).
146 Pimenta, P. F., Touray, M. & Miller, L. The journey of malaria sporozoites in the mosquito salivary gland. *J Eukaryot Microbiol* **41**, 608-624 (1994).
147 De Meillon, B. Malaria survey of South-West Africa. *Bull World Health Organ* **4**, 333-417 (1951).
148 Metselaar, D. Two malaria surveys in the central mountains of Netherlands New Guinea. *Am J Trop Med Hyg* **8**, 364-367 (1959).
149 Macdonald, G. Epidemiological basis of malaria control. *Bull World Health Organ* **15**, 613-626 (1956).
150 Senn, N. *et al.* Population hemoglobin mean and anemia prevalence in Papua New Guinea: new metrics for defining malaria endemicity? *PLoS One* **5**, e9375, doi:10.1371/journal.pone.0009375 (2010).
151 Okiro, E. A. *et al.* Age patterns of severe paediatric malaria and their relationship to Plasmodium falciparum transmission intensity. *Malar J* **8**, 4, doi:1475-2875-8-4 (2009).
152 Snow, R. W. & Marsh, K. The consequences of reducing transmission of Plasmodium falciparum in Africa. *Adv Parasitol* **52**, 235-264 (2002).
153 McGregor, I. A. The Passive Transfer of Human Malarial Immunity. *Am J Trop Med Hyg* **13**, SUPPL 237-239 (1964).
154 Baird, J. K. *et al.* Adult Javanese migrants to Indonesian Papua at high risk of severe disease caused by malaria. *Epidemiol Infect* **131**, 791-797 (2003).

155 O'Meara, W. P. *et al.* Relationship between exposure, clinical malaria, and age in an area of changing transmission intensity. *Am J Trop Med Hyg* **79**, 185-191, doi:79/2/185 [pii] (2008).

156 Snow, R. W. *et al.* Relation between severe malaria morbidity in children and level of Plasmodium falciparum transmission in Africa. *Lancet* **349**, 1650-1654, doi:S0140-6736(97)02038-2 (1997).

157 Djimde, A. A. *et al.* Clearance of drug-resistant parasites as a model for protective immunity in Plasmodium falciparum malaria. *Am J Trop Med Hyg* **69**, 558-563 (2003).

158 Langhorne, J., Ndungu, F. M., Sponaas, A. M. & Marsh, K. Immunity to malaria: more questions than answers. *Nat Immunol* **9**, 725-732, doi:ni.f.205 (2008).

159 Doolan, D. L., Dobano, C. & Baird, J. K. Acquired immunity to malaria. *Clin Microbiol Rev* **22**, 13-36, Table of Contents, doi:22/1/13 (2009).

160 Cohen, S., Mc, G. I. & Carrington, S. Gamma-globulin and acquired immunity to human malaria. *Nature* **192**, 733-737 (1961).

161 Riley, E. M. *et al.* Naturally acquired cellular and humoral immune responses to the major merozoite surface antigen (PfMSP1) of Plasmodium falciparum are associated with reduced malaria morbidity. *Parasite Immunol* **14**, 321-337 (1992).

162 Marsh, K. & Kinyanjui, S. Immune effector mechanisms in malaria. *Parasite Immunol* **28**, 51-60, doi:PIM808 (2006).

163 Conway, D. J. Molecular epidemiology of malaria. *Clin Microbiol Rev* **20**, 188-204, doi:20/1/188 (2007).

164 Anders, R. F., McColl, D. J. & Coppel, R. L. Molecular variation in Plasmodium falciparum: polymorphic antigens of asexual erythrocytic stages. *Acta Trop* **53**, 239-253, doi:0001-706X(93)90032-7 [pii] (1993).

165 Kyes, S., Horrocks, P. & Newbold, C. Antigenic variation at the infected red cell surface in malaria. *Annu Rev Microbiol* **55**, 673-707, doi:10.1146/annurev.micro.55.1.673 (2001).

166 Kinyanjui, S. M., Conway, D. J., Lanar, D. E. & Marsh, K. IgG antibody responses to Plasmodium falciparum merozoite antigens in Kenyan children have a short half-life. *Malar J* **6**, 82, doi:1475-2875-6-82 (2007).

167 Ferrante, A. & Rzepczyk, C. M. Atypical IgG subclass antibody responses to Plasmodium falciparum asexual stage antigens. *Parasitol Today* **13**, 145-148, doi:S0169475897898122 [pii] (1997).

168 Dorfman, J. R. *et al.* B cell memory to 3 Plasmodium falciparum blood-stage antigens in a malaria-endemic area. *J Infect Dis* **191**, 1623-1630, doi:JID33747 (2005).

169 Belnoue, E. *et al.* Vaccination with live Plasmodium yoelii blood stage parasites under chloroquine cover induces cross-stage immunity against malaria liver stage. *J Immunol* **181**, 8552-8558, doi:181/12/8552 [pii] (2008).

170 Roestenberg, M. *et al.* Protection against a malaria challenge by sporozoite inoculation. *N Engl J Med* **361**, 468-477, doi:361/5/468 (2009).

171 Hoffman, S. L. *et al.* Protection of humans against malaria by immunization with radiation-attenuated Plasmodium falciparum sporozoites. *J Infect Dis* **185**, 1155-1164, doi:JID010922 (2002).

172 Beier, J. C., Davis, J. R., Vaughan, J. A., Noden, B. H. & Beier, M. S. Quantitation of Plasmodium falciparum sporozoites transmitted in vitro by experimentally infected Anopheles gambiae and Anopheles stephensi. *Am J Trop Med Hyg* **44**, 564-570 (1991).

173 Nardin, E., Zavala, F., Nussenzweig, V. & Nussenzweig, R. S. Pre-erythrocytic malaria vaccine: mechanisms of protective immunity and human vaccine trials. *Parassitologia* **41**, 397-402 (1999).

174 Garcon, N., Heppner, D. G. & Cohen, J. Development of RTS,S/AS02: a purified subunit-based malaria vaccine candidate formulated with a novel adjuvant. *Expert Rev Vaccines* **2**, 231-238, doi:ERV020207 (2003).

175 Molineaux, L. & Gramiccia, G. *The Garki project: research on the epidemiology and control of malaria in the Sudan Savanna of West Africa.*, (World Health Organization, 1980).

176 Druilhe, P. & Perignon, J. L. A hypothesis about the chronicity of malaria infection. *Parasitol Today* **13**, 353-357, doi:S0169475897010958 [pii] (1997).

177 Babiker, H. A., Creasey, A. M., Bayoumi, R. A., Walliker, D. & Arnot, D. E. Genetic diversity of Plasmodium falciparum in a village in eastern Sudan. 2. Drug resistance, molecular karyotypes and the mdr1 genotype of recent isolates. *Trans R Soc Trop Med Hyg* **85**, 578-583 (1991).

178 Bruce, M. C. *et al.* Cross-species interactions between malaria parasites in humans. *Science* **287**, 845-848, doi:8243 [pii] (2000).

179 Richie, T. L. Interactions between malaria parasites infecting the same vertebrate host. *Parasitology* **96 (Pt 3)**, 607-639 (1988).

180 al-Yaman, F. *et al.* Reduced risk of clinical malaria in children infected with multiple clones of Plasmodium falciparum in a highly endemic area: a prospective community study. *Trans R Soc Trop Med Hyg* **91**, 602-605 (1997).

181 Mayor, A. *et al.* Plasmodium falciparum multiple infections in Mozambique, its relation to other malariological indices and to prospective risk of malaria morbidity. *Trop Med Int Health* **8**, 3-11, doi:968 [pii] (2003).

182 Owusu-Agyei, S., Smith, T., Beck, H. P., Amenga-Etego, L. & Felger, I. Molecular epidemiology of Plasmodium falciparum infections among asymptomatic inhabitants of a holoendemic malarious area in northern Ghana. *Trop Med Int Health* **7**, 421-428, doi:881 [pii] (2002).

183 Sama, W., Owusu-Agyei, S., Felger, I., Dietz, K. & Smith, T. Age and seasonal variation in the transition rates and detectability of Plasmodium falciparum malaria. *Parasitology* **132**, 13-21, doi:S0031182005008607 (2006).

184 Struik, S. S. & Riley, E. M. Does malaria suffer from lack of memory? *Immunol Rev* **201**, 268-290, doi:10.1111/j.0105-2896.2004.00181.x (2004).

185 Smith, T., Felger, I., Tanner, M. & Beck, H. P. Premunition in Plasmodium falciparum infection: insights from the epidemiology of multiple infections. *Trans R Soc Trop Med Hyg* **93 Suppl 1**, 59-64 (1999).

186 James, S. P. *Malaria at home and abroad*. (William Wood & Co., 1920).

187 Garnham, P. C. Malarial immunity in Africans; effects in infancy and early childhood. *Ann Trop Med Parasitol* **43**, 47-61 (1949).

188 Collins, W. E. & Jeffery, G. M. A retrospective examination of the patterns of recrudescence in patients infected with Plasmodium falciparum. *Am J Trop Med Hyg* **61**, 44-48 (1999).

189 Ocana-Morgner, C., Mota, M. M. & Rodriguez, A. Malaria blood stage suppression of liver stage immunity by dendritic cells. *J Exp Med* **197**, 143-151 (2003).

190 Ploemen, I. H. *et al.* Visualisation and quantitative analysis of the rodent malaria liver stage by real time imaging. *PLoS One* **4**, e7881, doi:10.1371/journal.pone.0007881 (2009).

191 Franke-Fayard, B. *et al.* A Plasmodium berghei reference line that constitutively expresses GFP at a high level throughout the complete life cycle. *Mol Biochem Parasitol* **137**, 23-33, doi:10.1016/j.molbiopara.2004.04.007 (2004).

192 Tarun, A. S. *et al.* Quantitative isolation and in vivo imaging of malaria parasite liver stages. *Int J Parasitol* **36**, 1283-1293, doi:S0020-7519(06)00239-6 (2006).

193 Bruna-Romero, O. *et al.* Detection of malaria liver-stages in mice infected through the bite of a single Anopheles mosquito using a highly sensitive real-time PCR. *Int J Parasitol* **31**, 1499-1502, doi:S002075190100265X [pii] (2001).

194 Goncalves, L. A., Vigario, A. M. & Penha-Goncalves, C. Improved isolation of murine hepatocytes for in vitro malaria liver stage studies. *Malar J* **6**, 169, doi:1475-2875-6-169 (2007).

195 Prudencio, M., Rodrigues, C. D., Ataide, R. & Mota, M. M. Dissecting in vitro host cell infection by Plasmodium sporozoites using flow cytometry. *Cell Microbiol* **10**, 218-224 (2008).

196 Irizarry, R. A. *et al.* Exploration, normalization, and summaries of high density oligonucleotide array probe level data. *Biostatistics* **4**, 249-264, doi:10.1093/biostatistics/4.2.249 (2003).

197 Gentleman, R. C. *et al.* Bioconductor: open software development for computational biology and bioinformatics. *Genome Biol* **5**, R80, doi:gb-2004-5-10-r80 (2004).

198 Gautier, L., Cope, L., Bolstad, B. M. & Irizarry, R. A. affy--analysis of Affymetrix GeneChip data at the probe level. *Bioinformatics* **20**, 307-315, doi:10.1093/bioinformatics/btg405 (2004).
199 R. Gentleman, V. C., S. Dudoit, R. Irizarry, W. Huber *Bioinformatics and Computational Biology Solutions using R and Bioconductor (Limma: linear models for microarray data (397--420) by Gordon K. Smyth)*. 397--420 (Springer, 2005).
200 Falcon, S. & Gentleman, R. Using GOstats to test gene lists for GO term association. *Bioinformatics* **23**, 257-258, doi:btl567 (2007).
201 Biewenga, J. *et al.* Macrophage depletion in the rat after intraperitoneal administration of liposome-encapsulated clodronate: depletion kinetics and accelerated repopulation of peritoneal and omental macrophages by administration of Freund's adjuvant. *Cell Tissue Res* **280**, 189-196 (1995).
202 Van Rooijen, N. & Sanders, A. Kupffer cell depletion by liposome-delivered drugs: comparative activity of intracellular clodronate, propamidine, and ethylenediaminetetraacetic acid. *Hepatology* **23**, 1239-1243, doi:S0270-9139(96)00187-5 (1996).
203 Van Rooijen, N. & Sanders, A. Liposome mediated depletion of macrophages: mechanism of action, preparation of liposomes and applications. *J Immunol Methods* **174**, 83-93 (1994).
204 Patel, B. N. *et al.* Ceruloplasmin regulates iron levels in the CNS and prevents free radical injury. *J Neurosci* **22**, 6578-6586, doi:20026652 (2002).
205 Mmbando, B. P. *et al.* Epidemiology of malaria in an area prepared for clinical trials in Korogwe, north-eastern Tanzania. *Malar J* **8**, 165, doi:1475-2875-8-165 (2009).
206 Collins, W. E. & Jeffery, G. M. A retrospective examination of sporozoite- and trophozoite-induced infections with Plasmodium falciparum in patients previously infected with heterologous species of Plasmodium: effect on development of parasitologic and clinical immunity. *Am J Trop Med Hyg* **61**, 36-43 (1999).
207 Haldar, K., Murphy, S. C., Milner, D. A. & Taylor, T. E. Malaria: mechanisms of erythrocytic infection and pathological correlates of severe disease. *Annual review of pathology* **2**, 217-249 (2007).
208 Henke, J. M. & Bassler, B. L. Bacterial social engagements. *Trends Cell Biol* **14**, 648-656, doi:S0962-8924(04)00263-6 (2004).
209 Nussler, A. K. *et al.* In vivo induction of the nitric oxide pathway in hepatocytes after injection with irradiated malaria sporozoites, malaria blood parasites or adjuvants. *Eur J Immunol* **23**, 882-887 (1993).
210 Guha, M., Kumar, S., Choubey, V., Maity, P. & Bandyopadhyay, U. Apoptosis in liver during malaria: role of oxidative stress and implication of mitochondrial pathway. *FASEB J* **20**, 1224-1226, doi:fj.05-5338fje (2006).
211 Armitage, A. E., Pinches, R., Eddowes, L. A., Newbold, C. I. & Drakesmith, H. Plasmodium falciparum infected erythrocytes induce hepcidin (HAMP) mRNA synthesis by peripheral blood mononuclear cells. *Br J Haematol* **147**, 769-771, doi:BJH7880 (2009).
212 de Mast, Q. *et al.* Assessment of urinary concentrations of hepcidin provides novel insight into disturbances in iron homeostasis during malarial infection. *J Infect Dis* **199**, 253-262, doi:10.1086/595790 (2009).
213 Ganz, T. Hepcidin--a peptide hormone at the interface of innate immunity and iron metabolism. *Curr Top Microbiol Immunol* **306**, 183-198 (2006).
214 Nemeth, E. *et al.* Hepcidin regulates cellular iron efflux by binding to ferroportin and inducing its internalization. *Science* **306**, 2090-2093, doi:1104742 [pii]
10.1126/science.1104742 (2004).
215 Heppner, D. G., Hallaway, P. E., Kontoghiorghes, G. J. & Eaton, J. W. Antimalarial properties of orally active iron chelators. *Blood* **72**, 358-361 (1988).
216 Goma, J., Renia, L., Miltgen, F. & Mazier, D. Effects of iron deficiency on the hepatic development of Plasmodium yoelii. *Parasite* **2**, 351-356 (1995).
217 Goma, J., Renia, L., Miltgen, F. & Mazier, D. Iron overload increases hepatic development of Plasmodium yoelii in mice. *Parasitology* **112 (Pt 2)**, 165-168 (1996).

218 Stahel, E. *et al.* Iron chelators: in vitro inhibitory effect on the liver stage of rodent and human malaria. *Am J Trop Med Hyg* **39**, 236-240 (1988).

219 Smith, T. *et al.* Relationship between the entomologic inoculation rate and the force of infection for Plasmodium falciparum malaria. *Am J Trop Med Hyg* **75**, 11-18, doi:75/2_suppl/11 [pii] (2006).

220 Sazawal, S. *et al.* Effects of routine prophylactic supplementation with iron and folic acid on admission to hospital and mortality in preschool children in a high malaria transmission setting: community-based, randomised, placebo-controlled trial. *Lancet* **367**, 133-143, doi:S0140-6736(06)67962-2 (2006).

221 Tanner, M. & de Savigny, D. Malaria eradication back on the table. *Bull World Health Organ* **86**, 82, doi:S0042-96862008000200002 [pii] (2008).

222 Bruce-Chwatt, L. J. Malaria and its control: present situation and future prospects. *Annu Rev Public Health* **8**, 75-110, doi:10.1146/annurev.pu.08.050187.000451 (1987).

223 Vekemans, J., Leach, A. & Cohen, J. Development of the RTS,S/AS malaria candidate vaccine. *Vaccine* **27 Suppl 6**, G67-71, doi:S0264-410X(09)01528-X (2009).

224 Boyd, M. F. Consecutive Inoculations with Plasmodium Vivax and Plasmodium Falciparum. *American Journal of Tropical Medicine and Hygiene* **1**, 10 (1939).

225 Troye-Blomberg, M. & Berzins, K. Immune interactions in malaria co-infections with other endemic infectious diseases: implications for the development of improved disease interventions. *Microbes Infect* **10**, 948-952, doi:S1286-4579(08)00191-3 (2008).

226 Beier, M. S. *et al.* Identification of malaria species by ELISA in sporozoite and oocyst infected Anopheles from western Kenya. *Am J Trop Med Hyg* **39**, 323-327 (1988).

227 Bruce, M. C. & Day, K. P. Cross-species regulation of Plasmodium parasitemia in semi-immune children from Papua New Guinea. *Trends Parasitol* **19**, 271-277, doi:S1471492203001168 [pii] (2003).

228 Lorenzetti, A. *et al.* Mixed Plasmodium falciparum infections and its clinical implications in four areas of the Brazilian Amazon region. *Acta Trop* **107**, 8-12, doi:S0001-706X(08)00081-8 (2008).

229 Matsuzaki, G. & Umemura, M. Interleukin-17 as an effector molecule of innate and acquired immunity against infections. *Microbiol Immunol* **51**, 1139-1147, doi:JST.JSTAGE/mandi/51.1139 [pii] (2007).

230 Yeaman, M. R. & Yount, N. Y. Unifying themes in host defence effector polypeptides. *Nat Rev Microbiol* **5**, 727-740, doi:nrmicro1744 (2007).

231 Hughes, D. T. & Sperandio, V. Inter-kingdom signalling: communication between bacteria and their hosts. *Nat Rev Microbiol* **6**, 111-120, doi:nrmicro1836 (2008).

232 Lowery, C. A., Dickerson, T. J. & Janda, K. D. Interspecies and interkingdom communication mediated by bacterial quorum sensing. *Chem Soc Rev* **37**, 1337-1346, doi:10.1039/b702781h (2008).

233 Roux, A., Payne, S. M. & Gilmore, M. S. Microbial telesensing: probing the environment for friends, foes, and food. *Cell Host Microbe* **6**, 115-124, doi:S1931-3128(09)00249-2 (2009).

234 Dockrell, H. M., de Souza, J. B. & Playfair, J. H. The role of the liver in immunity to blood-stage murine malaria. *Immunology* **41**, 421-430 (1980).

235 Dobano, C., Rogerson, S. J., Taylor, T. E., McBride, J. S. & Molyneux, M. E. Expression of merozoite surface protein markers by Plasmodium falciparum-infected erythrocytes in peripheral blood and tissues of children with fatal malaria. *Infect Immun* **75**, 643-652, doi:IAI.01527-06.01527-06 (2007).

236 Faucher, J. F. *et al.* The impact of malaria on common lipid parameters. *Parasitol Res* **88**, 1040-1043, doi:10.1007/s00436-002-0712-6 (2002).

237 Sibmooh, N. *et al.* Increased fluidity and oxidation of malarial lipoproteins: relation with severity and induction of endothelial expression of adhesion molecules. *Lipids Health Dis* **3**, 15, doi:10.1186/1476-511X-3-15 (2004).

238 Urban, B. C., Ing, R. & Stevenson, M. M. Early interactions between blood-stage plasmodium parasites and the immune system. *Curr Top Microbiol Immunol* **297**, 25-70 (2005).

239 Erdman, L. K., Finney, C. A., Liles, W. C. & Kain, K. C. Inflammatory pathways in malaria infection: TLRs share the stage with other components of innate immunity. *Mol Biochem Parasitol* **162**, 105-111, doi:S0166-6851(08)00208-9 (2008).

240 Coban, C., Ishii, K. J., Horii, T. & Akira, S. Manipulation of host innate immune responses by the malaria parasite. *Trends Microbiol* **15**, 271-278, doi:S0966-842X(07)00070-4 (2007).

241 Schofield, L. Intravascular infiltrates and organ-specific inflammation in malaria pathogenesis. *Immunol Cell Biol* **85**, 130-137, doi:7100040 (2007).

242 Playfair, J. H., De Souza, J. B., Dockrell, H. M., Agomo, P. U. & Taverne, J. Cell-mediated immunity in the liver of mice vaccinated against malaria. *Nature* **282**, 731-734 (1979).

243 Trinchieri, G. & Sher, A. Cooperation of Toll-like receptor signals in innate immune defence. *Nat Rev Immunol* **7**, 179-190, doi:nri2038 (2007).

244 Leiriao, P. *et al.* HGF/MET signalling protects Plasmodium-infected host cells from apoptosis. *Cell Microbiol* **7**, 603-609 (2005).

245 Heussler, V., Rennenberg, A. & Stanway, R. Host cell death induced by the egress of intracellular Plasmodium parasites. *Apoptosis* **15**, 376-385, doi:10.1007/s10495-009-0435-6.

246 Schaible, U. E. & Kaufmann, S. H. Iron and microbial infection. *Nat Rev Microbiol* **2**, 946-953, doi:nrmicro1046 (2004).

247 Ganz, T. Hepcidin, a key regulator of iron metabolism and mediator of anemia of inflammation. *Blood* **102**, 783-788, doi:10.1182/blood-2003-03-0672 (2003).

248 Cox, F. E. Concomitant infections, parasites and immune responses. *Parasitology* **122 Suppl**, S23-38 (2001).

249 Fujita, N. *et al.* Hepcidin expression in the liver: relatively low level in patients with chronic hepatitis C. *Mol Med* **13**, 97-104, doi:10.2119/2006-00057.Fujita (2007).

250 Nagashima, M. *et al.* Regulatory failure of serum prohepcidin levels in patients with hepatitis C. *Hepatol Res* **36**, 288-293, doi:S1386-6346(06)00276-2 (2006).

251 Nishina, S. *et al.* Hepatitis C virus-induced reactive oxygen species raise hepatic iron level in mice by reducing hepcidin transcription. *Gastroenterology* **134**, 226-238, doi:S0016-5085(07)01810-0 (2008).

252 Howard, C. T. *et al.* Relationship of hepcidin with parasitemia and anemia among patients with uncomplicated Plasmodium falciparum malaria in Ghana. *Am J Trop Med Hyg* **77**, 623-626, doi:77/4/623 [pii] (2007).

253 de Mast, Q. *et al.* Mild increases in serum hepcidin and interleukin-6 concentrations impair iron incorporation in haemoglobin during an experimental human malaria infection. *Br J Haematol* **145**, 657-664, doi:BJH7664 1365-2141.2009.07664.x (2009).

254 Ganz, T. Iron in innate immunity: starve the invaders. *Curr Opin Immunol* **21**, 63-67, doi:S0952-7915(09)000.coi.2009.01.011 (2009).

255 van Dooren, G. G., Stimmler, L. M. & McFadden, G. I. Metabolic maps and functions of the Plasmodium mitochondrion. *FEMS Microbiol Rev* **30**, 596-630, doi:FMR027 1574-6976.2006.00027.x (2006).

256 Sherman, I. W. *Molecular Approaches to Malaria*. (ASM Press, 2005).

257 Le Roch, K. G. *et al.* Discovery of gene function by expression profiling of the malaria parasite life cycle. *Science* **301**, 1503-1508, doi:10.1126/science.1087025(2003).